

Investigations on halobacterial transducers with respect to membrane potential sensing and adaptive methylation

**Dissertation zur Erlangung des Doktorgrades
der Fakultät für Chemie und Pharmazie
der Ludwig-Maximilians-Universität München**



**Matthias Koch
aus Eschwege**

2005

Erklärung:

Diese Dissertation wurde im Sinne von § 13 Abs. 3 bzw. 4 der Promotionsordnung vom 29. Januar 1998 von Prof. Dr. Dieter Oesterhelt betreut.

Ehrenwörtliche Versicherung:

Diese Dissertation wurde selbstständig, ohne unerlaubte Hilfe angefertigt.

München, 25.08.2005

.....
(Matthias Koch)

Dissertation eingereicht am 9.9.2005

1. Gutachter: Prof. Dr. Dieter Oesterhelt
2. Gutachter: Prof. Dr. Karl-Peter Hopfner

Mündliche Prüfung am 14.12.2005

This dissertation was generated between October 1999 and August 2005 at the Max-Planck Institute of Biochemistry in Martinsried, in the Department of Membrane Biochemistry under the guidance of Prof. Dr. Dieter Oesterhelt.

Parts of this work were previously published:

Poster presentation at the International Conference on Halophilic Microorganisms, Sevilla, Spain, September 23 - 27, 2001

Poster presentation at the Gordon Research Conference on Sensory Transduction In Microorganisms, Ventura, CA, USA, January 11 - 16, 2004

Koch, M.K., and Oesterhelt, D. (2005) MpcT is the transducer for membrane potential changes in *Halobacterium salinarum*. *Molecular Microbiology* **55**: 1681-1694.

Sprüche des Konfuzius

Dreifach ist des Raumes Maß:
Rastlos fort ohn Unterlaß
Strebt die *Länge*; fort ins Weite
Endlos giebet sich die *Breite*;
Grundlos senkt die *Tiefe* sich.

Dir ein Bild sind sie gegeben:
Rastlos vorwärts mußt du streben,
Nie ermüdet stillestehn,
Willst du die Vollendung sehn;
Mußt ins Breite dich entfalten,
Soll sich dir die Welt gestalten;
In die Tiefe mußt du steigen,
Soll sich dir das Wesen zeigen.

Nur Beharrung führt zum Ziel,
Nur die Fülle führt zur Klarheit,
Und im Abgrund wohnt die Wahrheit.

Friedrich Schiller (1759-1805)

Table of Contents

1 SUMMARY	1
2 INTRODUCTION	5
2.1 The halophilic archaeon <i>Halobacterium salinarum</i>	5
2.1.1 Taxonomy, ecology and metabolic properties.....	5
2.1.2 Morphology and swimming behavior.....	7
2.2 Signal transduction and taxis in bacteria and archaea	8
2.2.1 Histidine-aspartate phosphorelay (HAP) systems are an integral part of most common prokaryotic sensory pathways.....	9
2.2.2 The molecular machinery mediating enterobacterial signal transduction as a paradigm of prokaryotic signaling systems.....	10
2.2.3 Transducers relay external stimuli to the cell interior, and changes in their methylation status are involved in adaptation to a given stimulus intensity.....	14
2.3 Halobacterial signal transduction at a molecular level	18
2.3.1 The halobacterial Che protein machinery displays similarities to that of <i>B. subtilis</i>	18
2.3.2 Halobacterial transducers are class III transducers involved in sensing a variety of stimuli.....	20
2.3.3 Methylation of Htrs.....	21
2.4 Bacteriorhodopsin-dependent phototaxis in <i>H. salinarum</i>	22
2.4.1 The proton motive force (pmf).....	23
2.4.2 Hints towards an involvement of the signaling chain.....	23
2.5 Objectives of the thesis	25
3 RESULTS AND DISCUSSION	26
3.1 Identification of MpcT (Htr14) as the transducer for $\Delta\Psi$ changes in <i>H. salinarum</i>	26
3.1.1 Construction of retinal-protein knockout strains	26
3.1.2 Transducer inventory of <i>H. salinarum</i>	29
3.1.3 Generation of <i>htr</i> -deletions in strains MKK101 and MKK102.....	31
3.1.4 Red-blue colony selection as a new method facilitating the screening of halobacterial transformants.....	32
3.1.5 BR-dependent phototaxis is mediated by Htr14 and involves stimulus-induced methanol release.....	34
3.1.6 Htr14 is also responsible for HR-dependent photoresponses.....	36
3.1.7 Htr14 is bound to the plasma membrane and can exist in differently methylated forms.....	37
3.1.8 Mass spectrometrical analysis identified four methylatable residues in Htr14 and suggests a set of Htr14 species consistent with that seen on immunoblots.....	39

TABLE OF CONTENTS

3.1.9 The buffering capacity of the <i>H. salinarum</i> cytoplasm argues for a change in $\Delta\Psi$ as the stimulus that is sensed via Htr14.....	42
3.1.10 MpcT (Htr14) by itself probably serves as the $\Delta\Psi$ sensor.....	46
3.1.11 Structural and clustering model for <i>E. coli</i> Tsr and MpcT.....	50
3.1.12 Summary of MpcT (Htr14) action and outlook.....	59
3.2 Mass spectrometrical identification of methylation sites in Htrs.....	62
3.2.1 Starting point and strategy for the investigation of Htr methylation.....	62
3.2.2 An evaluation of MALDI-TOF MS experiments provided first hints towards the detectability of methylated peptides via MS.....	65
3.2.3 LC ESI Q-TOF MS(/MS) after in-gel Asp-N digestion of the respective Htrs is the method of choice to investigate Htr-methylation.....	67
3.2.4 Mascot MS/MS ions searches with the detected peptide fragment masses identified differently methylated forms of certain Htr peptides.....	70
3.2.5 For a number of Htrs either the methylation sites or the individual methylated residues could be identified via tandem MS (MS/MS).....	74
3.2.6 MS/MS spectra can provide different levels of information concerning the methylation of transducer peptides.....	77
3.2.7 Deamidations at position 2 of heptad -11 of Htr4 and Htr15 only in wild-type but not in the $\Delta cheB$ strain identify CheB as the deamidase of <i>H. salinarum</i>	82
3.2.8 Methylation sites within the methylatable regions of membrane-bound Htrs were identified in heptads -13, -12, +13, +15 and +17.....	83
3.2.9 Transducer evolution could be explained by a scenario different from the insertion/deletion (indel)-hypothesis.....	86
3.2.10 An additional methylatable site was identified in the signaling region of Htr14 (MpcT) in heptad +2.....	89
3.2.11 Summary of Htr methylation and outlook.....	90
4 MATERIALS AND METHODS.....	94
4.1 Chemicals and enzymes.....	94
4.1.1 Chemicals.....	94
4.1.2 Kits and Enzymes.....	95
4.2 Microbiological materials and methods.....	96
4.2.1 Strains and culture conditions.....	96
4.2.2 Plasmids.....	99
4.2.3 Media and antibiotics.....	101
4.2.4 Transformation of <i>E. coli</i>	103
4.2.5 Transformation of <i>H. salinarum</i>	104
4.3 Methods of molecular biology.....	107
4.3.1 Preparation and sequencing of DNA.....	107

4.3.2	Generation of PCR fragments and plasmid construction.....	109
4.3.3	Southern blot analysis.....	111
4.4	Methods for protein analysis.....	112
4.4.1	Protein preparation from <i>H. salinarum</i> cells.....	112
4.4.2	Determination of protein concentration.....	113
4.4.3	SDS PAGE.....	113
4.5	Immunochemical methods.....	115
4.5.1	Production of antibodies.....	115
4.5.2	Western blot analysis.....	115
4.6	Analysis of Htr-methylation by mass spectrometry.....	117
4.6.1	Preparation and MALDI-TOF MS analysis of tryptic peptides from membrane and cytosolic proteins of strain TOM.....	117
4.6.2	In-gel Asp-N digest of proteins from 1-D SDS-PAGE gels.....	117
4.6.3	LC MS/MS of the generated peptides.....	118
4.6.4	Analysis of raw MS/MS data by Mascot MS/MS ions search.....	119
4.7	Behavioral studies of <i>H. salinarum</i>.....	120
4.7.1	Selection of motile halobacterial cells via swarm plates.....	120
4.7.2	Investigation of phototactic responses via motion analysis	120
4.7.3	Analysis of the adaptive release of volatile methyl groups.....	122
4.8	Additional methods.....	124
4.8.1	Determination of protein contents and buffering capacities of halobacterial cell fractions.....	124
4.8.2	Measurements of pH changes in cell suspensions upon changes in illumination.....	125
4.9	Computer programs.....	125
5	REFERENCES.....	127
6	APPENDIX.....	134
6.1	Abbreviations.....	134
6.2	Lists of Tables and Figures.....	136
6.3	Plasmid maps.....	138
6.4	Oligonucleotide primers for PCR.....	140
6.5	Southern blots to verify the <i>htr</i>-deletions in strains derived from MKK101	144
6.6	Details on <i>htrs</i> and their gene products.....	148
6.7	Databases of Htr-peptide sequences.....	150
6.8	Additional MS/MS spectra.....	151
6.9	Domain organization of the Htrs, Tsr, Tar and McpB.....	154
6.10	Scheme of the features and methylation sites of Htrs, Tsr, Tar and McpB.....	156

1 SUMMARY

The halophilic archaeon *H. salinarum* is found in environments of high salinities like solar salterns or salt lakes, which are characterized by intense illumination and a shortage of oxygen. Its capability of phototrophic growth, which is based on the action of the light-driven proton pump bacteriorhodopsin (BR), is therefore crucial for an optimal thriving in its natural habitat. To reach the best illumination conditions, *H. salinarum* makes use of phototaxis, which under conditions of low irradiation requires the interaction of the retinal-containing photoreceptors sensory rhodopsin I or II with their respective transducers HtrI and HtrII. Like Htrs mediating chemotactic signals, these Htrs also communicate their signal input via cytosolic Che proteins to the flagellar motor. The cellular response is an alteration in the switching frequency of flagellar rotational direction, which can be observed in a microscopic cell tracking setup, e.g. as the reversal of swimming direction upon switching-off green to orange light. The investigation of mutants, which lacked the sensory rhodopsins and contained either BR or the light-driven chloride pump halorhodopsin (HR) as their only retinal protein, has previously revealed phototactic responses at high irradiance in the absence of respiration. The results of these experiments pointed to the involvement of a transducer and to a change in the electrical potential component of the proton motive force across the cell membrane as the signal that is sensed via this transducer.

In a deletion approach, mutants carrying single deletions of all 18 known or putative halobacterial transducer (*htr*) genes were constructed in a strain containing BR as the only retinal protein. To facilitate clone selection after halobacterial transformation, the method of red-blue selection was developed in the course of this study, and is now generally applied in the lab. It is based on the expression of the *bgaH* gene, which is present in the plasmids and encodes a β -galactosidase that is active at high salt concentrations. Clones containing the plasmid DNA develop a blue color when grown in the presence of X-gal and can therefore be distinguished from red clones, which lack the plasmid DNA, e.g. after a second recombination event has removed the plasmid DNA together with the gene to be deleted.

The methylatable membrane-bound transducer Htr14, which lacks an extracellular domain, was identified as the transducer, that is responsible for BR- and HR-dependent photosensing, which includes adaptive methylation. Based on the determinations of a minimal light-off-stimulus length of 200 ms, the net proton flux across the cell membrane within this time, and the cytoplasmic buffering capacity, it was concluded that indeed the change of the membrane

potential ($\Delta\Delta\Psi$) and not that of intracellular pH, is the signal-generating event. Htr14 was therefore renamed to Membrane potential change Transducer, or MpcT. It is the first transducer for which the causative stimulus could be defined as a change in membrane potential, as opposed to changes in intracellular pH, ATP concentration or redox state.

The good conservation of the N-terminal sequence of MpcT in its putative *N. pharaonis* ortholog and also in a putative sensor histidine protein kinase from *H. salinarum* suggests that $\Delta\Delta\Psi$ sensing takes place via this region of the proteins either directly, or indirectly via interaction with another protein that acts as the actual sensor. The apparently independent transcription of the *mpcT* gene might indicate a direct sensor function for MpcT, because all genes encoding receptors or binding proteins, for which an interaction with an Htr has been reported previously, are cotranscribed with the gene encoding the respective Htr.

Immunoblot analysis revealed several differently methylated MpcT species, which could be distinguished due to their different electrophoretic mobilities on SDS polyacrylamide gels. Mass spectrometrical analysis confirmed that for these transducer species an increase in mobility on the gel correlates with an increase in methylation, and identified a total of four methylatable Glu residues. Three of them are present at two methylation sites within the predicted methylatable regions of MpcT, and the fourth Glu is located within the signaling region. The term methylation site is used in this study, when referring to a pair of (mostly Glx) residues, which is normally located within a consensus sequence for methylation, that was derived previously for the *E. coli* methyltransferase CheR. One or both residues of such a site can accept a methyl group to form a methyl ester (in the case of a Gln, after preceding deamidation to a Glu). The methylation and demethylation of such transducer residues by the methyltransferase CheR and the methylesterase CheB, respectively, is known to play an important role in the adaptation of enterobacterial cells to a given stimulus strength, which enables the cells to sense such stimuli over a wide dynamic range of intensities. Similar functions were therefore expected for halobacterial CheR and CheB.

On the basis of published data, a structural and clustering model was generated for the *E. coli* transducer Tsr, which in principle allows for an interaction of the clustered transducers with CheA and CheW. Based on this model and on comparisons of the amino acid sequences of Tsr and MpcT, a structural model was proposed for MpcT, which might be helpful in the design of experiments leading to an elucidation of the molecular mechanisms of $\Delta\Delta\Psi$ sensing via MpcT.

At the beginning of this study, very little was known about the number and the positions of methylatable Htr residues. To investigate the methylation of membrane-bound Htrs, membrane protein preparations were subjected to 1-D SDS PAGE and the proteins with an apparent MW

between approx. 100 and 160 kDa, of which Htrs apparently constitute the major fraction, were excised from the gel in a number of slices and separately digested with the protease Asp-N. A subsequent investigation of the generated peptide mixtures via LC ESI Q-TOF MS/MS identified methylation sites comprising heptad positions 2 and 3 of one or more of the hydrophobic heptads -13, -12, +13, +15 and +17.

A hydrophobic heptad describes a succession of 7 amino acid residues, of which the first and the fourth are either hydrophobic, Ser or Thr, and a succession of such heptads is indicative of a coiled-coil structure. A heptad numbering for transducers is proposed, in which the numbers become increasingly negative/positive towards the N-/C-terminal end of the coiled coil, starting with +/- 0 for the two heptads framing and forming the hairpin turn of the predicted coiled coil. Depending on the quality of the MS/MS spectra and on the sequences of the investigated Htr peptides, in some cases only the methylation sites could be determined, whereas in others even the methylated residues could be identified.

Contrary to transducers from other organisms like *E. coli* and *B. subtilis*, in which only pairs of Glx residues have been reported to comprise methylation sites and only single residues have been reported to be methylated, the situation is different in *H. salinarum*. Individual halobacterial methylation sites were identified (in heptads -13 and +17, respectively, of Htr4), which contain an Asp or an Ala residue at heptad position 2 in combination with a methylatable Glu at heptad position 3. Furthermore, at sites containing two Glu residues, double methylations were detected frequently in Htrs from a $\Delta cheB$ mutant, but in several cases also in Htrs from wild-type cells. This demonstrates that pairs of methylated Glu residues are present in Htrs under physiological conditions *in vivo*.

While no indications were found towards deamidations of Asn residues in any of the investigated Htrs, the mass spectrometrical analyses pointed to Gln deamidations in heptad -12 of Htr6, heptad -11 of Htr4 and heptad -11 (and possibly also heptad -10) of Htr15. The detection of deamidations only in wild-type cells and not in a $\Delta cheB$ mutant suggests that halobacterial CheB, just like enterobacterial CheB, has a deamidase activity and, moreover, that it is the only deamidase acting on Htrs. This argues against a deamidase function of halobacterial CheD, despite the detection of such a function for its homolog in *B. subtilis*.

An increase of Htr methylation in the absence of CheB, which was deduced from band patterns seen on anti-Htr14 immunoblots comparing wild-type strain S9 to a $\Delta cheB$ mutant, could be confirmed via MS for Htr14 (MpcT), as well as for other Htrs. This study therefore provides the first direct experimental evidence confirming the assumed methylesterase function of CheB in

H. salinarum. However, the expected complete esterification of all methylatable Htr residues in the absence of CheB was not observed, which might indicate a restricted access of CheR to the remaining unmethylated Glu residues. Mass spectrometrical analysis of Htrs from a $\Delta cheR$ mutant demonstrated the complete absence of methylation in all detected methylatable peptides, which provided the first experimental evidence confirming the predicted methyltransferase activity of CheR in *H. salinarum*. The findings, that the methylatable site that was detected within the signaling region of MpcT is lacking the consensus sequence for methylation by CheR, and that the extent of methylation at this particular site is more or less identical in the presence and in the absence of CheB, point to a CheR/CheB-independent methylation in this particular case.

Methylation sites within the methylatable regions of transducers are assumed to define two faces on opposite sites of the dimer, each one resulting from a different monomer. In several Htrs these faces span 6 and possibly up to 8 heptads, and therefore the methylatable areas of these Htrs are larger than those known for other transducers like *E. coli* Tsr or *B. subtilis* McpB. Based on amino acid sequence alignments and on a comparison of the locations of methylation sites in these bacterial transducers with those of the newly identified sites in Htrs, a scenario for the generation of different transducer classes and of the groups of Htrs is proposed as an alternative to the indel (insertion/deletion)-hypothesis of transducer evolution (Le Moual and Koshland, 1996). It is suggested that in each case a primary genetic event at a single site of a transducer gene generated a modified but still active transducer, which maintained its methylation sites at the original locations. This primary event was then followed, in the course of evolution, by additional small changes leading to further modifications of the transducer, which in some cases included the loss of some of the original methylation sites and the development of new ones.

2 INTRODUCTION

2.1 The halophilic archaeon *Halobacterium salinarum*

2.1.1 Taxonomy, ecology and metabolic properties

As a member of the domain *Archaea* (phylum: *Euryarchaeota*, class: *Halobacteria*, order: *Halobacteriales*) *Halobacterium salinarum* belongs to the family *Halobacteriaceae*. Consisting entirely of halophiles *Halobacteriaceae* constitutes one out of three archaeal families containing halophilic members. The other two families *Methanospirillaceae* and *Methanosarcinaceae* also contain non-halophilic members. Table 2.1 shows that, as of May 2004, the family of *Halobacteriaceae* is divided into 18 genera containing 50 species (Garrity *et al.*, 2004).

Table 2.1. Genera and type strains of the family *Halobacteriaceae*

Genus (number of species)	Type strain [old name(s)]
I Halobacterium (1)	<i>Halobacterium salinarum</i> [<i>H. cutirubrum</i> , <i>H. halobium</i>]
II Haloarcula (6)	<i>Haloarcula vallismortis</i> [<i>Halobacterium vallismortis</i>]
III Halobaculum (1)	<i>Halobaculum gomorrense</i>
IV Halobiforma (2)	<i>Halobiforma haloterrestis</i>
V Halococcus (4)	<i>Halococcus morrhuae</i>
VI Haloferax (6)	<i>Haloferax volcanii</i> [<i>Halobacterium volcanii</i>]
VII Halogeometricum (1)	<i>Halogeometricum borinquense</i>
VIII Halomicrobium (1)	<i>Halomicrobium mukohataei</i> [<i>Haloarcula mukohataei</i>]
IX Halorhabdus (1)	<i>Halorhabdus utahensis</i>
X Halorubrum (9)	<i>Halorubrum saccharovororum</i> [<i>Halorubrobacterium saccharovororum</i>]
XI Halosimplex (1)	<i>Halosimplex carlsbadense</i>
XII Haloterrigena (2)	<i>Haloterrigena turkmenica</i> [<i>Halococcus turkmenicus</i>]
XIII Natrialba (6)	<i>Natrialba asiatica</i>
XIV Natrinema (3)	<i>Natrinema pellirubrum</i>
XV Natronobacterium (1)	<i>Natronobacterium gregoryi</i>
XVI Natronococcus (2)	<i>Natronococcus occultus</i>
XVII Natronomonas (1)	<i>Natronomonas pharaonis</i> [<i>Natronobacterium pharaonis</i>]
XVIII Natronorubrum (2)	<i>Natronorubrum bangense</i>

Taxonomic information was composed according to Garrity *et al.* (2004) and is available at <http://141.150.157.80/bergeysoutline/main.htm>

In the past, extensive taxonomic reclassification and renaming of strains has taken place on the basis of 16S rDNA sequencing and additional criteria. This is illustrated by the fact that 7 of the 18 type strains did not retain their original names, and that only 2 years earlier, in 2002 *Halobacteriaceae* was divided into only 15 genera containing 44 species (Oren, 2002). For example, strains which had been classified earlier as *Halobacterium halobium*, *Halobacterium*

salinarium and *Halobacterium cutirubrum* are now taxonomically united as a single species called *Halobacterium salinarum* (*H. salinarum*).

H. salinarum belongs to the group of extremely halophilic organisms, which require high salt concentrations of 2 - 4 M for optimal growth and can grow in media containing up to 5.2 M NaCl (30 %, saturation limit). It was first isolated from salted fish and is frequently found in aqueous environments with salinities close to saturation (4 - 5 M) like salt lakes or crystallizer ponds of solar salterns. These habitats usually appear red due to the massive growth of halophilic archaea which contain the carotenoid bacterioruberine for protection against photooxidative damage (Oren, 1994). Prokaryotic cell numbers in crystallizer ponds can exceed $10^7 - 10^8$ cells/ml, however, the number of recovered colony-forming cells was found to be only in the range of $10^4 - 10^6$ (Oren, 2002). Multi-pond solar salterns, which are used for the commercial production of salt, consist of a series of small, enclosed basins containing water of increasing salinities ranging from seawater to the NaCl-saturated brine of crystallizer ponds. They represent environments characterized by a shortage of oxygen and intense illumination (up to approx. 1000 W/m^2). The organic nutrients for *H. salinarum* are provided by the eukaryotic alga *Dunaliella salina*, which represents the major if not the only oxygenic phototroph growing even at extremely high salinities of up to 3.5 M NaCl and beyond (Fischer *et al.*, 1994), and by other photosynthetic organisms which grow in the preceding ponds of lower salinities.

Energy production in *H. salinarum* is possible via several different routes. In addition to its capability of aerobic and anaerobic respiration, the organism is able to use arginine for fermentative growth (Hartmann *et al.*, 1980). The key step of this process is the conversion of arginine to citrulline catalyzed by arginine deiminase (Ruepp and Soppa, 1996). In a second step, catalyzed by ornithine carbamoyltransferase, citrulline reacts with inorganic phosphate to ornithine and the high-energy compound carbamoyl phosphate which is finally used to generate ATP from ADP. *H. salinarum* can furthermore use light as a source of energy via the actions of two seven-transmembrane-helix proteins which function as light-driven ion pumps and contain a lysine-bound retinal as the photoreactive chromophore. Upon light-activation this retinal isomerizes from the all-trans to the 13-cis conformation, which induces a conformational change in the protein and finally results in the pumping of an ion across the cell membrane. In a cyclic process bacteriorhodopsin (BR) exports H^+ -ions, thereby providing the cell with the capacity for phototrophic growth, and halorhodopsin (HR) imports Cl^- -ions, which helps to maintain the osmotic balance during growth (reviewed by Oesterhelt, 1998).

2.1.2 Morphology and swimming behavior

H. salinarum exists in the form of rod-shaped cells of approximately 0.4 to 0.7 μm diameter and 2 to 6 μm length (Fig. 2.1), which exhibit unipolar flagellation with a tendency to bipolar flagellation in the stationary growth phase (Alam and Oesterhelt, 1984).



Figure 2.1 Electron micrographs of *H. halobium* (*H. salinarum*) cells with (A) bipolar and (B) monopolar flagellation.

Micrographs of cells from strain L-07 (retinal negative) were taken after shadowing with a carbon/platinum electron gun at a 25° angle and stabilization by a carbon backing film. Cell dimensions are approx. 0.4 x 2 μm . [adapted from: Alam and Oesterhelt, 1984]

A flagellar bundle consists of 5 - 10 individual flagellar filaments forming a right handed helix. It was suggested that each filament is driven by an individual motor and that the majority, if not all, of these motors rotate in the same direction at any given time (Marwan *et al.*, 1991). Observation of the flagellar bundles by high-intensity dark field microscopy revealed that (when viewed from the flagellum towards the cell body) clockwise (CW) rotation of the right-handed helical flagellar bundle pushes the cell forward, whereas counterclockwise (CCW) rotation makes the bundle pull the cell backward (Alam and Oesterhelt, 1984). This mechanism is quite different from that found in the peritrichously flagellated *E. coli* cells in which CCW rotation of the left-handed flagella produces forward swimming, whereas CW rotation or pauses of rotation leads to tumbling of the cells (Eisenbach, 1990).

Unstimulated halobacterial cells exhibit random switching of flagellar rotational direction leading to a random walk of the cells without any preferred direction (Fig. 2.2). A determination of the time course of spontaneous motor switching demonstrated that the switching probability is very low within the first few seconds after the preceding switching event and that the vast majority of cells switches after runs of approximately 6 to 80 s (Marwan *et al.*, 1991). In the presence of photo- or chemostimuli, the random walk can become biased because the motor switch is controlled by the halobacterial signaling chain.

The prolonged/shortened swimming into the direction of increasing/decreasing attractant stimulus intensity, respectively, results in a net movement of the cells towards optimal environmental conditions. Through the control of the motor switch by its environmental sensing

machinery *H. salinarum* is capable of phototaxis (Hildebrand and Dencher, 1975; Spudich and Stoeckenius, 1979a) as well as of chemotaxis (Storch *et al.*, 1999; Kokoeva and Oesterhelt, 2000).

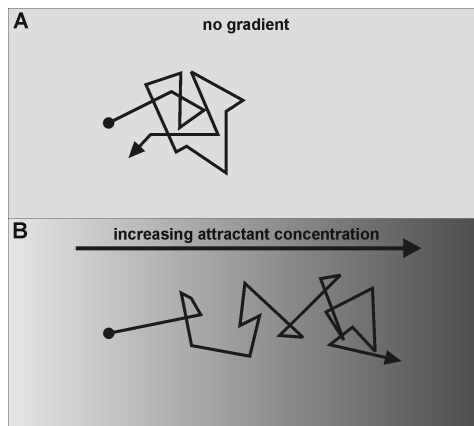


Figure 2.2 Random and biased random walk.

(A) In the absence of a stimulus gradient, halobacteria exhibit a random walk, which results in only small net changes of the original position of the cell. (B) In the presence of a stimulus-gradient, prolonged/shortened swimming phases in the direction of higher/lower attractant concentrations cause a biased random walk, which results in a net movement of the cell towards a more favorable environment.

2.2 Signal transduction and taxis in bacteria and archaea

In the course of evolution all organisms have acquired some sort of sensing capability for relevant parameters of their environment. The extent of these capabilities is growing with an organism's complexity, ranging from the rather simple machinery of unicellular prokaryotes to an extensive collection of different signaling pathways in multicellular eukaryotes.

Whereas in multicellular organisms intercellular communication, which is crucial for the coordinated interaction of different cell types, accounts for the major part of the signaling systems, the situation is different in prokaryotes. The prokaryotic signaling machinery is rather used to sense and respond to environmental parameters like light-intensity and wavelength, pH, temperature, osmolarity or concentrations of nutrients, harmful substances or terminal electron acceptors, like oxygen or nitrate.

However, intercellular communication is not completely absent in prokaryotes. In a growing number of bacterial species a population-density-sensing mechanism termed "quorum sensing" has been detected (reviewed in Henke and Bassler, 2004). The phenomenon was extensively studied in the marine bioluminescent Gram-negative bacterium *Vibrio fischeri* in which the expression of luminescence genes is induced when the cell density exceeds a certain threshold (approx. 10^{10} cells ml^{-1}). In quorum sensing the bacterial species produces a signal molecule termed autoinducer, which alters gene expression when it reaches a critical concentration in the medium. Autoinducers are often N-acyl-L-homoserine lactones (AHL), as in the case of LuxI / LuxR systems in Gram-negative bacteria (Stevens and Greenberg, 1997). Or they can be

modified oligopeptides, as in Gram-positive systems, which function via two-component signal transduction pathways.

2.2.1 Histidine-aspartate phosphorelay (HAP) systems are an integral part of most common prokaryotic sensory pathways

In a constantly changing environment it is of great importance that organisms can efficiently react to changes in parameters like those mentioned before, which are relevant for cell growth or survival. Such reactions take place in the form of either (i) movement towards favorable or away from unfavorable conditions or (ii) alterations in gene expression.

Most prokaryotic sensory pathways use histidine-aspartate phosphorelay (HAP) systems, which minimally consist of two components: a dimeric histidine protein kinase (HPK) and a response regulator (RR) protein (reviewed in West and Stock, 2001). Until 2004, more than 600 HAP systems had been detected in prokaryotic genomes (Ashby, 2004). Although eukaryotic signaling pathways usually depend on serine, threonine and tyrosine protein kinases, HAP systems are also present in many lower eukaryotes, like *Saccharomyces cerevisiae* or *Dictyostelium discoideum*, and even in plants, like for example *Arabidopsis thaliana*, which contains genes for 16 HPK and 24 RR homologs.

Most of the HPKs have a similar domain architecture: An N-terminal region, which comprises two transmembrane (TM) regions interrupted by a ligand-binding periplasmic domain, is followed by a cytoplasmic region consisting of a linker or HAMP (histidine kinases, adenylyl cyclases, methyl-binding proteins, phosphatases) domain (Aravind and Ponting, 1999), a dimerization domain, and a kinase domain which interacts with the corresponding RR. However, there are also HPKs with none, or more than two TM regions or with additional cytoplasmic domains.

The usual sequence of events in HAP systems is the following: (i) Binding of a ligand to the periplasmic domain of an HPK activates the kinase. (ii) This initiates a trans-autophosphorylation of a His residue present in one monomer of the HPK with the γ -phosphoryl group of an ATP molecule bound to the kinase domain of the other monomer. (iii) The subsequent transfer of this phosphoryl group from the His to a conserved Asp of the relevant RR then alters the activity of the RR's output domain. (iv) This generates a response, usually an alteration in the transcription of certain genes. (v) The RR is then deactivated by dephosphorylation, which can either take place spontaneously (with half-lives ranging from seconds to hours) or be enhanced by phosphatases.

2.2.2 The molecular machinery mediating enterobacterial signal transduction as a paradigm of prokaryotic signaling systems

Whereas most of the prokaryotic HAP systems are involved in the regulation of gene expression, the most extensively studied and probably best understood HAP system forms the central part of the prokaryotic chemotaxis machinery, for which the flagellar motor is the target (reviewed in Stock and Surette, 1996; Wadhams and Armitage, 2004). In this sensory system the external stimulus is not sensed directly by the periplasmic domain of the HPK but rather by membrane-spanning chemoreceptor proteins, which then relay the signal to the HPK. The chemoreceptors are also called transducers or methyl-accepting chemotaxis proteins (MCPs). The latter name results from the finding that they can be reversibly methylated at certain glutamate residues in the process of adaptation to stimulus intensity.

Because of the wealth of data which has been compiled within the last decades on the enteric chemotaxis machinery of the model organisms *Escherichia coli* and *Salmonella typhimurium*, it is now the best-understood example of such machineries and has become the paradigm of prokaryotic chemotactic signal transduction pathways. For all key components of this machinery structures are now available for either the complete protein or at least for separate domains (Fig. 2.3). The architectures and interactions of the *E. coli* components shall be described here in

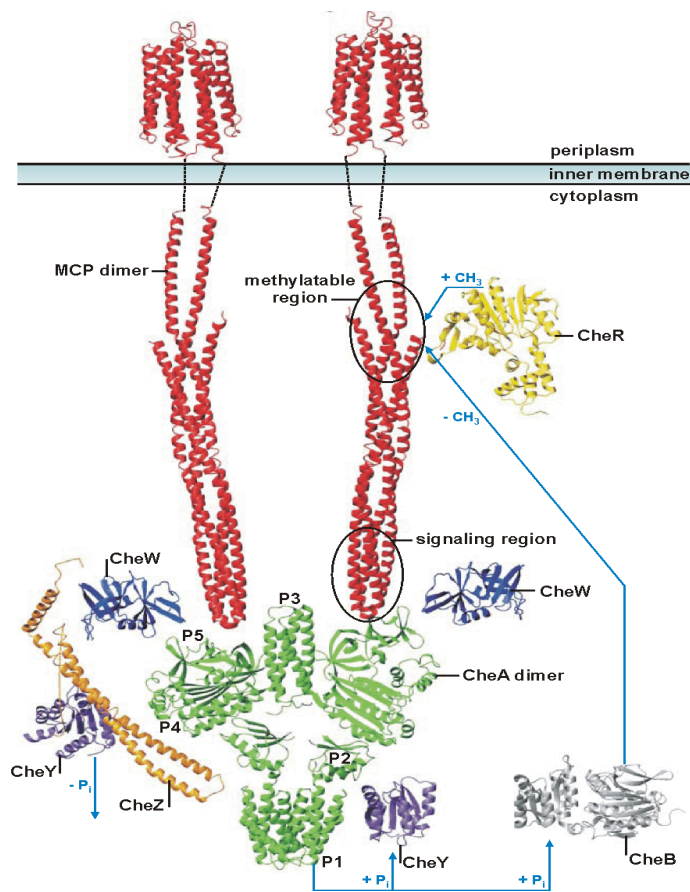


Figure 2.3 Structures and interaction pathways of chemosensory components of *E. coli* and *S. typhimurium*.

For the depicted structures, Protein Data Bank accession numbers, organisms of origin (*Eco*, *E. coli*; *Sty*, *S. typhimurium*; *Tma*, *T. maritima*) and year of deposition are indicated in parentheses: Tar periplasmic domain (1WAT, *Sty*, 1993); Tsr cytoplasmic domain (1QU7, *Eco*, 1999); CheA P1 domain (1I5N, *Sty*, 2001), P2 domain (1EAY, *Eco*, 1998) and P3 – P5 domains (1B3Q, *Tma*, 1998); CheW averaged NMR structure (1KOS, *Tma*, 2001); CheY (1EHC, *Eco*, 1996); CheR (1BC5, *Sty*, 1998); CheB (1A20, *Sty*, 1998); and CheZ with phosphorylated CheY bound (1KMI, *Eco*, 2001). The arrangement of the structures is not meant to imply that the domains or proteins are oriented or contact each other in the manner depicted. The dashed lines represent the TM regions and the HAMP domains of the MCPs, for which there are, as yet, no structures. Blue arrows indicate the process of phosphorylation (+ P_i) of the conserved Asp in the RRs CheY and CheB by the HPK CheA, the CheZ-enhanced dephosphorylation (- P_i) of CheY, and the processes of methyl esterification (+ CH₃) or methyl ester hydrolysis (- CH₃) of methylatable glutamate residues in the MCPs by CheR and (phosphorylated) CheB, respectively. [Modified from: Wadhams and Armitage, 2004]

some detail, especially because a partial homology exists between the components of the enterobacterial and the halobacterial system.

Transducer proteins of *E. coli*

E. coli has a set of 5 receptors/transducers which can sense external stimuli and relay this stimulation to the cytoplasmic Che machinery. Four of them are MCPs of 57 to 60 kDa and sense external substances. Each of these substances can be sensed by the relevant MCP's periplasmic ligand-binding domain. This happens either by direct interaction with the substance or via a substrate-loaded periplasmic binding protein (BP), which also acts as a component of an ATP-binding cassette (ABC) transporter: Tsr senses Ser. Tar senses Asp, and maltose via its BP. Trg senses ribose and galactose via their BPs. And Tap senses dipeptides via BPs (Levit *et al.*, 1998). The fifth transducer, Aer, is a 55 kDa MCP-like receptor, which is not subject to reversible methylation and lacks a periplasmic domain (Bibikov *et al.*, 2004). Aer is thought to mediate aerotactic responses by detecting oxygen-related cellular redox changes via a flavine adenine dinucleotide (FAD) prosthetic group bound to a cytoplasmic PAS (PER, ARNT, SIM) domain at its N-terminus (Taylor *et al.*, 1999). Structures of parts of the transducers are available for the periplasmic ligand-binding domain of Tar (Chi *et al.*, 1997) and for the part of the cytoplasmic domain of Tsr that is subject to reversible methylation and responsible for CheA-activation (Kim *et al.*, 1999).

After localization of chemoreceptors to the poles of cells was first demonstrated for *E. coli* by Maddock and Shapiro (1993), evidence has accumulated that transducers form large arrays at the cell poles in a wide evolutionary range of prokaryotic organisms ranging from bacteria to halophilic archaea (Fig. 2.4; Gestwicki *et al.*, 2000). Ames *et al.* (2002) proposed a model of

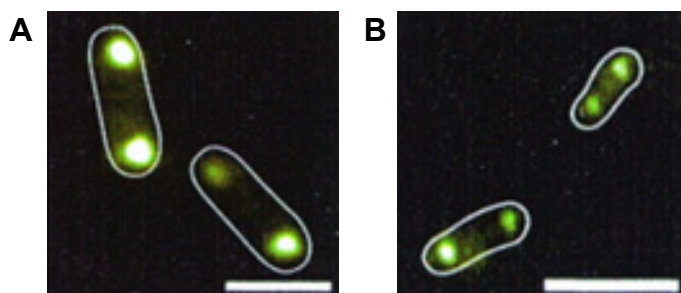


Figure 2.4 Polar clustering of transducers in *E. coli* and *H. salinarum*.

Fluorescence patterns for *E. coli* AW405 (A) and *H. salinarum* S9 cells (B) treated with an antibody raised against the *E. coli* transducer Trg and subsequently with a fluorescein-labeled anti-rabbit immunoglobulin G secondary antibody. Outlines of the cells are indicated. Bars, 2 μm . [Modified from: Gestwicki *et al.*, 2000]

cluster assembly, in which transducers of different specificities form mixed trimers of homodimers. These so-called receptor squads are thought to recruit CheA and CheW to their cytoplasmic tips, to form functional signaling teams, which cluster at the cell poles. As seen in the crystal structure of the cytoplasmic Tsr domain (Kim *et al.*, 1999), the trimer contact sites are

expected to be at the tip of the cytoplasmic four-helix coiled-coil structure formed by the transducer dimers. In *Rhodobacter sphaeroides* cells, a cytosolic cluster of transducers without TM regions is present in addition to the polar clusters of TM region-containing transducers (Wadhams *et al.*, 2003). Besides its particular transducers, each of these two cluster types contains a distinct set of CheA, CheW and CheR proteins, which do not localize to the other cluster type.

On the basis of a calculated model of a receptor cluster, Bray *et al.* (1998) suggested that clustering of transducers might play an important role in achieving the observed high sensitivity of chemosensing and the wide range of detectable concentrations (Tar can detect Asp concentrations below 5 nM and the detectable range spans 5 orders of magnitude up to a concentration of 1 mM Asp).

Overview of the sequence of events in the *E. coli* sensory pathway

Stimulation of transducers by a decrease in attractant or an increase in repellent stimulus strength starts the following sequence of events: it activates the HPK CheA, which after trans-autophosphorylation of its conserved His residue transfers the phosphoryl group to either one of the cognate RRs, CheY or CheB. Phosphorylated CheY (CheY-P) then diffuses to the flagellar motors (five to eight per *E. coli* cell) and induces switching from counterclockwise (CCW; viewed from the flagellum towards the cell) to clockwise (CW) rotation by interaction with the FliM switch proteins. This causes the left-handed helical flagellar bundle to fly apart and leads to a short phase of tumbling and reorientation of the cell, which subsequently resumes swimming into a new direction by CCW flagellar rotation. The decrease of the CheY-P concentration via hydrolysis to CheY, is enhanced by the phosphatase CheZ. Phosphorylation of the second RR, CheB, activates its methylesterase activity, which plays a role in the adaptation of the cell to a given stimulus intensity, as will be discussed below in more detail. As a consequence of this behavior, an increase/decrease of attractant concentrations prolongs/shortens the swimming phase of *E. coli*. The described biochemical processes are the basis of the observed biased random walk, which leads cells to a more favorable environment, as described above for *H. salinarum* (Fig. 2.2).

Structures for all components of the enteric sensory pathway are now available, though in some cases, as listed in the legend of Fig. 2.3, they could not be obtained directly for the enteric proteins but only for their homologs from the hyperthermophilic bacterium *Thermotoga maritima* (growth limit 90°C). Furthermore, the available structures do not always include the complete protein. For CheA, for example, a structure of a complete dimer has not been obtained,

so far. And in the case of the MCPs the structures of the transmembrane part and of the linker or HAMP domain are still not known.

A closer look at the Che proteins

Coupling of CheA to the cytoplasmic signaling regions of the transducers happens via the 18 kDa adaptor protein CheW. CheW has no catalytic activity and is rather thought to function as a scaffold protein which relays the signal from the transducer to CheA. The structure of CheW from *T. maritima*, obtained by solution NMR (Griswold *et al.*, 2002), displays great similarity to that of the CheA regulatory domain P5. CheA exerts its function as a dimer composed of two 71 kDa monomers. They both consist of 5 domains named P1 to P5, which are separated by hinges and linker regions (Bilwes *et al.*, 1999). The histidine phosphotransfer (HPt) domain P1 contains the phosphorylatable His (His48 in *E. coli*). P2 is responsible for binding to the RRs CheY and CheB. P3 is the dimerization domain. The kinase domain P4 of one monomer contains the ATP from which the γ -phosphoryl group is transferred to the His48 of the other monomer in a trans-autophosphorylation reaction. CheA activity is controlled by binding CheW plus transducer to the P5 regulatory domain. Depending on the state of the coupled transducer, P5 can control the access of the HPt domain P1 of the first monomer to the kinase domain P4 of the second monomer, and thereby either inhibit or activate the trans-autophosphorylation.

Being one of the two RRs acting as targets for CheA, the 14 kDa protein CheY contains a conserved Asp residue (Asp57 in *E. coli*) which is located inside an acidic binding pocket within the typical five α -helix, five β -strand structure of RRs. After phosphorylation, the produced CheY-P diffuses to the flagellar motor and interacts with the switch protein FlIM to induce a change of motor rotation. CheZ decreases the half-life of CheY-P to approx. 200 ms, compared to 20 s in its absence (Lukat *et al.*, 1991). It is a 24 kDa phosphatase which is assumed to form a dimer, but was also found to form oligomeric complexes in the presence of CheY-P (Blat and Eisenbach, 1996). A short half-life of CheY-P is important because a rapid decrease of the concentration of activated RR after the stimulation is a prerequisite for the temporal detection of gradients. Due to the small cell size, a temporal (at different times within a swimming phase) rather than a spatial (at different locations within a cell) detection of gradients is assumed as the mechanism of tactic sensing in prokaryotes (Schnitzer *et al.*, 1990).

In addition to CheY, the 37 kDa RR CheB is the second target of CheA. Phosphorylation of its N-terminal regulatory domain (at Asp56 in *E. coli*) to produce CheB-P stimulates the methylesterase activity of its C-terminal catalytic domain approx. 100-fold. In addition to being a methylesterase CheB can also function as a deamidase (Kehry *et al.*, 1983), converting certain

glutamine residues to glutamates, which thereby become targets for methylation. The constitutively active 33 kDa methyltransferase CheR, and CheB(-P) together mediate the reversible methylation of conserved glutamates or deamidated glutamines in the transducers, which plays an important role in the adaptation of the sensory system to different stimulus intensities. The transferred methyl groups originate from a cytoplasmic pool of S-adenosyl methionine (SAM) and are released in the form of methanol (Springer and Koshland, 1977; Stock and Koshland, 1978). In *E. coli*, CheR is targeted to the transducer cluster by binding to a C-terminal NWETF pentapeptide-motif (Djordjevic and Stock, 1998), which is present in the "high abundance" transducers Tar and Tsr, for which combined copy numbers between 3,300 and 37,000 per cell were detected in different strains and under different growth conditions (Li and Hazelbauer, 2004). The "low abundance" transducers Trg and Tap (together between 300 to 3,600 copies per cell) lack the NWETF motif and require the presence of Tsr or Tar for functional adaptation.

Involvement of the phosphotransferase system in *E. coli* chemotaxis

It should finally not be left unmentioned that *E. coli* cells are also chemotactic towards carbohydrates, like glucose, which are imported by the phosphoenolpyruvate-dependent phosphotransferase system (PTS). This kind of chemotaxis is not directly mediated by transducers, but rather based on a downregulation of CheA activity (leading to prolonged phases of smooth swimming) by the dephosphorylated form of one of the PTS components in the presence of high substrate concentrations. However, it only functions in the presence of MCPs, which are probably required to maintain a sufficient basal activity of CheA in the MCP-CheW-CheA complexes, without which the cells display a smooth swimming phenotype (Lux *et al.*, 1999).

2.2.3 Transducers relay external stimuli to the cell interior, and changes in their methylation status are involved in adaptation to a given stimulus intensity

Models for TM signaling and signal relay to the histidine kinase CheA

One of the unsolved questions in prokaryotic chemosensing asks how the external event of ligand binding is communicated along the transducer to its cytoplasmic tip, where the interaction with CheA takes place. Unlike, for example, eukaryotic receptor tyrosine kinases like the epidermal growth factor (EGF) receptor, where activation is a consequence of receptor dimerization in response to ligand-binding, the MCPs are not activated by a simple monomer to

dimer transition, because the dimer stability is independent of ligand binding to the transducer (Milligan and Koshland, 1988).

TM signaling must therefore take place within the dimer and could in principle be achieved by helix sliding, rotation or tilting, or via alterations in helix dynamics. Several models have been proposed for the mechanism of transducer activation by ligand binding (Kim, 1994). They include (i) the piston model, in which the TM helices move relative to each other and perpendicular to the membrane, (ii) the scissors model, in which ligand binding causes the periplasmic, as well as the cytoplasmic domains of the transducer monomers to approach each other in a scissor-like fashion and (iii) the supercoil model, in which ligand binding produces an unwinding of the supercoiled central 4-helix bundle of the dimer.

The model that currently seems to be best supported by experimental data is the swinging-piston model proposed by Chervitz and Falke (1996). It is based, besides other data, on an observed 1.6 Å downward displacement (towards the membrane) and a 5° tilt of helix $\alpha 4$ in the crystal structure of the periplasmic domain of Tar in the aspartate-occupied state, when compared to the apo structure of Tar. It was suggested that this 1.6 Å displacement is conveyed from the periplasmic domain via TM helix 2 and the cytoplasmic part of Tar to the signaling region, where it alters the activity of CheA. In support of the model, an approx. 1 Å intrasubunit piston-type downward movement of one TM helix relative to the other TM helix of Tar was observed upon ligand-binding (Ottemann *et al.*, 1999), when collecting electron paramagnetic resonance spectra of Tar, containing attached nitroxide spin labels.

A different approach to explain signaling via chemotaxis transducers was chosen by Kim *et al.* (2002). They compared the averaged main chain temperature (B) factors obtained by using a 13-residue sliding window along the crystal structures of the cytoplasmic part of wild-type Tsr, (denoted cTsrW and containing Q297, E304, Q311 and E493 at the four methylation positions) and of the Q₄-mutant cTsrQ, which contained Gln residues at all of these sites and is thereby mimicking the fully methylated transducer state (Dunten and Koshland, 1991). Upon observing higher B factors for cTsrW for the complete chain, they concluded that the overall structure of the Q-mutant is in a much less dynamic state. This led to the proposal that the process can be described by the "frozen dynamic" model of signaling, previously suggested by Kim (1994). The model assumes that repellent binding or transducer methylation converts the transducer to a frozen, less dynamic (signal "on") state, which can activate CheA more efficiently, whereas attractant binding or demethylation leads to a more dynamic (signal "off") state, for which the probability for an activating interaction with CheA decreases.

The phenomenon of adaptation

A key feature in prokaryotic chemosensing is the ability to detect small concentration gradients of attractants or repellents over a wide range of background concentrations. Transducer clustering is suspected to be a reason for the high sensitivity, and the wide dynamic range is attributed to a resetting of the transducers' sensitivity threshold by reversible methylation of conserved glutamate or (deamidated) glutamine residues in their cytoplasmic domains. This resetting process is called adaptation and is mediated by CheR and CheB, as discussed above.

A simple approach to explain the phenomenon of adaptation is based on a two-state model of the transducer-kinase complex (Fig. 2.5). The model assumes that the transducer can exist in an inactive and an active state, which inhibit and enhance CheA autophosphorylation, respectively.

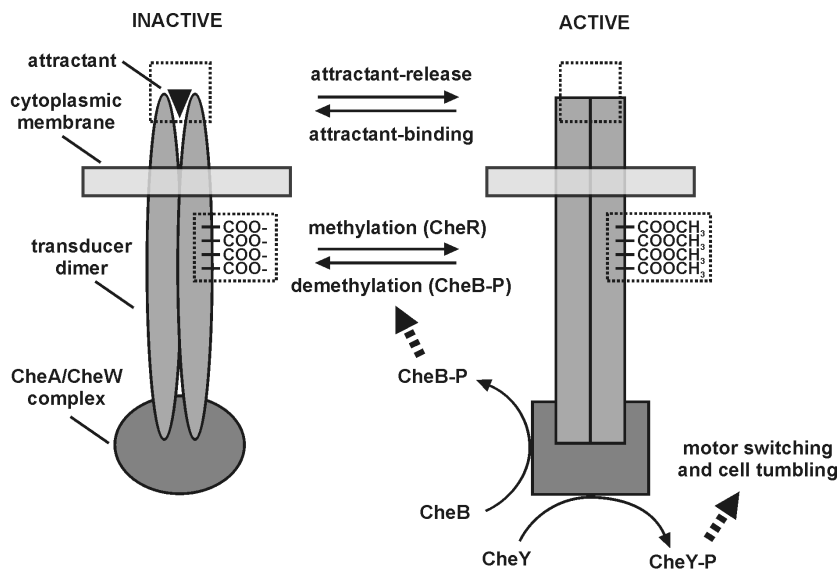


Figure 2.5 Two-state model of the transducer-kinase complex.

The model assumes two conformational states for the transducer dimer. The active state enhances, whereas the inactive state inhibits the activity of the kinase CheA, which is coupled to the transducer via CheW. The probability that the transducer is in the inactive/active state is highest, when the transducer is/is not bound to attractant and when it is fully demethylated/methylated (the content of the dotted boxes depicts the situations of highest probability for each state, with the methylation status only shown for one monomer). Adaptation to a certain attractant concentration is achieved via changes in the methylation status of the transducer. For an active transducer the probability to return to its inactive state is gradually increased by demethylation of methyl esterified glutamate residues, via phosphorylated CheB (CheB-P), which is produced by activated CheA. The probability that an inactive transducer returns to an active state, on the other hand, increases with increasing methylation via constitutively active CheR, when the concentration of CheB-P decreases.

Whereas attractant-binding increases the probability that the transducer is inactive, methylation increases the probability that it is active. Based on the two-state model, in which the transducer-kinase complexes act as independent units, allosteric models of multi-subunit transducer-kinase complexes were proposed, which assume interactions between different receptor-kinase complexes, and can thereby explain the observed signal amplification and high sensitivity of the system (Sourjik, 2004). They can be seen as extensions of the two-state model, in that the state

of a transducer (inactive or active) is not only stabilized by the mentioned criteria, but also by the conformational state of neighboring transducers in a larger array. According to such a model, attractant-binding to some of the transducers does not only induce an inactive conformation of these transducers, but via conformational interactions also of neighboring ones, which did not bind attractant.

The scenario for a tactic reaction and subsequent adaptation to an increase in repellent concentration is as follows: An increase in the number of repellent-bound transducers increases total CheA activity. This leads to enhanced phosphorylation of CheY, resulting in cell tumbling, and of CheB, resulting in the removal of methyl-groups, as methanol, from the esterified glutamates. The decrease in transducer methylation reduces total CheA activity and as a consequence the levels of CheY-P and CheB-P. When demethylation via CheB-P matches the rate of CheR-mediated remethylation, the total transducer methylation remains constant at the obtained lower level. Due to the decreased transducer methylation, the total CheA activity and therefore the motor switching frequency, are finally reset to the initial level, despite the fact that now more transducers contain bound repellent.

Adaptation to repellent and attractant stimuli can be observed by investigating the changes in the release of radioactively labeled methanol from cells treated with radiolabeled methionine, which is intracellularly converted to the methyl-donor S-adenosylmethionine (SAM) (Kehry *et al.*, 1984; a comprehensive review on the early studies of the role of protein methylation in sensory adaptation was written by Springer *et al.*, 1979). The observation of an increased/decreased methanol release upon repellent/attractant stimulation in *E. coli* is as predicted by the model. Interestingly, *B. subtilis* and *H. salinarum* show an increased release of methanol upon repellent as well as attractant stimulation. This might argue for a similar mechanism of adaptation in these organisms, which is different from that of *E. coli* (Bischoff and Ordal, 1992). For the *B. subtilis* asparagine receptor McpB, selective methylation changes at two particular sites are responsible for adaptation (Zimmer *et al.*, 2000). The overall methylation level of McpB does not change in response to attractant addition or removal. However, a methyl group-turnover could be observed, and was attributed to the selective removal of methyl groups from one of the sites followed by their addition to the other site.

Approaches to the determination of transducer methylation sites

Numerous forms of each methylated *E. coli* transducer are seen as a pattern of multiple bands on polyacrylamide gels (6 different Tar and estimated 12 to 20 different Tsr species were observed on a 2-D gel by Hazelbauer and Engström, 1981). In an approach to identify the

numbers and positions of their methylatable residues, transducers containing radioactively labeled methyl groups, that were added in the process of adaptation, were subjected to tryptic digest, and the resulting peptides were analyzed via reversed phase HPLC (Kehry and Dahlquist, 1982). In the case of Tsr, one Lys-containing peptide, designated K1, and one Arg-containing peptide, designated R1, were found to be methylated maximally four and two times, respectively (Kehry and Dahlquist, 1982). Sequence analysis of these peptides in their unmethylated forms, combined with the determination of the amounts of radioactivity that were released in each sequenator cycle, when sequencing the pooled forms of each methylated peptide, led to the identification of three methylated Glu residues in the K1 peptide and one in the R1 peptide (Kehry *et al.*, 1983).

A different approach was used by Terwilliger and Koshland (1984) to determine the sites of deamidation and methyl esterification in *S. typhimurium* Tar. Using *Staphylococcus aureus* V8 protease, which cleaves peptide bonds following glutamyl but not glutaminyl or methylated glutamyl residues, they generated fragments from the HPLC-separated forms of the two obtained methylatable tryptic peptides (these forms were designated K0 to K3 and R0 to R1, with respect to the number of methyl groups). After the identities of the two peptides had been determined via comparison of their amino acid composition to the predicted sequence of Tar, the fragment patterns of the HPLC runs, together with the determined amino acid composition of the fragments, identified three methylatable Glu residues in the Lys peptide (one generated by Gln deamidation), and one in the Arg peptide.

2.3 Halobacterial signal transduction at a molecular level

2.3.1 The halobacterial Che protein machinery displays similarities to that of *B. subtilis*

The sequence of genes in the *che* operon of *H. salinarum* is the following: *cheW1*, *Y*, *B*, *A*, *C1* (formerly *J*), *C3*, *D* and *R*. Additionally *cheW2* and *cheC2* are present at other positions on the chromosome (Rudolph and Oesterhelt, 1996; Ng *et al.*, 2000; <http://www.halolex.mpg.de>, Dieter Oesterhelt *et al.*, unpublished). The halobacterial operon displays similarities to the occurrence and arrangement of *che* genes in *B. subtilis* (<http://genolist.pasteur.fr/SubtiList/index.html>). In this bacterium, signals are also relayed to the flagellar motor via phosphorylation of CheY by CheA (a comprehensive review comparing the *B. subtilis* chemotactic system to those of other organisms was written by Szurmant and Ordal, 2004). However, opposite to the situation in *E.*

coli, CheA of *B. subtilis* is activated upon attractant binding to transducers to which it is coupled via the adaptor proteins CheW and/or CheV. The generated CheY-P then leads to prolonged phases of CCW rotation and therefore to smooth swimming. Whereas CheR and CheB function, like in *E. coli*, as methyltransferase and methylesterase, respectively, transducer deamidation in *B. subtilis* is catalyzed by CheD rather than by CheB (Kristich and Ordal, 2002). Furthermore, CheC acts as a phosphatase hydrolyzing CheY-P and is assumed to play an additional role in adaptation, like CheV.

H. salinarum CheA (71.8 kDa) displays approx. 34 % sequence identity with *B. subtilis* CheA and is essential for halobacterial taxis (Rudolph and Oesterhelt, 1996). For halobacterial CheA, but not for the CheA(H44Q) mutant lacking the conserved phosphorylatable His, autophosphorylation is observed *in vitro* in the presence of ATP/Mg²⁺. Addition to such a reaction mix of CheY (13.4 kDa), but not of a mutant CheY(D53A) lacking the conserved phosphorylatable Asp, leads to a rapid and complete dephosphorylation of CheA without the generation of detectable amounts of CheY-P. These results suggest that also halobacterial CheA and CheY form a HAP system, and that the half-life of native CheY-P is less than 5 s (Rudolph *et al.*, 1995), compared to 20 s for *E. coli* CheY-P in the absence of the phosphatase CheZ (Lukat *et al.*, 1991). The shorter half-life of halobacterial CheY-P is consistent with a lack of CheZ in *H. salinarum*.

Halobacterial CheB (36.5 kDa) contains a putative methylesterase domain (Rudolph *et al.*, 1995), consistent with the observed release of volatile methyl groups in response to attractants and repellents, a release pattern also found in *B. subtilis* (Alam *et al.*, 1989) but different from that in *E. coli*. *H. salinarum* mutants lacking CheB display a high frequency of motor switching (every 2 - 3 s), which is assumed to be caused by a high CheY-P level, due to a high transducer methylation and the complete transfer of phosphoryl groups from CheA to CheY, in the absence of competing CheB. Deletions of *cheY*, *cheA* or *cheB* genes lead to a complete loss of taxis in *H. salinarum* (Rudolph and Oesterhelt, 1996). Due to their similarity to *B. subtilis* CheR and CheD, *H. salinarum* CheR (30.5 kDa) and CheD (15.6 kDa) are expected to function as a methyltransferase and a Gln deamidase, respectively. It is presently not known why *H. salinarum* contains two presumptive coupling proteins CheW1 (19.2 kDa) and CheW2 (14.1 kDa) and why three homologous forms of CheC are found (20.9, 20.4 and 39.8 kDa), of which the biggest one (CheC3) represents a fusion of two CheC domains.

2.3.2 Halobacterial transducers are class III transducers involved in sensing a variety of stimuli

Molecular components of the halobacterial signaling machinery, including receptors, binding proteins and halobacterial transducers (Htrs), are employed in the detection of a variety of environmental stimuli. A total of 18 Htr-encoding genes (*htrs*) have been identified in the halobacterial genome on the basis of high homology to the well-conserved signaling region of eubacterial MCPs (Zhang *et al.*, 1996; Ng *et al.*, 2000; <http://www.halolex.mpg.de>).

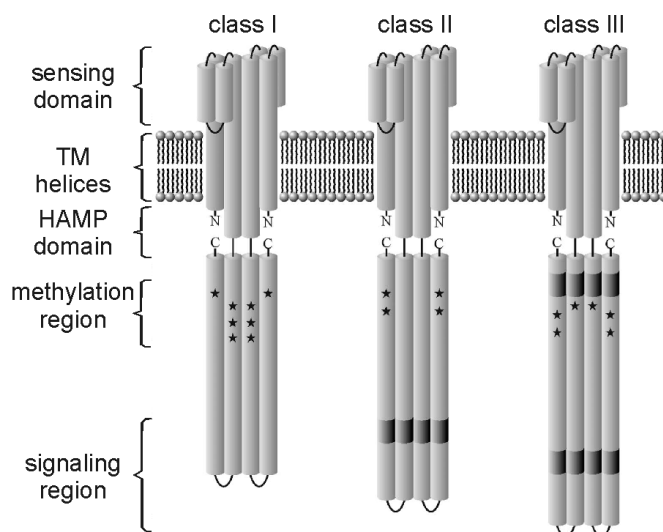


Figure 2.6 Schematic of the three transducer classes, according to Le Moual and Koshland (1996).

The classes were derived from multiple sequence alignments of the C-terminal cytoplasmic domains of transducers from different organisms. For each class a representative transducer dimer is depicted. 14-residue insertion/deletion (indel)-regions are shaded in dark gray. Stars indicate the sites of methylation for (from left to right) *E. coli* Tar, *M. xanthus* FrzCD and *B. subtilis* McpB. (adapted from Szurmant and Ordal, 2004)

Htrs are examples of class III transducers (Fig. 2.6), according to a classification scheme of Le Moual and Koshland (1996). On the basis of multiple sequence alignments of the C-terminal cytoplasmic domains of 29 putative transducers from different organisms to that of *E. coli* Tar, they propose three classes of transducers. The classification is based on the proposed presence or absence of 14-residue insertion/deletion (indel)-regions within the sequences. Class I transducers, like the enteric transducers, are lacking indel-regions. Class II transducers, like *Myxococcus xanthus* FrzCD, are suggested to contain 14-residue insertions closely before and after the signaling region. Class III transducers, like the *B. subtilis* transducers, are suggested to contain two additional 14-residue insertions, one N-terminally of the first and one C-terminally of the second methylation region.

In the process of elucidating the molecular details of the *H. salinarum* sensing machinery, several environmental stimuli had already been attributed to a number of Htrs at the beginning

of this study. Taxis towards orange and away from UV light, and taxis away from blue light, are mediated by the photoreceptors sensory rhodopsin I and II (SRI and SRII), respectively, together with their associated transducers HtrI and HtrII (Htr1 and Htr2) (Yao and Spudich, 1992; Seidel *et al.*, 1995; Zhang *et al.*, 1996). For HtrII, a function in serine chemotaxis has also been reported (Hou *et al.*, 1998). Photostimulation of SRI and SRII additionally causes the release of the switch factor fumarate, which, by an unknown mechanism, restores motor switching in the straight-swimming mutant strain M415 (Marwan and Oesterhelt, 1991). Aerotaxis is mediated by membrane-bound HtrVIII (Htr8) (Brooun *et al.*, 1998) and the soluble transducer HemAT (Htr10) (Hou *et al.*, 2000).

The transducers BasT (Htr3) (Kokoeva and Oesterhelt, 2000) and CosT (Htr5) (Kokoeva *et al.*, 2002) mediate taxis towards Leu, Ile, Val, Met and Cys, and to compatible solutes of the betaine family, respectively. These processes involve the putative binding proteins BasB and CosB, respectively (Kokoeva *et al.*, 2002). Chemotaxis towards Arg is mediated by the cytoplasmic transducer Car (Htr11) (Storch *et al.*, 1999). Responses to Asp, Glu and His were reported by Brooun *et al.* (1997) for a transducer from halobacterial strain Flx15, named HtrXI, which differs from Car (strain S9) at only 9 residues.

2.3.3 Methylation of Htrs

The chemosensory behavior of *H. salinarum*, including signal integration and adaptation, was first described more than 25 years ago (Spudich and Stoeckenius, 1979b; Schimz and Hildebrand, 1979). Signal integration was observed as the repression of a repellent stimulus by simultaneous application of an attractant stimulus of the correct strength, or as an additive effect of two attractant stimuli. Adaptation was seen as the return to normal frequencies of swimming reversals (in the investigated strains approx. once every 3 to 6 sec), after the application of a repellent/attractant stimulus of constant strength had temporarily decreased/increased this frequency. Since then evidence has accumulated that the reversible methylation of certain conserved glutamate residues in the Htrs, presumably mediated by CheR and CheB, plays an important role in the process of halobacterial adaptation to a given stimulus strength, similar to the situation in *E. coli*.

After treatment of cells with L-[methyl-³H]-methionine, fluorograms of SDS-PAGE gels showed a prominent group of radiolabeled bands between 90 and 135 kDa, from which volatile radioactivity could be released upon treatment with 0.5 M NaOH. It was assumed that, consistent with *E. coli*, these bands result from halobacterial MCPs to which the methyl groups are attached as methyl esters (Alam *et al.*, 1989). The same study showed that the methylation of

certain bands in the described group increased and decreased after the application of attractant (peptone) and repellent (phenol) stimuli, respectively. However, the methyl group turnover, seen as the release of volatile radioactivity, increased upon both kinds of stimuli.

The observation that the band patterns on immunoblots, that were generated with antibodies raised against the *E. coli* transducers Trg and Tsr, respectively, are consistent with those obtained after methyl-³H-labeling, lead to the conclusions that (i) these bands actually result from MCPs and (ii) the structural features of MCPs are evolutionary conserved between bacteria and archaea (Alam and Hazelbauer, 1991).

At the beginning of the present study very little was known about the identity of the methylatable residues in Htrs. By sequence comparison to a consensus sequence for transducer methylation by the methyltransferase CheR, reported for enteric bacteria (Terwilliger *et al.*, 1986), three potential methylation sites containing Glu pairs were identified in Htr1 and one in Htr2. Mutagenic substitution of an Ala pair for one of these (Glu265-Glu266) in Htr1 and for the homologous pair (Glu513-Glu514) in Htr2 eliminates methylation completely in Htr1 and almost completely in Htr2. This was demonstrated by the complete and almost complete absence, respectively, of the Htr1 and Htr2 bands on fluorographs after SDS-PAGE of proteins from these mutants (Perazzona and Spudich, 1999). No information was available concerning the positions of methylatable residues in any of the remaining transducers.

2.4 Bacteriorhodopsin-dependent phototaxis in *H. salinarum*

Besides the mentioned photosensing capabilities that rely on the interaction of SRI/SRII with their relevant transducers HtrI/HtrII, there is also a BR-dependent halobacterial phototaxis. More than two decades ago, the detection of a halobacterial photoresponse to changes in light intensity at high irradiance was proposed to be mediated by BR (Baryshev *et al.*, 1981). The proposal was based on the observation that cyanide, an inhibitor of the respiratory chain, or dicyclohexylcarbodiimide (DCCD), an inhibitor of the proton-translocating H⁺-ATPase, both enhanced the sensitivity of cells to a sudden decrease of green light intensity. BR, as well as the respiratory chain and the H⁺-ATPase, are generators of proton motive force (pmf) across the cell membrane. Inhibition of respiration or H⁺-ATPase activity leads to a decreased pmf in the dark, and therefore to a greater drop of pmf upon a decrease of irradiance.

2.4.1 The proton motive force (pmf)

The pmf across a membrane, usually given in mV, is a measure of the driving force for the translocation of protons. It can be calculated from the electrochemical potentials μ_{H^+} of the protons on either side of the membrane, and is negative for a higher μ_{H^+} on the outside, consistent with an energy requirement for the translocation of protons towards the outside. With F as the Faraday constant ($96,500 \text{ C mol}^{-1}$) the following relation exists:

$$\text{pmf} = - (1/F) \cdot \Delta\mu_{\text{H}^+} = - (1/F) \cdot (\mu_{\text{H}^+} (\text{out}) - \mu_{\text{H}^+} (\text{in}))$$

As protons are charged particles, the pmf is composed of two constituents: (i) the electrical potential difference ($\Delta\Psi = \Psi (\text{out}) - \Psi (\text{in})$) across this membrane and (ii) the difference in the concentrations of protons on both sides, which can be expressed as the difference in pH ($\Delta\text{pH} = \text{pH} (\text{out}) - \text{pH} (\text{in})$). Therefore its value at 30°C is given by the following equation (where R stands for the gas constant and T for the absolute temperature):

$$\begin{aligned} \text{pmf [mV]} &= - (1/F) \cdot \Delta\mu_{\text{H}^+} = \Delta\Psi + 2.3 RT/F \cdot \Delta\text{pH} = \\ &= \Delta\Psi + 60 \cdot \log ([\text{H}^+]_{\text{in}} / [\text{H}^+]_{\text{out}}) = \Delta\Psi + 60 \cdot \Delta\text{pH} \end{aligned}$$

The free enthalpy (ΔG) necessary to transport protons across the cell membrane in the direction of a more positive membrane potential (under physiological conditions the cell exterior), can be calculated for a pmf of -100 mV (inside negative) as follows:

$$\begin{aligned} \Delta G_{(\text{in} \rightarrow \text{out})} &= \Delta\mu_{\text{H}^+ (\text{in} \rightarrow \text{out})} = - F \cdot \text{pmf}_{(\text{in} \rightarrow \text{out})} \\ &= - 96,500 \text{ J mol}^{-1} \text{ V}^{-1} \cdot - 0.1 \text{ V} = + 9.65 \text{ kJ mol}^{-1} \end{aligned}$$

At a given membrane potential of -100 mV and in the absence of a pH gradient, this is the energy that the proton pump BR initially has to provide to pump protons towards the outside of the cell. Upon continued pumping the electrical potential across the membrane becomes more negative and an additional pH gradient develops. Both events increase the pmf, and therefore the energy needed to pump protons against the pmf. Details on the structures and mechanisms of action of BR and the other retinal proteins are reviewed by Oesterhelt (1998).

2.4.2 Hints towards an involvement of the signaling chain

In the course of the investigations on halobacterial phototaxis it was found that oxygen-depleted Pho81-B4 cells, which contain BR as their only functional retinal protein, are sensitive to changes at high irradiance levels, whereas Flx15 cells containing only SRI and SRII are sensitive to changes at low irradiance levels. These observations demonstrate that the combination of the two systems enables wild-type cells to react not only to different wavelengths of light but also within a wide range of light intensities (Bibikov *et al.*, 1991). As such a wide

range can be expected under the given environmental conditions, a broad detection range should represent an evolutionary advantage to the cells. No photoresponses are seen in cells lacking all retinal proteins.

BR-mediated photosensitivity decreases upon addition of 0.1% (29 mM) of the fermentative substrate arginine, which besides light and respiration can also be used to generate pmf. This finding, the mentioned effects of cyanide and DCCD, and last but not least comparable signal processing and adaptation times for SRI- and BR-mediated photosensing (in both cases average reversal-response times are 1.5 s, and adaptation takes approx. 4 s after a repellent and 20 - 40 s after an attractant stimulus), all argue for an interaction of a putative "pmf-sensor" with components of the halobacterial signal transduction chain (Bibikov *et al.*, 1993). Grishanin *et al.* (1996) proposed that a change of the membrane potential ($\Delta\Psi$), rather than of the pH difference across the membrane (ΔpH), is essential for the communication of changes in illumination from BR to the taxis system. The underlying observation was that the addition of the hydrophobic cation tetraphenylphosphonium (TPP^+), known for its ability to quench $\Delta\Psi$, decreased the sensitivity of cells to BR-mediated photosensing, whereas the addition of ammonium acetate, expected to decrease ΔpH , was without effect.

The direct activation of the flagellar motor switch by a decrease of the pmf is unlikely, and therefore also the possibility that BR-dependent phototaxis might not involve a transducer and the CheA/CheY two-component system. This is based on the finding that BR-containing cells of strain M415 do not switch upon a light stepdown, although, in principle they are able to switch spontaneously when supplemented with fumarate (Bibikov *et al.*, 1993).

Taken together these findings strongly point to an involvement of the halobacterial signaling chain in BR-dependent phototaxis and to the membrane potential component of the pmf as the detected signal.

2.5 Objectives of the thesis

The present thesis aims at the investigation of two different phenomena: (i) bacteriorhodopsin (BR)-dependent phototaxis and (ii) the methylation of halobacterial transducers (Htrs).

(i) In the case of BR-dependent photosensing published experiments have pointed to the involvement of a transducer and have suggested, that the sensed stimulus is a change in the electrical potential component of the proton motive force across the cell membrane.

After the generation of a genetically well-defined strain, which contains BR as the only retinal protein, and assuming that this kind of sensing functions via a single transducer, a deletion approach, by which single *htr* genes are removed from this strain's genome, shall be used to identify the responsible Htr. After its identification via investigation of the mutant cells with appropriate assays, this transducer shall be further characterized concerning its molecular properties. Moreover, additional experiments shall be performed to more thoroughly investigate the nature of the sensed stimulus.

(ii) The ultimate goal of investigations on transducer methylation is to understand on a molecular level the phenomenon of cellular adaptation to a given stimulus intensity. The published information on the molecular details of Htr methylation is restricted to the identification of one methylation site, each, in Htr1 and Htr2.

A method shall therefore be established for the identification of a larger amount of methylation sites, to obtain an overview of the numbers and locations of such sites under physiological conditions in additional Htrs, and possibly even of the methylated residues. Furthermore, the effects of CheR and CheB on transducer methylation in *H. salinarum* shall be investigated, to check if the experimental data will confirm their proposed functions.

The identification of methylation sites and positions will then allow to compare the methylation of Htrs to that of other transducers, and will provide the basis for further investigations on the dynamics of transducer methylation in response to attractant or repellent stimuli.

3 RESULTS AND DISCUSSION

3.1 Identification of MpcT (Htr14) as the transducer for $\Delta\Psi$ changes in *H. salinarum*

3.1.1 Construction of retinal-protein knockout strains

The aim of this study was to identify the transducer that is responsible for bacteriorhodopsin (BR)-mediated phototaxis and to gain further insights into the nature of this phenomenon. The chosen strategy for its identification was the generation of *htr*-deletion mutants in a halobacterial strain which contains BR as the only retinal protein.

Although strain Pho81-B4, which had previously been used to demonstrate BR-mediated taxis (Bibikov *et al.*, 1991), met this requirement and was available in the lab, two reasons argued against the use of this strain. (i) Its parent strain Pho81 (Sundberg *et al.*, 1985), as well as Flx15 (Spudich and Spudich, 1982) the parent of Pho81 were both obtained by mutagenesis using N-methyl-N'-nitro-N-nitrosoguanidine, followed by mutant screening procedures. It can be expected that in addition to the loss of functional retinal proteins the two rounds of chemical mutagenesis have caused major changes in the genomes of these strains as compared to the wild-type genome. (ii) Pho81-B4 was generated by transformation of Pho81 with a plasmid containing the *bop* gene and a mevinolin resistance-conferring gene. The thereby acquired mevinolin resistance would have excluded the use of mevinolin as the selective agent for further transformations of Pho81-B4.

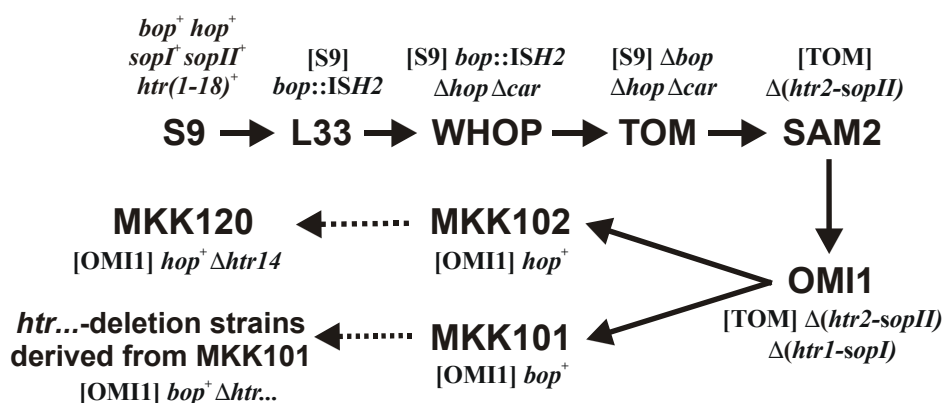


Figure 3.1 Overview of the generated strains leading to retinal protein-deficient strain OMI1, and strains MKK101 and MKK102.

The latter were produced from OMI1 by complementation with the *bop* and *hop* gene, respectively, and are the strains of origin for the subsequent *htr*-deletions. The relevant genotypes are indicated (*bop*: bacterioopsin, *hop*: haloopsin, *sopI*: sensory opsin I, *sopII*: sensory opsin II, *htr*: halobacterial transducer, *car*: *htr11*, *ISH2*: halobacterial insertion element 2). The genotype of a new strain is identical to that of the attributed strain in brackets, except for the explicitly added differences.

As an alternative to Pho81, strain OMI1 (Masato Otsuka, unpublished) was chosen as the parent for the strains to be generated in the course of this study. OMI1 was constructed via defined genetic manipulations instead of chemical mutagenesis (Fig. 3.1). Strain L33 served as the parent strain for these manipulations. It was generated from strain S9 (Wagner *et al.*, 1981) and contained an *ISH2* insertion element interrupting its *bop* gene (DasSarma *et al.*, 1983). Strains WHOP and TOM (Besir, 2001), and strains SAM2 and OMI1 (Masato Otsuka, unpublished) were produced from L33 by successive deletion of all 4 retinal-protein genes.

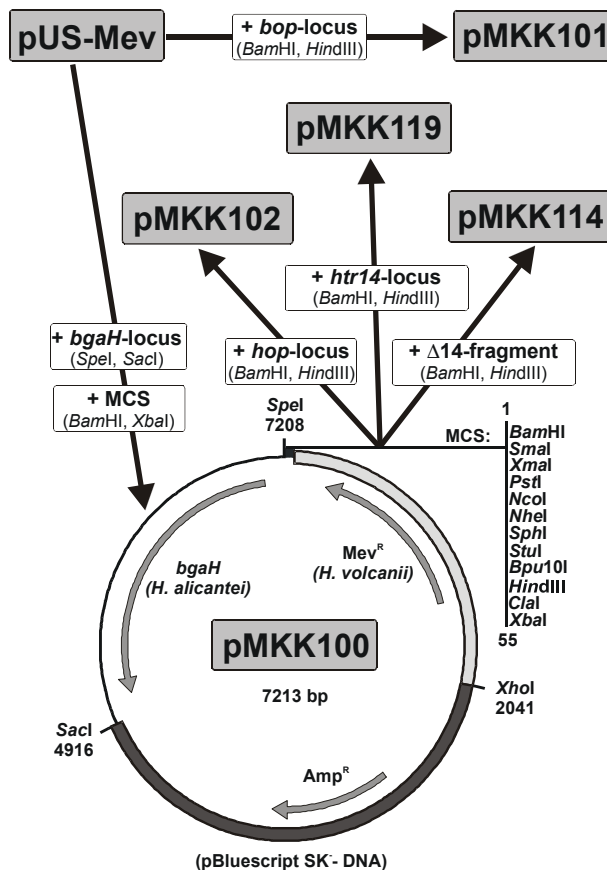


Figure 3.2 Schematic of the construction of plasmids pMKK101, pMKK102, pMKK114 and pMKK119 to exemplify the genetic strategies employed.

To generate pMKK101 the *bop* locus (Fig. 3.3) was amplified via PCR from genomic DNA, digested with *Bam*HI and *Hind*III, and then cloned into plasmid pUS-Mev digested with *Bam*HI and *Hind*III. To allow for red-blue selection of colonies, the *bgaH*-locus from *Haloflex alicantei* was cloned between *Spe*I and *Sac*I sites of pUS-Mev. Furthermore, a multiple cloning site (MCS) was introduced between the *Bam*HI and *Xba*I sites to produce pMKK100. By cloning PCR-generated DNA fragments, flanked by the appropriate restriction sites, into the MCS, additional deletion and complementation plasmids mentioned in the text were generated. This is described in detail in Table 4.2 and exemplified here by deletion plasmid pMKK114 and complementation plasmids pMKK102 and pMKK119. *Mev*^R and *Amp*^R indicate the markers for mevinolin- and ampicillin-resistance, respectively.

To produce the parent strain for the *htr*-deletion mutants, MKK101, the wild-type *bop* allele was restored in OMI1 at its original position using pUS-Mev-derived plasmid pMKK101 (Fig. 3.2). For investigations on HR-dependent photoreactions another strain, MKK102, was generated from OMI1 by restoration of the wild-type *hop* allele at its original position using pMKK100-derived plasmid pMKK102.

Southern-blot or PCR analysis of the retinal protein gene loci of OMI1, MKK101 and MKK102 confirmed the expected genotypes (Fig. 3.3). OMI1 and all strains derived from it also lack the genes for the transducers Htr1, Htr2 and Car (Htr11). The loss of the *car* gene probably happened during strain construction via a partial loss of DNA from the 284 kDa halobacterial plasmid pHS3 (<http://www.halolex.mpg.de>) which encodes Car.

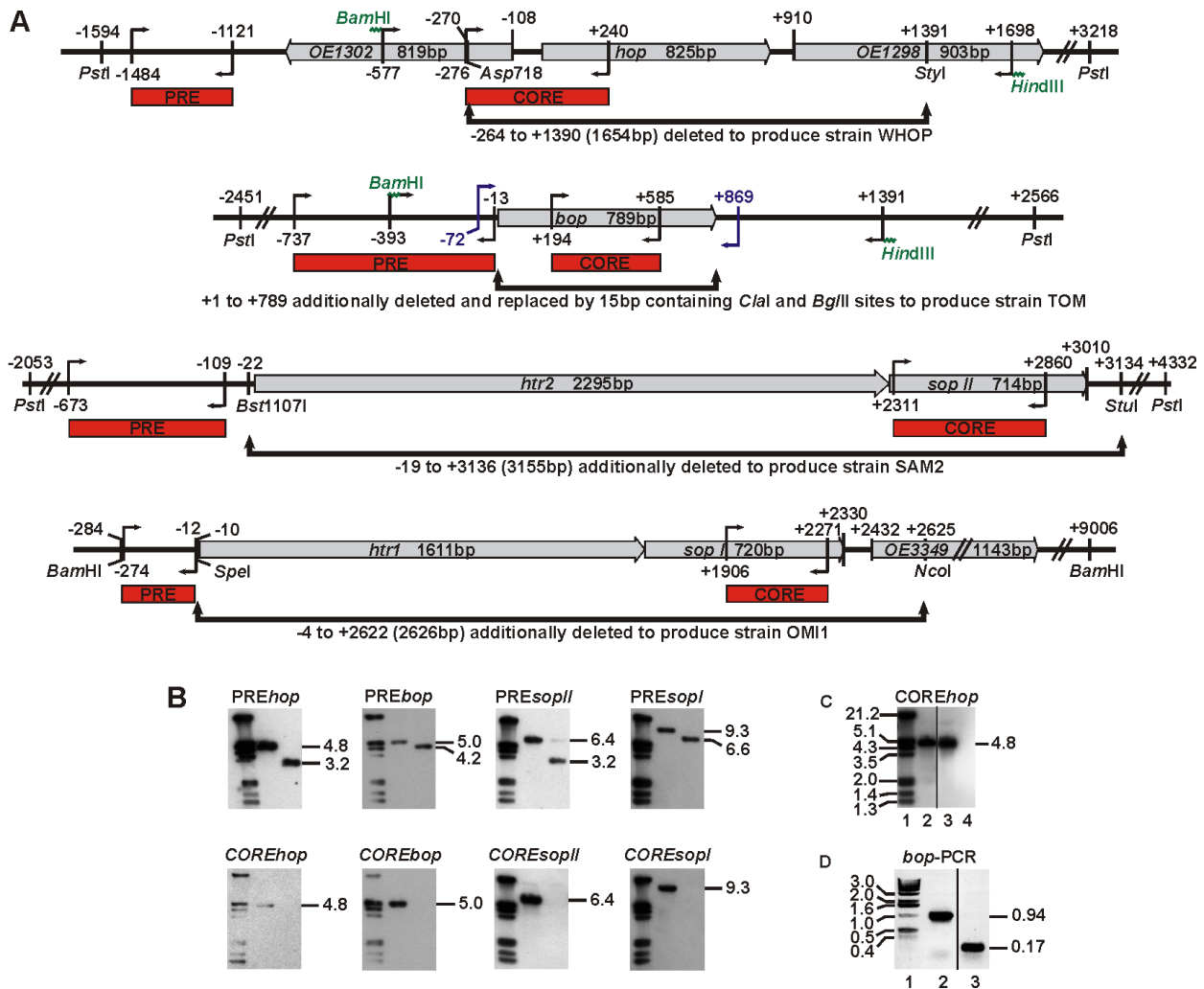


Figure 3.3 Genotypic analysis of strains OMI1, MKK101 and MKK102.

(A) Gene loci of the four halobacterial retinal protein genes (*hop*, *bop*, *sopI* and *sopII*). Genes deleted in strain OMI1 are depicted as thick arrows containing the gene length in base pairs and the gene name, according to <http://www.halolex.mpg.de>. Cleavage sites of relevant restriction enzymes are shown. All numbers indicate nucleotide positions given relative to the start of the open reading frame (orf) of the corresponding retinal protein gene. PCR primers are depicted as bent arrows with the position of the first matching 5'-nucleotide indicated. Restriction sequences, attached to or contained in the primer sequences, are indicated by a zigzag line. They were used for cloning the generated PCR fragments to produce complementation vectors. Boxes labeled PRE and CORE depict the DIG-11-dUTP-labeled DNA probes used in Southern-blot analysis at their hybridization positions. (B) Southern-blot analysis of the four retinal protein gene loci in strains S9 (wt) and OMI1. Genomic DNA was cleaved with *Bam*HI in case of the PRE_{sopI} and CORE_{sopI} blots and with *Pst*I in all other cases. Middle and right lanes represent strains S9 and OMI1, respectively. Left lanes show the positions of marker bands of which the sizes (in kilobasepairs) are given in (C). In all depicted blots generated with PRE DNA probes the size difference of the recognized DNA fragments from S9 and OMI1 matches the size of the deleted DNA regions. On the blots produced with CORE DNA probes band positions were identical to the PRE blots for S9, but bands were missing for OMI1, indicating the absence of the respective opsin gene in the latter. (C) Southern-blot analysis of strain MKK102 using DNA probe CORE_{hop}. The presence of the 4.8 kb band for MKK102 demonstrates the successful complementation with the *hop* gene. Lane 1: marker bands, lanes 2 - 4: *Pst*I-digested MKK102-, S9- and OMI1-DNA, respectively. (D) PCR analysis of *bop*-complemented strain MKK101. Lane 1 shows marker bands with their sizes indicated. PCR was performed with MKK101- and OMI1-DNA (lanes 2 and 3, respectively) using the primers with starting positions -72 and +869, as shown in (A). Vertical black lines on blot (C) and gel (D) indicate that lanes were not directly adjacent.

3.1.2 Transducer inventory of *H. salinarum*

***H. salinarum* strain R1 contains a total of 18 transducers (Htrs)**

At the beginning of this study the annotation of the genome sequence of halobacterial strain R1 was an ongoing project in the lab (Dieter Oesterhelt *et al.*, unpublished; <http://www.halolex.mpg.de>) and the annotated genome sequence of halobacterial strain NRC-1 (Ng *et al.*, 2000) was not available, yet. To successfully apply the strategy of generating single-*htr*-deletions in strain OMI1, it was advisable to know the complete set of *htr* genes in the halobacterial genome. This should exclude that the responsible transducer would escape the investigation.

BLAST searches (Altschul *et al.*, 1990) with published Htr-sequences against the 6-frame translations of the R1 nucleotide sequence revealed a total of 18 transducer genes. The classification criterion for a transducer gene was the presence of the highly conserved signaling region within its corresponding gene product, which was checked by alignment of the amino acid sequences (Fig. 3.30B). After the publication of the annotated NRC-1 sequence a comparison to the annotated R1 sequence revealed that the nucleotide sequence of the chromosome is practically identical in both strains, apart from the positions and numbers of integrated halobacterial insertion elements (ISH).

The nucleotide sequences at all 17 chromosomal transducer loci are identical in both strains. However, the start codons for *htrs* 3, 16 and 18 were found to be incorrectly assigned for NRC-1. Alternative start codons 5' to the ones assigned for NRC-1 result in 5'-extensions of the corresponding open reading frames (orfs). These extensions encode amino acid sequences with significant similarity among each other and also to other transducers (data not shown). This clearly indicates that the longer gene versions are correct.

One of the transducer genes (*htr11*, *car*) of strain R1 is not encoded on the chromosome (2001 kb) but on plasmid pHS3 (284 kb) and is completely missing in the NRC-1 genome. Transducer genes are not present on any of the other 3 halobacterial plasmids pHS1 (148 kb), pHS2 (195 kb) and pHS4 (41 kb) (see: <http://www.halolex.mpg.de>).

The chromosomal locations of the 17 *htr* genes, 10 *che* genes and 4 retinal-protein genes are depicted in Fig. 3.4. On the basis of amino acid sequence homology and predicted TM helices, the transducers can be divided into 5 groups: Htrs 9, 10, 11, 12, 13 and 15 (group 1) lack TM helices; Htrs 1 and 14 (group 2) contain 2 TM helices connected by a short hairpin loop; Htrs 2, 3, 4, 5, 6, 16 and 18 (group 3) contain 2 TM helices with an extensive extracellular domain in

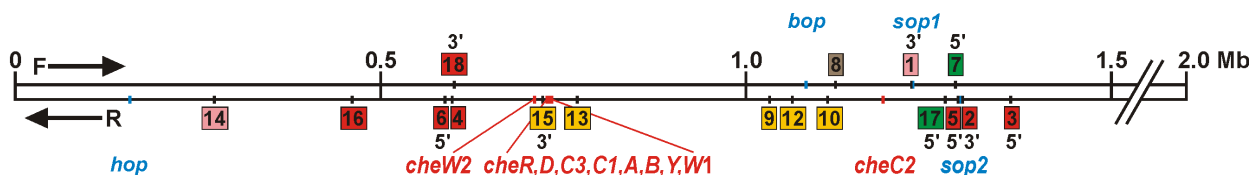


Figure 3.4 Chromosomal locations of halobacterial genes encoding transducers, opsins and Che-proteins.

The upper and the lower horizontal line symbolize the forward (F) and the reverse (R) strand, respectively, of the 2 Mb chromosome of halobacterial strain R1. The positions of transducer genes (black), opsin genes (blue) and Che protein genes (red) are marked on their respective coding strand (<http://www.halolex.mpg.de>). The numbers of the corresponding transducers are shown in boxes with a color code reflecting the number of their predicted transmembrane helices (TM): 0 TM, yellow; 2 TM but no extracellular domain, pink; 2 TM plus extracellular domain, red; 3 TM, green; 6 TM, brown. The existence of a transcription unit with the orf at the 3' end or at the 5' end of an *htr* is indicated by attributing 3' or 5' to the respective box. Exact *htr* positions and identifiers of these adjacent orfs are listed in Table 6.2.

between; Htrs 7 and 17 (group 4) contain 3 TM helices and lack an extracellular domain; Htr8 (group 5) contains 6 TM helices and also lacks an extracellular domain.

Several of the *htr* genes form a transcription unit with an adjacent gene. This is indicated by a short distance between or even a short overlap of successive genes with the same orientation. Most common is an overlap of 4 bases (e.g. an ATGA-overlap of start and stop condon). For several of these transcription units it was demonstrated that the products of their genes form a functional unit.

The 3'-end of *htr1* overlaps with *sopI* (encoding the photoreceptor SRI which interacts with Htr1) and the 3'-end of *htr2* is separated by only 2 nucleotides from *sopII* (encoding the photoreceptor SRII which interacts with Htr2). The 5'-ends of *htr3* (*basT*) and *htr5* (*cosT*) are overlapping with *basB* and *cosB*, respectively, which encode putative extracellular lipid-anchored ligand-binding proteins for the respective transducers (Kokoeva *et al.*, 2002). The 5' end of *htr6* and the 3' end of *htr18* overlap with adjacent orfs *OE2170R* (*tmcC*) and *OE2196F* (*potD*), respectively. The products of the latter show homology to periplasmic substrate-binding proteins and contain a lipid-anchor motif like BasB and CosB (Fig. 3.5). This suggests that Htr6 and Htr18 are chemotaxis transducers of unknown specificity which interact with a coproduced lipid-anchored binding protein.

Genes *htr7* and *htr17* both encode transducers with 3 TM regions and overlap at their 5'-ends with orfs *OE3472F* and *OE3438R*, respectively, which encode small polypeptides consisting solely of 3 TM regions (Fig. 6.7B). This might hint to a physical interaction of these polypeptides with the TM regions of Htr7 and Htr17, respectively, possibly resulting in heterotetrameric complexes with a 12-TM-region topology resembling that expected for Htr8 dimers.

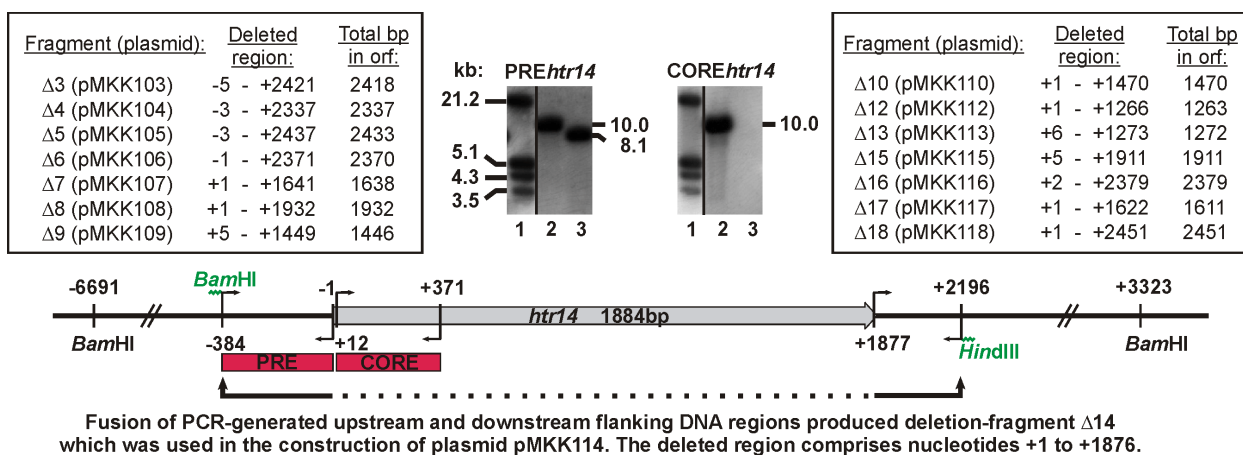


Figure 3.6 Southern-blot analysis of the *htr*-deletion strains derived from strain MKK101, exemplified by MKK114.

The *htr14* locus is shown with nucleotide positions given relative to the start of the orf. PCR primers are depicted as bent arrows, with the position of the first matching 5'-nucleotide indicated. Restriction sequences attached to primers are symbolized by a zigzag line. These sequences were used for insertion of the PCR fragment $\Delta 14$, which lacks the coding region of *htr14*, into plasmid pMKK100 to produce the deletion plasmid pMKK114. Southern blots of *Bam*HI-digested DNA from strain MKK101 (lanes 2) and from *htr14*-deletion strain MKK114 (lanes 3) were produced using the DIG-labeled DNA probes PRE*htr14* and CORE*htr14*, whose hybridization positions are indicated. Lanes 1 show marker bands. All other *htr* genes were deleted similarly, with the exception of *htr1*, *htr2* and *htr11* (*car*) which were already missing in MKK101. The boxes contain information about the other *htr*-deletion fragments. The DNA regions missing in the fragments and in the corresponding plasmids and deletion strains are given with respect to the first nucleotide (+1) of the orf.

3.1.4 Red-blue colony selection as a new method facilitating the screening of halobacterial transformants

The generation of transformed halobacterial cells, which have lost the originally introduced plasmid DNA again and have therefore regained their sensitivity to mevinolin, is a lengthy procedure taking several weeks due to long generation times of halobacteria (a minimum of 5 to 6 hours in complex liquid medium under standard conditions during the exponential growth phase, as compared to 20 min for *E. coli* cells). In view of the relatively high number of halobacterial mutants to be constructed it seemed appropriate to review the established technique of mutant generation and to optimize it.

At the beginning of this study, the standard procedure of mutant screening after transformation with a "suicide plasmid", which lacks a halobacterial origin of replication, took approximately 7 weeks. It involved a first round of clone selection on medium containing mevinolin as selective agent. Mevinolin inhibits 3-hydroxy-3-methylglutaryl-coenzyme A (HMG-CoA) reductase, a key enzyme in the synthesis of isoprenoids, the precursors of archaeal lipids. Resistance against mevinolin results from a mutation in the promoter of an HMG-CoA reductase-encoding gene from *Haloferax volcanii*, that leads to overproduction of the reductase when this gene is introduced via a plasmid into halobacterial cells (Lam and Doolittle, 1992). Mevinolin-resistant

cells are generated by a single recombination event, by which they integrate the entire plasmid DNA into their genome. Reculturing such cells without selective pressure allows for a second recombination event in a small fraction of the cells, which leads to a loss of the plasmid DNA.

In a second selection step hundreds of clones had to be tested for plasmid loss, by transfer to plates with and without mevinolin ("double-picking"). Whether the second recombination had generated the desired genotype (e.g. a gene-deletion) or restored the genotype of the parental strain, was investigated by Southern-blot analysis of the clones unable to grow on mevinolin (for a description of the events taking place after transformation with a suicide plasmid, see Fig. 4.1).

To facilitate clone selection, the *bgaH* gene from *Haloferox alicantei* (Holmes and Dyall-Smith, 2000) was introduced into the plasmids as a reporter gene. It encodes a β -galactosidase that is active in the presence of high salt concentrations and was previously used in halobacterial promoter studies (Patenge *et al.*, 2000). The presence of *bgaH* in the plasmids (Fig. 3.2) allowed for red-blue selection of plasmid-DNA-deficient (red, due to BR and bacterioruberin) versus plasmid-DNA-containing (blue, due to β -galactosidase-activity) halobacterial clones, when growing the cells on plates containing X-gal (Fig. 3.7).

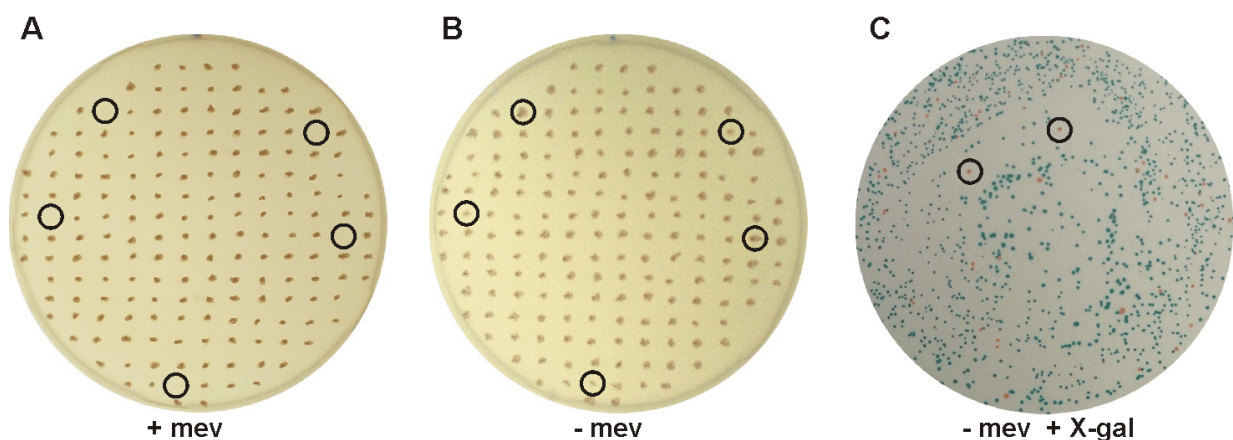


Figure 3.7 Selection of halobacterial transformants via the "double-picking" technique or via red-blue-clone-selection.

The established method of clone selection involved the transfer of each selected clone to two plates of complete medium, the first of which (A) contained mevinolin as the selective agent, whereas the second one (B) lacked mevinolin. Circles mark the clones which did not grow on the first plate because they had lost the DNA of the introduced plasmid together with the mevinolin resistance gene in a second recombination event. These clones were candidates for cells containing the desired mutation and were therefore picked on the second plate (circles). (C) Plating of cells transformed with a plasmid containing the *bgaH* gene in addition to the mevinolin resistance-conferring gene can be done on plates lacking mevinolin but containing X-gal. Clones which have lost the plasmid DNA after the second recombination event can be directly identified on the plate as red clones. Two of them are marked by circles. The majority of blue clones still contains the plasmid DNA and can therefore produce the *bgaH*-encoded β -galactosidase which converts X-gal into a blue dye.

The use of this selection method has a number of advantages: (i) Blue colonies clearly attest to the success of the transformation. This prevented the erroneous selection of untransformed clones which, for reasons that are unclear, were occasionally able to form colonies on mevinolin-containing plates. (ii) Transformed cells, which have lost the plasmid-DNA in a second recombination event, can now directly be identified as red colonies on plates lacking mevinolin. This avoids the laborious task of double-picking hundreds of clones per transformation, and thereby saves approx. two to three weeks of time which is needed for unambiguous identification of clones that are not growing on mevinolin-containing plates.

3.1.5 BR-dependent phototaxis is mediated by Htr14 and involves stimulus-induced methanol release

Cell tracking demonstrates that Htr14 is the transducer responsible for BR-mediated phototaxis

As previously shown by tracking of Pho81-B4 cells (Bibikov *et al.*, 1993), the BR-dependent photoresponse is characterized by a significant increase in the number of reversing cells when orange light is switched off. The percentage of cells, which reverse their swimming direction within 4 s after a light-off stimulus, increases with increasing initial light intensity. With less than ca. 20% reversals in the absence of a stimulus, a maximum of ca. 85 - 95% reversals is reached with Pho81-B4 cells when the prestimulus irradiance exceeds 150 - 200 W/m², values which could be confirmed with MKK101 cells.

To identify the Htr involved in this response, computerized cell-tracking experiments were performed (Fig. 3.8, see Fig. 4.3 for the experimental setup). The characteristic photoresponse was observed with MKK101 and all of the *htr*-deletion strains derived from it, except MKK114 ($\Delta htr14$). The photoresponse was restored in the unresponsive strain by complementation with *htr14*, i.e., in strain MKK119. The response was investigated under conditions of oxygen depletion, which leads to a low pmf in the dark. Since the pmf is the driving force for flagellar rotation, the drop in pmf could be observed as a progressive immobilization of the cells during preincubation in the dark. Motility returned upon reillumination because of the pmf-regenerating proton-transport activity of BR.

Addition of the respiratory-chain inhibitor cyanide to the cell suspension allowed for investigation of the BR-dependent photoresponse in the presence of oxygen. Cyanide-treated MKK101 cells that were not oxygen-depleted performed more photostimulated reversals as the concentration of cyanide increased. The cyanide effect was seen at concentrations as low as 0.1 mM, increased in a concentration-dependent manner up to approximately 2 mM, and then

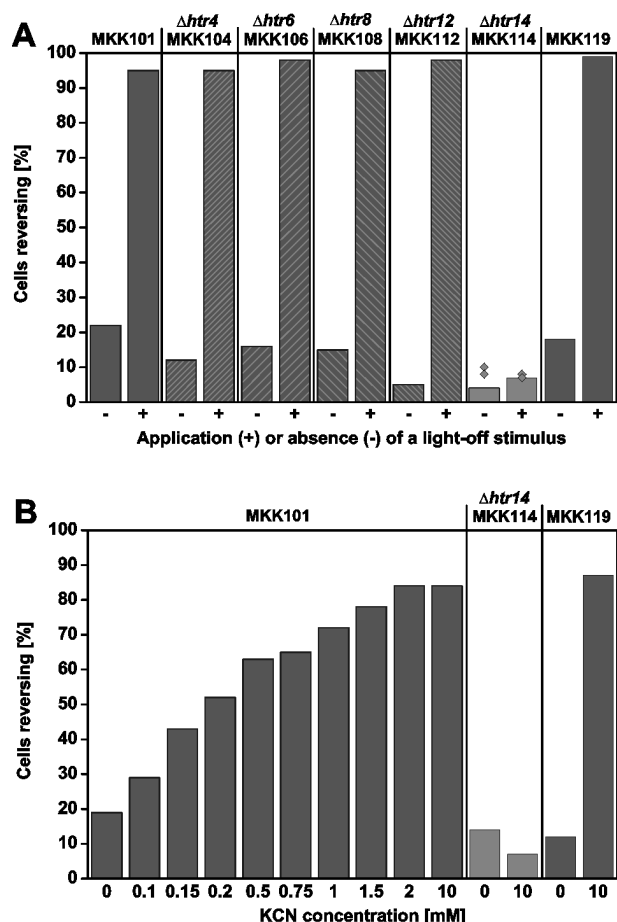


Figure 3.8 Cell-tracking experiments with BR-containing strain MKK101 ($\Delta htr1 \Delta htr2 \Delta htr11$) and derived *htr*-mutants.

(A) The percentage of oxygen-depleted cells reversing within 4 s was determined either without (-) or with the application (+) of a 3 s orange-light-off stimulus (300 W/m²). Results are shown for strain MKK101, MKK101-mutants carrying an additional deletion of the *htr* indicated above the strain name, and the *htr14*-complemented strain MKK119. Results for two additional MKK114 clones are depicted as diamonds. MKK101-mutants in which *htrs* 3, 5, 7, 9, 10, 13, 15, 16, 17 or 18 are deleted gave results (data not shown) which were in exactly the same range as those obtained for all depicted strains except MKK114. Each value shown is based on the observation of 61 to 201 cells (mean of 97) whose tracks were collected in 20 measurements within 10 min.

(B) Cells from strains MKK101 (*htr14*⁻), MKK114 ($\Delta htr14$) and MKK119 (*htr14*-complemented) were analyzed as in (A), but this time with the indicated concentrations of cyanide in the resuspension buffer and without preincubation in the dark, i.e. without oxygen depletion. In each case, light-off stimuli (390 W/m²) were applied to the cells. Each value is based on the tracking of 100 to 284 cells (mean of 153) whose tracks were collected in 30 measurements within 15 min.

A variable range of 5 to 25%, for spontaneous, and 83 to 98%, for light-induced, reversals was found, under oxygen depletion as well as in the presence of saturating cyanide, when analyzing different strains or when the same strain was analyzed on different days.

remained constant at least up to 10 mM. As expected, in the presence of 10 mM cyanide no photoresponse was seen with MKK114 but the response was restored in MKK119.

Flow-assay analysis indicates that adaptive methylation plays a role in BR-dependent photosensing via Htr14

As an alternative approach to investigate BR-dependent photosensing by MKK101 cells, an assay was employed that measures the adaptive release of volatile radioactive methyl groups (as methanol) from transducers (Alam *et al.*, 1989). After radioactive labeling and immobilization of the cells in a transparent syringe-filter unit, a constant flow of chase buffer was applied, and the cells were subjected to orange-light stimuli (for a description of the setup see Fig. 4.5).

To demonstrate functional adaptation, L-leucine stimuli were used as a control. Without cyanide in the chase buffer, none of the tested strains showed a release of methanol upon light stimulation (data not shown), whereas L-leucine evoked methanol release in all experiments. When 10 mM cyanide was present, strong demethylation signals could be produced in MKK119 cells with orange-light-on or -off stimuli (Fig. 3.9 A). These signals were absent with MKK114,

confirming the findings of the cell-tracking experiments. For OMI1 cells, which lack all retinal proteins, no demethylation response could be observed upon photostimulation, however, it was seen in response to L-leucine (data not shown).

While the cell-tracking experiments demonstrated that Htr14 is the only transducer whose absence abolishes BR-dependent phototaxis, and therefore indicated that Htr14 mediates this process, the methanol-release experiments additionally showed that adaptive methylation is involved in Htr14-dependent sensing.

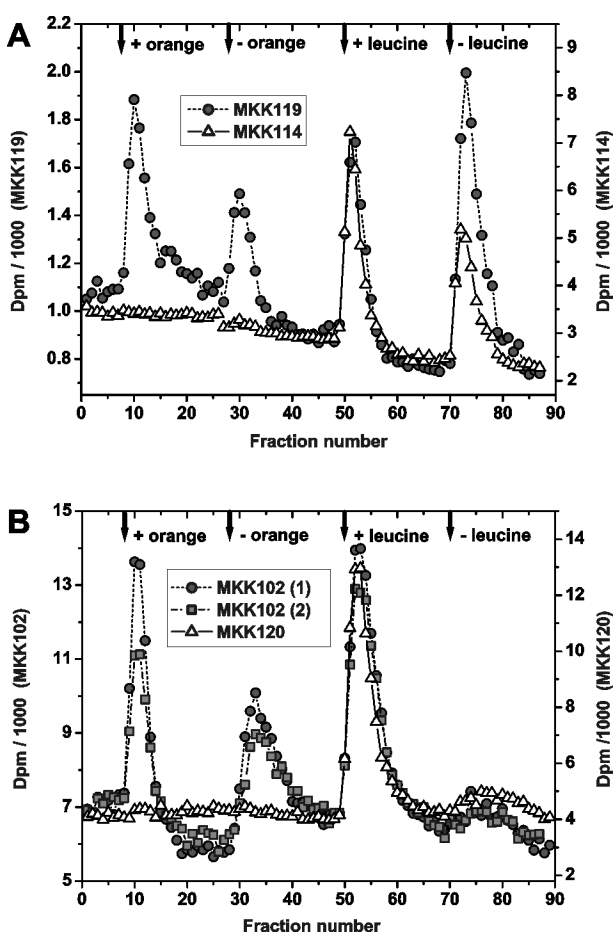


Figure 3.9 Stimulus-induced release of ^3H -labeled methanol from whole cells immobilized in a transparent $0.22\ \mu\text{m}$ filter unit.

Cells of the different strains were radiolabeled and treated as described in Materials and Methods. A constant flow (1.5 ml/min) of chase buffer containing 10 mM cyanide was applied to the cells. Fractions of 18 s were collected and their content of volatile radioactivity was determined. Stimulus addition (+) or removal (-) is indicated by arrows (orange: $640\ \pm\ 80\ \text{nm}$ light at $120\ \text{W/m}^2$; leucine: 10 mM L-leucine in chase buffer with cyanide). Individual curves were normalized to the + leucine-peak. (A) Responses of BR-containing strains MKK114 ($\Delta htr14$) and MKK119 (*htr14*-complemented). (B) Responses of HR-containing strains MKK102 (*htr14*, separate results for two different clones) and MKK120 ($\Delta htr14$). All responses were confirmed in additional, independent experiments.

3.1.6 Htr14 is also responsible for HR-dependent photoresponses

Upon illumination, HR pumps chloride ions into anaerobic dark-adapted cells, thereby increasing the $\Delta\Psi$ -component of the pmf as demonstrated by a transient (several-minute) generation of maximal (aerobic) cellular ATP level with concomitant acidification of the cytosol (Mukohata and Kaji, 1981). When tracking motile MKK102 cells in the presence of 10 mM cyanide, swimming reversals upon light-off stimuli could not be detected (data not shown), a result which contrasts with the observation of a reversal response in strain Pho81-HR, reported

by Grishanin *et al.* (1996). Both strains contain HR as the only retinal protein, although in the case of Pho81-HR it was overproduced.

Fig. 3.9 B shows results of methanol-release experiments using MKK102 and an *htr14*-deletion strain derived from it (MKK120). Upon a light-off stimulus, methanol was released only from MKK102 cells, i.e., only when Htr14 was present. This result demonstrates that Htr14 also mediates HR-dependent photoresponses. The reason why MKK102 cells did not exhibit swimming reversals upon a decrease in irradiance is unclear.

3.1.7 Htr14 is bound to the plasma membrane and can exist in differently methylated forms

Immunoblot analysis demonstrated membrane localization for Htr14

A visual inspection of the amino acid sequence of Htr14 identified a hydrophobic region, including residues 28 to 76, that lacks charged amino acids. This stretch could accommodate two transmembrane helices connected by a hairpin loop, as depicted in Fig. 3.14. To determine the cellular localization of Htr14, an antiserum (anti-Htr14_{D585}) was generated against a synthetic peptide which contains a stretch of amino acids present in the C-terminal region of the protein (D585 to S606). The antiserum is highly specific as demonstrated by the complete absence of reactivity with proteins from the *htr14*-deletion strain MKK114 (data not shown). Immunoblots of the cytosolic and membrane protein fractions of strains MKK101, S9 and the *cheB*- and *cheR*-deletion strains WFS101 and WFS102, respectively, show that the majority of cellular Htr14 pelleted together with the membranes (Fig. 3.10). The small amount of apparently cytosolic Htr14 might result from incomplete pelleting of small membrane fragments. Incomplete pelleting of halobacterial membranes was observed at a growing extent when cells were lysed in buffers of decreasing salt concentration (data not shown). These results suggest that Htr14 is anchored to the membrane, probably via the two predicted N-terminal transmembrane helices.

Htr14 can exist in differently methylated forms distinguishable by their electrophoretic mobilities

To examine the extent of Htr14-methylation, the mobility of Htr14 in SDS-PAGE gels was compared for strains MKK101, S9, WFS101 and WFS102 (Fig. 3.10 A). In strain WFS101 ($\Delta cheB$) Htr14 should be fully methylated, because methyl groups can be added by the methyltransferase CheR but not removed by the methylesterase CheB, whereas in strain WFS102 ($\Delta cheR$) Htr14 should be completely unmethylated.

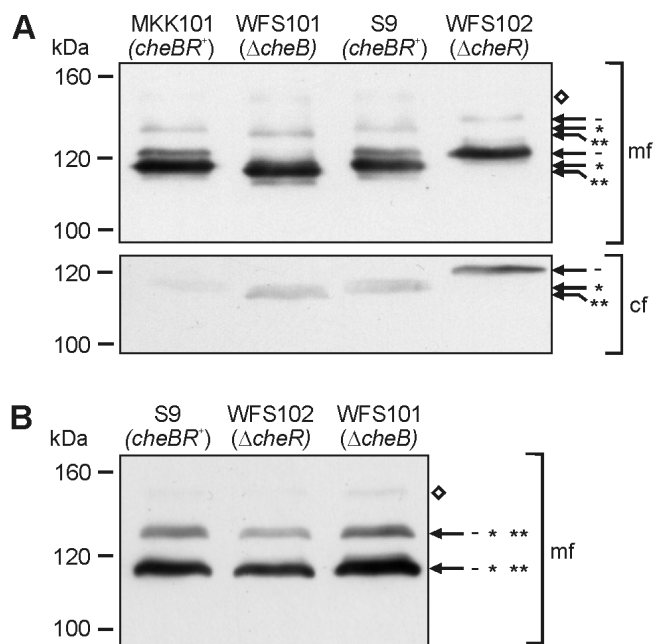


Figure 3.10 Immunoblot analysis of the cellular localization and the methylation status of Htr14 in different halobacterial strains with anti-Htr14_{D585} serum.

Cytosolic (cf) and membrane (mf) protein fractions (15 µg protein per lane) were subjected to SDS-PAGE (8% polyacrylamide) followed by immunoblotting as described in Materials and Methods. The relevant strain genotypes concerning the methyltransferase and the methylesterase genes *cheR* and *cheB*, respectively, are indicated in parentheses. Arrows mark the band positions attributed to putatively unmethylated (-), moderately methylated (*) and highly methylated (**) species of Htr14, which are the most prominent (or the only) species in the $\Delta cheR$ -, *cheBR*⁺- and $\Delta cheB$ -strains, respectively.

(A) The majority of cellular Htr14 pellets with the membrane fraction but small amounts are also present in the cytosolic fraction. All depicted lanes are from the same blot with identical exposure times. The pattern of bands at a MW between 115 and 122 kDa is present again at higher MW in the

lanes of the membrane fractions. Below the main Htr14 band an additional band is seen with the membrane fraction of the $\Delta cheB$ -strain at approx. 113 kDa and with that of *cheBR*⁺ strain S9 at approx. 115 kDa. (B) Different immunoblot, obtained after identical treatment of the protein samples as in A but with 6 M urea additionally present in the separating gel. The methylation-dependent differences in electrophoretic mobility observed in A are abolished. A pattern of three Htr14 species with different mobilities (the lower ones marked by arrows, the very faint upper one by a diamond) is seen for all strains and is also present in A where it is overlaid by the methylation-dependent motility differences.

The major Htr14 species in the cytosolic as well as in the membrane protein fractions of the investigated strains appear in 3 bands at apparent molecular weights (MW) of approx. 122, 117 and 115 kDa. Of these three bands only the one at 122 kDa is present in strain WFS102. This band is therefore assigned to an unmethylated Htr14 species, consistent with the previous observation that decreasing degrees of methylation of *E. coli* transducers cause them to run with progressively higher apparent MW (Boyd and Simon, 1980). For strain WFS101 the main band runs at 115 kDa and is attributed to a highly methylated Htr14 species. For strains S9 and MKK101 the strong band at 117 kDa is attributed to a moderately methylated Htr14 species. Above this band another, weaker band at 122 kDa points to the additional presence of an unmethylated Htr14 species in these strains. The faint bands observed in the membrane protein fractions of WFS101 at a MW below 115 kDa and for S9 and MKK101 below 117 kDa might indicate that a minor fraction of the major Htr14 species in these strains is methylated at an additional site. It is unlikely that these bands result from methylation-independent differences in Htr14 mobility, as for strain WFS102 no such band is present below 122 kDa.

The described pattern for the major Htr14 species in the investigated strains is repeated at higher molecular weights. This points to differences between Htr14 species, which cause different mobilities under the used electrophoresis conditions, in addition to the mobility

differences that are due to different extents of Htr14 methylation. Methylation-independent differences in electrophoretic mobility were also reported for *E. coli* transducers Tsr and Tar (Hazelbauer and Engström, 1981). This might point to an additional, still unspecified type of transducer modification that is conserved among members of the kingdoms of bacteria and archaea. The methylation-dependent mobility differences could be abolished by addition of 6 M urea to the sample buffer and gel, whereas methylation-independent mobility differences persisted (Fig. 3.10 B). A discrepancy between apparent (approx. 122 kDa for unmethylated Htr14) and calculated (65.6 kDa) MW has been noted previously for halobacterial proteins and is thought to be due to their acidic nature (Monstadt and Holldorf, 1991).

3.1.8 Mass spectrometrical analysis identified four methylatable residues in Htr14 and suggests a set of Htr14 species consistent with that seen on immunoblots

As discussed in detail in Chapter 3.2, mass spectrometrical analysis of the membrane-bound transducers demonstrated that Htr14 from wild-type cells contains three methylatable glutamate pairs. This was found by LC-ESI-Q-TOF-MS (liquid chromatography - electrospray ionization - quadrupole - time of flight - mass spectrometry) analysis of peptide mixes resulting from in-gel Asp-N digestion of the proteins contained in thin slices of an SDS-PAGE gel of an S9 membrane protein preparation. Htr14 was identified in three adjacent gel slices. In case of the slice containing the Htr14 species of intermediate electrophoretic mobility (at approx. 117 kDa), the major part of Htr14 methylation was found on the first glutamate within the pair E310/E311 and on the second glutamate within the pair E506/E507 (Fig. 3.11). The first pair is located within a sequence that is well conserved among the 18 Htrs (Fig. 3.14 and 3.30A) and perfectly matches the consensus sequence for transducer methylation by CheR in *E. coli* (Nowlin *et al.*, 1987): A/S-X-X-E-E*-X-A/S/T-A-S/T/A (with X symbolizing an arbitrary amino acid and the asterisk marking the methylation site). Perazzona and Spudich (1999) had previously shown that mutations within this conserved halobacterial sequence, which convert E265/E266 of Htr1 and E513/E514 of Htr2, respectively, to alanine pairs, completely and almost completely abolish methylation of these transducers, respectively. The sequence surrounding E506/E507 of Htr14 also matches the *E. coli* methylation consensus, except that the last residue is a glutamate.

In addition to these major sites of methylation, another site was detected in Htr14 derived from this gel slice. It is located within the signaling region of Htr14 on the second glutamate of the pair E415/E416 and is not surrounded by the CheR-methylation consensus sequence. Only very low levels of methylation were found at this site. The protein-containing slices were cut out of

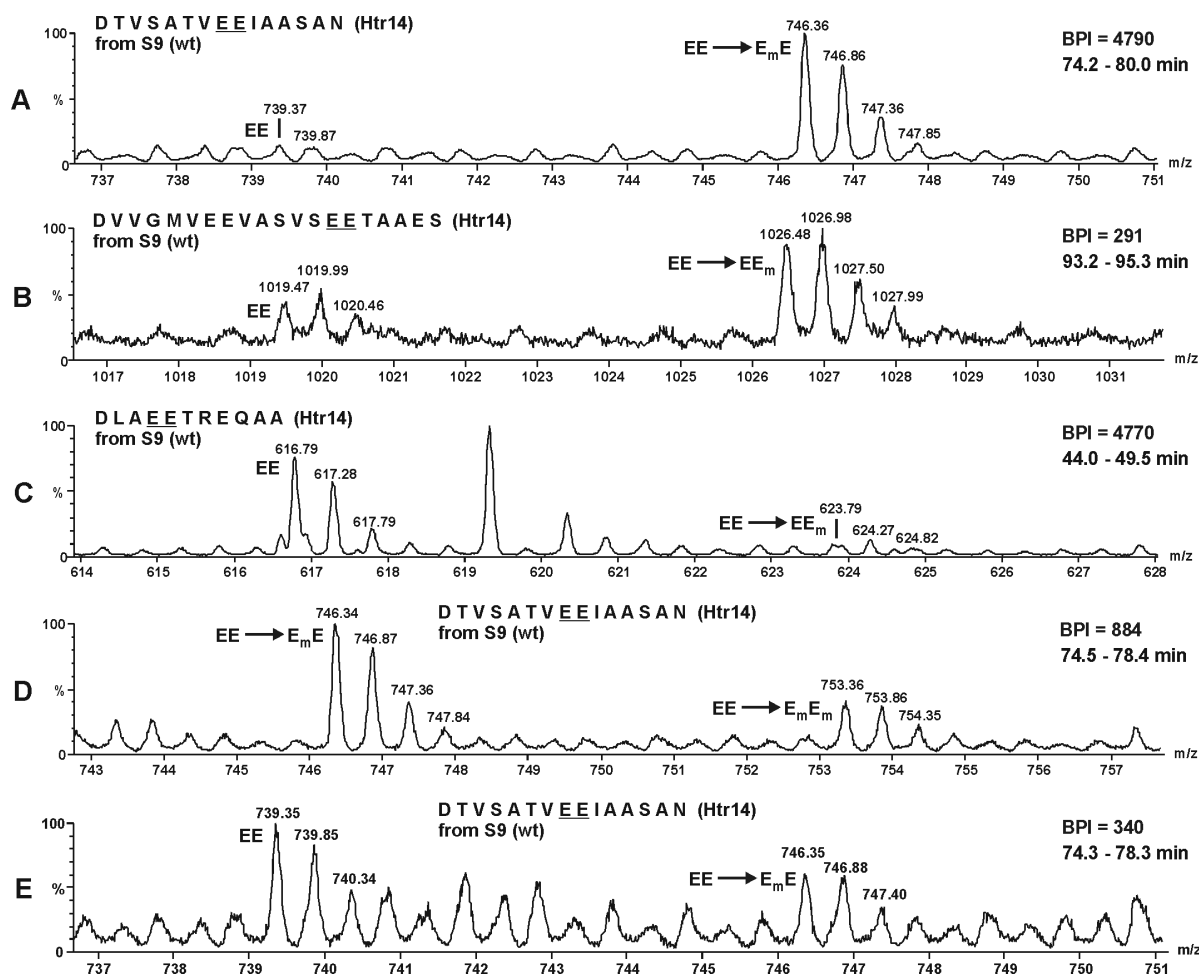


Figure 3.11 Mass spectra in the mass-per-charge ranges of the three methylatable peptides of Htr14.

For (A-C) the middle one of three adjacent Htr14-containing slices from an SDS PAGE gel of a membrane protein preparation from S9 cells was subjected to in-gel Asp-N digestion and the depicted spectra were obtained via LC-ESI-Q-TOF MS of the generated mix of peptides as described in Materials and Methods. (A) Mass-per-charge (m/z) range expected for the doubly charged Htr14-peptide containing the E310/E311 pair (underlined) in the unmethylated and the singly methylated form. (B) and (C) Corresponding spectra for the m/z range of the Htr14-peptides containing the E513/E514 and the E415/E416 pairs, respectively. The spectra were integrated over the complete time of elution (indicated on the right) of both forms of the peptide, with the methylated form starting to elute from the LC column approximately 1 to 4 min after the start of the elution of the unmethylated form. For each spectrum the intensity of the highest peak (BPI) is indicated in arbitrary units. The respective elution intervals (and the integrated BPI-values, which are corresponding to the respective peptide species and can be used to estimate the ratio of the differently methylated forms of a peptide) are the following, listed for the unmethylated / methylated peptides: (A) 74.2 - 75.0 min (245) / 76.8 - 80.0 min (4570), (B) 93.2 - 93.7 min (92) / 94.5 - 95.3 min (250), (C) 44.0 - 49.5 min (3580) / 48.0 - 49.5 min (204).

(D) The m/z range expected for the doubly charged Htr14-peptide containing the E310/E311 pair (underlined) in the singly and doubly methylated form. In this case Htr14 originated from the gel-slice adjacent to the one used for (A-C), in the direction of higher protein mobility. In this gel-slice an unmethylated form of this peptide was not detectable. Elution intervals (and integrated BPI-values) for the singly / doubly methylated peptides were 74.5 - 76.5 min (854) / 75.8 - 78.4 min (322). The depicted spectrum comprises the complete elution intervals of both forms.

(E) Mass spectrum corresponding to the one shown in (A) but generated from the peptide mix originating from the gel slice adjacent to that used for (A-C), in the direction of lower protein mobility. Elution intervals (and integrated BPI-values) for the unmethylated / singly methylated peptide were 74.3 - 75.5 min (259) / 77.1 - 78.3 min (172). Attribution of the different peptide-forms to the peaks as indicated in MS spectra (A-E) was in all cases confirmed by MS/MS analysis.

the gel and subjected to MS analysis without knowing the exact positions of the bands for the different Htr14 species. These are only visible on an immunoblot and it is therefore not exactly known which fractions of the individual bands were contained in the different investigated slices.

Due to the repeated interruptions of the MS-analysis caused by the acquisition of MS/MS spectra, a quantification of the differently methylated species via integration of the MS signals yields only approximate values. Despite these limitations, such a quantification suggests that the main form of Htr14 identified in the central gel slice carries two methyl groups, one at each major site. In the adjacent gel slice corresponding to higher protein mobility, mass spectrometrical analysis identified only the singly and the doubly methylated but not the unmethylated form of the Htr14 peptide containing the E310/E311 pair (Fig. 3.11 D). In the adjacent gel slice corresponding to lower protein mobility the unmethylated form was more abundant than the singly methylated form and the doubly methylated form could not be detected (Fig. 3.11 E).

These results are consistent with the band pattern on the immunoblot, which points to a higher mobility of Htr14 species with increasing levels of methylation. In view of the MS analysis, the bands on the immunoblot are interpreted in the following way: The 122 kDa band seen for the *cheR*-deletion strain corresponds to unmethylated Htr14. For strains S9 and MKK101 (both *cheBR*⁺) the weak band at 122 kDa reflects the presence of some unmethylated Htr14. The strong band at 117 kDa probably results from an overlay of intermediately methylated Htr14 forms, of which Htr14 methylated at the two major methylation positions E310 and E507 is the main species. In the *cheB*-deletion strain WFS101, unmethylated Htr14 is absent. But instead of an expected single band of high mobility, corresponding to an Htr14 species that should be fully methylated at all four methylatable glutamates, in addition to the major band at 115 kDa, another weak band is seen at approx. 117 kDa. This offers two alternative interpretations: (i) Htr14 species which are not fully methylated are present in this strain in vivo despite the absence of CheB, or (ii) Htr14 is fully methylated in vivo but loses part of its methylation due to ester hydrolysis during sample preparation for SDS-PAGE. Hydrolysis is unlikely, however, because a pH of 7.0 was never exceeded between cell lysis and the start of the electrophoresis, and hydrolysis during the gel-run would have caused a smear rather than discrete bands.

The faint bands at approx. 113 kDa for the Δ *cheB* strain and at approx. 115 kDa for the *cheBR*⁺ strain S9 might result from a small fraction of the main Htr14 species in the respective strains that is additionally methylated at the site within the signaling region.

3.1.9 The buffering capacity of the *H. salinarum* cytoplasm argues for a change in $\Delta\Psi$ as the stimulus that is sensed via Htr14.

Determination of the buffering capacity of halobacterial cell fractions

To assess which of the two constituents of the pmf, ΔpH or $\Delta\Psi$, is actually sensed during BR- and HR-mediated photosensing, the minimum stimulus length, required to elicit a reversal response, was compared with the time that is necessary to generate significant changes in $\Delta\Psi$ and in internal pH (pH_i). When orange light of 390 W/m^2 was switched off for 800, 500 and 200 ms, the percentages of MKK101 cells that reversed within 4 s were determined to be 85, 65 and 40%, compared to 20% in the absence of a stimulus (Fig. 3.12). These data demonstrate that 200 ms of darkness (and apparently even a stimulus of slightly shorter duration) is sufficient to elicit a reversal response in MKK101 cells, which is in accordance with previous results obtained with Pho81-B4 cells (Bibikov *et al.*, 1993).

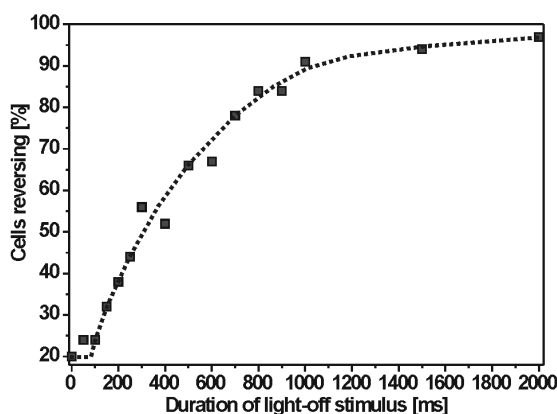


Figure 3.12 Tracking of MKK101 cells in the presence of 5 mM cyanide after light-off stimuli of varying durations.

The BR-dependent photoresponse of MKK101 cells was investigated as described in Materials and Methods. Light-off stimuli were ranging in duration from 0 to 2000 ms. All measurements were performed on the same cells which were kept on the microscopic slide for a total of 8.5 h under permanent illumination ($580 \pm 50 \text{ nm}$ at 390 Wm^{-2}), interrupted only by the light-off stimuli. The depicted values were determined in random succession and are each based on the tracking of between 191 to 696 cells (mean of 332) whose tracks were collected in one or two sets of 30 measurements within 15 min.

To estimate how rapidly pH_i changes after the light is shut off, it is necessary to know the cytoplasmic buffering capacity at a given pH_i and to compare it with the net rate of proton transport across the plasma membrane after stimulus application. Therefore the buffering capacities of halobacterial cell fractions were determined at different pH values via titration with NaOH (Fig. 3.13). The pH values of MKK101 and S9 lysates were 6.6 and 6.8, respectively. Between pH 6.5 and 7.0, the buffering capacities of S9 and MKK101 cytosolic fractions were between 400 and 250 nmol H^+ per pH unit per mg protein. The protein concentrations of the cytosolic fractions of MKK101 and S9 cells were 0.30 ± 0.02 and 0.32 ± 0.01 mg per ml of cell suspension at an optical density of 1.0 at 600 nm (ODml), respectively, and cell lysates both contained 0.43 ± 0.01 mg per ODml.

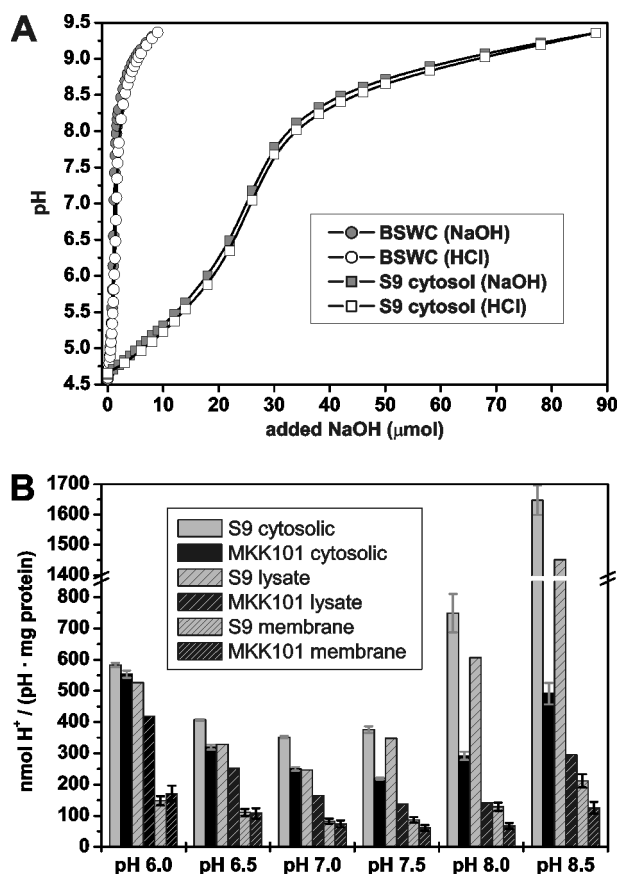


Figure 3.13 Determination of the buffering capacities of cell lysates, cytosolic and membrane fractions from halobacterial strains S9 and MKK101 at different pH values.

All titrations were performed as exemplified in (A), which shows titration curves of 40 ml basal salt medium without citrate (BSWC) in the absence (left curves) and presence (right curves) of S9 cytosolic fraction. The amounts of HCl added during the back-titration are not shown but correspond to the amounts of NaOH shown on the abscissa. (B) Buffering capacities of the different fractions at several pH values. Grey error bars show the values calculated from NaOH and HCl titrations relative to their mean value, which is shown by the column. Black error bars reflect the variation of three protein determinations via the BCA assay and are given as the standard deviation about the mean.

With $1.4 \cdot 10^9$ cells per ODml, the number of protons that must be transported out of a cell at pH_i values between 6.5 and 7.0 to increase its cytosolic pH by 0.1 was calculated to be between $5.1 \cdot 10^6$ and $3.1 \cdot 10^6$ for a 1 femtoliter cell. This number is in good agreement with the value of $8 \cdot 10^6$ protons calculated earlier for a 1.4 femtoliter cell of strain R1M1 at pH 7.0 (Michel and Oesterhelt, 1980).

Determination of the rate of proton transport across the membranes of MKK101 cells upon light-off and -on stimuli

The maximum number of H^+ ions transported per second across the cell membrane of an average MKK101 cell was determined by measuring the pH change in the cell suspension when switching off orange light of 80 W/m^2 (Table 3.1). With a buffering capacity of the cell suspension of 0.150 ± 0.008 pH units per 100 nmol H^+ , and with $7.0 \cdot 10^9$ cells in the assay, a maximum transport rate of $48,000 \pm 5000 \text{ H}^+$ per second and cell was found. When using light intensities of or below 80 W/m^2 the initial rates seen when switching off the light were approximately proportional to the original light intensity and remained constant for at least 10 to 12 s before they began to decrease. The maximally observed decrease of external pH upon switching off the light (0.020 ± 0.001 pH units) was reached after approximately 60 s and corresponded to ca. $1.1 \cdot 10^6$ protons per cell and a change in pH_i of ca. 0.03 pH units. With a

value of 36,000 +/- 5000, the maximum net proton transport rate induced by switching on light of 80 Wm⁻² was slightly lower and was maintained for 20 - 33 s.

Table 3.1. Rates of net proton transport across MKK101 cell membranes induced by illumination changes.

<i>Change of irradiance [Wm⁻²]</i>	<i>Maximum transport rate [$\Delta\text{pH}_e \text{ min}^{-1}$]^a</i>	<i>Maximum transport rate [$\text{H}^+ \text{ cell}^{-1} \text{ s}^{-1}$]</i>	<i>Time period of maximum H⁺-transport</i>	<i>Maximum stimulus-induced ΔpH_e and time until accomplishment</i>
0 → 80	+ 0.043	40,900	25 s	0.027 -- 60 s
80 → 0	- 0.055	52,200	12 s	-
0 → 80	+ 0.041	38,900	24 s	0.027 -- 60 s
80 → 0	- 0.057	54,100	11 s	0.020 -- 60 s
0 → 80	+ 0.036	34,200	32 s	-
80 → 0	- 0.050	47,500	11 s	0.020 -- 60 s
0 → 80	+ 0.041	38,900	20 s	0.025 -- 60 s
80 → 0	- 0.048	45,600	12 s	0.019 -- 54 s
0 → 80	+ 0.030	28,500	33 s	0.022 -- 67 s
80 → 0	- 0.046	43,700	11 s	0.018 -- 60 s
0 → 37	+ 0.015	14,200	31 s	0.012 -- 82 s
37 → 0	- 0.016	15,200	-	-
0 → 18	+ 0.005	4,700	-	0.004 -- 66 s
18 → 0	- 0.009	8,500	-	-

a: ΔpH_e : change of pH in the extracellular medium of the cell suspension; + and - indicate H⁺-transport into and out of the cells, respectively. With a buffering capacity of 0.150 +/- 0.008 pH units per 100 nmol H⁺, a change of 0.1 pH unit in the cell suspension corresponds to 5.7·10⁶ H⁺ transported per cell.

Comparison of light-off stimulus-induced changes in intracellular pH and in membrane potential

The initial transport rates allowed an estimation of the maximum change in pH_i that can be expected when the light is switched off for 200 ms. Assuming a 5-fold higher transport rate in the cell tracking experiments, when the pre-stimulus irradiance was 390 instead of 80 W/m², the maximum number of H⁺ ions transported across the membrane within the first 200 ms would be 48,000, corresponding to a change in pH_i of only 48,000 / 3.1·10⁷ = 0.0015 pH units. Even a 10-fold greater change in pH_i would not be expected to alter the protonation state of amino acid residues significantly. These considerations lead to the conclusion that the event that is sensed via Htr14 is not a change in pH_i (ΔpH_i) but should rather be a change in $\Delta\Psi$ ($\Delta\Delta\Psi$).

As previously determined for halobacterial strain R1M1 (Michel and Oesterhelt, 1976), the $\Delta\Psi$ of oxygen-depleted dark-adapted cells at an external pH between 6.0 and 6.8 can be increased from ca. -90 mV to ca. -130 mV upon illumination with 73 W/m² for 15 min. The difference of

40 mV should therefore be a good estimate for the maximum initial drop of $\Delta\Psi$ when light is switched off under the conditions of the performed experiments. A $\Delta\Delta\Psi$ of 1 mV requires the net transport of 330 charges across the cell membrane for an average *H. salinarum* cell (Michel and Oesterhelt, 1980). A transport rate of 48,000 charges per second per cell upon switching off 80 W/m² light, which represents a minimum rate for net charge transport in our cell tracking experiments (in which the pre-stimulus irradiance, and therefore the expected transport rate, was 5-fold higher), would thus correspond to a drop of 29 mV within 200 ms. It can therefore be concluded that a $\Delta\Delta\Psi$ that can be sensed by the cell can be generated within less than one hundred milliseconds and must be maintained for a few hundred ms to be sensed.

Changes in cellular ATP levels or in respiratory electron transport can be excluded as the stimulus for Htr14.

Changes in irradiance also influence, via pmf changes, the cellular ATP level and electron flow through the respiratory chain. In principle, these factors could be alternatives to $\Delta\Psi$ as the parameter monitored by the cells. A decrease in ATP level might cause decreased phosphorylation of one or more proteins which in their dephosphorylated state might induce a reversal response via the transducer. When switching off the light, the decrease of cellular ATP concentration within the 200 ms stimulus time, however, would only be about 10 μ M, corresponding to < 0.3% of the ATP level under the given conditions (Wagner *et al.*, 1978). The changes in ATP levels that occur during stimulus application should, therefore, not be responsible for significant changes in the phosphorylation levels of putative signaling proteins.

Changes in electron flow through the respiratory chain would shift the redox state of chain components. Any of these, through direct or indirect interaction with Htr14, could cause the repellent response. Such a mechanism has been proposed for the *E. coli* aerotaxis transducer Aer, which is thought to sense the redox state of the electron transport system via an FAD cofactor non-covalently bound to its PAS domain (reviewed by Taylor *et al.*, 1999). For Tsr, which can also mediate aerotactic responses in *E. coli* but is lacking a prosthetic group, Rebbapragada *et al.* (1997) proposed a pmf-sensing function. However, electron transport sensing could not be excluded under the respiration conditions prevailing in those experiments.

In halobacteria, light inhibition of respiration in the presence of oxygen is the consequence of a pmf-increase (Oesterhelt and Krippahl, 1973). A decrease of oxygen concentration in the medium also causes chain components to assume a reduced state, although in the latter case the pmf falls rather than increases. The BR-dependent photoresponse, however, is observed in the presence of cyanide or in the absence of oxygen. Since alternative terminal electron acceptors

were absent in the performed experiments, both conditions should prevent electron flow through the respiratory chain, thereby eliminating the possibility of changes in the redox state of chain components.

After excluding redox-state sensing and the generation of sufficient changes in pH_i and cellular ATP concentration within the period of stimulus application, the only viable explanation is that Htr14 responds to changes in $\Delta\Psi$. Therefore, Htr14 was renamed as the Membrane potential change Transducer, or MpcT.

3.1.10 MpcT (Htr14) by itself probably serves as the $\Delta\Psi$ sensor

A high sequence homology between MpcT and its putative ortholog from *N. pharaonis* is present in the N-terminal but not in the C-terminal region

The question remains whether MpcT detects $\Delta\Delta\Psi$ directly or in conjunction with another protein or proteins. A known example of $\Delta\Delta\Psi$ sensing is the voltage-gated K⁺ channel KvAP from *Aeropyrum pernix* for which a positively charged but otherwise very hydrophobic "sensor paddle" domain was suggested to move perpendicular to the plane of the membrane upon a $\Delta\Delta\Psi$, thereby inducing a conformational change in the gating part of the channel (Jiang *et al.*, 2003).

One might speculate that $\Delta\Delta\Psi$ sensing via MpcT occurs by a similar mechanism, either involving a membrane-embedded segment of MpcT containing charged residues or via an interaction of MpcT with another protein containing such a segment. For the predicted TM regions (maybe in combination with some charged, also membrane-embedded residues from the N-terminal region) both options are possible, whereas the Pro-rich C-terminal region of MpcT would seem to require interactions with another protein or proteins. These two regions in MpcT are quite dissimilar in their primary sequence to the corresponding regions of other Htrs. Together with the linker region (between the second TM region and the putative coiled-coil region) they are proposed to be situated close to the membrane, as depicted in a hypothetical working model of an MpcT structure on the basis of a proposed structure of *E. coli* Tsr (Fig. 3.16).

When the amino acid sequence of MpcT was compared with that of its putative ortholog from the halophilic archaeon *Natronomonas pharaonis* (Michaela Falb *et al.*, unpublished), no significant sequence identity could be found for the C-terminal region downstream of position 552 of MpcT (Fig. 3.14). However, in both proteins this region contains a stretch of 33 residues with a proline content of 21% in MpcT and 18% in its putative ortholog, which is unusually high

residues 245 to 552 of MpcT), this intermediate region consists of an additional stretch of residues. This stretch comprises putatively α -helical regions (as deduced from the presence of hydrophobic heptad sequences), interrupted by a region of unknown structure, that contains a sequence which was named GDL-motif (Fig. 3.14). A GDL-motif was found to be indicative of the beginning of the "connector region" within a "HAMP domain" of a transducer. HAMP domains comprise a common structural element that was identified by sequence comparisons of sensor kinases and MCPs (Aravind and Ponting, 1999), and are frequently found in histidine protein kinases, adenyl cyclases, methyl-binding proteins and phosphatases.

The N-terminal region of MpcT also exhibits significant homology to that of the putative *H. salinarum* histidine kinase OE2712R

A comparison of MpcT with proteins from *H. salinarum* strain R1 (Dieter Oesterhelt *et al.*, unpublished; <http://www.halolex.mpg.de>) discovered protein OE2712R (the equivalent of protein Vng1193c from *Halobacterium sp.* NRC-1 (Ng *et al.*, 2000)). OE2712R is 39% identical (from position 25 to 180) to the mentioned N-terminal region of MpcT (Fig. 3.15).

The C-terminal region of OE2712R (from position 183 to 392), however, is 32% identical to the putative histidine protein kinase (HPK) domain of halobacterial KinA (OE2961F, Vng1374g). His203 of OE2712R corresponds to the conserved phosphorylatable His405 of *B. subtilis* histidine kinase A (Wang *et al.*, 2001). Assuming that the same signal is sensed by MpcT and OE2712R, these findings suggest that the N-terminal rather than the C-terminal regions of MpcT and OE2712R are responsible for the input of the $\Delta\Psi$ signal. In the case of MpcT, the output is likely to be via an interaction of its cytoplasmic signaling region with the associated HPK, CheA, which then relays the signal via the response regulator CheY to the flagellar motor as the final target. In the case of the putative sensor kinase OE2712R, the output might be a change in an intrinsic HPK activity and involve transcriptional regulation via an unknown response regulator. OE2712R is expected to form dimers just like Htrs or like other known HPKs, e.g. CheA. None of the other Htrs show a comparable similarity between a transducer region and a region from a putative sensor kinase.

deletion of this gene in strain MKK101 had no detectable effect on BR-dependent phototaxis (data not shown), which excludes it as being a partner with MpcT in $\Delta\Psi$ sensing.

Although a role for MpcT as the direct sensor of changes in $\Delta\Psi$ is supported by the absence of a cotranscribed receptor gene, it cannot yet be ruled out that one or more additional proteins are required to interact with MpcT in the process of $\Delta\Psi$ sensing. However, contrary to signaling via Htr1 and Htr2, which in both cases requires a physical interaction with the corresponding photoreceptors, such an interaction of MpcT with BR or HR is not assumed. A $\Delta\Psi$, generated via BR or HR, should be detectable anywhere along the cell membrane, and does not necessarily require a protein-protein interaction between the sensor and the generator of $\Delta\Psi$. As photostimuli can be sensed in both combinations, BR/MpcT or HR/MpcT, a physical interaction would require that MpcT interact alternatively with two different receptors, *i.e.* with BR as well as with HR. Taking into account the differences especially in the structures of the membrane-exposed surfaces, the tilt of the helices and the photocycles of HR and BR, this seems rather unlikely.

3.1.11 Structural and clustering model for *E. coli* Tsr and MpcT

Generation of a model for *E. coli* Tsr, which is consistent with the EM data of overexpressed Tsr

Based on the detected structural motifs of MpcT (Fig. 3.14) and on its homology to *E. coli* Tsr, a hypothetical structural model of MpcT is suggested (Fig. 3.16). It was constructed in analogy to a structural and clustering model of Tsr which was generated on the basis of: (i) the structure of a mutationally modified cytoplasmic Tsr fragment, cTsrQ (Kim *et al.*, 1999), (ii) the ligand-binding domain structure of *E. coli* Tar (Chi *et al.*, 1997), (iii) results obtained via cysteine- and disulfide-scanning mutagenesis within the "linker region" following transmembrane helix 2 (TM2) of *Salmonella typhimurium* Tar (Butler and Falke, 1998) and (iv) data from an electron microscopical study of detergent-treated membranes containing Tsr assemblies (Weis *et al.*, 2003).

Weis *et al.* attribute an observed discrepancy between the length of the cytoplasmic Tsr region estimated from their EM data, ca. 190 Å, and the length proposed by a hypothetical Tsr model of Kim *et al.* (1999), 260 Å, to a more compact arrangement of the "linker region", which is present in Tsr as well as in the other *E. coli* methyl-accepting chemotaxis proteins (MCPs). These approximately 50 amino acids adjacent to TM2 constitute a HAMP domain (Aravind and Ponting, 1999). Appleman and Stewart (2003) analyzed the "HAMP linkers" present in the 5

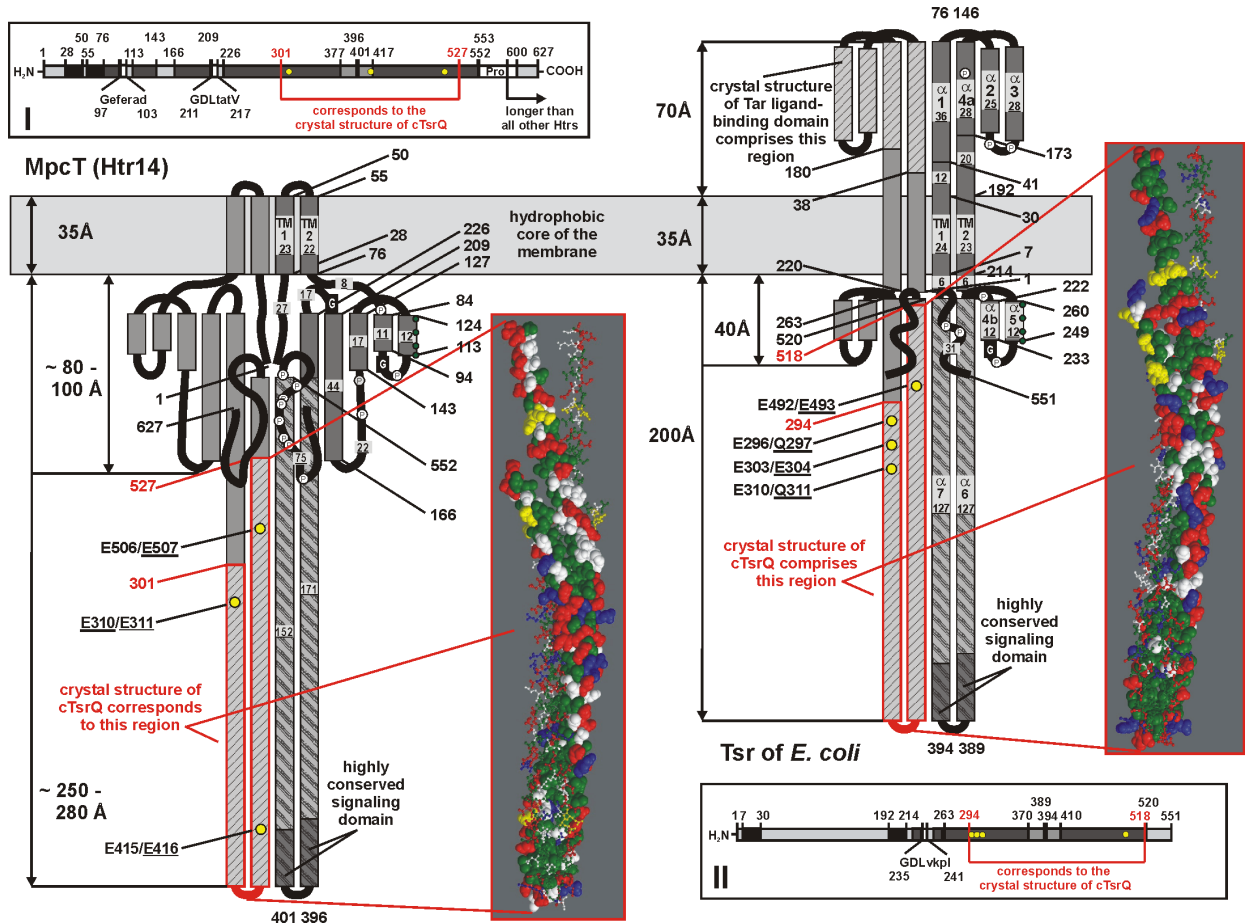


Figure 3.16 Proposed structures of halobacterial MpcT (Htr14) and *E. coli* Tsr.

Upper right: Proposed structure of Tsr on the basis of the cTsrQ structure, the *E. coli* Tar ligand-binding domain structure, cysteine- and disulfide-scanning mutagenesis experiments and EM data obtained from membrane preparations containing overexpressed Tsr, as described in detail in the text. Lower left: Proposed structure of MpcT on the basis of homology to Tsr, of predicted transmembrane regions and of proposed hydrophobic heptad regions, suggesting either an α -helical structure, or a coiled coil (thick hatching).

The parts of the molecules depicted as boxes are assumed to have an α -helical structure, whereas for those depicted as black lines no structural assumptions are made. Numbers on grey fields indicate the length of the corresponding regions, the remaining numbers indicate the positions of the first and last residues of the depicted segment. Green dots on helix $\alpha 5$ of Tsr represent residues M249, L252, L256 and M259. They correspond to residues in *S. typhimurium* Tsr, which are involved in the formation of $\alpha 5/\alpha 5$ contacts as determined by disulfide-scanning mutagenesis experiments. The corresponding residues in HAMP-region 1 of MpcT (I113, L116, F120 and M123) are also indicated by green dots. Yellow dots indicate experimentally confirmed methylation sites (underlining indicates the methylatable residue(s) of the Glx-pair, underlining is doubled for the major methylation positions). P, proline residue; G, GDL-motif indicating the beginning of the connector region within a HAMP domain.

The sphere representations of the coiled-coil regions show the cTsrQ structure (at the right), and a model of the corresponding MpcT region (at the left) generated on the basis of the cTsrQ coordinates via SWISS MODEL (<http://swissmodel.expasy.org>; Schwede *et al.*, 2003). In each case, one polypeptide chain of the transducer dimer is depicted as spheres and the second one as balls and sticks. Color code of the residues: yellow, Glx-pairs containing methylation sites; green, hydrophobic; red and blue, acidic and basic, respectively; white, all other residues.

Insets I and II represent MpcT and Tsr, respectively. Numbers indicate the first and last residue position of the depicted features. Black, transmembrane regions; dark grey, detected hydrophobic heptad; yellow dots, methylation sites; Pro, proline-rich region; white, GDL-motif with exact sequence indicated below (capital letters indicate conserved residues matching the consensus sequence, which was produced from an alignment of MCPs from different organisms (data not shown): GDLxxxh with x = arbitrary residue, h = hydrophobic residue).

MCPs and in 15 out of 30 known sensor kinases of *E. coli*. These HAMP linkers consist of two amphipathic sequences (AS-1 and AS-2) predicted to form two α -helices, which are joined by a connector with no obvious secondary structure, and which in Tsr extends from A233 to E248. Besides a Glu (E248 in Tsr) and a Met/Leu (M259 in Tsr) in AS-2, the only other highly conserved residue in these HAMP linkers is a Pro in AS-1 (P221 in Tsr, located 6 residues distal to the end of TM2).

Pro is known for its helix-breaking property. In the Tsr model it is therefore proposed that Pro221 generates a kink between (TM2-containing) helix α 4a and helix α 4b, displacing the

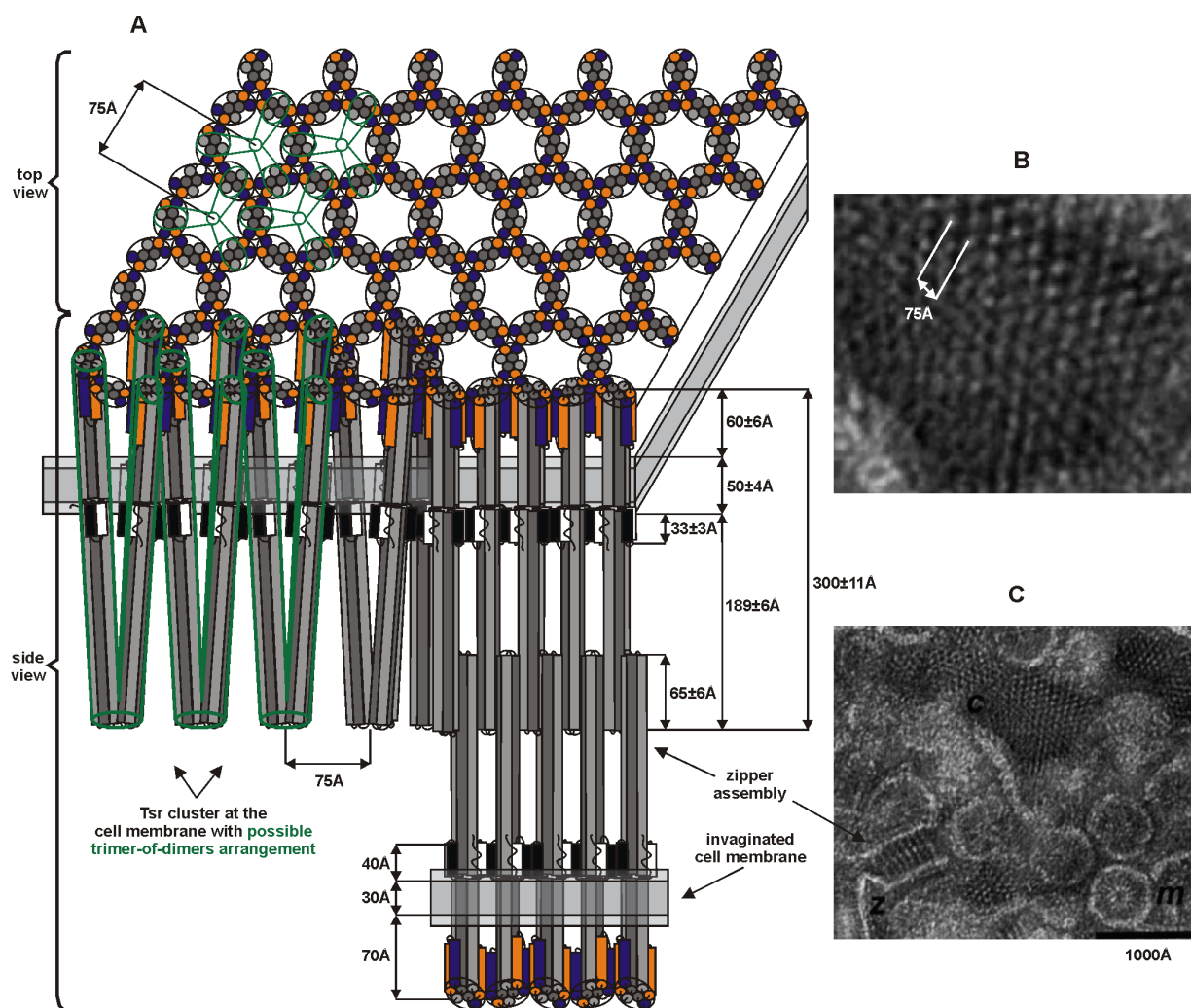


Figure 3.17 Clustering of overexpressed Tsr in the *E. coli* membrane.

(A) Schematic model of the arrangement of Tsr molecules in the proposed hexagonal cluster (the actual geometry of the periplasmic dimer-dimer-contacts might be slightly different). Indicated in green is a possible formation of trimers of dimers. Zipper-like structures, which were observed in EM pictures and were found to result from membrane invaginations, are depicted at the lower right. (B) A magnified view of a crystalline patch, seen in the EM pictures shown in C, displays a hexagonal structural array with a lattice constant of 75 Å. (C) Overview of the structures seen in EM pictures of overexpressed Tsr. Indicated are crystalline patches (c), zipper-structures (z) and micellar structures (m). EM pictures B and C were taken from Weis *et al.* (2003), and the values for the distances shown in A were observed in such pictures in the same study. These values are in complete agreement with the distances predicted by the depicted clustering model.

latter to the side of the central coiled-coil axis (Fig. 3.16). The region, which comprises proposed helices $\alpha 4b$ and $\alpha 5$ of Tsr together with the connector in between, starts after Pro221 of AS-1 and ends behind the conserved M259 of AS-2. The positioning of this region besides the coiled coil (formed by helices $\alpha 6$ and $\alpha 7$) produces a thickening of the Tsr dimer close to the membrane, and results in a total length of approx. 200 Å for the Tsr cytoplasmic domain when measured starting at the hydrophobic core of the membrane.

The model therefore exactly matches the length of the putative Tsr structures seen in the EM pictures of Weis *et al.* (2003), and suggests that $\alpha 4b$ and $\alpha 5$ cause the staining that is seen in these pictures directly beneath the membrane (extending ca. 33 Å from the hydrophilic border of the membrane into the cytosol) (Fig. 3.17). The average dimensions of the Tsr-containing structures detected by Weis *et al.* in detergent-treated membranes are almost identical (0.6% difference) to those seen in tomograms of fixed, cryosectioned cells overproducing Tsr (Lefman *et al.*, 2004), suggesting that the observed distances should closely match the actual situation in the cell.

Hexagonal arrays of Tsr dimers which contact each other via their HAMP domains might form the basis of transducer clustering

Cysteine- and disulfide-scanning mutagenesis experiments with *E. coli* membrane preparations containing overproduced *S. typhimurium* Tar (10 - 20% of the total membrane protein) were used to determine the solvent exposure of the residues in the HAMP linker region of Tar and to identify intersubunit contact sites (Butler and Falke, 1998). Tar is 53% identical to *E. coli* Tsr between P221 and Q260 of Tsr. Application of the solvent-exposure data from Tar to Tsr suggests an α -helical region between positions 215 and 230, a middle section with an ordered structure that is at least partially shielded from solvent, and a second α -helical region comprising residues 245 to 260. These limits for the α -helical regions approximately correspond to those predicted by Appleman and Stewart (2003), which are reflected in the presented Tsr model. The disulfide-scanning experiments identified only four residues in the HAMP linker, which efficiently form disulfide bonds between Tar molecules in which one of the linker residues (a different one in each experiment) is replaced by a cysteine. The obtained results suggest that only helices $\alpha 5$, but not helices $\alpha 4b$ or middle sections, form symmetric contacts between Tar subunits. Butler and Falke suggested that the $\alpha 5/\alpha 5$ disulfide products result from contacts formed between helices $\alpha 5$ and $\alpha 5'$, which originate from the two subunits of the same dimer.

Based on the suggested Tsr structure, the alternative explanation of interdimer contacts within an ordered array of transducers is proposed (Fig. 3.18A), in which all structural dimensions are in accordance with the EM data of Weis *et al.* (2003). In cells overproducing transducers, such an array can be expected, even in the absence of CheA and CheW, as demonstrated by the mentioned EM studies. The proposal of interdimer contact sites formed by three transducers predicts a maximum crosslinking efficiency of 67%, if each transducer contains only one cysteine that is located at the identical position along the contact face in all transducers. The three highest efficiencies observed for the mentioned four residues in $\alpha 5$ of Tar were between 58 and 63%, which is in accordance with the demands of the model.

Transducers like Tsr and Tar can form heterotrimers of homodimers *in vivo* (Studdert and Parkinson, 2004). These mixed trimers are expected to link up to form receptor clusters. If such clusters form in cells that lack Che proteins but contain a mix of overproduced Tar and Tsr, which both contain a single cysteine at the homologous position, replacing one of the contact-forming $\alpha 5$ -residues, then the Tsr structure and clustering model predicts the following result: interdimer contacts between the transducers should allow the formation of mixed disulfide-linked products containing Tar and Tsr. These products should be absent in the case of intradimer $\alpha 5/\alpha 5'$ -contacts because transducers only form homodimers. It will be interesting to see, whether the predicted Tar-Tsr crosslinking products can be found experimentally. The assumption of $\alpha 5/\alpha 5$ -contacts between different transducers in the receptor cluster furthermore predicts a good conservation of the involved residues. Indeed, with the exception of one position containing a Val in Tar, only Met, Leu and Ile are present at these positions in all *E. coli* and *S. typhimurium* transducers (except Aer, which differs from the remaining transducers also in other respects, for example methylation-independent signaling (Bibikov *et al.*, 2004)). Because of their high similarity, mutual substitution of these residues should have almost no effect on the contact face geometry.

Figure 3.18 Section of the suggested hexagonal array of Tsr molecules, viewed from the plane of the membrane into the cytosol, and proposed arrangement of CheW and CheA in such an array.

(A) In Tsr-overproducing cells, Tsr molecules are proposed to form the depicted hexagonal array with a lattice constant of 75 Å, consistent with the EM data of Weis *et al.* (2003). In this array Tsr dimers contact each other via their helices $\alpha 5$. Grey discs symbolize the membrane-spanning helices $\alpha 1$ and $\alpha 4a$ (in the plane of the membrane, numbers not shown) and helices $\alpha 6$ and $\alpha 7$ (in the cytosol). The latter helices form a coiled coil with their counterparts from the other subunit of the dimer (primed helices). White and black discs symbolize helices $\alpha 4b$ and $\alpha 5$, respectively, which are positioned besides the coiled coils, directly beneath the membrane and are expected to cause staining at these sites in EM pictures, which display a side-view of the depicted arrangement (as indicated in red). As indicated in green, the signaling regions of three dimers could form direct contacts (in the absence of Che proteins). The C-terminal region of Tsr (residues 521 to 551) is not depicted. It could be positioned besides helices $\alpha 4b$ and $\alpha 7$ without disturbing the proposed hexagonal array.

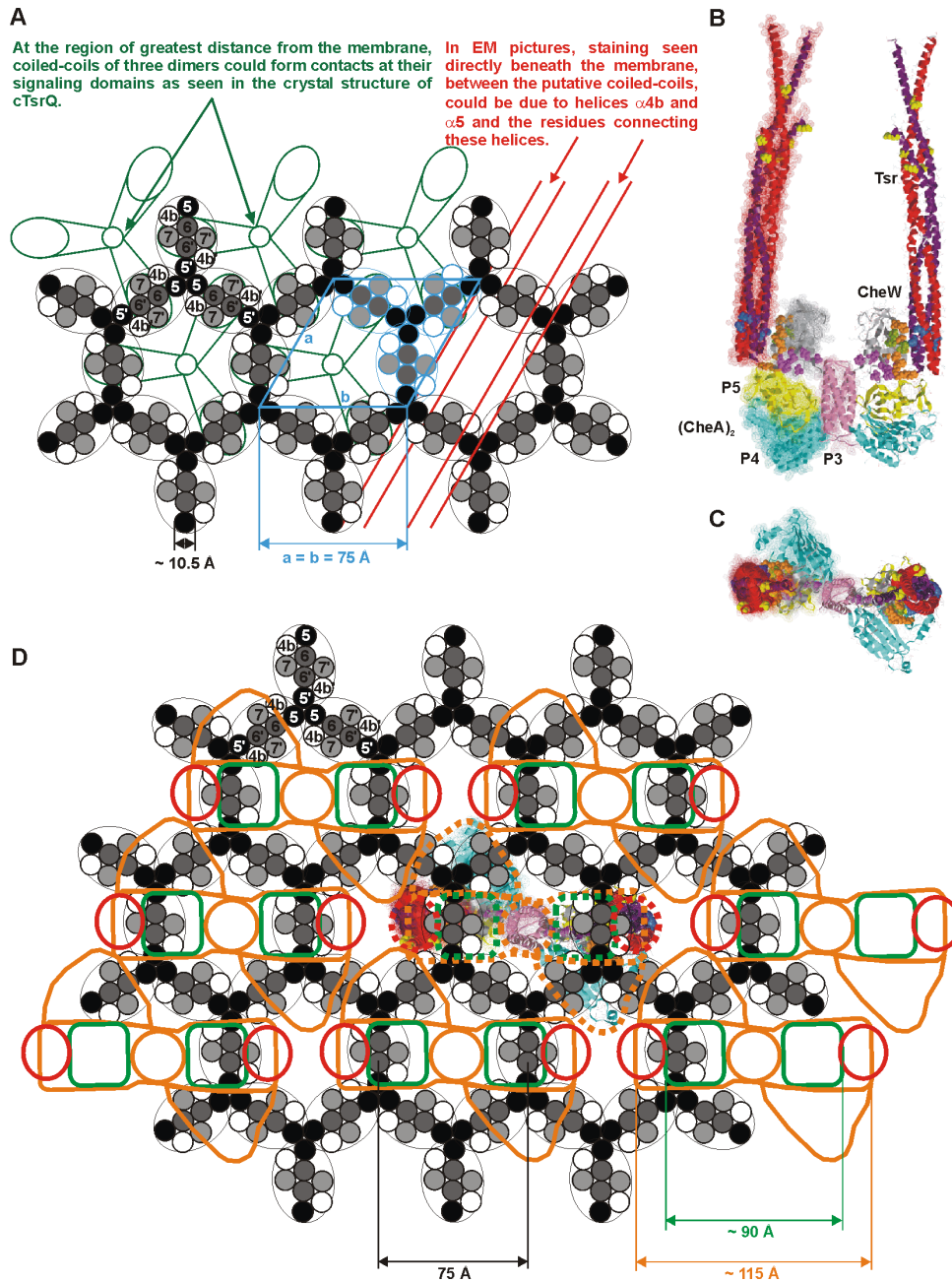


Figure 3.18 (B) and (C) Side- and top-view, respectively, of a proposed arrangement of the coiled-coil regions of two Tsr molecules bound via CheW molecules to a CheA dimer. The model uses the *E. coli* Tsr crystal structure of Kim *et al.* (1999), the crystal structure of a *T. maritima* CheA-dimer (Bilwes *et al.*, 1999) comprising domains P3 (pink), P4 (blue) and P5 (yellow), but lacking P1 and P2, and furthermore a structure of *T. maritima* CheW, which best represents the average of the 20 NMR structures generated by Griswold *et al.* (2002). Model construction was as described in the text. In Tsr, yellow spheres indicate methylation sites, blue spheres indicate residues important for CheW binding and the two monomers are depicted as red and purple ribbons. In CheW, orange, orange (Liu and Parkinson, 1991) and green (Boukhvalova *et al.*, 2002) spheres indicate the residues important for Tsr binding and purple spheres those important for CheA binding. All these highlighted residues in *T. maritima* CheW correspond to residues identified via mutational studies in *E. coli* CheW. In the left half of the model, dots around the ribbons indicate the space-filling structure of the molecules. (D) Overlay of the Tsr array and schematic images of CheA dimers (orange) bound to CheW monomers (green), according to the described model. The molecules are shown at their correct relative sizes, viewed from the plane of the membrane into the cytosol. The depicted arrangement requires that the cytosolic tips of the Tsr molecules bound to CheW are located at the positions indicated by the red circles. These positions are approx. 20 Å away from the tip-position of a coiled coil that is perfectly orthogonal to the membrane. The top view already shown in C is displayed in the center of the array to visualize the exact relative dimensions.

The dimensions of the proposed hexagonal Tsr array should in principle allow for an interaction of Tsr with CheA and CheW

In view of the known interactions of transducers with CheA and CheW as the basis for tactic signaling, the question arises whether the dimensions of the proposed transducer array would spacially allow for an interaction with CheA and CheW molecules. To check this it is necessary to know the dimensions of dimeric CheA and monomeric CheW and to compare them to those of the clustered Tsr dimers. For CheA the crystal structure of Bilwes *et al.* (1999) was used. It shows a dimer of *Thermotoga maritima* CheA (residues 290 to 671) which comprises the dimerization domain (P3), the kinase domain (P4) and the regulatory domain (P5) but lacks the histidine phosphotransfer domain (P1) and the CheY/CheB-binding domain (P2). The latter two domains are expected to be located adjacent to the kinase domain and to be facing away from the membrane towards the cytoplasm. For CheW the solution structure of Griswold *et al.* (2002) was used, which was obtained for CheW from *T. maritima*. CheA and CheW from *T. maritima* have approximately the same size as and share significant homology with CheA and CheW from *E. coli*. They are therefore considered to be adequate models to visualize molecule interaction surfaces on the basis of data obtained for CheA, CheW and Tsr from *E. coli* and to compare the dimensions of these molecules to those in the proposed Tsr array.

Fig. 3.18 B and C show a side- and a top-view, respectively, of a CheA dimer and two CheW monomers connecting two Tsr dimers. This arrangement would be consistent with the dimensions in the Tsr array if the cytoplasmic end of each Tsr dimer is displaced approx. 20 Å towards the outside with respect to the central twofold axis of CheA. Over an estimated length of 200 Å for the cytoplasmic part of Tsr this displacement would cause a tilt angle of only 6 degrees relative to a Tsr arrangement orthogonal to the membrane. The depicted model was constructed using the following considerations: (i) The CheW residues for which mutational experiments in *E. coli* proposed an interaction with Tsr (Liu and Parkinson, 1991; Boukhvalova *et al.*, 2002) were positioned to face those Tsr residues for which similar experiments proposed an interaction with CheW (Liu and Parkinson, 1991). (ii) The CheW residues for which mutational experiments pointed to an interaction with the regulatory domain of CheA were positioned to point towards the cytosol. (iii) A CheA dimer was arranged with the regulatory domains pointing towards the membrane and the kinase domains (and therefore the adjacent P1 and P2 domains) pointing towards the cytoplasm. This is the generally expected CheA orientation, which would allow the diffusion of CheY to the CheY/CheB-binding domain P2. (iv) A docking of the Tsr-bound CheW molecules to the CheA regulatory domains was only possible after the mentioned slight displacement of the coiled coils of the Tsr molecules away

from their orthogonal positions. The CheW-contacting surface of CheA has not been determined experimentally so far, and is here proposed to be the surface of the regulatory domain that is orthogonal to the twofold symmetry axis of the CheA dimer.

The dimensions of the proposed transducer array should therefore in principle allow the formation of CheA/CheW/Tsr complexes. This might point to the existence of transducer arrays with the described dimensions not only in Tsr-overproducing cells but also in chemotactically active wild-type cells. The arrangement of CheA/W within the array depicted in Fig. 3.18D is considered to be the most probable one, as it appears to allow for the docking of the highest number of CheA/W to an array of the given dimensions. On the basis of the presently available data in the literature it cannot be excluded, however, that CheW is contacting a different face of the CheA regulatory domain, producing a different CheA/CheW complex geometry leading to an overall arrangement different from the one depicted. Such different arrangements should, however, in each case lead to a lower number of bound CheA/CheW.

The overall stoichiometry of the depicted arrangement would be six Tsr dimers per two CheW monomers per one CheA dimer (6 : 1 : 1). Maximally 33% of the Tsr dimers could therefore be complexed (via a single dimer face) to CheA/CheW at any time. The determination of the total cellular stoichiometries of the signaling complex components in *E. coli* resulted in a ratio of 3.4 transducer dimers per 1.6 CheW monomers per one CheA dimer (Li and Hazelbauer, 2004). When taking into account that this ratio of 3.4 : 0.8 : 1 reflects the total cellular amount of these proteins and that one should expect a certain amount of unbound CheA and CheW in the cell, then the 6 : 1 : 1 stoichiometry within the proposed array seems to represent a reasonable value.

Description of a structural MpcT model generated on the basis of the proposed Tsr model

Based on the homology between MpcT and Tsr, a hypothetical structural model of MpcT was devised which takes into account putative structural motifs of MpcT that were derived from its amino acid sequence.

An inspection of all halobacterial transducer sequences revealed the presence of two HAMP domains in transducers (like MpcT) which contain two predicted TM regions (Fig. 6.7). The first of these domains (HAMP-1) is adjacent to TM2, similar to the situation in Tsr, and the second (HAMP-2) is located N-terminally to the predicted coiled coil of the methylatable and signaling regions (Fig. 3.16). Transducers with 3 or 6 TM regions contain only HAMP-2, and HAMP domains are completely absent in the transducers lacking TM regions. Within HAMP-2 the sequence GDLTxRh (x and h symbolize arbitrary residues and hydrophobic residues,

respectively) was noted, which is 98% conserved among all TM region-containing transducers. It contains the consensus sequence GDLxxxh, which was deduced via an inspection of HAMP domains in transducers from a number of other organisms (data not shown). This sequence indicates the beginning of the connector region within a HAMP domain and was termed the GDL-motif.

With the sequence GEFERAD, MpcT displays the poorest conservation of the GDL-motif of HAMP-1, when compared to the other transducers. Nevertheless, the residues corresponding to the putative $\alpha 5/\alpha 5$ contact-forming residues in Tsr are well conserved in all HAMP-1 domains, including that of MpcT. In analogy to Tsr, HAMP-1 of MpcT (residues 84 to 124) is therefore proposed to be localized besides the coiled coil and might form interdimer contacts in an array of transducer dimers, similar to that described in the Tsr model. Such arrays could provide the basis for a cellular localization at the poles, which has been observed not only for bacterial but also for halobacterial transducers (Gestwicki *et al.*, 2000). The region C-terminal to HAMP-1 is also suggested to be arranged at the side of the putative coiled coil and to have a partially α -helical structure. The proposed arrangement is based on the detection of hydrophobic heptad sequences (Fig. 3.14) expected to form α -helical regions, and on the assumption that the two HAMP domains in MpcT have a tertiary structure similar to that proposed for the HAMP domain in the Tsr model. The exact arrangement and dimensions of the proposed lateral helices are not known at present. The Pro-rich C-terminal tail is also thought to be located besides the coiled coil.

The putative four-helix coiled coil should mainly determine the length of the cytoplasmic part of MpcT. Especially the region between the methylation sites is expected to be structurally very similar to that of Tsr. Sphere models of this region, which are based on the known structure of cTsrQ, display the conserved hydrophobic contact face (appearing predominantly green in Fig. 3.16) between the dimer-subunits and show very similar positions for the methylation sites in Tsr and MpcT. If halobacterial transducers form a hexagonal array similar to that proposed for Tsr (and other *E. coli* transducers), then the model would provide sufficient space to the side of the central coiled coil to position the additional helices besides the putatively contact-forming first HAMP domain.

In the proposed model, the complete cytoplasmic region of the MpcT dimer is approximately 250-280 Å long. A central four-helix coiled-coil structure is surrounded by at least eight additional helices in a stretch of 80 to 100 Å beneath the hydrophobic core of the membrane.

This would still allow for good accessibility for CheR and CheB to the methylation sites within the glutamate pairs E310/E311 and E500/E507, just as in the Tsr model.

Though presently only based on sequence analysis and similarity considerations, the proposed MpcT model should, nevertheless, provide a basis for the design of future experiments (e.g. scanning mutagenesis or construction of hybrid transducers) aiming at the elucidation of the MpcT structure and the mechanism of sensing.

3.1.12 Summary of MpcT (Htr14) action and outlook

Fig. 3.19 summarizes the current view of the halobacterial signaling machinery. In addition to the known cytoplasmic and membrane-bound transducers involved in chemo- and aerotaxis and the two phototaxis transducers Htr1 and Htr2, this study identified MpcT as the transducer mediating BR-dependent phototaxis. After exclusion of significant changes in intracellular pH or ATP concentration or in the redox states of electron transport chain components under the

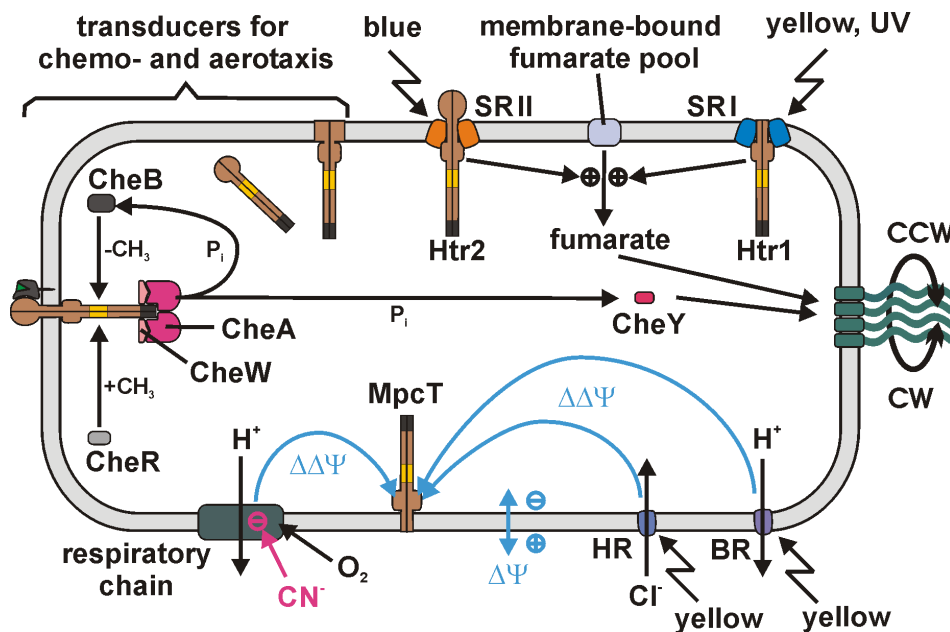


Figure 3.19 Overview of the involvement of transducer proteins (Htrs) in halobacterial signal transduction.

Htrs are depicted as dimers (brown) and are shown in their expected topology. The Htr-regions involved in adaptation (yellow) and in signal relay (dark grey) to the flagellar motor via Che proteins are indicated. The actions of the Che-protein machinery, described in the text, are only illustrated for the Htr on the left, for which an interaction with a substrate-loaded, membrane-anchored binding protein is indicated. CheD and CheC (CheJ) proteins are omitted for clarity. Htr1 and Htr2 transduce light signals via direct interaction with their corresponding receptors, SRI and SRII. Repellent light signals mediated by SRI and SRII elicit the release of the switch factor fumarate from a membrane-bound fumarate pool. MpcT senses changes in $\Delta\Psi$, generated via light-dependent changes in ion-transport activity of BR or HR. Signaling via MpcT occurs either in the absence of oxygen or in the presence of cyanide. Both conditions inhibit the respiratory chain and produce a decreased level of membrane energization (low $\Delta\Psi$). The relative sizes of receptors, binding proteins, transducers and Che proteins approximately reflect their corresponding molecular masses, however, the depicted arrangement of the molecules is not meant to predict the interacting molecular surfaces or the stoichiometries of interaction.

conditions of the BR-dependent photoresponse, it was concluded that the stimulus sensed via MpcT is a change in the electrical potential across the cell membrane.

The detection of such changes should be possible anywhere along the membrane and is not expected to require an interaction of MpcT with BR or HR. The lack of cotranscription for *mpcT* suggests that $\Delta\Delta\Psi$ sensing can be done by MpcT alone and does not require an additional receptor protein, although the need for an additional receptor cannot be completely ruled out at the moment.

A good conservation of the N-terminal sequence of MpcT in its putative *N. pharaonis* ortholog and furthermore in a putative sensor kinase from *H. salinarum* might indicate that $\Delta\Delta\Psi$ sensing takes place within this region in all three proteins. In a proposed structural model for MpcT, this region is localized close to and spanning the cell membrane. It therefore meets the expected fundamental feature of a $\Delta\Delta\Psi$ sensing module, i. e. membrane permeation. It also contains the membrane-proximal HAMP-domain of MpcT, which is suggested to participate in the clustering of MpcT, possibly together with further Htrs of different specificities. This would be in analogy to a clustering model which was devised for *E. coli* Tsr on the basis of the available data in the literature.

MpcT can exist as differently methylated species, which differ by their electrophoretic mobilities on SDS PAGE gels. In addition to CheR-dependent methylation, however, an additional, presently unknown MpcT modification exists, which produces differently mobile MpcT species also in $\Delta cheR$ strains.

MS analysis revealed four glutamate residues in MpcT at which methylation was found to varying extents. Particularly interesting in this respect is that for the first time a double methylation of a glutamate pair in a transducer was demonstrated. So far only single methylations have been reported in the literature. Another surprising result was the unprecedented presence of a methylated glutamate within the signaling region of MpcT. In this case, which will be discussed in more detail in Chapter 3.2.10, the sequence surrounding the glutamate pair does not match the methylation consensus sequence for CheR. It will be interesting to find out whether a methylation will also be detectable in the $\Delta cheR$ strain, which would point to the existence of an additional methyltransferase.

MpcT has so far been the only Htr for which a methylation within the signaling region was detected. However, in view of the well conserved sequence surrounding this methylation site, one might speculate that this kind of methylation also exists in other transducers and somehow interferes with the binding of CheW/CheA to transducers in general.

After the detection of MpcT as the responsible transducer for $\Delta\Delta\Psi$ and its characterization concerning methylation states and a possible domain architecture, two questions remain to be answered: (i) Does MpcT sense $\Delta\Delta\Psi$ by itself or does it react with another presumably membrane-spanning protein which functions as the sensor? (ii) If MpcT is the sensor itself, which parts of MpcT are involved, and what is the mechanism of $\Delta\Delta\Psi$ sensing on the molecular level?

To answer these questions, the following strategies could be helpful. (i) Crosslinking experiments on membrane preparations containing a tagged version of MpcT might be used to identify possible membrane-bound interaction partners of MpcT. This could be done by using the photoactivatable crosslinking reagent tris(2,2'-bipyridyl)ruthenium(II) followed by affinity chromatography on a column that specifically binds the tag attached to MpcT. MS analysis could then be used to identify the proteins bound to MpcT, and would be followed by testing if some of these proteins qualify as possible candidates for a $\Delta\Delta\Psi$ sensor. Finally, deletion analysis should show if one of these candidates is actually required for $\Delta\Delta\Psi$ sensing. (ii) Hybrid transducers should be constructed to investigate the indications that the N-terminal part of MpcT is responsible for the signal input. If this is the case, then hybrids consisting of the N-terminal part of MpcT joined to the C-terminal part of another transducer might be sensitive to $\Delta\Delta\Psi$ stimuli. On the other hand, a hybrid consisting of the N-terminal part of the putative sensor kinase OE2712R and the C-terminal part of MpcT would allow to analyze a presumptive conserved function for the N-terminal part in both proteins. (iii) Furthermore, a cysteine or alanine scanning mutagenesis approach might be used to identify amino acid residues in MpcT that are potentially involved in $\Delta\Delta\Psi$ sensing. These residues could either be necessary for a transducer-sensor interaction or they could constitute the molecular basis of $\Delta\Delta\Psi$ sensing by MpcT itself.

3.2 Mass spectrometrical identification of methylation sites in Htrs

3.2.1 Starting point and strategy for the investigation of Htr methylation

At the beginning of this study, very little was known about the methylation sites of Htrs and the exact positions of the methylatable residues. The term "methylation site" is used throughout this work to describe a pair of (mostly Glu or Gln) residues, which is located within a CheR recognition consensus sequence of a transducer and can accept a methyl group to produce a methyl ester at the first and/or the second residue (in case of Gln only after preceding deamidation to Glu). Such a methylatable residue within a transducer is called a "methylation position".

A mutagenesis study, in which the residues of putative methylation sites were exchanged for Ala-pairs, had previously identified exactly one and at least one methylation site in Htr1 and Htr2, respectively (Perazzona and Spudich, 1999). In the mentioned study, single Ala-substitutions within the Glu265-Glu266 pair of Htr1 furthermore pointed to Glu265 as the methylatable residue, because only the E265A but not the E266A mutation led to a complete loss of Htr1 methylation.

Information about methylation positions, that are based on mutagenization, however, has to be considered with some caution, as mutagenization does not only eliminate the putatively methylatable residue, but also modifies the CheR recognition sequence. Furthermore, a mutagenesis approach would not be practicable to analyze the methylation of the 18 Htrs, which most probably contain several methylation sites each. To compare the methylation situation of all Htrs, or even of only a subfraction, a substantial set of data is needed and these data should reflect the *in vivo* methylation of wild-type transducers under physiological conditions more closely than a mutagenesis approach.

Due to the recent advancements in the techniques of mass spectrometrical protein analysis, especially in the area of tandem mass spectrometry (MS/MS) of peptides resulting from protein digests, mass spectrometry (MS) appeared to be the method of choice for a comprehensive analysis of physiological transducer methylation. The big advantage of MS/MS analysis of peptides, compared to simple MS analysis, is the fact that the peptide-fragment pattern obtained by collision-induced dissociation (CID) allows for an "*in silico* sequencing" of the peptide. This is done by comparing the obtained fragment masses to calculated fragment masses of peptides, which were produced by *in silico* digest of proteins from a database. This method does not only

allow the unambiguous identification of a peptide but also makes possible the determination of the residues, which carry post-translational modifications like a methylation.

To get a first impression of the positions and the number of putative methylation sites in Htrs, the sequences of other transducers with known methylation sites, like *E. coli* Tsr and *B. subtilis* McpB, were aligned to those of the Htrs. As shown for Htr14 in Fig. 3.20, the cytoplasmic coiled-coil region of all Htrs consists of a succession of hydrophobic heptads, i. e. of groups of seven residues, in which the first and the fourth positions are almost entirely occupied by hydrophobic residues, Ser or Thr. By numbering the heptads with increasingly negative values towards the N-terminus and increasingly positive values towards the C-terminus, starting adjacent to the hairpin turn of the coiled coil, these heptads can be used to define the distance between a methylation site and the hairpin turn.

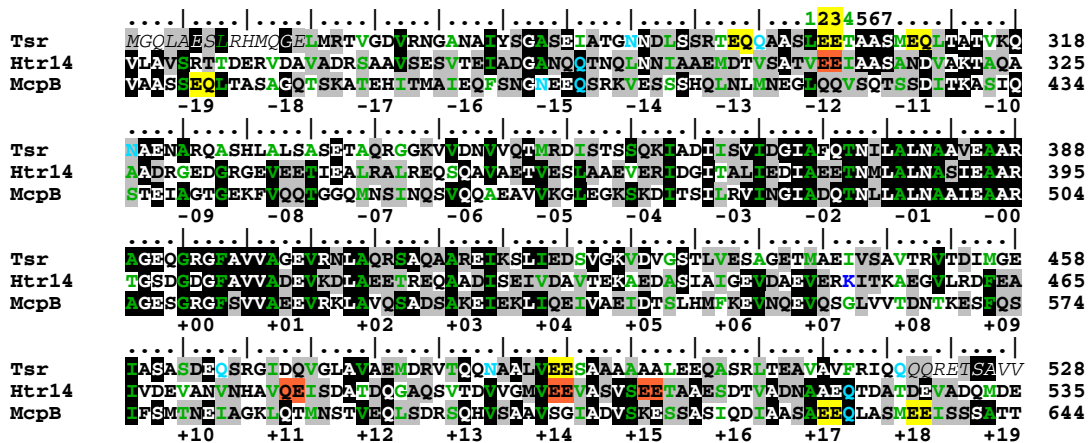


Figure 3.20 Hydrophobic heptads in the putative coiled-coil regions of Tsr, Htr14 and McpB.

An ungapped alignment of *E. coli* Tsr (249-528), *H. salinarum* Htr14 (256-535) and *B. subtilis* McpB (365-644) demonstrates high homology within the signaling region (identical residues are highlighted in black, similar residues according to the BLOSUM62 matrix in grey). It furthermore reveals an uninterrupted succession of hydrophobic heptads in which positions 1 and 4 (numbering as indicated above the alignment) are made up almost entirely of hydrophobic residues, Ser or Thr (green). Only occasionally Gln or Asn are present at these positions (turquoise) and charged residues are completely absent, with the exception of one Lys in Htr14 (blue). Heptads were designated according to the following scheme: the two heptads containing the hairpin turn of the coiled coil (according to the cTsrQ structure of Kim *et al.* (1999)) were named -0 and +0. To neighboring heptads increasingly higher numbers were assigned with increasing distance from the turn. Attributed signs are negative towards the N-terminus and positive towards the C-terminus. Published methylation sites of Tsr and McpB (highlighted yellow) in each case comprise a pair of Glx residues at heptad positions 2 and 3 in some of the heptads ≥ 11 and ≤ 19 . All Glx pairs present in Htr14 at heptad positions 2 and 3 in the described regions (highlighted orange) are considered as potential candidates for methylation sites.

Using this heptad-numbering scheme, the published methylation sites of *E. coli* Tsr localize to the Glx-pairs at positions 2 and 3 of heptads -11, -12, -13 and +14, whereas those of *B. subtilis* McpB localize to the Glx-pairs at the corresponding positions in heptads +17, +18 and -19. An inspection of all Htr14 heptads from -19 to -11 and from +11 to +19 shows 4 Glx pairs

comprising positions 2 and 3 of heptads +11, -12, +14 and +15, which represent a first selection of candidates for methylation sites in Htr14.

As shown on a model of the cytoplasmic region of Htr14 (Fig. 3.21), the residue pairs at positions 2 and 3 of each group of 4 heptads of the same absolute value are arranged within the transducer dimer in a plane perpendicular to the coiled coil's long axis. Although the described arrangement is only clearly seen in the model up to approx. heptads +/-10 (at greater distances from the hairpin turn, the helices fly apart in the cTsrQ structure), a continuation of the perfect coiled-coil structure is expected beyond this position for Tsr and the other transducers because of the unchanged persistence of the heptad pattern. If this is the case, one would predict that positions 2 and 3 in heptads -11, -12, -13 and +14 (which represent the methylation sites in Tsr) form two faces of successive sites, one on each side of the Tsr (or Htr14) dimer. When looking at positions 2 and 3 of heptads -1, -2, -3 and +4, for which the relative arrangement within the coiled coil is expected to be identical to that in heptads -11, -12, -13 and +14, the presence of these positions on one face of the dimer is clearly seen for the monomer depicted as spheres in Fig. 3.21. A similar arrangement on opposite faces of the dimer is predicted for positions 2 and 3 in heptads +17, +18 and -19 of McpB (or Htr14). This finding points to a possible scheme for the arrangement of methylation sites and predicts that in a particular transducer methylation sites should not be expected in two heptads of the same number but with opposite signs.

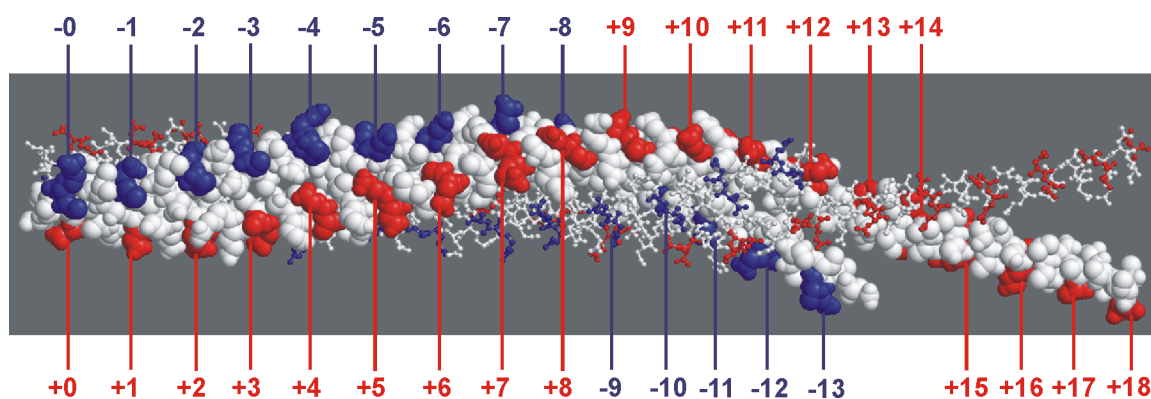


Figure 3.21 Heptad positions 2 and 3 within the coiled coil of Htr14 (modeled on the cTsrQ-structure). Structural model of the presumptive coiled coil region of dimeric Htr14 generated via SWISS MODEL (Schwede *et al.*, 2003) using the coordinates of the cTsrQ structure of Kim *et al.* (1999). The two monomers are depicted as spheres, and as balls and sticks, respectively. Residues at positions 2 and 3 of the heptads, which were numbered according to Fig. 3.20, are indicated in blue if they are N-terminal and in red if they are C-terminal of the coiled coil's hairpin turn. Especially in the region of the model, which contains heptads 0 to 10, all 4 helices comprising the coiled coil are closely contacting each other, as expected for such a structure. Here the residues at positions 2 and 3 of corresponding heptads from all 4 helices are located in a plane perpendicular to the coiled coil's long axis.

3.2.2 An evaluation of MALDI-TOF MS experiments provided first hints towards the detectability of methylated peptides via MS

To find out, whether methylated Htr peptides can in principle be detected via MS, MALDI-TOF (matrix-assisted laser desorption/ionization-time of flight) MS spectra, which had led to the identification of Htrs in the course of the ongoing lab-project of *H. salinarum* proteome analysis (Klein *et al.*, 2005; Tebbe *et al.*, 2005), were checked for the presence of peaks corresponding to putatively methylated peptides from these Htrs. These spectra had been obtained from peptide mixtures, which were generated by tryptic in-gel digest of silver-stained protein spots on 2-D gels of either cytosolic or membrane protein preparations.

Using the computer program Mascot (Matrix Science Inc., Boston, MA, USA), searches had been performed against a database containing all sequences of *H. salinarum* proteins that were predicted from the complete annotated genome sequence (<http://www.halolex.mpg.de>). These searches used the peak lists generated via MALDI-TOF MS of the described peptide mixtures. Spectra of those gel spots, in which one or more Htrs had previously (in the course of the proteome analysis) been identified by Mascot via an automated search algorithm called peptide mass fingerprinting (PMF), were checked manually for the presence of peaks, which correspond to the masses of peptides that contain potentially methylatable residues. Such peptides had been determined before as candidates for methylation by inspection of positions 2 and 3 of the relevant heptads, as described above for Htr14. In a number of cases, pairs of peaks with a mass difference of 14 Da were detected, in which the single peaks were consistent with the masses calculated for the unmethylated and the singly methylated form of such peptides. The difference of 14 Da is in accordance with the mass of a methylene group, which comprises the difference between a carboxyl group and its methyl ester. The described peak pairs were detected for some membrane-associated (Htrs 1, 2, 3, 4, and 6) as well as presumably cytosolic Htrs (Htrs 11 and 13). A selection is shown in Fig. 3.22.

For peptide A186 - R208 from cytosolic Htr13 and peptide A513 - R544 from membrane-associated Htr6, the masses observed in the spectra point to a deamidation of the pair's Gln residue to a Glu. The phenomenon of deamidation has been described for *E. coli* transducers but this was the first indication that deamidation also exists in *H. salinarum*. The peak observed at the mass corresponding to the deamidated and singly methylated form of the Htr13 peptide A186 - R208 has a much lower intensity than that corresponding to the unmethylated form of the deamidated peptide. This suggests that Htr13 is methylatable at this site (probably only after

preceding deamidation), but in the investigated protein sample only a small fraction of Htr13 was actually carrying a methyl group there.

Fig. 3.22G shows a complete spectrum of a peptide mix, which results from a 2-D gel spot containing Htr3 and Htr6. Three isolated peak pairs, each comprising a difference of 14 Da, can

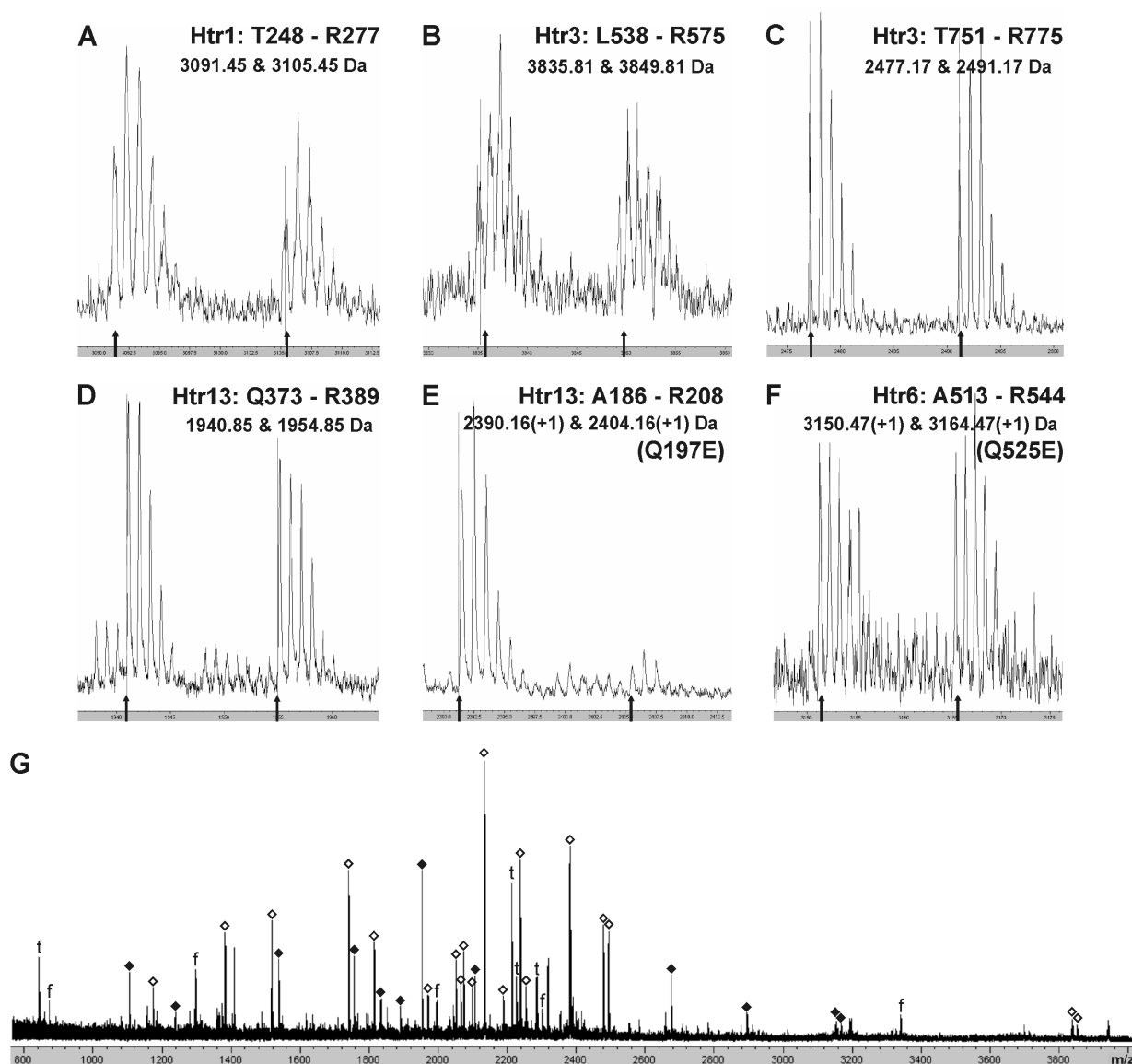


Figure 3.22 MALDI-TOF mass spectra of some methylatable Htr peptides resulting from tryptic digests of protein spots from 2-D gels.

Proteins were obtained from a total membrane protein preparation of strain TOM (A, B, C, F, G) or from a fraction of a cytosolic preparation of the same strain, generated by size exclusion chromatography (D, E). Samples were prepared and subjected to 2-D gel electrophoresis, tryptic digest and MALDI-TOF MS analysis, as described in Materials and Methods. (A-F) Arrows mark the exact positions on the m/z axis that correspond to the masses of the unmethylated and singly methylated Htr peptides after protonation ($[M-H]^+$), as listed above the spectrum. In the case of E and F the observed masses are 1 Da higher than calculated but match exactly if a deamidation is assumed that converts the Gln of each peptide to a Glu. (G) Complete spectrum obtained from a gel spot containing Htr3 and Htr6. Peaks matching the calculated masses within a range of < 200 ppm are attributed to peptides from Htr3 (open diamonds) and Htr6 (filled diamonds). Peaks which are frequently observed in other MALDI spectra of similar preparations were marked t (for trypsin fragments) and f (for other unassigned frequently observed peaks). Note the pairs of peaks differing by 14 Da (the mass of a CH_2 -group) which are centered at approx. 2484, 3158 and 3843 Da.

be clearly seen and correspond to the masses expected for the unmethylated and singly methylated forms of two peptides from Htr3 and one from Htr6.

Although this analysis of MALDI-TOF MS spectra has demonstrated for the first time, that methylated Htr peptides can be detected via MS and that the methylation sites are present in peptides which were predicted to be methylated, the approach has several drawbacks (Table 3.2). (i) Only 11 of the 18 Htrs could be identified as yet via this method. (ii) The putatively methylatable peptides produced by tryptic digest of Htrs are rather large, due to a low content of Lys and Arg residues in the methylatable regions. The peptide sizes therefore often exceed the detection limit of the method, or the detected mass peaks have only a low intensity, hardly above the background. (iii) MALDI-TOF MS analysis cannot unambiguously assign a particular peptide to a mass peak, due to the lack of additional fragmentation information. (iv) Furthermore, no information is provided about the methylation positions within the peptides.

Table 3.2. Comparison of the number of residues in those Htr-peptides that contain the putative methylation site at heptad position -12 and were generated by digestion with either trypsin or Asp-N.

<i>Htr</i>	1	2	3	4	5	6	7	8	9	10	11	12	13	14	15	16	17	18
tryptic peptide ^a	<u>30</u>	<u>40</u>	<u>38</u>	<u>33</u>	39	<u>32</u>	42	28	59	20	<u>31</u>	49	<u>23</u>	48	84	56	35	33
Asp-N- peptide ^b	<u>16</u>	<u>17</u>	<u>17</u>	<u>14</u>	<u>13</u>	<u>22</u>	<u>18</u>	<u>13</u>	32	20	28	13	17	<u>15</u>	31	21	21	<u>13</u>

a: Underlining indicates that peaks with masses consistent with those of the unmethylated and singly methylated forms of the corresponding peptide were identified via MALDI-TOF MS in the course of the *H. salinarum* proteome analysis project in the lab. Italicized numbers correspond to peptides which exceed the detection range of the MS setup (800 - 4,000 Da). Strike-through indicates that the corresponding Htrs have, so far (until August 2005), completely escaped an identification via MALDI-TOF MS.

b: Double underlining indicates that the corresponding peptide was identified via LC ESI Q-TOF MS/MS in the course of this study.

3.2.3 LC ESI Q-TOF MS(/MS) after in-gel Asp-N digestion of the respective Htrs is the method of choice to investigate Htr-methylation

To obtain information about as many methylation sites as possible in a high number of Htrs, a different approach had to be taken, with the aim to overcome the drawbacks of the described MALDI-TOF MS method. The fact that 7 Htrs completely escaped the detection via this method might partly be due to a low content of these transducers in the cell and therefore on the 2-D gels. The finding, that Htrs present in the membrane protein fraction were shown via immunoblot to comigrate with bands visible after Ponceau S-staining of the corresponding nitrocellulose blots (Fig. 3.23), suggested that the staining of these bands might be due to the presence of Htrs at these positions. An immunoblot was generated with antiserum HC23 (Zhang

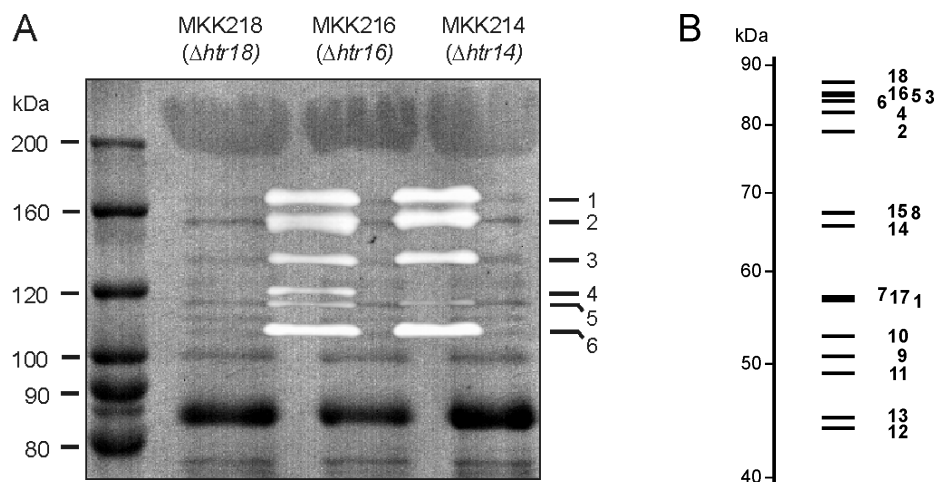


Figure 3.23 Htr positions on a nitrocellulose blot after SDS PAGE of membrane protein preparations from different *htr*-deletion mutants derived from strain S9, and calculated gel-band pattern of the Htrs.

(A) After 8 % polyacrylamide gel electrophoresis of the membrane protein fractions from the indicated strains (20 μ g total protein per lane), proteins were blotted onto a nitrocellulose membrane and visualized by Ponceau S staining. The pattern of bands on X-ray film, obtained for the MKK216 and MKK214 lanes after immunodetection with anti-Htr-signaling-region antiserum HC23 (obtained from M. Alam) and anti-rabbit IgG (Sigma) as secondary antibody, is shown as an overlay of white bands. The overlay is slightly shifted to the left of the corresponding lanes on the blot to better visualize the correlation of immunological 1, 2, 3 and 5 to the Ponceau S-stained bands. Immunosignal 4 is absent for the *htr14*-deletion strain MKK214 and can therefore be attributed to Htr14. Immunosignal 6 results from Htr1, as it is absent in strains lacking Htr1 (not shown). (B) Theoretical band pattern on the basis of the calculated molecular masses of the Htrs. Numbers attributed to the theoretical bands refer to the corresponding Htrs.

et al., 1996), that was raised against the peptide VIDIAEQTNMLALNASIEAARAG representing the conserved signaling region of the Htrs (but lacking an amino acid between I2 and D3, which is present in all 18 Htrs and was not included in the peptide for unknown reasons). The blot identified membrane-bound Htrs in the region corresponding to apparent molecular weights (MWs) between approx. 105 and 170 kDa. The apparent agreement of the immunosignals with several bands on the blot suggested that membrane-bound Htrs might represent the most abundant protein species at this MW range in SDS-PAGE gels, although their calculated MWs range from 56.6 kDa for Htr1 to 87.0 kDa for Htr18 (Fig. 3.23B). If Htrs comprise a considerable part of the proteins in this region, then slices from 1-D gels instead of spots from 2-D gels could be used for MS analysis. This would allow to easily obtain bigger amounts of Htrs and maybe to identify also Htrs of low abundance.

To overcome the low detection efficiency of the large peptides, which result from tryptic digest of the putatively methylatable regions of Htrs, a different protease was chosen. Asp-N, which specifically cleaves polypeptides N-terminally of aspartate residues, produces peptides of more appropriate sizes and is therefore better suited for the analysis of Htr methylation (Table 3.2).

Information about the methylation site(s) within a peptide or even about the exact position(s) of the methylated residue(s) can be obtained via fragmentation of the methylated peptide followed by MS analysis of the fragments. To achieve this, the technique of LC ESI Q-TOF (liquid chromatography electrospray ionization quadrupole time-of-flight) MS/MS was chosen. The chromatographical separation of the peptide mixture on a reversed phase column was followed by nanospray ionization and analysis of the thereby generated peptide ions via Q-TOF MS/MS. The chromatography step provided a second level of separation after the gel electrophoresis. This was especially important because the 1-D gel slices contained mixtures of several different proteins. The resulting peptide mixtures were therefore rather complex and could not be resolved properly when applied directly to the mass spectrometer in an "offline measurement" (data not shown).

In a number of independent experiments, slices from Coomassie-stained 1-D SDS-PAGE gels of membrane protein preparations from wild-type strain S9 or from $\Delta cheB$ strain WFS101 were excised from several gel lanes. In each experiment, the corresponding slices were pooled to increase the amount of protein and treated as described in Materials and Methods. The exact positions of the gel slices, and the Htrs identified in each of these slices are shown for an S9 membrane protein preparation (Fig. 3.24). In addition to the 12 detected Htrs, approx. 20 - 25 other proteins could be identified in the region between approx. 100 and 160 kDa. Some of these

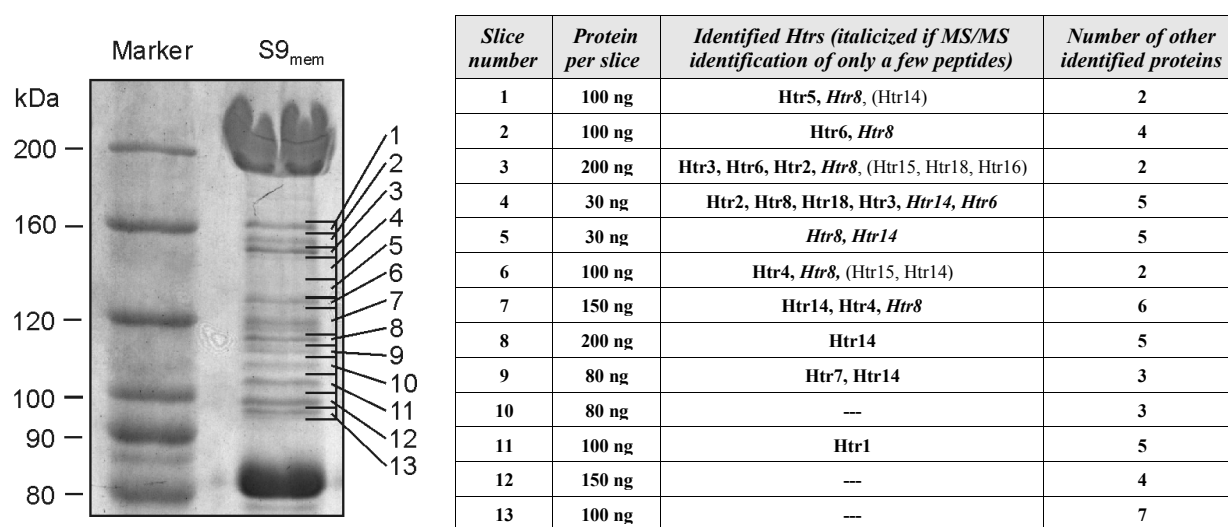


Figure 3.24 Positions of the excised gel slices used for LC ESI Q-TOF MS/MS analysis and the Htrs identified in these slices.

Gel slices were excised, as indicated, from an SDS polyacrylamide gel (8%) of a membrane protein preparation from strain S9 (15 μ g per lane), which was obtained as described in Materials and Methods. Protein amounts in each slice were estimated from the intensity of the Coomassie stain by comparison to the known amounts of marker proteins (approx. 500 ng per band). In each case, identical slices from 6 lanes were pooled for subsequent Asp-N-digests and LC ESI Q-TOF MS/MS analysis. Htrs identified in the slices of the depicted gel are listed. Htrs, which were additionally identified at the corresponding gel positions in comparable experiments are added in parentheses. Furthermore, the number of reliably identified additional proteins is given for each slice.

non-Htr proteins were detected in several different slices (8 out of 13 slices in the case of the cell surface glycoprotein, which mainly migrates as a very thick band centered at approx. 200 kDa). For most slices from this region either the majority of all MS/MS-identified peptides resulted from Htrs (slices 1, 3, 4, 6 and 8) or an Htr was the protein with the highest number of identified peptides (slices 9 and 11). The inferred prevalence of Htrs in the mentioned gel-slices and their relative positions on the gel suggested the following assignment of the gel-slices shown in Fig. 3.24 (including their major Htr species) to the immunobands of Fig. 3.23: slice 1 (Htr5) to band 1, slices 3 and 4 (Htrs 2, 3, 6, 8, 18) to band 2, slice 6 (Htr4) to band 3, slices 7/8 (Htr14) to band 4, slice 9 (Htr7) to band 5 and slice 11 (Htr1) to band 6. The remaining slices either contained only minor amounts of Htrs, or Htrs were not detected at all. The thereby proposed positions of the different Htrs on the gel is only partly consistent with that expected from the calculated MWs, which points to a significant influence of one or more additional Htr characteristics on their mobilities, besides the MW. The positions at which Htrs could be identified in the gel of Fig. 3.24 are in good agreement with the results obtained in similar experiments.

The identification of Htr14 peptides in slices 4 to 9 is consistent with the detection of several distinct Htr14 immunosignals in the region between approx. 115 and 150 kDa (Fig. 3.10). Similarly, peptides of Htr8 were identified in slices 1 to 7. These findings might hint to the existence of several different species not only of Htr14 but also of Htr8, which can be distinguished by their different mobilities on SDS PAGE gels.

3.2.4 Mascot MS/MS ions searches with the detected peptide fragment masses identified differently methylated forms of certain Htr peptides

The fragment masses detected in the Q-TOF MS/MS experiments were used to search for matches in different databases using the MS/MS ions search option of the program Mascot. Three different databases were used: (i) One contained the complete set of 2821 sequences of halobacterial proteins according to the annotation status of Halolex (<http://www.halolex.de>) in September, 2004. It was used to find out how many proteins could be detected in the respective gel slices. (ii) A second database contained the sequences of the 18 Htrs, and additionally a number of modified peptide sequences, which were derived from the peptide sequences obtained by theoretical Asp-N digestion of these Htrs, by allowing glutamine deamidation to glutamate at potential methylation sites. The Htr regions, within which such modifications were considered, were predicted via alignments of Htrs with *E. coli* Tsr and *B. subtilis* McpB, for which the methylation sites are known. These regions comprise all sites which were considered to be

potentially methylatable, i. e. all sites containing a pair of Glx residues, or a pair of an Asp and a Glx residue, at heptad positions 2 and 3, which are located in the region between and including heptads 11 and 19. This database was normally used to identify Htr peptides, which can become deamidated and/or methylated. (iii) To check if deamidations can also occur at unexpected sites, a third database was used. In addition to the sequences of peptides generated by *in silico* Asp-N-digestion of all Htrs, it furthermore contained sequences of peptide species derived from these peptides. These species were generated by producing all sequence permutations after allowing for all single or multiple replacements of glutamines by glutamates or asparagines by aspartates, followed by a second *in silico* Asp-N digestion. This additional step was necessary because each replacement of an Asn by an Asp created an additional Asp-N cleavage position (as Asp-N cleaves specifically N-terminally of Asp but not of Asn). To illustrate the contents of the second and third databases, their first entries are shown in Table 6.3.

Using the third database, no additional peptides were identified in any of the investigated peptide mixtures. It is therefore unlikely that Asn residues anywhere in the Htrs, or Gln residues at positions different from those within the potentially methylatable Htr regions are subject to deamidation in the cell.

A comparison of the retention times of the MS/MS-identified unmethylated, singly methylated and doubly methylated forms of Htr peptides eluting from the LC column revealed that per added methyl group the peptide eluted approx. 2 to 3 min later. The retention times of the differently methylated forms of the peptide were therefore used as an important additional criterion besides the identification of the different peptide forms via MS/MS. Fig. 3.25 shows the situation for the different forms of peptide DEMSATIEEVAASA of Htr4, which were obtained once (A) from wild-type strain S9 and once (B) from the $\Delta cheB$ mutant WFS101, which lacks the putative methylesterase CheB and was therefore predicted to contain maximally methylated transducers. In case of the S9 preparation, the form containing a doubly methylated glutamate pair was not identified via MS/MS. However, as shown in Fig. 3.25B, it is clearly present in the preparation containing Htr4 from WFS101, where it eluted approx. 2 min after the singly methylated form. The fact, that in the MS spectrum resulting from the S9 preparation a weak signal at the mass expected for the doubly methylated peptide was found approx. 2 min after the elution of the singly methylated form, suggests that the doubly methylated form was also present in S9. The low signal intensity might have been the reason why no MS/MS spectrum was recorded.

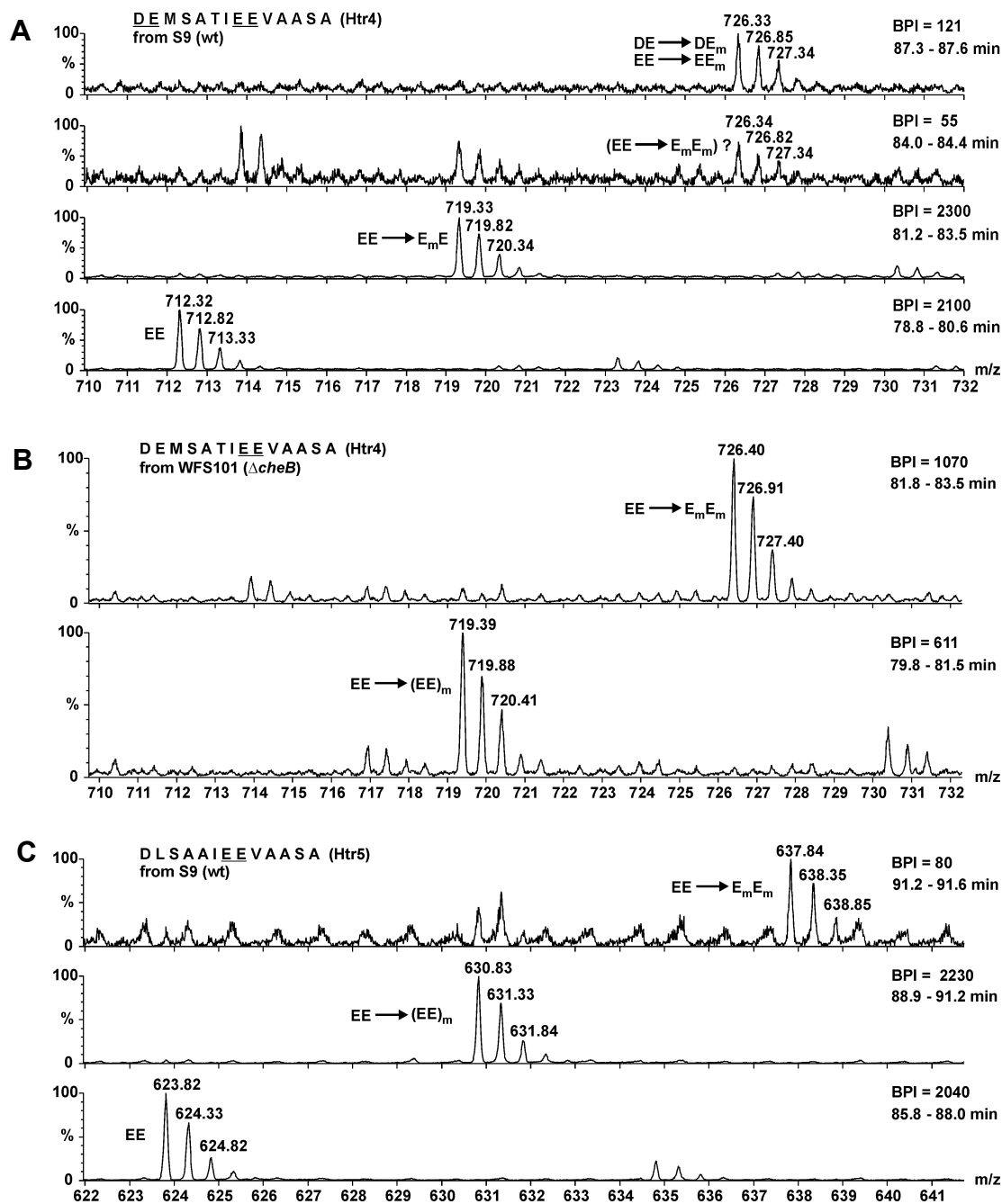


Figure 3.25 MS spectra in the mass-per-charge (m/z) ranges of the differently methylated forms of those peptides of Htr4 and Htr5 that contain the first methylatable site, present in heptad -12.

Peptide sequences are shown with the methylation sites underlined. All spectra result from the integration of the signals obtained within the complete time of elution (shown to the right) of those species whose mass is annotated. The intensity of the highest peak in each spectrum (BPI) is given in arbitrary units and can be used for a crude estimation of the relative abundance of the different species. An E followed by a subscript m indicates the methylated glutamate residue identified via MS/MS. A glutamate pair in parentheses followed by a subscript m indicates that MS/MS did not clearly determine, which of the glutamates within the pair was methylated. (A) Peaks corresponding to the unmethylated, singly and doubly methylated forms of the Htr4 peptide from S9 cells. The question mark indicates the absence of an MS/MS spectrum for the corresponding (putative) peptide species. (B) Peaks corresponding to the singly and doubly methylated form of the same peptide, this time from the $\Delta cheB$ mutant WFS101. No significant peaks were present at the m/z value of the unmethylated peptide after integration of the signals measured between 70 and 80 min (data not shown). (C) Peaks corresponding to the unmethylated, singly and doubly methylated forms of the Htr5 peptide from S9 cells.

In addition to the proposed DEMSATIEEVAASA species that carries both methyl groups within the Glu pair, another doubly methylated form of this peptide was identified via MS/MS (Fig. 3.27C), which carries the first methylgroup within the DE pair and the second one within the EE pair (Fig. 3.25A, upper spectrum). Though the MS/MS spectrum could not distinguish between a methylation of the Asp or the Glu residue of the first site, it is proposed that the Glu residue carries the methyl group, as there have been no confirmed methylations of Asp residues in any of the Htrs, so far. Moreover, one should expect that the methylation of the Asp residue would have prevented the Asp-specific cleavage by Asp-N. This is the first example of a transducer methylation site that consists of a DE pair. The discovery of a DE methylation site receives additional support from the detection of deamidation in up to three DQ pairs in Htr4 and Htr15, which are described in detail in Chapter 3.2.7. For none of these sites the mass spectrometrical analysis pointed to a methylation, but as deamidation is a prerequisite for methylation, one might expect that, after deamidation, these sites also become subject to methylation just like the DE pair in peptide DEMSATIEEVAASA.

A comparison of the relative intensities of the different forms of Htr4 peptide DEMSATIEEVAASA, obtained from S9 and WFS101, and of Htr5 peptide DLSAAIEEVAASA, obtained from S9, clearly shows an increased methylation in the absence of CheB (Fig. 3.25). Though the base peak intensities (BPI) of the MS spectra, which were integrated over the total time of elution of each peptide form, can only give a crude estimation of the relative amounts of the peptide forms (because the acquisition of MS spectra was permanently interrupted by the recording of MS/MS spectra), the tendency is obvious. The ratios of unmethylated to singly methylated to doubly methylated peptide forms were: (i) 2040 : 2230 : 80 for the Htr5 peptide from S9, (ii) 2100 : 2300 : ~50 for the Htr4 peptide from S9 and (iii) ~0 : 611 : 1070: for the same peptide from the $\Delta cheB$ mutant WFS101. This clear shift towards higher methylation in the absence of CheB is consistent with the Htr14 band patterns seen on immunoblots of membrane protein preparations from S9 and WFS101 (Fig. 3.10), and additionally supports a methylesterase function for CheB. The fact, that for Htr14 from the $\Delta cheR$ mutant WFS102 only the upper one of the main Htr14 bands was visible on this immunoblot, supported the expected methyltransferase function for CheR, and is consistent with the complete absence of methylated peptides in spectra obtained from Htr peptides, which were produced from WFS102 (data not shown).

While a DEMSATIEEVAASA species, which is methylated at both positions of the Glu pair, was only proposed on the basis of a peak of the correct mass within the expected time of elution

for this species, the doubly methylated form of DLSAAIEEVAASA was clearly identified via MS/MS (Fig. 3.29B). This is the first time that a double methylation was clearly identified within a transducer methylation site. The finding deserves special attention, because the peptide originated from a transducer that was obtained from wild-type cells. It therefore shows that double methylations at a single Glu pair can occur under physiological conditions in wild-type cells and do not necessarily require the functional knock-out of the methyltransferase CheB. However, in the absence of CheB the relative amount of the doubly methylated peptide form drastically increases relative to the situation in wild-type cells, as can be seen when comparing Figs. 3.25A and B. It is not clear why in the absence of CheB still differently methylated transducer species were present. One would expect that without the CheB methyltransferase activity CheR should convert all transducers to the state of highest possible methylation. The continued presence of partially methylated peptide species in the $\Delta cheB$ mutant hints to the presence of an additional methyltransferase or to the inaccessibility of certain methylatable residues to the methyltransferase CheR.

3.2.5 For a number of Htrs either the methylation sites or the individual methylated residues could be identified via tandem MS (MS/MS).

To illustrate how the identification of individual methylated residues in transducers was achieved via Mascot MS/MS ions searches using the peak lists generated in Q-TOF MS/MS experiments, the single steps shall be briefly described here.

Table 3.3 shows the beginning of a typical Mascot results page. The search against the database of all *H. salinarum* protein sequences produced a list of "significant hits", which comprises the proteins, for which the highest number of peptides were attributed to MS/MS spectra. With increasing hit number, the total score of the MS/MS identifications, which is a measure of the reliability of these identifications, decreases. In the case of a low score, individual inspections of the MS/MS spectra become necessary to decide whether or not to trust the suggested identification. Following these suggested protein identifications on the results page, are lists of those peptide species of each identified protein, which were attributed to MS/MS spectra.

The score of each suggested peptide identification increases with the number of experimentally determined fragment masses, which could be matched to the calculated masses. The performed Q-TOF MS/MS experiments mainly produced peptide fragments of the b- and y-series, which comprise the sets of N-terminal and C-terminal fragments, respectively, after fragmentation by disruption of a single peptide bond at all possible positions within the peptide species (Fig.

3.26). The peptides generated by Asp-N were usually fragmented into y- and b-series of comparable intensities, contrary to tryptic peptides, which all contain a C-terminal Arg or Lys, so that their fragmentation produces a y-series of considerably higher intensity compared to the

Table 3.3. Example of a Mascot MS/MS ions search result: suggested protein-identifications and peptide-list underlying the identification of the first protein.

MS data file : bea125_6.raw
Database : Hsal_ok_040923 (2821 sequences; 787650 residues)

Significant hits:

1. OE1536R transducer protein Htr14
2. OE1737R DnaK-type molecular chaperone Hsp70
3. OE6059R iron-sulfur protein homolog/glycerol-3-phosphate dehydrogenase homolog
4. OE3167F transducer protein HtrVIII
5. OE5203F arginine--tRNA ligase (EC 6.1.1.19)
6. OE3474R transducer protein CoST
7. OE1500R pyruvate, water dikinase (EC 2.7.9.2) (phosphoenolpyruvate synthase)
8. OE2871F probable 3-hydroxyacyl-CoA dehydrogenase (EC 1.1.1.157)

1.	OE1536R (transducer protein Htr14)			Mass: 65616 Da	Score: 1585	Queries matched: 44	
RT	Observed	Mr(expt)	Mr(calcd)	Delta	Miss	Score	Expect Peptide
50.3	382.683	763.351	763.339	0.013	1	9	1.6 DDFTVPA
68.3	386.177	770.339	770.381	-0.042	0	12	0.84 DEPAAAVV
67.6	416.240	830.465	830.439	0.027	0	9	3 DIGITALIE
38.2	431.698	861.382	861.408	-0.026	0	46	0.00037 DAVTEKAE
40.8	437.717	873.420	873.419	0.001	1	16	0.63 DERVDAVA
47.8	446.216	890.418	890.461	-0.043	0	32	0.0087 DALARQAF
51.5	446.231	890.447	890.461	-0.014	0	(14)	0.62 DALARQAF
39.8	454.205	906.396	906.393	0.003	0	19	0.14 DSGGESVAVS
39.1	473.245	944.476	944.493	-0.017	0	44	0.00076 DVAKTAQAAA
42.8	516.777	1031.539	1031.561	-0.022	0	53	7.2e-005 DAVLAVSRTT
38.0	518.207	1034.399	1034.415	-0.016	1	51	9.9e-005 DNAAEQTDAT
86.7	526.274	1050.533	1050.523	0.010	0	46	0.00042 DEIASLVASF
38.1	529.200	1056.385	1056.436	-0.051	1	49	0.0001 DQPQPASDAE
39.8	535.238	1068.461	1068.472	-0.011	1	51	0.00013 DDSPTAQPPAA
38.8	546.735	1091.456	1091.473	-0.017	1	55	4.2e-005 DATDQGAQSVT
81.8	566.292	1130.570	1130.586	-0.016	0	31	0.012 DFVEPLVALE
45.4	580.789	1159.564	1159.583	-0.020	1	56	3.4e-005 DAARAGDLTATV
88.4	582.294	1162.574	1162.587	-0.013	0	43	0.00067 DFNQLLETLA
88.1	583.784	1165.553	1165.550	0.002	1	62	8.9e-006 DDEIASLVASF
47.2	597.252	1192.490	1192.536	-0.046	1	62	7.8e-006 DDIAAGEFERA
41.4	616.773	1231.531	1231.568	-0.037	0	58	2e-005 DLAEETREQAA
65.1	620.781	1239.547	1239.551	-0.004	0	50	0.00014 DSLEAYTAELE
85.2	716.854	1431.693	1431.691	0.001	0	101	1.1e-009 DELAEQTAALAGML
48.9	717.847	1433.680	1433.700	-0.019	0	(52)	8.6e-005 DRSAAVSESVTEIA
52.6	717.861	1433.707	1433.700	0.007	0	61	1.3e-005 DRSAAVSESVTEIA
75.2	724.852	1447.689	1447.686	0.002	0	(52)	0.00011 DELAEQTAALAGML (M-oxid.)
73.0	739.362	1476.709	1476.694	0.015	0	(50)	0.00013 DTVSATVEEIAASAN
75.8	746.365	1490.715	1490.710	0.006	0	69	1.7e-006 DTVSATVEEIAASAN (D/E-methyl.)
45.5	753.359	1504.704	1504.694	0.010	0	97	2.6e-009 DGMQSNLEVASRQA
41.3	761.353	1520.691	1520.689	0.002	0	(89)	1.5e-008 DGMQSNLEVASRQA (M-oxid.)
51.9	762.871	1523.728	1523.722	0.006	0	61	1.1e-005 DEVANVNHAVQEIS
43.0	767.340	1532.665	1532.648	0.018	1	54	4.7e-005 DEEGVPDSGGESVAVS
83.1	774.368	1546.721	1546.718	0.002	1	26	0.031 DELAEQTAALAGMLD
74.2	820.365	1638.716	1638.708	0.008	0	63	5.9e-006 DESVPGAFGESITEMA
61.9	611.266	1830.775	1830.817	-0.041	0	(53)	3.4e-005 DGANQQTNQLNNAEEM
61.8	916.423	1830.832	1830.817	0.015	0	(61)	9.9e-006 DGANQQTNQLNNAEEM
44.9	924.422	1846.829	1846.811	0.017	0	112	6.9e-011 DGANQQTNQLNNAEEM (M-oxid.)
91.8	1019.467	2036.919	2036.910	0.010	0	(55)	2.2e-005 DVVGMVEEVASVSEETAAES
93.2	684.645	2050.913	2050.925	-0.012	0	(41)	0.00058 DVVGMVEEVASVSEETAAES (D/E-methyl.)
93.5	1026.477	2050.940	2050.925	0.014	0	91	6.9e-009 DVVGMVEEVASVSEETAAES (D/E-methyl.)
79.8	685.304	2052.891	2052.904	-0.014	0	(10)	0.63 DVVGMVEEVASVSEETAAES (M-oxid.)
79.8	1027.467	2052.920	2052.904	0.016	0	(29)	0.01 DVVGMVEEVASVSEETAAES (M-oxid.)

The original list was slightly changed in its format and edited manually: The columns QUERY and RANK were removed, and the approx. retention times in minutes (RT) for the generation of the MS/MS spectra were added. Accounted modifications were: methionine oxidation (M-oxid.) and methyl esterification of D or E (D/E-methyl.). Information on Mascot search results in general can be found at <http://www.matrixscience.com>.

b-series. Table 3.4 shows, as a typical example, an overview of the calculated fragment masses for one of the peptides listed in Table 3.3, with the matches to experimentally determined fragment masses indicated. The big advantage of the MS/MS analysis of Htr peptides is that not only the number of methyl groups present on a peptide can be identified, but also the approximate or even the exact position of the methyl group on the peptide, depending on the quality of the spectrum.

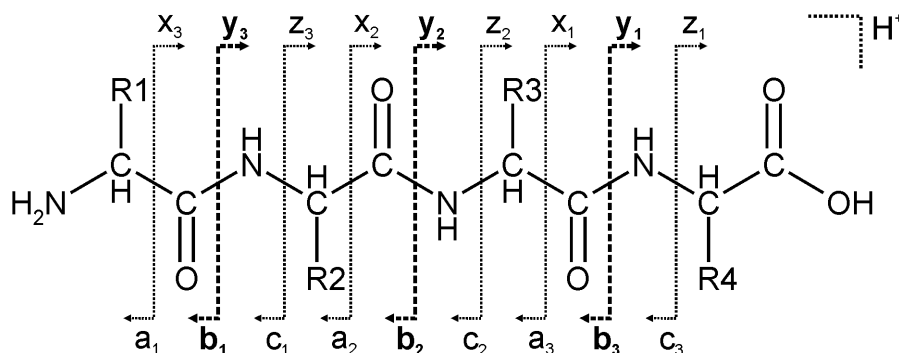


Figure 3.26 Fragments of the b- and y-series comprise the major part of the peptide-fragments generated during ESI-Q-TOF MS/MS analysis.

Collision-induced fragmentation of peptides leads to mostly singly-charged fragments. The charge resulting from protonation can either be positioned on the fragment comprising the N-terminal part (a-, b- and c-fragments) or on that comprising the C-terminal part (x-, y- and z-fragments). Bond breakage occurs most frequently within the peptide bonds generating b- and y-fragments, which are numbered as indicated.

In the depicted list of fragment masses, the determined matches suggest a methylation at E8 of peptide DTVSATVEEIAASAN of Htr14. A closer look at the MS/MS spectrum was needed (Fig. 3.28D), however, to confirm the suggestion of the Mascot search. It had to take into consideration the peak intensities and check for the absence of peaks which would be expected if E9 instead of E8 were methylated. The spectrum shows almost complete sets of b- and y-fragments and some additional a-fragments. As only Asp or Glu residues can in principle be converted to methyl esters, information about the methylation site is provided by all b-fragments smaller than b₈ or b₉ and by all y-fragments greater than y₆ or y₇ (depending on the methylation position), because only these fragment masses would be different if the Asp instead of one of the Glu residues were methylated. To determine the exact methylation position within the Glu pair, however, only the masses corresponding to fragments b₈ and y₇ can be used, because all other b- and y-fragments would have the same mass, whether E8 or E9 carried the methyl group. A search within the MS/MS spectrum for alternative masses differing from those of b₈ or y₇ by 14 Da, which would be expected for the E9 methylation, did not identify significant peaks. This supported the Mascot identification of E8 as the methylated residue in this Htr14 peptide.

Table 3.4. Mascot search result for the MS/MS fragmentation of the singly methylated Htr14-peptide DTVSATVEEIAASAN which was specified in the peptide list of Table 3.3.

Monoisotopic mass of neutral peptide Mr(calc): 1490.71

Variable modifications: E8 Methyl ester (DE)

Ions Score: 70 **Expect:** 5.6e-008

Matches (Bold Red): 83/215 fragment ions using 107 most intense peaks

#	<i>a</i>	<i>a</i> ⁰	<i>b</i>	<i>b</i> ⁰	Seq.	<i>y</i>	<i>y</i> ⁰	#
1	88.04	70.03	116.03	98.02	D			15
2	189.09	171.08	217.08	199.07	T	1376.69	1358.68	14
3	288.16	270.14	316.15	298.14	V	1275.64	1257.63	13
4	375.19	357.18	403.18	385.17	S	(1176.57)	1158.56	12
5	446.22	428.21	474.22	456.21	A	1089.54	1071.53	11
6	547.27	529.26	575.27	557.26	T	(1018.51)	1000.49	10
7	646.34	628.33	674.34	656.32	V	917.46	899.45	9
8	789.40	771.39	817.39 [b ₈ [!] : 803.39]	799.38 [b ₈ ⁰ : 785.38]	E _m	818.39	800.38	8
9	918.44	900.43	946.44	928.43	E	675.33 [y ₇ [!] : 689.33]	657.32 [y ₇ ⁰ : 671.32]	7
10	1031.53	1013.51	1059.52	1041.51	I	546.29	528.28	6
11	1102.56	1084.55	1130.56	1112.55	A	433.20	415.19	5
12	1173.60	1155.59	1201.59	1183.58	A	362.17	344.16	4
13	1260.63	(1242.62)	1288.63	1270.62	S	291.13	273.12	3
14	1331.67	1313.66	1359.66	1341.65	A	204.10		2
15					N	133.06		1

The list contains the calculated fragment masses for this peptide in case of a methylation at E8. Matches to the experimentally determined fragment masses are shown in red. A manual evaluation of the MS/MS spectrum showed that the values in parentheses were incorrectly assigned by the used algorithm. The b'- and y'-fragment masses which would be different for a methylation at E9 instead of E8 were manually added in brackets. The superscript zero indicates the loss of a water molecule (18 Da) from the corresponding fragment. The corresponding MS/MS spectrum is shown in Fig. 3.28D.

Similar analyses of Mascot results were performed in the course of this study for each of the identified methylation sites or methylation positions in Htr peptides. Some examples of MS/MS spectra will be discussed below to illustrate the different levels of information provided by these spectra, depending on their quality.

3.2.6 MS/MS spectra can provide different levels of information concerning the methylation of transducer peptides

Fig. 3.27 shows MS/MS spectra, which were attributed via Mascot to different forms of the Htr4 peptide DEMSATIEEVAASA. The MS/MS spectra were recorded within the time of elution of the different molecular species shown in Fig. 3.25A and B. This provided the basis for the attribution of the MS/MS-identified peptide forms to these integrated MS spectra. Whereas spectra A and B of Fig. 3.27 show most of the peaks well above the background level, spectra C

and D are of poorer quality and display a high level of background signals. However, as the elution times of the corresponding species are in agreement with the finding that per added methyl group the peptides elute approx. 2 - 3 min later, even the spectra of lower quality were considered to have reliably identified the peptide species.

Unambiguous identifications of the methylation positions in peptides can be based on either (i) the presence of significant mass peaks only for a methylation at one and not for the alternative methylation at the other residue of a methylation site or (ii) the complete absence of another methylatable residue within the complete peptide or at the identified methylation site.

The case of two potentially methylatable residues at a methylation site is shown in Fig. 3.27B. Here the presence of significantly higher peaks corresponding to the masses of fragments y6 and b8, as compared to peaks corresponding to the masses of fragments y6' and b8' (which would be expected in case of a methylation at the other Glu of the pair), argues for a methylation exclusively at or at least with a strong preference for the indicated position. Similar situations are depicted for two peptides from Htr14 (Fig. 3.28C and D). In both cases the MS/MS spectra unambiguously identified the exclusive (or strongly preferred) methylation position in the respective peptide.

Examples of unambiguous identifications of the methylation position due to the absence of a second methylatable residue are shown in Fig. 3.28A and B. The detection of the methylated form of Htr4 peptide DAAAEQATTLS is of particular interest, because it demonstrates that this peptide includes a physiological methylation site, which contains an Ala residue (at heptad position 2), a finding that was unprecedented. This might shed new light on the fact that Perazzona and Spudich (1999) saw a methylation in Htr1 only for the mutated methylation site containing the residues Glu265Ala266 but not for Ala265Glu266. At the first glance, the fact that methylation is seen in Htr4 at the site Ala738Glu739 seems to contradict the finding that in Htr1 methylation was only seen for the reverse order of residues. However, the investigated sites are located within the N-terminal methylatable region of Htr1, and the C-terminal methylatable region of Htr4, respectively. The methylatable Glu is therefore in both cases pointing away from the signaling region, so that the Ala-containing methylatable sites have the same spatial orientation within the transducer dimers. The detection of a methylation in Htr2 peptide DEVAGISQETAAQATAVA (obtained from the $\Delta cheB$ mutant WFS101) points to a second methylation site in addition to the one identified by Perazzona and Spudich (1999), and might explain why they saw some remaining methylation after mutating the methylation site Glu513Glu514 to a pair of alanines.

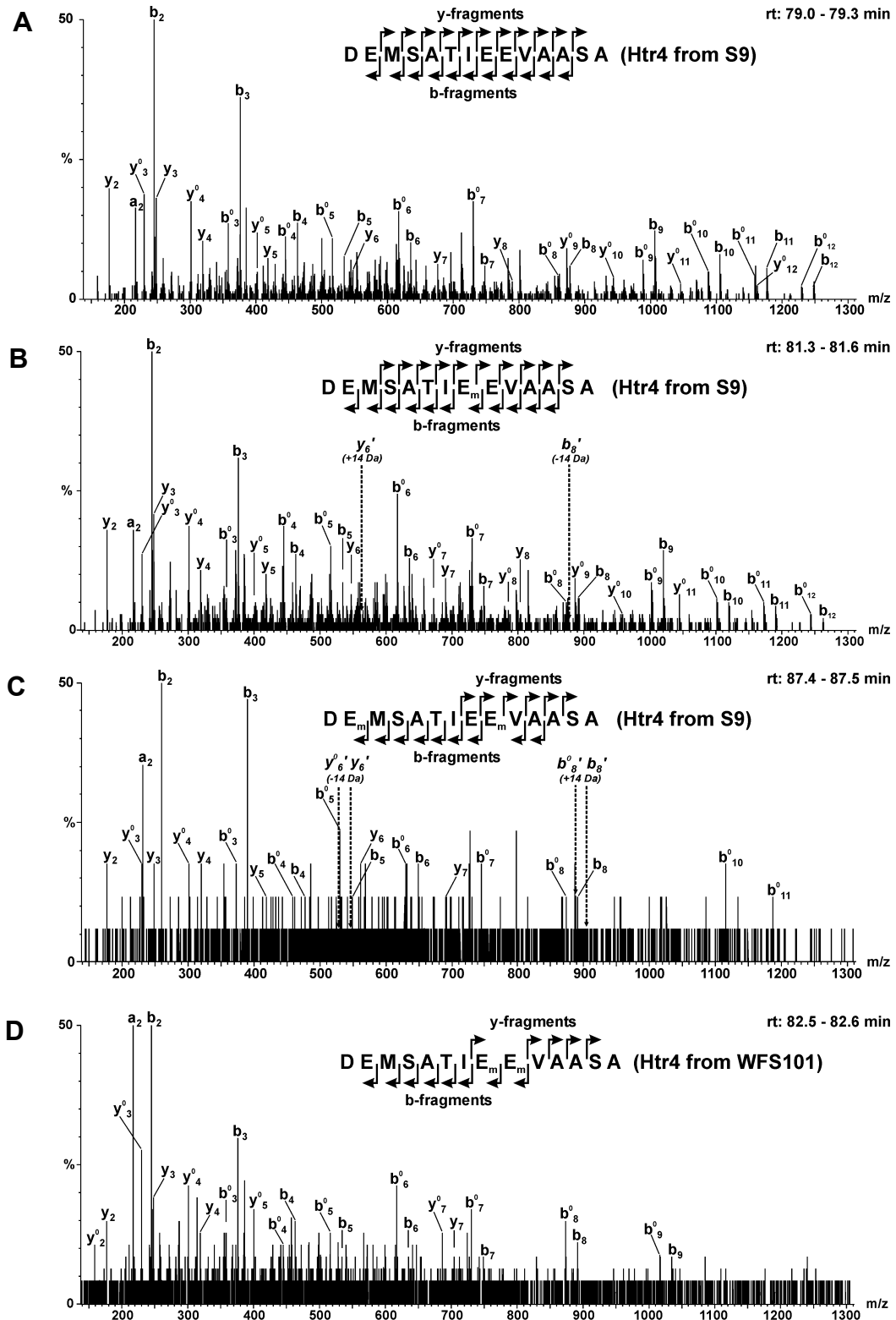


Figure 3.27 MS/MS spectra of the differently methylated forms of peptide DEMSATIEEVAASA of Htr4. Each spectrum was produced by fragmentation of the respective peptide species and was recorded within the indicated interval of retention times (rt). All signals which correspond to the masses of predicted a-, b- or y-fragments are annotated. Arrows above and below the peptide sequence indicate the presence of signals for the indicated y- and b-fragments. A subscript m marks a methylated residue. Intensities are given relative to the base peak (here b_2 which is cut off at 50%). Primed fragment designations in combination with dotted arrows indicate the height of signals present at positions that would be calculated if the other glutamate were the methylated residue within the pair. Spectra are shown for the unmethylated (A), singly methylated (B) and doubly methylated (C) peptide species identified in strain S9 and for the doubly methylated species from $\Delta cheB$ strain WFS101 (D).

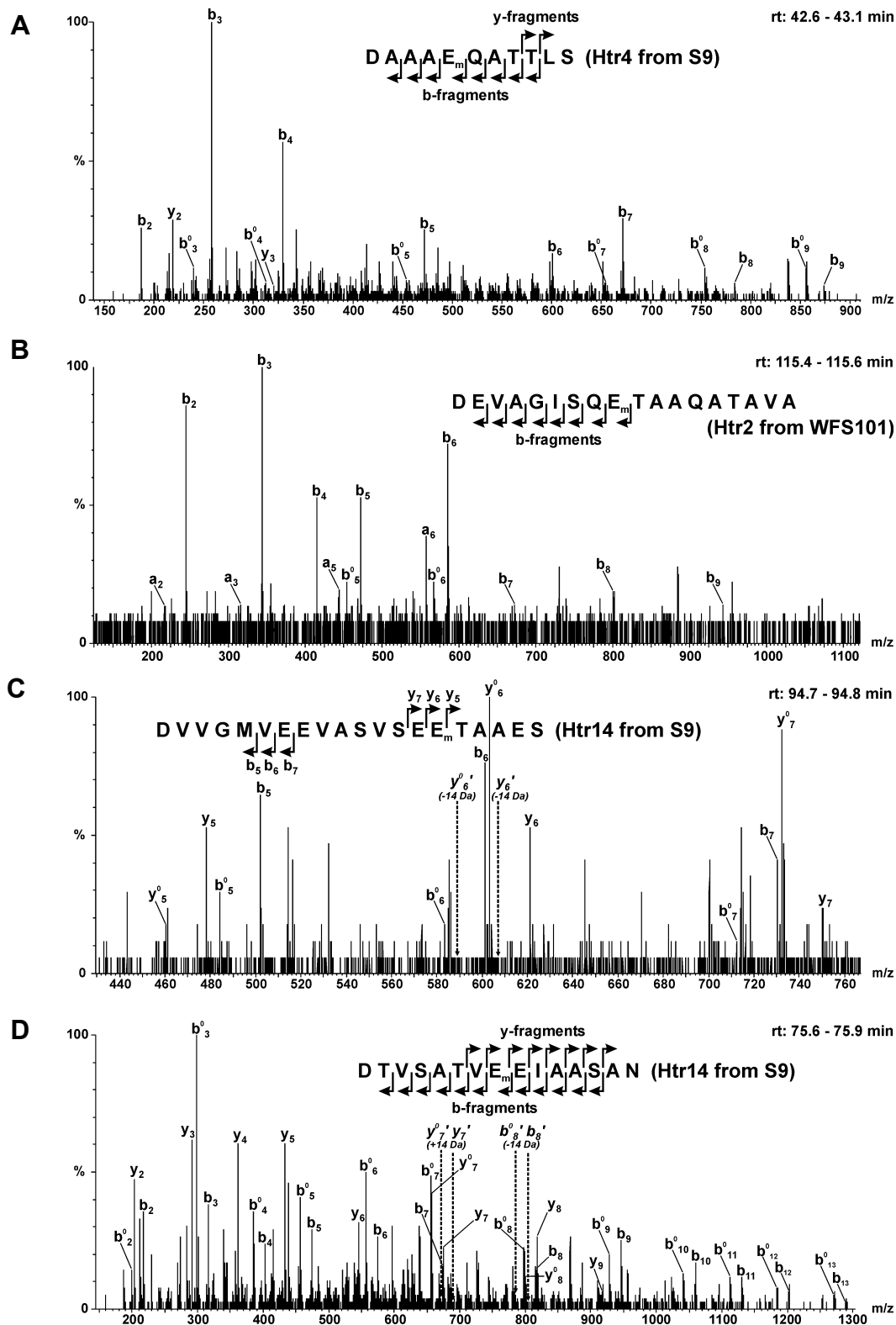


Figure 3.28 Unambiguous MS/MS identifications of the methylated glutamate residue in different peptides.

Spectra were recorded and annotated as described in Fig. 3.27. Identifications of the methylated positions are unambiguous, either due to the absence of a second glutamate at the methylation site (A, B), or due to the absence of significant alternative MS/MS signals that would be present if the other glutamate of the pair were methylated (C, D). In (C) only the fragments present within the depicted region of the spectrum are indicated on the peptide sequence. A magnified view of the m/z region between 650 and 850 of (D) is shown in Fig. 6.4A. The positions of the absent alternative signals are indicated by primed fragment designations in combination with dotted arrows.

In the case of the Htr5 peptide DLSAAIEEVAASA only the methylation site could be unambiguously identified but not the methylation position (Fig. 3.29A). Although the peak pattern pointed to a slight preference for the first methylation position, the MS/MS spectrum also contained significant mass peaks consistent with a methylation at the alternative position. This points to the possibility that in the main fraction of the Htr5 molecules the methyl group was attached to the first Glu and in the remaining molecules it was present at the second Glu.

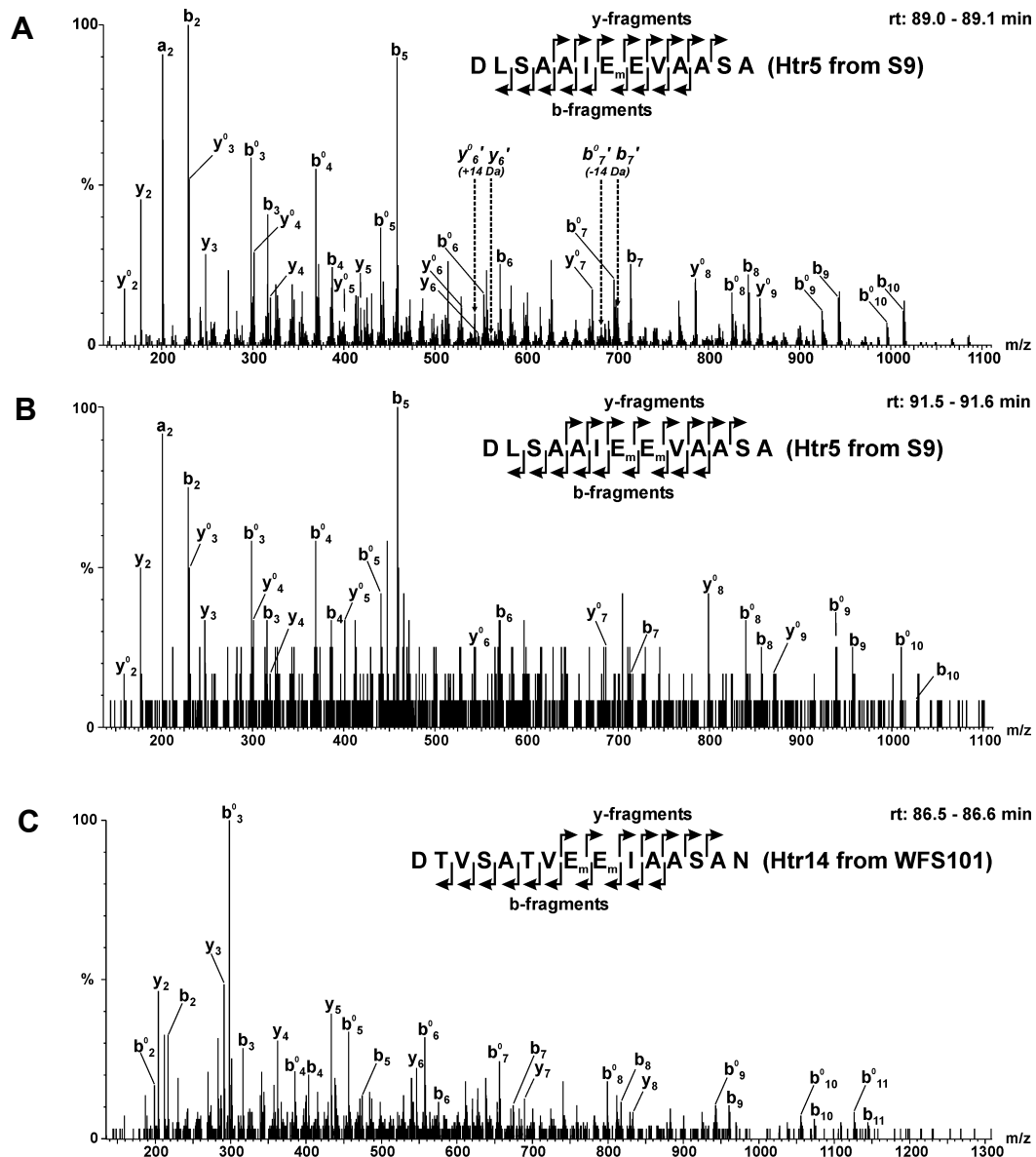


Figure 3.29 Examples of an unambiguous identification of the methylation site but not of the methylated glutamate residue (A), and for doubly methylated sites in a peptide derived from strain S9 (B) and in a peptide from the $\Delta cheB$ mutant WFS101 (C).

Spectra were recorded and annotated as described in Fig. 3.27. (A) Significant peaks are present at m/z values expected for an alternative methylation at the other glutamate of the pair, as indicated by primed fragment designations in combination with dotted arrows. Fig. 6.5 in the Appendix shows an MS/MS spectrum of a peptide of the same sequence but obtained from Htr8 instead of Htr5, as concluded from the gel position. In both cases the methylation position could not be determined unambiguously, but the first position seemed to be at least preferred.

The detection of a doubly methylated form of the same peptide demonstrates that in wild-type cells both residues are able to accept methyl groups (Fig. 3.29B). In the face of the detected doubly methylated peptide species, the inability to clearly identify a single methylation position indicates similar probabilities for the formation and/or hydrolysis of a methyl ester bond at both positions of this methylation site.

As mentioned, methylatable Htr peptides obtained from the $\Delta cheB$ mutant WFS101 are usually not found in the unmethylated form, but rather in singly and doubly methylated forms. An example of an unambiguous identification of such a doubly methylated peptide is shown for the Htr14 peptide DTVSATVEEIAASAN (Fig. 3.29C).

3.2.7 Deamidations at position 2 of heptad -11 of Htr4 and Htr15 only in wild-type but not in the $\Delta cheB$ strain identify CheB as the deamidase of *H. salinarum*

The peptide DQVAETSQRAAALG of Htr4 from wild-type S9 cells, was identified in Q-TOF MS experiments in a form in which the first Gln was deamidated to a Glu. The identification was based on an MS/MS spectrum, which showed almost the complete b-series. A closer look at the relevant m/z region of MS spectra, which were integrated in temporal proximity to the recording time of the MS/MS spectrum, revealed the following situation: a species with the m/z value of the non-deamidated peptide (708.85 Da; 2+) eluted between 41.9 and 42.2 min with an integrated base peak intensity (BPI) of 440, whereas another species with the m/z value of the deamidated form (709.32 Da; 2+) eluted between 42.3 and 49.0 min with a BPI of 4,480. In the case of the $\Delta cheB$ mutant WFS101 the situation was different: here only a species corresponding to the non-deamidated form was present, eluted between 45.7 and 47.5 min and was identified via MS/MS with almost the complete b-series. Similar situations were seen when analyzing other membrane protein preparations from S9 or WFS101. This suggests that the majority of this peptide exists in the deamidated form in wild-type, whereas in the absence of CheB it is not deamidated.

In addition to the discussed Htr4 peptide, peptide DQVASAAEQAQ of Htr15 from wild-type S9 was also shown via MS/MS to exist in a form that is deamidated at the first Gln. A closer look at the corresponding integrated MS spectra identified three different species: (i) one eluted from 38.8 to 39.4 min (559.29 Da, BPI 67), (ii) one from 39.4 to 40.0 min (559.74 Da, BPI 437), (iii) and the last one from 40.0 to 41.0 min (560.23 Da, BPI 641). This result proposes that wild-type cells contain a low amount of the non-deamidated form in addition to the more abundant singly and doubly deamidated forms. For the presumptive doubly deamidated form, it is

assumed that the deamidations happened at the first and the second Gln of the sequence, which in Htr15 are at heptad position 2 in heptads -11 and -10, respectively (Fig. 3.30). As no Htr15 peptides were detected in the gel-slices from WFS101, it could not be checked whether the peaks attributed to the deamidated forms were absent in this $\Delta cheB$ mutant, as in the case of the Htr4 peptide. Why Htr15, for which no TM regions were predicted, was present in the membrane protein preparation of S9 is not clear. Perhaps it was bound to the membrane due to another mechanism (e. g. protein-protein interaction) or it was present in some aggregated form, which pelleted together with the membrane proteins.

Taken together, these results strongly suggest that, in addition to being a methyltransferase, CheB also functions as a deamidase in *H. salinarum*. It furthermore suggests that deamidations, at least at the described positions, are not catalyzed by another enzyme (e.g. CheD), which otherwise would have taken over the function of CheB in the $\Delta cheB$ mutant. This points to a different situation compared to *B. subtilis*, where CheD and not CheB was found to be responsible for the deamidation of a pair of Gln residues in transducer McpA (Kristich and Ordal, 2002). A possible influence on the expression of *cheD* by the deletion of *cheB* should be negligible, because in the *che*-operon (Fig. 3.4), the orf encoding CheR is transcribed following the orf encoding CheD, and it was shown that transducer methylation via CheR is functional in the $\Delta cheB$ mutant.

3.2.8 Methylation sites within the methylatable regions of membrane-bound Htrs were identified in heptads -13, -12, +13, +15 and +17.

The extensive analysis of MS/MS spectra, which were produced in the course of this study for Htr peptides obtained from different membrane protein preparations, identified a substantial number of methylation sites and in many cases also the methylated residue(s) within these sites (Fig. 3.30). All identifications were based on MS/MS spectrum analyses similar to those discussed in detail in the previous chapters. All detected methylation sites within the methylatable regions of Htrs comprise heptad positions 2 and 3 of heptads -13, -12, +13, +15 or +17. Like in *E. coli* Tsr or *B. subtilis* McpB, methylation was never detected within an individual Htr in two heptads of the same value but of opposite signs. As a consequence, the methylation sites of the two Htr monomers should define two faces of the coiled coil, which are located on opposite sides of the dimer.

Due to experimental limitations, not all peptides which putatively contain methylation sites could be analyzed via MS/MS. Peptides for which no data are available can be divided into three groups: (i) Peptides from soluble transducers, as these were not contained in the investigated membrane protein preparation. (ii) Peptides with a length of more than approx. 30 amino acids,

a size which appeared to be the upper limit for reliable peptide identification via the used LC ESI Q-TOF MS setup. (iii) Peptides from transducers of which generally only a very low number of peptides was detected, possibly due to the low abundance of these transducers in the preparation.

Based on the amino acid sequences surrounding and including the mass spectrometrically detected methylation sites, additional methylation sites are suggested at positions which meet the following criteria: (i) The sites comprise only residue pairs at positions 2 and 3 of those heptads for which methylation was shown experimentally with other Htrs. (ii) Methylatable residues within such pairs are only glutamates, which were either originally encoded by the transducer gene, or produced from Gln residues by CheB-mediated deamidation. (iii) Instead of a Glx, an Ala or an Asp can also be present at the first position of the pair. (iv) In the amino acid sequence surrounding the methylation site (5' - 6' - 7' - 1 - 2(Glx) - 3(Glx) - 4 - 5 - 6 - 7), positions 5^(o), 6^(o) and 7^(o) contain only the residues Ala, Ser, Thr, Val, Met, Leu or Ile, with a few exceptions derived from the experimentally determined sites: positions 6^(o) and 7^(o) can alternatively contain a Glu or an Asp, and position 6' can contain a Gly (as in Htr2 which also contains a Gln at position 7 in the sequence surrounding the site in heptad +15).

When applying the described criteria, additional sites are predicted in a number of Htrs within heptads -12, +13 and +17. Some of the predicted sites are consistent with the results of the MALDI-TOF MS experiments described in Chapter 3.2.2 (sites in heptads -12 and +13 of Htr 11 and Htr13). It appears that all 18 Htrs contain a methylation site within heptad -12. Within heptad -13, methylation was found for Htr4 and predicted for Htr 6. Furthermore, the detection (via MS/MS) of Gln deamidations within heptad -11 of Htr4 and Htr15 suggests that methylation is also possible within this heptad. The sites within the first methylatable region of enteric transducers like Tsr and Tar are also located within heptads -13 to -11 and are therefore present at the same distance from the hairpin turn as those of the Htrs.

Within the second methylatable region, some Htr methylation sites (heptad +13 or +15) are located at a distance from the signaling region, which is close to that found in Tsr and Tar (heptad +14). On the other hand, especially in the Htrs containing TM regions, a relatively well-conserved methylation site is present at heptad +17, at the same distance to the hairpin turn as the third site in McpB. No sites were detected in Htrs which are located at a greater distance from the signaling region than those in heptad +17.

Fig. 6.7 shows a schematic overview of all 18 Htrs, Tsr, Tar and McpB. The Htrs were grouped with respect to their predicted TM regions, and for all proteins different regions and

putative or identified methylation sites are indicated. All Htrs with two predicted TM regions contain two HAMP regions of which the central GDL-motifs are shown. Of these two HAMP regions, only the second, which is proximal to the predicted coiled-coil region, is present in the Htrs containing 6 or 3 TM regions and in Tsr, Tar and McpB. HAMP regions are completely absent in the Htrs lacking TM regions. The sequence of the GDL-motif proximal to the coiled coil is well conserved among the mentioned proteins, whereas that of the distal one is less conserved.

3.2.9 Transducer evolution could be explained by a scenario different from the insertion/deletion (indel)-hypothesis

In the TM region-containing Htrs, as well as in McpB, the GDL-motif proximal to the coiled coil localizes to a position which would correspond to a "theoretical heptad -26", whereas in Tar and Tsr the GDL-motif localizes to a "theoretical heptad -22" (the term theoretical is used to indicate that the described repeat pattern of hydrophobic residues is not continued up to these positions). The enterobacterial HAMP region is therefore located 4 heptads or 28 residues closer to the hairpin turn than that of Htrs or McpB. Le Moual and Koshland (1996) propose that class III transducers, like Htrs or McpB, evolved to class I transducers, like Tar or Tsr, by deletions of four 14-residue-insertion/deletion (indel)-regions within the coiled-coil domain. Two of these regions are proposed to have been deleted between the signaling region and the methylation regions, and the other two between the methylation regions and the HAMP region and the C-terminus, respectively (Fig. 2.6). The concomitant presence of the well-conserved Htr methylation site within heptad -12, and of a reasonably well-conserved site in heptad +17, raises doubts about the indel-hypothesis.

When applying this hypothesis to a hypothetical class III transducer with methylation sites within these two heptads (which is the case in some of the Htrs), a rather complicated scenario would have to be assumed for its conversion to a class I transducer of the enterobacterial type. The assumed four 14-residue deletions would produce a hypothetical class I transducer with methylation sites in heptads -10 and +15. A subsequent development into an enterobacterial transducer would require the loss of both methylation sites and the creation of new sites within neighboring heptads, one of them in heptad -12, i. e. at the same distance from the signaling region as the original site in the class III transducer. The conversion of a class III transducer to a class I transducer would therefore require (i) two pairs of concomitant deletion events within the transducer gene, with each pair producing a loss of exactly two times 14 amino acids at approx. equidistant positions N-terminally and C-terminally of the hairpin turn (which does not destroy

but only shortens the coiled coil), (ii) the loss of the displaced original methylation sites and (iii) the development of several new methylation sites, which in each case would require several mutations to produce a methylation consensus sequence. The same scenario is valid when taking McpB as the original class III transducer.

In the face of such a complicated sequence of events, one is tempted to think of a more simple mechanism, which could explain not only the generation of the different "classes", defined by Le Moual and differing primarily in the lengths of their predicted coiled-coil regions, but also that of the different groups of Htrs.

In Fig. 3.31 a simple scenario is proposed, by which the different transducer classes and the different groups of Htrs could be derived from a hypothetical ancestral transducer. The scenario

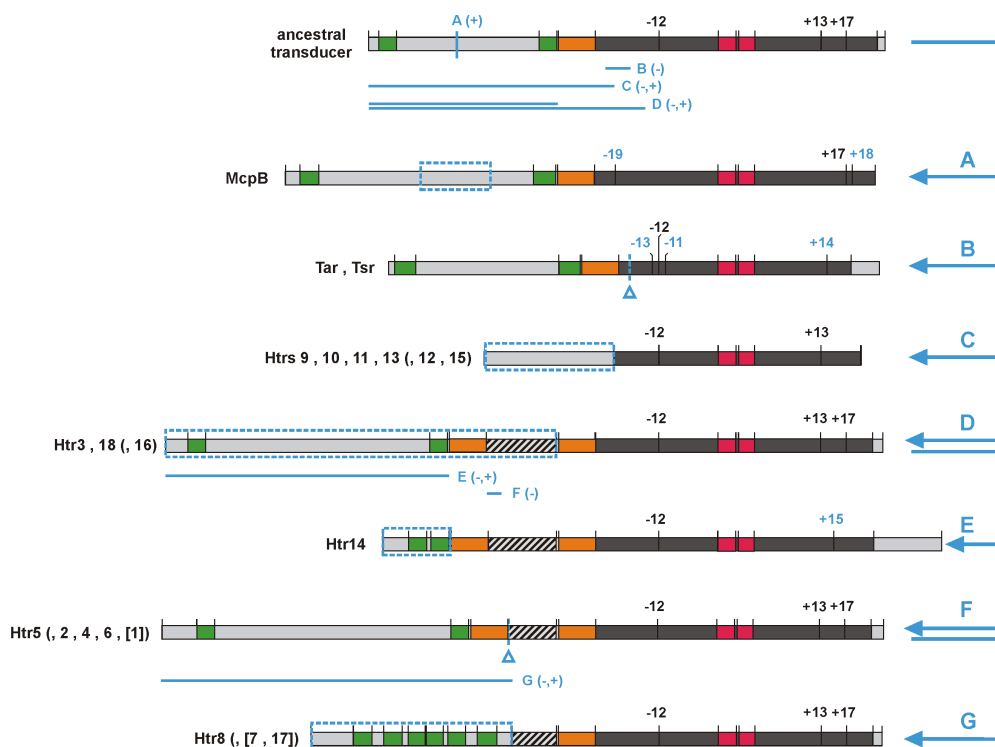


Figure 3.31 Hypothetical scenario for the generation of class I and class III transducers from a proposed common ancestor.

Transducers are depicted schematically with their different regions highlighted: green, TM region; orange, HAMP region; dark grey, predicted coiled-coil region; red, highly conserved signaling region containing the central hairpin turn; hatched, region proposed to be originating from a duplication of the N-terminal part of the coiled-coil region. New transducers are suggested to result from deletions (-) within the transducer of origin, from insertions (+), or from a replacement of their N-terminal sequences (-,+). In the generated transducers, a Δ marks the deleted region and a dotted box indicates either the inserted or the newly added N-terminal region. A possible set of methylation sites within the proposed ancestral transducer is indicated by the corresponding heptad numbers. For the other transducers heptad numbers are depicted for all putative and identified methylation sites. Transducers listed in parentheses show a slightly different set of methylation sites when compared with the corresponding depicted transducer(s), but their overall topology is very similar, with the following exceptions: Htrs 7 and 17 contain only 3 TM regions and Htr1 lacks the extracellular region between the TM regions. All transducers are proposed to have been generated by a single primary genetic event, as described by steps A to G in the schematic, which was then followed by several additional mutations leading to the loss of previous methylation sites, the generation of new ones (blue numbers), to changes in the C-terminal transducer part (like a trimming of the coiled-coil region, or shortening or elongation of the C-terminal region), and to changes within the putative N-terminal ligand-binding region.

assumes that each of the depicted transducer groups was generated by a primary genetic event, leading to either the loss of a single transducer region, the integration of an additional stretch of amino acids at a single location within the transducer, or the replacement of the N-terminal transducer region, either with a region originally encoded by a different orf, or by a longer version of the original N-terminal Htr region. As the primary event preserves the inner region of the coiled coil and thereby at least some and possibly all of the methylation sites at their original position, the adaptation mechanisms are expected to remain functional.

The transducers produced by the primary event are expected to have been further modified in an evolutionary process of functional optimization. For each transducer, such a process presumably included one or more of the following modifications: (i) the loss of some of the original and (ii) the generation of new methylation sites, (iii) the loss of the C-terminal part of the hydrophobic heptad pattern in response to the loss of the N-terminal counterpart (which is assumed to have occurred in the course of Tsr and Tar generation), (iv) a partial loss of the C-terminal part of the transducer (as in the case of the soluble Htrs), (v) an elongation of the C-terminal part (as seen for Htr14), (vi) changes in the extracellular domain leading to different ligand-binding specificities and (vii) minor sequence modifications throughout the whole transducer.

The described scenario is not meant to define the detailed sequence of evolutionary events in the course of transducer development. It rather intends to demonstrate that transducers might have evolved by single primary genetic events, instead of the two double events proposed by the indel-hypothesis. It is proposed that the primary events affected the region N-terminal of the first methylation region, and were followed by additional minor modifications, which could, for example, have lead to the formation of a new pattern of methylation sites. The analysis of Htr methylation in the course of this study has shown, that the methylation site-containing region of the presumed coiled coil does not only span 3 to 4 heptads as in the case of McpB and Tsr, respectively, but rather up to 6 (or even 7, if the deamidation in heptad -11 of Htr4 actually leads to a methylation at this site). The presence of methylation sites at different locations within such an extended part of the transducers seems to support the assumption, that a repositioning of methylation sites can take place in the aftermath of some primary genetic events, and has occurred without the interim loss of the transducers' functions and adaptive capabilities.

3.2.10 An additional methylatable site was identified in the signaling region of Htr14 (MpcT) in heptad +2

In peptide DLAEETREQAA, originating from the signaling region of Htr14, a methylation was detected at the second residue of the Glu pair, which localizes to position 3 of heptad +2. This finding was surprising because the detection of a methylated Glu within the signaling region of a transducer was unprecedented.

MS/MS spectra clearly identified the unmethylated and the singly methylated forms of this Htr14 peptide obtained from S9 cells (Fig. 3.32). Htr14 from the $\Delta cheB$ mutant WFS101 also contained either the unmethylated or the singly methylated form, the latter also exclusively methylated at the second Glu (Fig. 6.6). No significant peaks corresponding to the mass of the doubly methylated form could be detected within 10 min after the elution of the singly methylated form, no matter whether it was obtained from S9 or WFS101 preparations (data not shown). This was unexpected, because in WFS101, methylatable peptides were usually found in

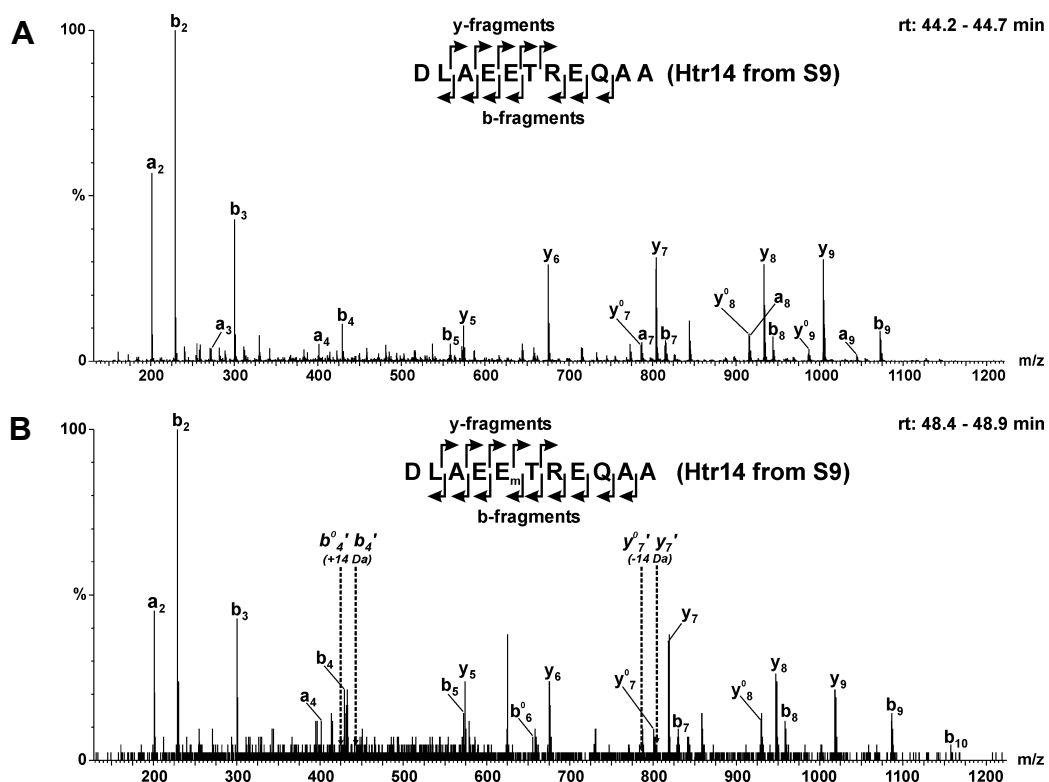


Figure 3.32 MS/MS spectra of the unmethylated and the methylated form of peptide DLAEETREQAA which originates from the signaling region of Htr14 from strain S9.

Spectra were recorded and annotated as described in Fig. 3.27. (A) Unmethylated peptide. (B) Singly methylated peptide. Strong signals are present for y_7 , y_7^0 and b_4 whereas no significant signals exist at the m/z values calculated for a methylation at the other glutamate of the pair, as indicated by primed fragment designations in combination with arrows. This suggests that the second glutamate is either the only or the predominantly methylated residue of the peptide. Spectra of the same peptide species but derived from the $\Delta cheB$ mutant WFS101 are shown in Fig. 6.6.

singly and doubly methylated rather than unmethylated forms, as shown above. Furthermore, the sequence surrounding this methylation site (KDLAEEETREQ) is very different from the described consensus sequence for CheR-dependent methylation. These findings might indicate that methylation at this site is not regulated via the CheR/CheB system.

As this methylation site is present in the highly conserved signaling region, many Htrs exhibit a very similar sequence there (however, in *E. coli* Tsr and *B. subtilis* McpB a Glu pair is not present in this heptad). Although a methylation within the Htr signaling region could only be shown for Htr14, so far, it might therefore be a more common phenomenon. With the ongoing developments in the field of mass spectrometry, which are expected to result in a further increase of sensitivity, it should be possible in the near future to detect more peptides containing this site. This will allow to analyze if other Htrs can also be methylated within their signaling region and whether this methylation is actually independent of CheR and CheB.

3.2.11 Summary of Htr methylation and outlook

In the present study, a mass spectrometrical approach was used to analyze the methylation of the membrane-bound transducers of *H. salinarum*, after a mutagenesis approach was excluded as not practicable for the analysis of an initially estimated number of 24 to 48 methylation sites (2 to 4 sites in each of the 12 Htrs that contain TM regions). After the analysis of MALDI-TOF MS spectra of mixtures of tryptic Htr peptides provided first hints towards the detectability of this post-translational protein modification, the analysis of Asp-N-digested Htrs with LC ESI Q-TOF MS/MS was used to obtain the majority of the results. After immunoblot experiments suggested that Htrs comprise the major fraction of the proteins of apparent MWs between 100 and 160 kDa, 1-D SDS PAGE was used for protein separation and to obtain sufficient protein amounts to allow for the detection of even the presumably low-abundant Htrs.

The use of specifically designed peptide databases led to the detection of Gln deamidations to Glu, which only occurred within the determined methylation regions, and furthermore to the exclusion of Asn deamidations to Asp anywhere in the Htrs. The elution times of the different peptide forms, which were found to increase by approx. 2 to 3 minutes per added methyl group, were in each case used as an additional criterion to support the MS/MS identifications of the different peptide species. In each case, the identified methylation sites comprised either a GlxGlx pair, a DE pair, or an AE pair at heptad positions 2 and 3, mainly in heptads -12, +13 or +17, in some cases in heptads -13 or +15, and possibly also in heptads -10 and -11 (if the deamidations detected in the latter two heptads are indicative of a subsequent methylation). The deamidations of several DQ pairs in Htr4 and Htr15 were only detected in Htrs, which resulted

from wild-type strain S9 and were absent in the $\Delta cheB$ mutant WFS101, which suggests that CheB is the only deamidase acting on Htrs of *H. salinarum*. The observation of an increased Htr methylation in the absence of CheB, which was visible either as a downward shift of Htr14 bands on an immunoblot or as an increase in the relative amount of the higher methylated, compared to the lower methylated peptide species, identified CheB as either the main or even the only methylesterase active in Htr demethylation. In the absence of CheR, on the other hand, only the Htr14 species of lowest mobility was present on the immunoblot and no methylated Htr peptides were detected via MS/MS, which supports the expected methyltransferase activity of CheR.

Depending on the quality of the generated MS/MS spectra and on the individual peptide sequences, a preferred methylation position could be identified for some of the sites, whereas at other sites either a distinction was not possible, a single methylation was found at either the first or the second position, or both positions simultaneously carried a methyl group. Doubly methylated sites were found in several peptides of Htrs, which were obtained from a $\Delta cheB$ mutant, but also in peptides obtained from S9. This demonstrates that under physiological conditions wild-type *H. salinarum* cells contain transducers with doubly methylated sites, which has, as yet, not been shown for transducers from other organisms.

The detection of a second methylation site in Htr2 from the $\Delta cheB$ mutant WFS101, in addition to the main site in heptad -12, might explain why Perazzona and Spudich (1999) saw some remaining Htr2 methylation after mutating the Glu pair at the main site to a pair of alanines. The fact that Ala or Asp were also detected at Htr methylation sites besides Glu and Gln, might explain why in the mentioned study the replacement of the second Glu of the Htr1 methylation site by an Ala did not abolish methylation, although the consensus sequence for CheR methylation, deduced from the transducer methylation sites known at that time, did not include an Ala at heptad positions 2 or 3.

Although the present study could mass spectrometrically identify a number of Htr methylation sites and has proposed additional sites on the basis of their surrounding sequences and their heptad location within the methylatable region, some sites might have escaped an identification. Possible reasons could be that (i) such sites were only methylated to a very low extent, (ii) no form of the peptide carrying the site was ever detected mass spectrometrically, (iii) the peptide contained additional, unexpected modifications, which were not considered in the used databases, or (iv) the criteria used for the proposal of additional sites in non-identified peptides were too restrictive. On the basis of the identified or deduced methylation sites and of sequence

alignments of Htrs and other transducers, a model was proposed as an alternative to the indel-hypothesis of Le Moual and Koshland (1996), to explain the generation of the different transducer classes and Htr groups on the basis of single primary genetic events. These events are proposed to have produced modified transducers, which were still capable of adaptation due to the preservation of their methylation sites. It is suggested that these transducers were then optimized in an evolutionary process, which in some cases included a relocation of the methylation sites to another position within the methylatable region.

The methylatable regions of Htrs can span up to 7 heptads in Htr4 (-11 to +17) and possibly even 8 heptads in Htr15 (-10 to +17) and are therefore larger than those which had previously been characterized in other transducers like McpB and Tsr, where they span only 3 to 4 heptads. As deduced from the spatial arrangement of heptad positions 2 and 3 in an "ideal" coiled coil, the methylation sites in all discussed transducers are predicted to define two opposed faces of the coiled coil, one on each transducer monomer.

Finally, the discovery of a methylation site at position 3 of heptad +2 within the signaling region of Htr14 was totally unexpected. The absence of the CheR methylation consensus sequence and an identical methylation pattern in the presence and in the absence of CheB might point to a CheR/CheB-independent methylation system. This finding was particularly interesting, because a direct influence on CheW/CheA binding to the transducer should be expected for a methylation within the signaling region. Due to a high homology of the sequence surrounding this site in a number of Htrs, it might be expected that also other Htrs can be methylated at this position.

Differentially isotopically labeled Htr-peptides could be used in the future to quantitate the *in vivo* changes in Htr-methylation upon stimulation of the cells

The new MS-based method for the analysis of Htr methylation, which was developed in the course of this study, is not restricted only to the identification of methylation sites or methylated residues of the Htrs. It should moreover be possible to also use it in a quantitative approach to investigate changes in the degree of Htr methylation or of changes in the preferred methylated residue, after Htrs were stimulated with light or chemicals. The results of these investigations are expected to allow for a distinction between global and local methylation changes in transducers in the course of adaptation. This is of particular interest, e. g. for future computer simulations of the halobacterial signal transduction pathways, because it is still unclear whether the stimulation of a particular transducer induces methylation changes only locally, on the stimulated transducer or on a certain subgroup of the transducer ensemble, or globally, on all

transducers of the cell. It is furthermore not known, whether in *H. salinarum* an increase of attractant stimulus strength leads to an increase in transducer methylation, as was shown for *E. coli* transducers (reviewed in Stock and Surette, 1996), or if the net methylation of the Htrs remains unchanged, due to a demethylation of some residues and a concomitant methylation of others, as proposed for *B. subtilis* McpB (Zimmer *et al.*, 2000).

A possible approach for the quantification of methylation changes in Htrs is the following: A halobacterial culture is separated into two identical fractions, one of which is stimulated by application of an attractant or a repellent stimulus. The cells are immediately lysed and the membrane protein fractions are electrophoretically separated via SDS PAGE in the presence of urea, which eliminates the mobility differences between differently methylated forms of an Htr. After excision of gel bands containing Htrs, followed by in-gel Asp-N digestion, the peptides from the unstimulated and the stimulated sample are differentially isotopically labeled by D0- and D4-nicotinoylation, respectively, of their Lys residues as well as their N-termini, using N-nicotinoyloxy-succinimide (Nic-NHS) (Schmidt *et al.*, 2005). D4-nicotinoylation adds nicotinoyl-groups, which contain 4 deuterium atoms instead of the 4 hydrogens that are present in the D0-nicotinoyl-groups.

A subsequent MS/MS analysis will identify the elution times of the different peptides and will be followed by an MS scan of the same sample. Via integration of the generated MS spectra from the start of elution of the D4-labeled to the end of elution of the D0-labeled form of a particular peptide (D4-labeled peptides elute slightly earlier than the corresponding D0 (H4)-labeled ones), the ratios of these peptides can be determined. Such ratios for a number of non-methylatable peptides from Htrs or from other proteins will provide an internal standard to which the ratios determined for the differently methylated species of the methylatable peptides can be compared. If the stimulation has caused an increase of methylation at a site in a certain peptide, then the ratio of D4-labeled peptide species to D0-labeled species should be the same for all unmethylated peptides, but it should increase for the methylated form of the peptide and decrease for its unmethylated form, indicating an increase of methylation at this site upon stimulation of the cells.

Quantification experiments are under way and will hopefully provide deeper insights into the dynamics of Htr methylation during the process of adaptation in the near future.

4 MATERIALS AND METHODS

4.1 Chemicals and enzymes

4.1.1 Chemicals

All chemicals used in the course of this study were purchased at the highest purity grade available from Sigma-Aldrich (Taufkirchen, Germany) or Merck (Darmstadt, Germany). Exceptions are indicated within the methods chapters or are listed below:

Ammonium peroxodisulfate	Biorad, Munich, Germany
Bacto™ agar	Difco, Detroit, MI, USA
Bacto™ tryptone	Difco, Detroit, MI, USA
Bacto™ yeast extract	Difco, Detroit, MI, USA
Benchmark Protein ladder	Invitrogen, Karlsruhe, Germany
BMA Seakem™ LE agarose	Biozym, Hess. Oldendorf, Germany
Bromophenolblue	Difco, Detroit, MI, USA
CSPD chemiluminescent substrate	Roche Diagnostics, Mannheim, Germany
DIG-11-dUTP	Boehringer-Mannheim, Mannheim, Germany
DNA ladder 100bp	Peqlab, Erlangen, Germany
DNA molecular weight marker III, DIG-labeled	Roche Diagnostics, Mannheim, Germany
L-[methyl- ³ H]-methionine	Amersham Biosciences, Freiburg, Germany
N-2-Hydroxyethylpiperazine-N'-2-ethanesulfonic acid (HEPES)	Biomol, Hamburg, Germany
Neutralized bacteriological peptone L34	Oxoid, Basingstoke, Hampshire, UK
Tetramethylethylenediamine (TEMED)	Serva Feinbiochemika, Heidelberg, Germany
Protogel (30 % acrylamide, 0.8 % bisacrylamide)	National diagnostics, Atlanta, GA, USA

4.1.2 Kits and Enzymes

All restriction enzymes were purchased from New England Biolabs, Beverly, MI, USA. Other enzymes or kits used in the course of this study are listed below:

ABI Prism BigDye™ Terminator Cycle Sequencing Ready Reaction Kit	Applied Biosystems, Foster City, CA, USA
Anti Digoxigenin AP F _{ab} fragments	Roche Diagnostics, Mannheim, Germany
BCA Protein Assay Reagent Kit	Pierce, Rockford, IL, USA
EZ™ Antibody Production and Purification Kit	Pierce, Rockford, IL, USA
Pfu Turbo™ DNA polymerase	Stratagene, La Jolla, CA, USA
QIAprep™ Spin Miniprep Kit	Qiagen, Hilden, Germany
QIAquick™ Gel Extraction Kit	Qiagen, Hilden, Germany
SuperSignal™ West Pico Chemiluminescent Substrate	Pierce, Rockford, IL, USA
T4 DNA ligase	Gibco BRL, Berlin, Germany

4.2 Microbiological materials and methods

4.2.1 Strains and culture conditions

Overview of strains

The following table lists the *E. coli* and *H. salinarum* strains that were used or generated in the course of this study.

Table 4.1. Overview of strains

Strain (lab-designation)	Relevant description ^{a,b} [source or reference]
<i>E. coli</i>:	
XL1-Blue MRF'	$\Delta(mcrA)183 \Delta(mcrCB-hsdSMR-mrr)173 endA1 supE44 thi-1 recA1 gyrA96 relA1 lac$ [F' <i>proAB lacI^qZ</i> Δ M15 Tn10 (Tet ^R)] [Stratagene, La Jolla, CA, USA]
<i>H. salinarum</i>:	
S9	<i>bop</i> ⁺ , <i>hop</i> ⁺ , <i>htr1</i> ⁺ , <i>sopI</i> ⁺ , <i>htr2</i> ⁺ , <i>sopII</i> ⁺ , <i>htr11</i> ⁺ (Mev ^S) [Wagner <i>et al.</i> , 1981]
S9 _{mot}	Genotype of S9. A highly motile single colony isolate of the S9 strain collected from expanding rings on a swarm plate [Storch <i>et al.</i> , 1999]
L33	Like S9, except <i>bop::ISH2</i> . Derived from parent strain S9 by spontaneous insertion of the insertion element <i>ISH2</i> into the <i>bop</i> gene after treatment of S9 cells with UV light [Wagner <i>et al.</i> , 1981]
WHOP	Like S9, except <i>bop::ISH2</i> , Δhop , $\Delta htr11$. Derived from parent strain L33 by deletion of the <i>hop</i> gene and partial loss of DNA, including the <i>htr11</i> gene, from plasmid PHS3 (284 kDa). Together with the <i>hop</i> gene, the flanking genes <i>oe1302</i> and <i>oe1298</i> were also deleted [Besir, 2001]
TOM	Like S9, except Δbop , Δhop , $\Delta htr11$. Generated from parent strain WHOP by deletion of the <i>bop</i> gene [Besir, 2001]
SAM2	Like TOM, except $\Delta(htr2-sopII)$. Generated from parent strain TOM by deletion of the <i>sopII</i> and <i>htr2</i> genes [Masato Otsuka, unpublished]
OMI1 (NAOMI)	Δbop , Δhop , $\Delta(htr1-sopI)$, $\Delta(htr2-sopII)$, $\Delta htr11$ Generated from parent strain SAM2 by deletion of the <i>sopII</i> and <i>htr2</i> genes. Together with <i>htr2</i> and <i>sopII</i> , the downstream flanking gene <i>oe3349</i> was also deleted [Masato Otsuka, unpublished].
OMI1 _{mot} (NAOMI _{mot})	Genotype of OMI1. Motile OMI1 _{mot} cells resulted from a single colony isolate from a plate of cells that were selected from the outer ring of the third out of three consecutive swarm plates.
MKK101 (NABOCO)	Like OMI1, except <i>bop</i> ⁺ . Generated from OMI1 _{mot} by restoration of the wild-type <i>bop</i> locus, using plasmid pMKK101 [this work]
MKK102 (NAHOCO)	Like OMI1, except <i>hop</i> ⁺ . Generated from OMI1 _{mot} by restoration of the wild-type <i>hop</i> locus using plasmid pMKK102 [this work]
MKK103 (NABOCO Δ 3)	Like OMI1, except <i>bop</i> ⁺ and $\Delta htr3$. Generated from MKK101 by deletion of <i>htr3</i> using plasmid pMKK103 [this work]
MKK104 (NABOCO Δ 4)	Like OMI1, except <i>bop</i> ⁺ and $\Delta htr4$. Generated from MKK101 by deletion of <i>htr4</i> using plasmid pMKK104 [this work]
MKK105 (NABOCO Δ 5)	Like OMI1, except <i>bop</i> ⁺ and $\Delta htr5$. Generated from MKK101 by deletion of <i>htr5</i> using plasmid pMKK105 [this work]

Strain (lab-designation)	Relevant description ^{a,b} [source or reference]
MKK106 (NABOCOΔ6)	Like OMI1, except <i>bop</i> ⁺ and Δ <i>htr6</i> . Generated from MKK101 by deletion of <i>htr6</i> using plasmid pMKK106 [this work]
MKK107 (NABOCOΔ7)	Like OMI1, except <i>bop</i> ⁺ and Δ <i>htr7</i> . Generated from MKK101 by deletion of <i>htr7</i> using plasmid pMKK107 [this work]
MKK108 (NABOCOΔ8)	Like OMI1, except <i>bop</i> ⁺ and Δ <i>htr8</i> . Generated from MKK101 by deletion of <i>htr8</i> using plasmid pMKK108 [this work]
MKK109 (NABOCOΔ9)	Like OMI1, except <i>bop</i> ⁺ and Δ <i>htr9</i> . Generated from MKK101 by deletion of <i>htr9</i> using plasmid pMKK109 [this work]
MKK110 (NABOCOΔ10)	Like OMI1, except <i>bop</i> ⁺ and Δ <i>htr10</i> . Generated from MKK101 by deletion of <i>htr10</i> using plasmid pMKK110 [this work]
MKK112 (NABOCOΔ12)	Like OMI1, except <i>bop</i> ⁺ and Δ <i>htr12</i> . Generated from MKK101 by deletion of <i>htr12</i> using plasmid pMKK112 [this work]
MKK113 (NABOCOΔ13)	Like OMI1, except <i>bop</i> ⁺ and Δ <i>htr13</i> . Generated from MKK101 by deletion of <i>htr13</i> using plasmid pMKK113 [this work]
MKK114 (NABOCOΔ14)	Like OMI1, except <i>bop</i> ⁺ and Δ <i>htr14</i> . Generated from MKK101 by deletion of <i>htr14</i> using plasmid pMKK114 [this work]
MKK115 (NABOCOΔ15)	Like OMI1, except <i>bop</i> ⁺ and Δ <i>htr15</i> . Generated from MKK101 by deletion of <i>htr15</i> using plasmid pMKK115 [this work]
MKK116 (NABOCOΔ16)	Like OMI1, except <i>bop</i> ⁺ and Δ <i>htr16</i> . Generated from MKK101 by deletion of <i>htr16</i> using plasmid pMKK116 [this work]
MKK117 (NABOCOΔ17)	Like OMI1, except <i>bop</i> ⁺ and Δ <i>htr17</i> . Generated from MKK101 by deletion of <i>htr17</i> using plasmid pMKK117 [this work]
MKK118 (NABOCOΔ18)	Like OMI1, except <i>bop</i> ⁺ and Δ <i>htr18</i> . Generated from MKK101 by deletion of <i>htr18</i> using plasmid pMKK118 [this work]
MKK119 (NABOCOΔ14+14)	Like OMI1, except <i>bop</i> ⁺ . Generated from MKK114 by restoration of the wild-type <i>htr14</i> locus using plasmid pMKK119 [this work]
MKK120 (NAHOCOΔ14)	Like OMI1, except <i>hop</i> ⁺ and Δ <i>htr14</i> . Generated from MKK102 by deletion of <i>htr14</i> using plasmid pMKK114 [this work]
MKK121 (NABOCOΔ <i>oe1534</i>)	Like OMI1, except <i>bop</i> ⁺ and Δ <i>oe1534</i> . Generated from MKK101 by deletion of <i>oe1534</i> using plasmid pMKK121 [this work]
MKK203 (S9Δ3)	Like S9, except Δ <i>htr3</i> . Generated from S9 _{mot} by deletion of <i>htr3</i> using plasmid pMKK103 [this work]
MKK204 (S9Δ4)	Like S9, except Δ <i>htr4</i> . Generated from S9 _{mot} by deletion of <i>htr4</i> using plasmid pMKK104 [this work]
MKK205 (S9Δ5)	Like S9, except Δ <i>htr5</i> . Generated from S9 _{mot} by deletion of <i>htr5</i> using plasmid pMKK105 [this work]
MKK206 (S9Δ6)	Like S9, except Δ <i>htr6</i> . Generated from S9 _{mot} by deletion of <i>htr6</i> using plasmid pMKK106 [this work]
MKK207 (S9Δ7)	Like S9, except Δ <i>htr7</i> . Generated from S9 _{mot} by deletion of <i>htr7</i> using plasmid pMKK107 [this work]
MKK208 (S9Δ8)	Like S9, except Δ <i>htr8</i> . Generated from S9 _{mot} by deletion of <i>htr8</i> using plasmid pMKK108 [this work]
MKK209 (S9Δ9)	Like S9, except Δ <i>htr9</i> . Generated from S9 _{mot} by deletion of <i>htr9</i> using plasmid pMKK109 [this work]
MKK210 (S9Δ10)	Like S9, except Δ <i>htr10</i> . Generated from S9 _{mot} by deletion of <i>htr10</i> using plasmid pMKK110 [this work]
MKK212 (S9Δ12)	Like S9, except Δ <i>htr12</i> . Generated from S9 _{mot} by deletion of <i>htr12</i> using plasmid pMKK112 [this work]

Strain (lab-designation)	Relevant description ^{a,b} [source or reference]
MKK213 (S9Δ13)	Like S9, except Δ <i>htr13</i> . Generated from S9 _{mot} by deletion of <i>htr13</i> using plasmid pMKK113 [this work]
MKK214 (S9Δ14)	Like S9, except Δ <i>htr14</i> . Generated from S9 _{mot} by deletion of <i>htr14</i> using plasmid pMKK114 [this work]
MKK215 (S9Δ15)	Like S9, except Δ <i>htr15</i> . Generated from S9 _{mot} by deletion of <i>htr15</i> using plasmid pMKK115 [this work]
MKK216 (S9Δ16)	Like S9, except Δ <i>htr16</i> . Generated from S9 _{mot} by deletion of <i>htr16</i> using plasmid pMKK116 [this work]
MKK217 (S9Δ17)	Like S9, except Δ <i>htr17</i> . Generated from S9 _{mot} by deletion of <i>htr17</i> using plasmid pMKK117 [this work]
MKK218 (S9Δ18)	Like S9, except Δ <i>htr18</i> . Generated from S9 _{mot} by deletion of <i>htr18</i> using plasmid pMKK118 [this work]
WFS101 (S9Δ <i>cheB</i>)	Like S9, except Δ <i>cheB</i> . Generated from S9 by deletion of <i>cheB</i> (the deleted region ^c includes the DNA from position +19 to +1026 of the orf starting with: ATGACA...) [Wilfried Staudinger, unpublished]
WFS102 (S9Δ <i>cheR</i>)	Like S9, except Δ <i>cheR</i> . Generated from S9 by deletion of <i>cheR</i> (the deleted region ^c includes the DNA from position +91 to +807 of the orf starting with: TTGACT...) [Wilfried Staudinger, unpublished]
<p>a: Information about all mentioned halobacterial genes, their sequences and additional names is available at the database http://www.halolex.mpg.de (Dieter Oesterhelt <i>et al.</i>, unpublished). b: In addition to the systematic designations (<i>htr1 - 18</i>), final names were assigned to the <i>htrs</i> 1, 2, 3, 5, 8, 10, 11, 14 and their gene products after the elucidation of a biological function, as described in the Introduction Chapter. c: Nucleotide positions are given relative to the first nucleotide of the orf (+1).</p>	

Culturing of *E. coli*

E. coli cells were grown in LB medium, supplemented with ampicillin if appropriate, at 37°C with constant shaking at 250 rpm. To isolate single cultures, cells were plated onto agar plates containing LB medium and ampicillin. The cells were incubated over night at 37°C.

Culturing of *H. salinarum*

Unless otherwise stated, halobacterial cells were grown aerobically in the dark in complete medium at 40°C under constant shaking at 100 rpm as described by Oesterhelt and Krippahl (1983) until they reached an optical density between 0.7 and 1.0. Optical density was monitored at 600 nm in a spectrophotometer (Ultrospec3000, Pharmacia Biotech, Uppsala, Sweden). If not otherwise described, 35ml of medium in a 100 ml Erlenmeyer flask were inoculated with 100 μl (1/350) of stock culture. For long term storage 15 ml of a fresh halobacterial culture grown to an OD₆₀₀ between 0.5 and 0.9 were transferred to a 20 ml polyethylene vial (Polyvials, Zinsser Analytic, Frankfurt). The vial was tightly closed and stored at room temperature in the dark. Cells stored in the described way can easily be used to produce fresh cultures for at least 4 years, probably longer.

4.2.2 Plasmids

Overview of plasmids

The following overview lists the plasmids used in the course of this work together with a description of their generation and of essential features. All inserts are characterized by the positions of their first and last nucleotides which are flanked by the (introduced) restriction sites. In the case of deletion mutants the positions of the deleted nucleotides are also given. All positions are given with respect to the first (+1) nucleotide of the respective open reading frame.

Table 4.2. Overview of plasmids.

Plasmid name (lab-designation)	Description of the plasmid [source or reference]
pUS-Mev	6304 bp vector derived from pBluescript SK ⁻ (Stratagene, La Jolla, USA) by cloning 1400 bp of <i>H. salinarum</i> sequence containing the <i>bop</i> gene between <i>Bam</i> HI and <i>Hind</i> III sites and 1994 bp of <i>H. volcanii</i> sequence containing the mevinolin resistance gene between <i>Hind</i> III and <i>Xho</i> I sites of the multiple cloning site (MCS) [Schweiger, 1996; Pfeiffer <i>et al.</i> , 1999]
pMKK101 (pM@bop1)	6689 bp vector derived from pUS-Mev by replacing the <i>bop</i> -containing sequence between <i>Bam</i> HI and <i>Hind</i> III sites with the <i>Bam</i> HI/ <i>Hind</i> III-digested <i>bop</i> -locus insert: -387 to +1390 (<i>bop</i> : 789 bp) [this work]
pMKK012 (pM@Δ <i>htr</i> 12)	5557 bp vector derived from pUS-Mev by replacing the <i>bop</i> -locus sequence between <i>Bam</i> HI and <i>Hind</i> III sites with the <i>Bam</i> HI/ <i>Hind</i> III-digested Δ <i>htr</i> 12 insert: -292 to +1620 but lacking +1 to +1266 (<i>htr</i> 12: 1263 bp) [this work]
pMKK112 (pM@βΔ <i>htr</i> 12)	7819 bp vector derived from pMKK012 by insertion of the <i>Spe</i> I/ <i>Sac</i> I-digested <i>bgaH</i> -locus between the <i>Spe</i> I and <i>Sac</i> I sites: -141 to +2145 (<i>bgaH</i> : 1992 bp) [this work]
pMKK103 (pM@βΔ <i>htr</i> 3)	7713 bp vector derived from pMKK112 by replacing the Δ <i>htr</i> 12 insert between <i>Bam</i> HI and <i>Hind</i> III sites with the <i>Bam</i> HI/ <i>Hind</i> III-digested Δ <i>htr</i> 3 insert: -297 to +2669 but lacking -5 to +2421 (<i>htr</i> 3: 2418 bp) [this work]
pMKK104 (pM@βΔ <i>htr</i> 4)	7756 bp vector derived from pMKK112 by replacing the Δ <i>htr</i> 12 insert between <i>Spe</i> I and <i>Hind</i> III sites with the <i>Spe</i> I/ <i>Hind</i> III-digested Δ <i>htr</i> 4 insert: -302 to +2627 but lacking -3 to +2337 (<i>htr</i> 4: 2337 bp) [this work]
pMKK105 (pM@βΔ <i>htr</i> 5)	7759 bp vector derived from pMKK112 by replacing the Δ <i>htr</i> 12 insert between <i>Spe</i> I and <i>Hind</i> III sites with the <i>Spe</i> I/ <i>Hind</i> III-digested Δ <i>htr</i> 5 insert: -300 to +2732 but lacking -3 to +2437 (<i>htr</i> 5: 2433 bp) [this work]
pMKK106 (pM@βΔ <i>htr</i> 6)	7776 bp vector derived from pMKK112 by replacing the Δ <i>htr</i> 12 insert between <i>Bam</i> HI and <i>Hind</i> III sites with the <i>Bam</i> HI/ <i>Hind</i> III-digested Δ <i>htr</i> 6 insert: -301 to +2674 but lacking -1 to +2371 (<i>htr</i> 6: 2370 bp) [this work]
pMKK107 (pM@βΔ <i>htr</i> 7)	7772 bp vector derived from pMKK112 by replacing the Δ <i>htr</i> 12 insert between <i>Bam</i> HI and <i>Hind</i> III sites with the <i>Bam</i> HI/ <i>Hind</i> III-digested Δ <i>htr</i> 7 insert: -300 to +1939 but lacking +1 to +1641 (<i>htr</i> 7: 1638 bp) [this work]
pMKK108 (pM@βΔ <i>htr</i> 8)	7719 bp vector derived from pUS-Mev by replacing the <i>bop</i> -locus sequence between <i>Bam</i> HI and <i>Hind</i> III sites with the <i>Bam</i> HI/ <i>Hind</i> III-digested Δ <i>htr</i> 8 insert: -315 to +2163 lacking +1 to +1932 (<i>htr</i> 8: 1932 bp). Additionally the <i>bgaH</i> -locus sequence was inserted between the <i>Spe</i> I and <i>Sac</i> I sites as in the construction of pMKK112 [this work]
pMKK109 (pM@βΔ <i>htr</i> 9)	7830 bp vector derived from pUS-Mev by replacing the <i>bop</i> -locus sequence between <i>Bam</i> HI and <i>Hind</i> III sites with the <i>Bam</i> HI/ <i>Hind</i> III-digested Δ <i>htr</i> 9 insert: -328 to +1774 but lacking +3 to +1449 (<i>htr</i> 9: 1446 bp). Additionally the <i>bgaH</i> -locus sequence was inserted between the <i>Spe</i> I and <i>Sac</i> I sites as in the construction of pMKK112 [this work]

Plasmid name (lab- designation)	Description of the plasmid [source or reference]
pMKK110 (pM@βΔhtr10)	7935 bp vector derived from pUS-Mev by replacing the <i>bop</i> -locus sequence between <i>Bam</i> HI and <i>Hind</i> III sites with the <i>Bam</i> HI/ <i>Hind</i> III-digested Δhtr10 insert: -402 to +1830 but lacking +1 to +1470 (<i>htr10</i> : 1470 bp). Additionally the <i>bgaH</i> -locus sequence was inserted between the <i>Spe</i> I and <i>Sac</i> I sites as in the construction of pMKK112 [this work]
pMKK111 (pM@βΔhtr11)	7817 bp vector derived from pMKK112 by replacing the Δhtr12 insert between <i>Spe</i> I and <i>Hind</i> III sites with the <i>Spe</i> I/ <i>Hind</i> III-digested Δhtr11 insert: -345 to +1664 but lacking -3 to +1356 (<i>htr11</i> : 1359 bp) [this work]
pMKK113 (pM@βΔhtr13)	7777 bp vector derived from pMKK112 by replacing the Δhtr12 insert between <i>Bam</i> HI and <i>Hind</i> III sites with the <i>Bam</i> HI/ <i>Hind</i> III-digested Δhtr13 insert: -296 to +1576 but lacking +4 to +1273 (<i>htr13</i> : 1272 bp) [this work]
pMKK100 (pM@βMaster)	7213 bp vector derived from pUS-Mev by insertion of the <i>Spe</i> I/ <i>Sac</i> I-digested <i>bgaH</i> -locus between the <i>Spe</i> I and <i>Sac</i> I sites: -141 to +2145 (<i>bgaH</i> : 1992 bp). Furthermore the <i>bop</i> -containing sequence between <i>Bam</i> HI and <i>Xba</i> I sites was replaced with the <i>Bam</i> HI/ <i>Xba</i> I-digested MCS-1 insert containing a multiple cloning site (MCS) especially designed for this vector to contain a maximum number of unique cutting sites for the most common restriction enzymes (48 bp between <i>Bam</i> HI and <i>Xba</i> I sites) [this work]
pMKK114 (pM@βΔhtr14)	7877 bp vector derived from pMKK100 by replacing the MCS sequence between <i>Bam</i> HI and <i>Hind</i> III sites with the <i>Bam</i> HI/ <i>Hind</i> III-digested Δhtr14 insert: -384 to +2196 but lacking +1 to +1876 (<i>htr14</i> : 1884 bp) [this work]
pMKK115 (pM@βΔhtr15)	7930 bp vector derived from pUS-Mev by replacing the <i>bop</i> -locus sequence between <i>Bam</i> HI and <i>Hind</i> III sites with the <i>Bam</i> HI/ <i>Hind</i> III-digested Δhtr15 insert: -326 to +2338 but lacking +5 to +1911 (<i>htr15</i> : 1911 bp). Additionally the <i>bgaH</i> -locus sequence was inserted between the <i>Spe</i> I and <i>Sac</i> I sites as in the construction of pMKK112 [this work]
pMKK116 (pM@βΔhtr16)	7762 bp vector derived from pUS-Mev by replacing the <i>bop</i> -locus sequence between <i>Spe</i> I and <i>Hind</i> III sites with the <i>Spe</i> I/ <i>Hind</i> III-digested Δhtr16 insert: -324 to +2649 but lacking +2 to +2379 (<i>htr16</i> : 2379 bp). Additionally the <i>bgaH</i> -locus sequence was inserted between the <i>Spe</i> I and <i>Sac</i> I sites as in the construction of pMKK112 [this work]
pMKK117 (pM@βΔhtr17)	7755 bp vector derived from pMKK112 by replacing the Δhtr12 insert between <i>Bam</i> HI and <i>Hind</i> III sites with the <i>Bam</i> HI/ <i>Hind</i> III-digested Δhtr17 insert: -295 to +1908 but lacking +1 to +1622 (<i>htr17</i> : 1611 bp) [this work]
pMKK118 (pM@βΔhtr18)	7962 bp vector derived from pUS-Mev by replacing the <i>bop</i> -locus sequence between <i>Spe</i> I and <i>Hind</i> III sites with the <i>Spe</i> I/ <i>Hind</i> III-digested Δhtr18 insert: -459 to +2788 but lacking -1 to +2451 (<i>htr18</i> : 2451 bp). Additionally the <i>bgaH</i> -locus sequence was inserted between the <i>Spe</i> I and <i>Sac</i> I sites as in the construction of pMKK112 [this work]
pMKK119 (pM@βhtr14)	9757 bp vector derived from pMKK100 by replacing the MCS sequence between <i>Bam</i> HI and <i>Hind</i> III sites with the <i>Bam</i> HI/ <i>Hind</i> III-digested <i>htr14</i> -locus sequence: -384 to +2196 (<i>htr14</i> : 1884 bp) [this work]
pMKK121 (pM@βΔoe1534)	7798 bp vector derived from pMKK100 by replacing the MCS sequence between <i>Bam</i> HI and <i>Hind</i> III sites with the <i>Bam</i> HI/ <i>Hind</i> III-digested Δoe1534 insert: -299 to +1093 but lacking +1 to +771 (<i>oe1534</i> : 771 bp) [this work]
pMKK102 (pM@βhop2)	9448 bp vector derived from pMKK100 by replacing the MCS sequence between <i>Bam</i> HI and <i>Hind</i> III sites with the <i>Bam</i> HI/ <i>Hind</i> III-digested <i>hop</i> -locus sequence: -577 to +1698 (<i>hop</i> : 825 bp) [this work]

4.2.3 Media and antibiotics

Media for *E. coli*

LB medium (Sambrook et al., 1989)

1 %	tryptone	10 g	tryptone
0.5 %	yeast extract	5 g	yeast extract
0.5 %	NaCl	5 g	NaCl
		ad 1 l	H ₂ O

TB medium (Sambrook et al., 1989)

1.2 %	tryptone	12 g	tryptone
2.4 %	yeast extract	24 g	yeast extract
0.35 %	glycerol	4 ml	87 % glycerol
17 mM	KH ₂ PO ₄	2.31 g	KH ₂ PO ₄
72 mM	K ₂ HPO ₄	12.54 g	K ₂ HPO ₄
		ad 1 l	H ₂ O

Tryptone, yeast extract and glycerol are dissolved and autoclaved in 900 ml H₂O. After cooling to ~ 60 °C 100 ml of sterile 170 mM KH₂PO₄ / 720 mM K₂HPO₄ are added.

SOC medium (Sambrook et al., 1989)

2 %	tryptone	20 g	tryptone
0.5 %	yeast extract	5 g	yeast extract
8.6 mM	NaCl	0.5 g	NaCl
2.5 mM	KCl	10 ml	0.25 M KCl
10 mM	MgCl ₂	5 ml	2 M MgCl ₂
20 mM	glucose	20 ml	1 M glucose
		ad 1 l	H ₂ O

The filter-sterilized solutions of MgCl₂ and glucose are added after autoclaving and cooling to ~ 60 °C.

All media were prepared with deionized water. For LB and SOC media the pH was adjusted to 7.0 with NaOH, TB medium had a pH of 7.5. Sterilization was done by autoclaving. For the preparation of agar plates 15 g of agar were added per 1 l of medium. If appropriate, ampicillin was added after the medium had cooled down to approximately 50 °C.

Media and solutions for *H. salinarum****Complete medium (Oesterhelt and Krippahl, 1983)***

81 mM	MgSO ₄	20 g	MgSO ₄ · 7 H ₂ O
10 mM	Na ₃ -citrate	3 g	Na ₃ -citrate · 2H ₂ O
4.3 M	NaCl	250 g	NaCl
27 mM	KCl	2 g	KCl
1% (w/v)	peptone (L34, Oxoid)	10 g	peptone (L34, Oxoid)
		ad 1 l	H ₂ O

pH is adjusted to 7.0 with NaOH.

Basal salt solution (BS)

Like complete medium but without peptone.

Basal salt solution without citrate (BSWC)

Like complete medium but without peptone and without citrate.

20 mM HEPES-buffered basal salt solution (BSH)

Like basal salt solution but additionally buffered with 20 mM HEPES (20 ml 1 M HEPES, pH 7.0 ad 1 l).

All media and solutions were prepared with deionized water. Sterilization of the medium - and of the solutions if appropriate - was done by autoclaving. For the preparation of agar plates 15 g of agar were added per 1 l of medium. If appropriate the antibiotic mevinolin was added after cooling down of the medium to approximately 50 °C.

Swarm plates contained 0.25 % agar in complete medium.

Antibiotics

The following antibiotics were used in the course of this study:

<i>Antibiotic</i>	<i>Stock solution</i>	<i>Final concentration</i>
ampicillin	100 mg/ml in water (filter sterilized)	100 µg/ml
mevinolin (lovastatin)	10 mg/ml in ethanol	10 µg/ml

The mevinolin (monacolin K, lovastatin, 404.5 g/mol) stock solution was prepared by ethanol extraction of Mevinacor™-tablets (MSD Sharp & Dohme, Haar, Germany). 10 tablets of 20 mg lovastatin each were ground up in a mortar and suspended in 20 ml of ethanol. The suspension was shaken in a Falcon tube at room temperature for 1 hour and centrifuged at 5000·g for 5 min. The supernatant was filtered through a sterile 0.22 µm PVDF-filter. All antibiotics were stored at - 20 °C.

4.2.4 Transformation of *E. coli*

Production of electrocompetent *E. coli*

5 ml of an over night culture of XL1-Blue MRF' cells (35ml LB medium, inoculated from a plate, 37 °C, 250 rpm) were added to 500 ml of TB medium. The cells were grown at 37 °C and 250 rpm to a density of $OD_{600} = 0.9 - 1.2$, cooled down to 4 °C and collected by centrifugation (GS3 rotor, 3000·g, 20 min, 4 °C). The centrifugation step and all further steps were performed at 0 - 4 °C using sterile equipment and solutions. The cells were gently suspended and washed 3 times in decreasing amounts of 10 % glycerol (500 ml, 250 ml and 50 ml). The final pellet was resuspended with 1 ml of 10 % glycerol. Aliquots of 90 µl, each containing approximately $20 \cdot 10^9$ cells, were frozen in liquid N₂ and stored at - 70 °C.

Electrotransformation of *E. coli*

90 µl aliquots of electrocompetent cells stored at -70 °C were thawed on ice. All following steps until the electrotransformation event were performed on ice. 45 µl of the cells were added to an appropriate amount of plasmid DNA in a microfuge tube (0.2 – 0.5 ng of plasmid DNA for plasmid production or 2µl of a ligation mixture containing 10 – 40 ng of total DNA per µl). After incubation on ice for 10 min the cells were transferred to a sterile electrotransformation cuvette (2 mm electrode distance, Biorad, Munich, Germany) and incubated for additional 2-5 min. The electrotransformation was performed in a Gene Pulser (Biorad, Munich, Germany) with the following settings: 2.5 kV, 400 Ω, 25 µF. Time constants were between 8 and 9 ms. The electrotransformed cells were immediately diluted with 500 µl of SOC medium. After incubation for 30 – 60 min in a test tube at 37 °C and 250 rpm to allow for their regeneration, the cells were plated onto ampicillin-containing LB agar plates and incubated at 37 °C overnight.

A 4 ml over night culture of a single colony from the plate in ampicillin-containing LB medium was used for DNA isolation with the QIAprep™ Spin Miniprep Kit, which usually yielded 50 µl of 200 - 600 µg plasmid DNA per µl.

4.2.5 Transformation of *H. salinarum*

PEG transformation of *H. salinarum*

Transformation of *H. salinarum* was performed according to the method of Cline *et al.* (1989) with some modifications.

To increase their transformation competence halobacterial cells were cultured in 35 ml of complete medium to a cell density of $OD_{600} = 0.3 - 0.4$ (late log phase), then diluted 200-fold into 35 ml of complete medium and recultured. After the cells had grown to $OD_{600} = 0.3 - 0.4$ two or three times, they were finally grown to a cell density of $OD_{600} = 0.5 - 0.8$.

2 ml of this halobacterial culture were centrifuged in a microfuge tube (2 min, 8000·g, RT). After complete removal of the supernatant the pellet was gently resuspended in 200 μ l of spheroplasting solution (SPS). 5 μ l of 0.5 M EDTA in SPS (f.c. was 12.5 mM EDTA) were then added to convert the cells to spheroplasts. It was found that EDTA concentrations as low as 2.5 mM produced spheroplasts rather quickly (2 - 5 min) whereas higher concentrations slowed down spheroplast formation (at a f.c. of 50 mM EDTA the same sample still showed ~ 30% rod shaped cells after 20 min).

When spheroplast formation was complete, the spheroplasts were added to a 2 ml microfuge tube containing a mix of 4 μ l of a plasmid-DNA solution (2 - 3 μ g DNA) with 10 μ l of 1 M NaCl. Gentle mixing was followed by an incubation for 2 - 5 min at RT. 220 μ l of 60 % PEG₆₀₀ in SPS were transferred to the lid of the tube and mixed with the spheroplasts by closure of the lid and immediate vigorous shaking of the tube to prevent cell lysis caused by an excessively high PEG₆₀₀ concentration. After incubation at RT for 15 min the tube was filled up with 1.6 ml of complete medium and centrifuged (2 min, 8000·g, RT). After careful removal of the supernatant (decanting followed by a short spin and complete removal of the remaining liquid) the spheroplasts were gently resuspended in 2 ml of complete medium and pelleted and resuspended as before but this time in 600 μ l.

To allow the cells to recover their S-layer the microfuge tube was placed into a horizontal position and incubated for 24 h at 37 °C at 250 rpm. An aliquot of 50 - 100 μ l of the cells was plated onto agar plates containing complete medium and mevinolin as selective agent. The remaining cells were pelleted, resuspended in 50 μ l of complete medium and also plated. Colonies were usually visible after the plates had been incubated for 10 - 20 days at 40 °C in a closed box. The box additionally contained an open dish filled with 4 M NaCl to prevent the plates from drying out.

In the case of transformations with *bgaH*-containing plasmids (i.e. for all plasmids used in this study except pMKK101) the plates additionally contained 1 µg X-gal (Gerbu Biochemicals, Gaiberg, Germany) per ml medium.

SPS (*Spheroplasting solution, contains no Mg²⁺*)

2 M	NaCl	11.7 g	NaCl
25 mM	KCl	2.5 ml	1 M KCl
50 mM	Tris/HCl, pH 8.75	5 ml	1 M Tris/HCl, pH 8.75
15 % (w/v)	sucrose	15 g	sucrose
		ad 100 ml	H ₂ O

The pH is adjusted to 8.75 with 10 M NaOH.

0.5 M EDTA in SPS (*EDTA chelates Mg²⁺ thereby damaging the S-layer*)

0.5 M	EDTA	9.3 g	EDTA
2 M	NaCl	5.85 g	NaCl
25 mM	KCl	1.25 ml	1 M KCl
50 mM	Tris/HCl, pH 8.75	2.5 ml	1 M Tris/HCl, pH 8.75
15 % (w/v)	sucrose	7.5 g	sucrose
		ad 50 ml	H ₂ O

To dissolve EDTA the pH is adjusted to 8.75 with 10 M NaOH.

60 % PEG₆₀₀ in SPS (*PEG makes the membrane permeable for DNA*)

Like SPS but additionally containing 60 % (w/v) of PEG₆₀₀ (Merck, Darmstadt, Germany).

All solutions were sterilized by filtration through an 0.22 µm filter (Rotilabo™ Spritzenfilter, Roth, Karlsruhe, Germany) and kept at 4 °C until use. Immediately before use they were brought to RT.

Clone selection by double picking

Cells transformed with a suicide plasmid have integrated the complete plasmid DNA into their genome by homologous recombination and have thereby acquired resistance to mevinolin (Fig. 4.1). A transformed colony from a mevinolin-containing plate was selected and recultured two or three times to an OD₆₀₀ of 0.5 - 0.8 in 35 ml complex medium without mevinolin. This allowed for a second recombination event in some of the cells by which they lost the plasmid DNA, either producing wild-type cells or the desired genotype. Growing cells from such a culture on plates lacking mevinolin was followed by picking 300 to 600 clones and transferring each one to a plate with and a plate without mevinolin (double-picking). The clones which did not grow on the mevinolin-containing plate were picked on the plate without mevinolin, recultured in 35 ml complex medium and subjected to Southern blot analysis to identify those which had the desired genotype.

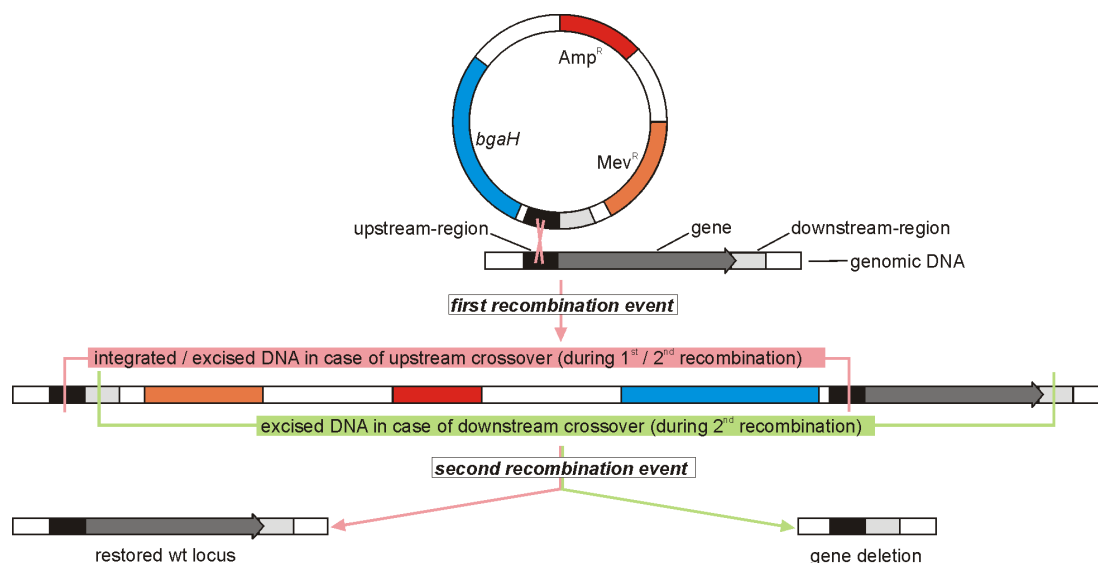


Figure 4.1 Schematic description of a halobacterial transformation with a suicide plasmid.

Transformation of halobacterial cells with a suicide plasmid, which lacks a halobacterial origin of replication, happens via homologous recombination. The complete plasmid DNA, including the mevinolin resistance gene and *bgaH*, is thereby integrated into the halobacterial genome, in the case of deletion plasmids either into the region upstream or downstream of the gene that is to be deleted. Cells which have integrated the plasmid DNA are mevinolin-resistant and turn blue on plates containing X-gal, due to the *bgaH*-encoded β -galactosidase activity. When such cells are grown in the absence of mevinolin, a second recombination can take place by which the plasmid DNA is removed from the genome. If this second recombination happens within the same region as the first (here the upstream-region), then the wild type situation is restored. However, if it happens within the other region of homology (here the downstream-region), then not only the plasmid DNA but also the gene of interest are excised from the genome resulting in a deletion genotype. With equally long regions of upstream and downstream homology in the plasmid, probabilities are equal for wild-type regeneration and for the generation of a gene deletion.

Clone selection by red-blue selection

Alternatively, when the plasmids contained the *bgaH* gene, transformed cells were plated on mevinolin-containing plates which additionally contained 1 μ g X-gal (Gerbu Biochemicals, Gaiberg, Germany) per ml medium. It was freshly applied to the plates > 3 hours before spreading the cells, by plating a fresh mixture of 40 μ l of water with 40 μ l of X-gal stock solution (40 mg/ml in dimethylformamide). After the colonies had grown to an optimal size at 40°C, the plates were kept at room temperature for 1 to 4 days until unambiguous differentiation between blue and red colonies was possible.

To generate cells with the desired genotype, a blue colony was picked on the mevinolin-containing plate, regrown three times in 35 ml of fresh complex medium as described and then plated on X-gal-containing plates without mevinolin. On such plates, in addition to blue colonies some red ones (1 - 5%) were also present. In $\geq 50\%$ of the red colonies the genotype of the parental strain was restored, whereas the rest had the desired genotype, which was finally verified via Southern-blot analysis.

4.3 Methods of molecular biology

4.3.1 Preparation and sequencing of DNA

Preparation of unpurified ("crude") halobacterial DNA

Halobacterial genomic DNA for use in PCRs and Southern blots was prepared by lysing cells with water. This was done by spinning down 2 ml of a fresh halobacterial culture (1 min, 12,000·g) of an OD₆₀₀ of 0.7 +/- 0.1 and careful removal of the complete supernatant (by a second short spin of the microfuge tube after decanting the supernatant followed by the removal of remaining medium with a pipet tip). Complete lysis of the cells was achieved by addition of 400 µl of water to the pellet, immediately followed by intensive mixing with the pipet to produce a uniform lysate without DNA clots. One microliter of such "crude" genomic DNA, which was prepared as described from a culture of an OD₆₀₀ of 0.7, is estimated to contain approx. 10 to 20 ng of DNA from 5·10⁶ cells. Stored at 4°C the DNA preparation can be used as a template in PCRs at least for several weeks.

Isolation of plasmid DNA from *E. coli* cells

Plasmid DNA was isolated from *E. coli* cells using the QIAprep Miniprep kit (Qiagen, Hilden, Germany). In brief, a clone of transformed cells was selected on an ampicillin-containing agar plate and the cells were grown overnight in 5 ml of LB medium (37°C, 250 rpm). Cells from 4 ml of this culture were pelleted and treated according to the manufacturer's protocol. The final elution from the QIAprep column with 2 mM Tris/HCl at pH 8.5 usually yielded 50 µl of plasmid DNA (200 - 600 ng/µl).

Isolation of DNA fragments from agarose gels

Electrophoretic separation of DNA fragments was done in gels of 1 - 1.5% agarose in 1 x TAE buffer at 5 V/cm. The samples were applied to the gels dissolved in 1 x DNA sample buffer. To isolate specific DNA fragments from such gels, the QIAquick Gel Extraction kit (Qiagen, Hilden, Germany) was used. In brief, a gel slice containing only the desired fragment was excised from the gel and treated according to the manufacturer's protocol.

50 x TAE buffer (Sambrook et al., 1989)

2 M	Tris/acetate, pH 8.5	242 g	Tris base
		57.1 ml	CH ₃ COOH
100 mM	EDTA	37.2 g	Na ₂ EDTA·2H ₂ O
		ad 1000 ml	H ₂ O

The final 1 x TAE electrophoresis buffer is 40 mM Tris/acetate, pH ~8.3 and 2 mM EDTA.

6 x DNA sample buffer

47% (v/v)	glycerol	5.4 ml	87% glycerol
10 mM	Tris/HCl pH 7.0	100 µl	1 M Tris/HCl, pH 7.0
0.025%	bromophenolblue	125 µl	2% bromophenolblue in 20% ethanol
0.025%	xylene cyanol FF	125 µl	2% xylene cyanol FF in 20% ethanol
		ad 10 ml	H ₂ O

Determination of DNA concentration

The concentrations of solutions of plasmid DNA or PCR products after purification via agarose gels were determined with a Gene Quant II spectrophotometer (Pharmacia Biotech, Uppsala, Sweden) by measuring the absorption at 260 nm. For a pathlength of 1 cm an absorption of 1.0 corresponds to a concentration of double stranded DNA of 50 µg/ml.

Sequencing of DNA

Sequencing of DNA templates present in the generated plasmids was done using the method of Sanger. With this method DNA fragments of different lengths are produced by DNA polymerase-mediated elongation of an appropriate primer on a template DNA, using a reaction mix which contains low concentrations of each of the four dideoxynucleotides (ddATP, ddGTP, ddCTP and ddTTP) in addition to the four common deoxynucleotides (dNTPs). Each of these ddNTPs is labeled with a different fluorophore and when the polymerase adds one of them instead of the corresponding dNTP, the elongation of the DNA fragment is terminated and the fragment is labeled with the respective fluorophore. Electrophoretic separation of the generated DNA fragments, in combination with laser-excitation of the eluting fluorophores and fluorescence detection, produces a sequence of the four different fluorescence signals. This sequence corresponds to that of the bases in successively longer DNA fragments.

In this study the ABI PRISM BigDye Terminator Cycle Sequencing kit (Applied Biosciences, Foster City, CA, USA) was used. The Terminator Ready Reaction Mix contained the dye-labeled ddNTPs (BigDye terminators), dNTPs (dATP, dCTP, dTTP and dUTP), AmpliTaq DNA polymerase and MgCl₂ in Tris/HCl buffer at pH 9.0. The DNA fragments were generated from the template DNA by subjecting the sequencing reaction mix to thermocycling as described below. The product of the sequencing reaction was purified via MicroSpin G-50 columns

according to the manufacturer's protocol (Amersham Biosciences, Freiburg, Germany) to remove excessive dNTPs and BigDye terminators. The eluates were dried in a Speedvac for 45 min. Sequencing was performed by gel electrophoresis in an ABI PRISM 377 DNA sequencer (Applied Biosystems, Foster City, CA, USA). For analysis of the electropherograms and to check the generated sequences via alignment to the expected sequences the computer program BioEdit was used.

Sequencing reaction mix:

100 - 200 fmol	plasmid DNA	1.5 μ l	plasmid solution produced by a QIAprep miniprep (200 - 600 ng/ μ l)
10 pmol	primer	1 μ l	10 pmol/ μ l primer solution
	Terminator Ready Reaction mix	5 μ l	Terminator Ready Reaction mix
625 mM	betaine	2 μ l	5 M betaine
		ad 16 μ l	H ₂ O

Thermocycling program (30 cycles of steps 1 - 3):

Step:	Temperature:	Time:	Description:
1	96°C	10 s	Melting
2	50°C	5 s	Primer annealing
3	60°C	4 min	Elongation
4	4°C	hold	Storage

4.3.2 Generation of PCR fragments and plasmid construction

General strategy

PCR reactions were performed in a GeneAmp 9700 thermocycler (Applied Biosystems, Foster City) with Pfu-Turbo polymerase (Stratagene, La Jolla, CA, USA) according to the supplier's recommendations, using unpurified ("crude") genomic DNA from strain S9 as template. A typical PCR mixture had the following composition: 5 μ l of 10x Pfu-Turbo buffer, ~1 μ l of each primer (10 - 20 pmol), 5 μ l of a dNTP mixture (12.5 nmol of each dNTP), 1 μ l of "crude" DNA (200 - 500 ng), 3 μ l DMSO, water ad 50 μ l and finally 0.3 - 1.0 μ l Pfu-Turbo polymerase (0.8 - 2.5 U). The mixture was heated to 96°C for 2 min and then subjected to 30 cycles of melting- (96°C, 30 s), annealing- (5°C below the calculated annealing temperature, 30s) and extension- steps (72°C, 1 min per 500 bp). All generated DNA fragments used for the construction of deletion plasmids consisted of ca. 350 +/- 50 bp each, of upstream and downstream gene-flanking sequences, fused to each other and were generated and cloned as exemplified here by Δ 14.

The flanking sequences of the *htr14* gene were fused via recombinant PCR (Higuchi, 1990) to produce the deletion fragment Δ 14. As the first step, in two separate PCR reactions DNA fragments were produced which comprised 384 and 320 bp of the upstream and downstream

region of the gene, respectively. The following primers were used (with restriction sites underlined and positions of the 3' nucleotides given relative to that of the first nucleotide of the *htr14* coding region): USshr14.seq: 5'- GCT TGG ATC CGA GGC CTC CC-3' (*Bam*HI, -375), USshr14.rev: 5'- CGC TAC TGG CGC CTA ATC GTC TAT GTC CCC C-3' (-21), DSshr14.seq: 5'- ACG ATT AGG CGC CAG TAG CGG CCC CGC C-3' (+1894), DSshr14.rev: 5'- CGA GAA GCT TCT GTT CCG CGG-3' (*Hind*III, +2186). The 5'-regions of USshr14.rev and DSshr14.seq were designed such that the produced PCR fragments showed an overlap of 20 bp (representing the fused 10 bp upstream and downstream of the *htr14*-encoding region).

In a second step the purified PCR products together with the primers USshr14.seq and DSshr14.rev were subjected to another round of PCR yielding the deletion fragment $\Delta 14$, comprising 704 bp of fused upstream and downstream sequence lacking the coding region of *htr14* in between. The introduced restriction sites were used for inserting $\Delta 14$ into the multiple cloning site (MCS) of plasmid pMKK100 to produce pMKK114 (Fig. 3.2). All other deletion fragments were produced and cloned in a similar manner (for a list of the primers see Table 6.1).

pMKK100 and all derived plasmids are suicide plasmids. The *bgaH*-locus in pMKK100 consists of the *bgaH* gene together with 141 bp of its upstream and 153 bp of its downstream DNA sequence, flanked by attached *Spe*I and *Sac*I restriction sites, respectively. It was produced by PCR amplification of *Haloferax alicantei* DNA, present in plasmid pMHL32 (Holmes and Dyall-Smith, 2000).

The following PCR products were used in the construction of complementation plasmids: a DNA fragment comprising the *bop* locus from position -393 to position +1391 between included *Bam*HI and appended *Hind*III sites, one comprising the *hop* locus from position -577 to position +1698 between appended *Bam*HI and *Hind*III sites (Fig. 3.3), and one comprising the *htr14* locus from position -384 to position +2196 between appended *Bam*HI and *Hind*III sites (Fig. 3.6). The fragments were digested with *Bam*HI and *Hind*III and inserted into plasmid pUS-Mev (Pfeiffer *et al.*, 1999) in the case of the *bop*-containing fragment, and into plasmid pMKK100 in the case of the *hop*- and the *htr14*-containing fragments, to produce the complementation plasmids pMKK101, pMKK102 and pMKK119. The sequences of $\Delta 14$ and of all other deletion and complementation fragments were confirmed via sequencing of the respective plasmids (for a list of all plasmids see Table 4.2).

Restriction digest

Cleavage of DNA by endonucleases was mainly used for two purposes: (i) To create ligatable fragments from PCR products and plasmids. (ii) To produce a mixture of genomic DNA fragments with defined sizes for use in Southern blots. Three typical reaction mixtures are listed below. Buffers and BSA solution for the digestion mixtures were used as recommended by the manufacturer (New England Biolabs, Beverly, MA, USA), so that the activity of each endonuclease, also in double digests, was at least 75% of its maximum value under ideal buffer conditions.

Reaction mixtures for restriction digests

	Purified PCR-product as DNA-fragment:	Purified plasmid as DNA-fragment:	"Crude" genomic DNA as DNA-fragment:
10 x NE-buffer:	5 µl	5 µl	6 µl
10 x BSA solution:	5 µl	5 µl	6 µl
H ₂ O:	13 µl	13 µl	17 µl
DNA-fragment:	25 µl	25 µl	30 µl
endonuclease 1:	1 µl (10 - 20 U)	1 µl (10 - 20 U)	1 µl (10 - 20 U)
endonuclease 2:	1 µl (10 - 20 U)	1 µl (10 - 20 U)	---
total volume:	50 µl	50 µl	60 µl
incubation conditions:	37 °C, 2 - 12 h	37 °C, 2 - 12 h	37 °C, 16 - 24 h

Ligation

Ligations of endonucleolytically cleaved plasmids and PCR fragments were done with T4 DNA ligase (Gibco BRL, Berlin, Germany). The ratio of plasmid to insert was optimally 1 : 3. A typical example of a ligation reaction mixture and the incubation conditions are listed below.

Reaction mixture for T4 DNA ligase

		Example:
5 x reaction buffer:	4 µl	4 µl
plasmid:	3 - 30 fmol	20 fmol (106 ng) of an 8000 bp plasmid
insert:	9 - 90 fmol	60 fmol (32 ng) of an 800 bp insert
H ₂ O:	ad 20 µl total	ad 20 µl total
T4 DNA ligase:	1 µl (1U)	1 µl (1U)
total volume:	20 µl	20 µl
incubation conditions:	Mixing on ice, followed by 1 h at 14 °C and 1 h at 25°C. For transformations 2 µl of the reaction product is used per 45 µl of <i>E. coli</i> cells.	

4.3.3 Southern blot analysis

To produce the DIG-11-dUTP-labeled "PRE" and "CORE" DNA probes used in the Southern-blots, in a first step appropriate DNA sequences were amplified from genomic DNA by standard

PCRs with the primers listed in Table 6.1. The correctly sized products of the first PCRs were purified from agarose gels, and approx. 50 ng of purified product were used as the template for additional PCRs in which 1 nmol of DIG-11-dUTP was present in addition to the unlabeled dNTPs.

In each case the PRE and CORE probes hybridized to a region upstream of the gene and within the gene, respectively. To analyze the different strains, their (crude) genomic DNA was digested with an appropriate restriction enzyme (mostly *Bam*HI or *Pst*I), subjected to 1% agarose gel electrophoresis, vacuum-blotted and then UV-crosslinked to Hybond-N nylon membrane (Amersham Biosciences, Freiburg, Germany). To allow determination of the fragment sizes, one lane of the agarose gels always contained 8 µl of DIG-labeled DNA molecular weight marker (Roche Diagnostics, Mannheim, Germany). The total amount of DNA per lane corresponded to the DNA content of $30 \cdot 10^6$ cells (approximately 100 ng of digested DNA from 6 µl of a crude DNA preparation). The use of blocking reagent, hybridization procedure and chemiluminescent detection with CSPD was according to the manufacturer's protocols (Roche Diagnostics, Mannheim, Germany).

4.4 Methods for protein analysis

4.4.1 Protein preparation from *H. salinarum* cells

Preparation of membrane and cytosolic protein fractions for use in immunoblots and for MS analysis

Membrane and cytosolic fractions of halobacterial protein were prepared under high salt conditions (1.3 M) as follows: 450 ODml of cells from a 350 ml culture with an OD₆₀₀ of 1.4 were spun down, and resuspended in 20 ml of 30 % basal salt medium (30% complex medium without peptone) additionally containing 10 µg/ml PMSF, 20 mM HEPES pH 7.5 and 100 µg/ml DNase I. After sonication at 0 - 10°C (2 x 1 min, Branson sonifier 450, 1/2" disruptor horn, 30% duty cycle, level 6) the lysate was centrifuged at 6,300-g and 20°C for 20 min to remove unlysed cells and allow for DNase I action. The membrane protein fraction was obtained as a pellet after centrifugation (60Ti-rotor, Beckman, 200,000-g, 90 min, 4°C). After removing the supernatant the pellet was resuspended in 20 ml of the mentioned buffer and centrifuged as before. It was finally resuspended in 1 ml of protein resuspension buffer (20 mM HEPES pH 7.5, containing 10 µg/ml of PMSF and 1 mM EDTA). To avoid contamination of the cytosolic protein fraction with the pellet only the upper 7 ml of the supernatant of the first ultracentrifugation were carefully collected, the rest was discarded. After protein precipitation by

adding 6 volumes of acetone (-20°C) to the saved supernatant, followed by two washing steps with 40 ml ice cold 50% acetone to remove the salt, the precipitate was pelleted, dried and resuspended in 1 ml of protein resuspension buffer. Aliquots were stored at -70°C.

4.4.2 Determination of protein concentration

Protein concentrations of membrane and cytosolic fractions were determined with the BCA protein assay reagent kit (Pierce, Rockford, IL, USA) according to the manufacturer's recommendations. The method is based on the biuret reaction of Cu^{2+} with proteins in alkaline solution to form Cu^+ , followed by the sensitive and selective colorimetric detection of Cu^+ via its reaction with bicinchoninic acid (BCA) to form a blue complex with an absorption maximum at 562 nm. In brief, the assay was performed in a microplate in which different dilutions of a BSA standard (2 mg/ml) and different dilutions of protein samples of unknown concentrations were separately mixed with the reagent mix and then incubated at 60°C for 30 min. After the determination of absorption values at 490 nm in a Wallac 1420 multiwell plate reader (Perkin Elmer, Boston), a standard curve was generated with the BSA dilutions and used to determine the concentrations of the unknown samples.

4.4.3 SDS PAGE

Proteins from the halobacterial membrane or cytosolic fractions, which had been stored at -70°C, were incubated for 20 min at 40°C in 1 x SDS sample buffer prior to their electrophoretic separation (15 µg total protein per lane) in a discontinuous SDS PAGE according to Laemmli (1970). The acrylamide content was 3.9% for the stacking gel and 8% for the separating gel. The electrophoresis runs were performed in SE250 Mighty Small II miniature vertical slab gel units (Hoefer Scientific Instruments, San Francisco, CA, USA) under constant cooling with tap water. The 8 cm x 7 cm x 0.75 mm gels were subjected to currents of 5 mA per gel until the front of bromophenol blue reached the separating gel and ≤ 15 mA per gel for the remaining time at a maximum voltage setting of 150 V. The total electrophoresis time amounted to approx. 3.5 hours. In each case the BenchMark protein ladder (Invitrogen, Karlsruhe, Germany) was used as a molecular weight standard. In addition to the components listed below, the separating gel optionally also contained 6 M urea to reduce the number of bands detected on immunoblots.

The separated proteins were finally either analyzed immunochemically or via in-gel digestion followed by MS analysis of the generated peptides. To visualize protein bands, the gels were incubated with Coomassie stain for 15 min, followed by destaining in Destain-1 for 10 min and in Destain-2 for 30 min or up to several hours. Staining and destaining solutions were heated in

a microwave to approx. 40 - 50°C before the addition of the gels. To avoid contaminations in the subsequent MS analyses, these solutions were prepared from chemicals of the purity grade p.a. and from ultrapure water (18.2 MΩcm) generated with the Milli-Q PF Plus system (Millipore Corporation, Billerica, MA, USA).

3.9% Stacking gel (5 ml for 3 minigels)

3.9%	acrylamide (aa) / bisacrylamide (baa)-mix	650 µl	30% aa / 0.8% baa-mix
125 mM	Tris/HCl pH 6.8	630 µl	1 M (8x) Tris/HCl pH 6.8
0.1% (w/v)	SDS	50 µl	10% (w/v) SDS (350 mM)
ad 5 ml	H ₂ O	3.7 ml	H ₂ O
0.2%	TEMED	10 µl	TEMED
0.1% (w/v)	APS (add at last!)	50 µl	10% (w/v) APS

Addition of 20 µl of 2% bromophenol blue (in ethanol) slightly stains the gel and facilitates loading of the samples.

8% Separating gel (10 ml for 2 minigels)

8%	acrylamide (aa) / bisacrylamide (baa)-mix	2.7 ml	30% aa / 0.8% baa-mix
375 mM	Tris/HCl pH 8.8	2.5 ml	1.5 M (4x) Tris/HCl pH 8.8
0.1% (w/v)	SDS	100 µl	10% (w/v) SDS (350 mM)
ad 10 ml	H ₂ O	4.7 ml	H ₂ O
0.2%	TEMED	20 µl	TEMED
0.04% (w/v)	APS (to be added at last!)	40 µl	10% (w/v) APS

5 x SDS electrophoresis buffer (used as 1 x SDS electrophoresis buffer)

125 mM	Tris base	15.1 g	Tris base
960 mM	glycine	72 g	glycine
0.5% (w/v)	SDS	5 g	SDS
ad 1000 ml	H ₂ O	~ 1 l	H ₂ O

For use at the anode, the buffering capacity should be increased by addition of 7 g Tris base per liter 5 x buffer, resulting in a pH of approximately 8.8.

5 x SDS sample buffer (10 ml)

300 mM	Tris/HCl pH 6.8	3 ml	1 M Tris/HCl pH 6.8
9% (w/v)	dithiothreitol (580 mM)	900 mg	dithiothreitol
50% (v/v)	glycerol	5.9 ml	87% glycerol
12% (w/v)	SDS	1.2 g	SDS
0.03%	bromophenol blue	150 µl	2% bromophenol blue (in 20% ethanol)

The sample buffer was stored in aliquots at -20°C. When gel electrophoresis was followed by MS analysis or immunoblotting, protein samples were dissolved in 1 x SDS sample buffer, which additionally contained freshly added 1.5% (v/v) 2-mercaptoethanol, to ensure complete reduction of disulfide bonds.

Coomassie stain (500 ml)

0.1%	Coomassie brilliant blue R250	0.5 g	Coomassie brilliant blue R250
40% (v/v)	ethanol	200 ml	ethanol
10% (v/v)	acetic acid	50 ml	acetic acid
ad 500 ml	H ₂ O	250 ml	H ₂ O

Destain-1

Like Coomassie stain but without the Coomassie brilliant blue R250.

Destain-2

10% (v/v) acetic acid.

4.5 Immunochemical methods

4.5.1 Production of antibodies

Design and synthesis of antigenic peptides

The polyclonal antisera anti-Htr14_{D585} and anti-Htr14_{E172} were generated against synthetic peptides, comprising amino acids D585 to S606 and E172 to R195 of MpcT (Htr14), respectively, in both cases plus N-terminally attached glycyl-cysteine. The chosen sequences are present in regions of MpcT that have little or no homology to other halobacterial transducers. They were expected to be immunogenic because of their low hydrophobicity due to a high content of charged residues, and in the case of the D585 peptide additionally because of the presence of 3 prolines. Both peptides were synthesized in the Moroder department at the MPI of Biochemistry, Martinsried, via the solid phase method, and their purity was determined via mass spectrometry to be > 99% for the D585 peptide and > 95% for the E172 peptide. In each case the peptide was coupled via the cysteine to maleimide-activated keyhole limpet hemocyanine from the EZ antibody production and purification kit (Pierce, Rockford, IL, USA) according to the manufacturer's recommendations.

Immunization of rabbits and serum generation

Further treatment of the two conjugates was identical. After a conjugate was purified via the gel-filtration column of the kit as recommended, it was emulsified 1:1 with 0.5 ml of TiterMax Gold adjuvant (Sigma-Aldrich, Taufkirchen, Germany). Five hundred microliters of the mixture were subcutaneously injected into a rabbit immediately, followed by two booster shots with 250 µl each after 28 and 78 days. The blood was collected on day 92 and after clotting and centrifugation each antiserum was stored at -70°C and used without further purification. Both antisera showed high sensitivity as well as specificity, as demonstrated by the generation of clear signals on Western blots when used at a dilution of 1 : 30,000, whereas no signals were seen with cells lacking MpcT.

4.5.2 Western blot analysis

For immunodetection proteins were electrophoretically separated on an 8% SDS-PAGE gel and blotted onto nitrocellulose membrane (Schleicher and Schuell, Dassel, Germany) via tank blotting in Towbin buffer at 0°C for 1 hour at 100 V in a Trans-Blot electrophoretic transfer cell (Biorad, Munich, Germany). To check the transfer and to mark the positions of the protein molecular weight standard, the membrane was stained with 1 x Ponceau S.

After washing with TBS-T buffer and blocking for 30 min at 25°C, blots were incubated at 4°C over night either with anti-Htr14_{D585} at a dilution of 1 : 30,000 in blocking buffer, or with the "multiple antigenic peptide antibody HC23" (Zhang *et al.*, 1996) at a dilution of 1 : 5,000 in blocking buffer. After an additional washing step with TBS-T buffer, blots were incubated at 25°C for 1 - 2 hours with horseradish peroxidase-conjugated goat anti-rabbit IgG (Sigma-Aldrich, Taufkirchen, Germany) diluted 1 : 10,000 in blocking buffer, and finally developed with SuperSignal West Pico chemiluminescence substrate (Pierce, Rockford, IL, USA) according to the manufacturers' protocols.

Towbin buffer

25 mM	Tris	6 g	Tris
192 mM	glycine	28.8 g	glycine
20% (w/v)	methanol	400 ml	methanol
ad 2 l	H ₂ O	~ 1.6 l	H ₂ O

The final pH is approx. 8.3. The buffer was prepared fresh after 3 - 4 uses.

10 x Ponceau S solution

2%	Ponceau S	2 g	Ponceau S
30% (w/v)	trichloroacetic acid (TCA)	30 g	trichloroacetic acid
ad 100 ml	H ₂ O	ad 100 ml	H ₂ O

TBS-T buffer

20 mM	Tris/HCl pH 7.6	2.4 g	Tris
137 mM	NaCl	8 g	NaCl
ad 1 l	H ₂ O	ad 1 l	H ₂ O (pH adjusted to 7.6 with HCl)
0.05%	Tween-20	500 µl	Tween-20 (added after autoclaving)

Blocking buffer (TBS-T with 0.2% (w/v) casein)

300 mg I-block -reagent (purified casein, Applied Biosciences, Foster City, CA, USA) were added to 150 ml of TBS-T without Tween-20, and the mixture was heated on a hot plate until completely dissolved. After cooling to 25°C, 75 µl Tween-20 were added.

4.6 Analysis of Htr-methylation by mass spectrometry

4.6.1 Preparation and MALDI-TOF MS analysis of tryptic peptides from membrane and cytosolic proteins of strain TOM.

Membrane protein preparations ("high salt membrane fraction") of strain TOM (BR⁻, HR⁻) were produced as described by Klein *et al.* (2005). Separation via native 2-D PAGE, according to Schaegger *et al.* (1994), was followed by tryptic digest of the proteins contained in excised spots from the silver-stained gel and finally by MALDI-TOF MS analysis of the peptide mixes as described by Tebbe *et al.* (2005). All steps were performed by Birgit Bisle.

The gel chromatographical fraction (Sephadex G-200, "peak 2") of a cytosolic protein preparation of TOM, in which Htr13 was present, was subjected to 2-D gel electrophoresis (first dimension IEF, pH 4 - 5, second dimension SDS PAGE, 6 - 12 % polyacrylamide). This was followed by tryptic in-gel digest of the proteins contained in gel spots and MALDI-TOF MS analysis. All steps were performed by Christian Klein as described (Klein, 2005).

4.6.2 In-gel Asp-N digest of proteins from 1-D SDS-PAGE gels

For subsequent digests of well-defined subfractions of S9 membrane protein preparations with the protease Asp-N (specifically cleaving N-terminally of Asp), the proteins were first separated on an 8% polyacrylamide SDS gel (15 µg total protein per lane). Sets of gel slices containing proteins of identical mobility were then excised from 6 lanes, cut into pieces of approx. 1 mm³, and the pieces from each set were pooled in a 0.5 ml Protein LoBind tube (Eppendorf AG, Hamburg, Germany), resulting in total protein amounts between approx. 200 and 1000 ng per tube, as estimated from the intensity of Coomassie staining of the protein in the slices. All successive steps until the application of the generated peptide mixtures to the MS system were performed in such tubes to minimize sample loss by adsorption to the tube walls.

To remove the Coomassie stain from the gel pieces, they were subjected to alternating 10 min washing steps with 120 µl 50 % acetonitrile (50% ACN) and with 120 µl of digestion buffer (25 mM ammonium bicarbonate, adjusted to pH 7.5 with acetic acid). After the third incubation with 50% ACN and removal of the liquid, the gel pieces were dried in a centrifugal vacuum concentrator.

For in-gel digest of proteins, the gel pieces were then incubated for 4 hours at 37°C at 800 rpm in 35 µl digestion buffer containing 20 ng Asp-N (Roche Diagnostics, Mannheim, Germany), in accordance with the manufacturer's recommendation to use an Asp-N amount of 0.5 to 5% of

the protein mass in the gel. After removal of the peptide-containing digestion solution, the remaining peptides were extracted from the gel pieces in successive washing steps with 50 μ l water, followed by 50 μ l 2% FA and by 50 μ l 50% ACN in 2% FA. The extraction solutions were finally combined with the digestion solution to result in the final peptide mixture.

4.6.3 LC MS/MS of the generated peptides

For LC MS/MS identification of the peptides generated by Asp-N digest, the peptide mixtures were dried in a centrifugal vacuum concentrator and redissolved in 15 μ l of 2% FA. A desalting/filtering step was included prior to the MS analysis, to protect the sensitive valve system of the MS-setup: the peptide solutions were loaded onto self-packed micro RP (reversed phase) columns (two 1 mm diameter plugs of C18 "High Performance Extraction Discs", 3M Empore, St. Paul, MN, USA, that were stuffed into gel-loader tips), after the columns had been pre-rinsed with 15 μ l of isopropanol and equilibrated with 15 μ l of 2% FA. After washing the column once with 15 μ l of 2% FA, the samples were eluted slowly with 15 μ l of 80% methanol / 2% FA into a clean Protein LoBind tube and dried as above.

Each sample was redissolved in 20 μ l of 2% FA and approx. 50 to 200 ng of total peptide (as estimated based on the Coomassie-stained gel bands) in a final volume of 3 to 10 μ l 2% FA were automatically loaded to the LC MS system consisting of a CapLC micro HPLC system, a 10-port switching valve and a Q-ToF Ultima API mass spectrometer (Waters Corporation, Milford, MA, USA). In each run the peptide solution was loaded onto a self-packed 100 μ m x 25 mm trapping column (stationary phase was ReproSil-Pur 200 C18-AQ, 5 μ m, Dr. Maisch GmbH, Ammerbuch-Entringen, Germany) at a flow rate of 2 μ l/min of solvent A (0.5% FA / 2% ACN). After valve-switching, the sample was eluted from the trapping column via a self-packed nanoscale RP column (75 μ m x 150 mm, ReproSil-Pur 120 C18-AQ, 3 μ m). To elute the peptides from the stationary phase, a binary solvent gradient was applied (Fig. 4.2) starting with 100% solvent A and ending after 100 min with 100% of solvent B (0.5% FA / 80% ACN), followed by rinsing of the columns for 25 min prior to the next run. During the elution, the CapLC pumps provided a flow of 5.5 μ l/min of which approx. 200 nl/min were directed to the columns after flow splitting.

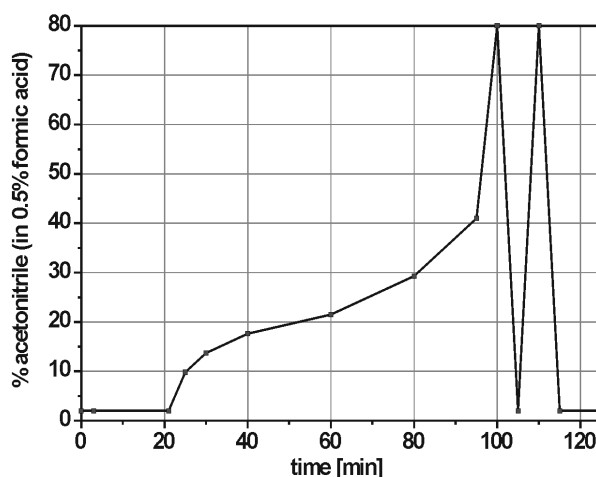


Figure 4.2 Solvent gradient used in the LC ESI Q-TOF experiments.

Peptide samples dissolved in 3 to 10 μl of 2% formic acid were flushed from the sample loop of the CapLC system to the trapping column by using solvent A (2% acetonitrile in 0.5% formic acid) at a flow rate of $2 \mu\text{l min}^{-1}$, starting at 0 min. Elution from the trapping column via the nano RP column to the nanospray needle started after 21 min by a stepwise linear increase of the ACN concentration in the eluent at a flow rate of $5.5 \mu\text{l min}^{-1}$, of which 200 nL were directed to the columns after flow splitting. The eluent was produced by mixing different amounts of solvents A and B (80% acetonitrile in 0.5% formic acid) at the times indicated in the diagram. The arrival of the eluent at the needle was delayed by approx. 7 min.

The outlet of the nano RP column was connected to a metal-coated fused-silica PicoTipTM needle (PicoTipTM FS360-20-10-D-20-C7, New Objective, Inc., Woburn, MA, USA), which was placed in front of the MS inlet. Automated data acquisition by the Q-TOF mass spectrometer was controlled by the vendor's software package Mass Lynx and began 20 min after the start of the sample transfer to the trapping column, i. e. one minute before the ACN concentration began to increase. According to the chosen acquisition parameters, only ions that were at least doubly charged were selected for fragmentation.

4.6.4 Analysis of raw MS/MS data by Mascot MS/MS ions search

Using the program Mascot Distiller (Matrix Science Inc., Boston, MA, USA; like the other Mascot software), the generated raw data of the obtained CID (collision-induced dissociation) spectra of each LC MS run were reduced to peak lists suitable for database searching. MS/MS ions searches were submitted by the program Mascot Daemon to a departmental Mascot Server, which allowed searches against customized databases, of which those described in Chapter 3.2.4 were used. The following search parameters were applied: Asp-N as enzyme, up to 1 miscleavage site, no fixed modifications, D/E-methylation and M-oxidation as variable modifications, $\pm 0.15 \text{ Da}$ peptide tolerance, $\pm 0.15 \text{ Da}$ MS/MS tolerance.

4.7 Behavioral studies of *H. salinarum*

4.7.1 Selection of motile halobacterial cells via swarm plates

To obtain reliable results when tracking halobacterial cells, only those with average swimming speeds $\geq 8 \mu\text{m/s}$ were accounted for in the analyses. To select such highly motile cells soft agar plates were employed, which contained 0.25% agar in complex medium. For this purpose 10 μl of a fresh culture of cells in the late logarithmic growth phase (OD_{600} of 0.5 - 0.8) were injected into the soft agar at the center of such a swarm plate and incubated at 40°C for 3 to 5 days.

Due to cell proliferation and concomitant consumption of nutrients a gradient of chemotactically active substances was generated. The cells reacted to this gradient producing a pattern of expanding rings in the soft agar. A sample of 20 μl was taken from the outermost ring, which is expected to contain the most motile cells, and this sample was used to reinoculate another swarm plate. The sample taken from the third plate was then used to inoculate 35 ml of complex medium. An appropriate dilution of the obtained culture was finally spread on a standard complex medium plate and single clones were selected, cultured and investigated under a light microscope with respect to their motilities.

The single colony isolate OMI1_{mot} was generated from OMI1 by this selection technique and represents the most motile of the investigated clones. It was transformed to generate strains MKK101 and MKK102 which were then directly used to create *htr*-deletion strains without additional clone selection steps via swarm plates. When swarm plate selection was applied to strains other than OMI1, the cells taken from the third swarm plate were cultured and then directly used in behavioral experiments, without the additional selection of the most motile single colonies.

4.7.2 Investigation of phototactic responses via motion analysis

Cellular motion was recorded under infrared observation light by collection of raw video data at a frequency of 10 frames per second using a VP110 video processor (Motion Analysis Corporation, Santa Rosa, CA, USA). Microscopic setup and motion analysis algorithms were essentially as described (Marwan and Oesterhelt, 1990) (Fig. 4.3). In all experiments, cells were tracked for 5 s, either under constant illumination with orange light or starting 1s before application of a 3 s light-off stimulus. Only cells with a minimum swimming speed of $8 \mu\text{m s}^{-1}$ were included in the calculation of the percentage of cells reversing within the last 4 s of tracking.

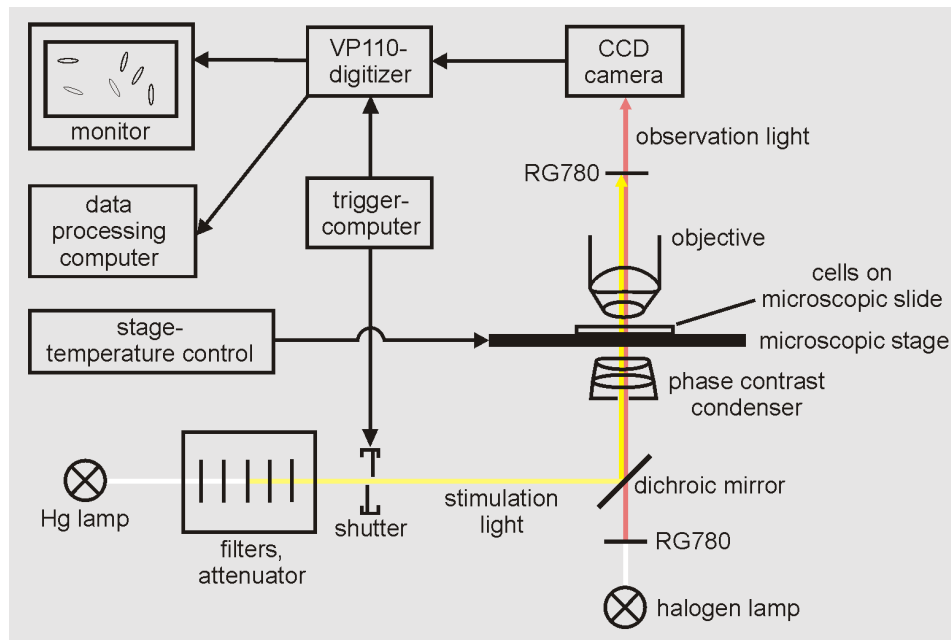


Figure 4.3 Cell-tracking setup for the analysis of the orange-light response of halobacterial cells.

Slides containing the cell preparations were kept at 25°C on a microscopic stage. Cell motion was recorded by an infrared-sensitive COHU 4912 CCD camera (COHU, San Diego, CA, USA) using infrared observation light provided by a 100 W halogen lamp (Osram, Munich, Germany) in combination with an RG780 cut-off filter (780 nm, Schott, Mainz, Germany). The observation light was passed through a phase contrast condenser and a 40x phase contrast objective. Orange stimulation light was generated by passing light from an HBO 100 W mercury lamp through a combination of cut-off and neutral glass filters (Schott) as described in the text. It reached the cells via a dichroic mirror and the condenser, but due to an additional RG780 cut-off filter it could not reach the CCD camera. A trigger computer controlled the shutter and the VP110 video processor, which processed the raw video data at a frequency of 10 frames per second. Further analysis of the digitized cell coordinates was performed on a personal computer (80486 PC) with the algorithms described by Marwan and Oesterhelt (1990).

After growing the cells under standard conditions, they were diluted to an OD_{600} of 0.3. In the case of oxygen depletion, this was done by adding basal salt medium (complex medium without peptone) buffered to pH 7.0 with 20 mM HEPES (BSH). For experiments to test the effects of cyanide, the cells were concentrated by centrifugation and resuspended in complex medium (pH 7.0) containing differing concentrations of KCN. When testing the reaction to light-off stimuli of different durations, cells of OD 0.78 were diluted 1 : 2 with complex medium (pH 7.5) containing 10 mM cyanide. In each case 8 μ l of diluted cell suspension were transferred to a microscopic slide and sealed under a coverslip (18x18 mm) by application of a molten mixture of paraffin wax and vaseline (2 : 1, w/w) to the edges of the slide, to avoid evaporation and to limit oxygen diffusion to the cells. To decrease the number of cells sticking to the glass surface, slides and coverslips were thoroughly cleaned with ethanol, incubated in freshly prepared aqueous 0.5% pectin solution (Sigma-Aldrich, Taufkirchen, Germany) for 2 min, and blown dry with pressurized air (Fig. 4.4).

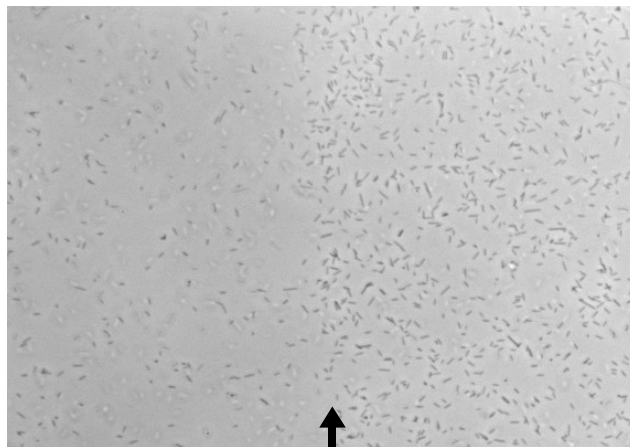


Figure 4.4 Microscopic slide after parts of the glass surface were coated with pectin.

Halobacterial cells are shown in the plane of the microscopic slide at the border of the pectin layer. The amount of cells sticking to the glass slide is significantly decreased, when the surface of the slide is additionally treated with pectin (left of the arrow), compared to a surface that was only cleaned with ethanol (right of the arrow).

For experiments carried out under conditions of oxygen depletion, cells were kept on the slide in the dark for more than one hour, and tracking was initiated after reillumination for at least 10 min. Light of 640 +/- 80 nm at an intensity of 300 W/m² in the plane of the cells was provided by a 100 W mercury lamp equipped with cut-off filters (Schott, Mainz, Germany) KG1, W360 and OG570. For investigation of the cyanide effect and for the measurements testing different stimulus durations, cells were applied to the slides and immediately illuminated with 580 +/- 50 nm light at an intensity of 390 W/m². Measurements started after 10 min of preillumination.

4.7.3 Analysis of the adaptive release of volatile methyl groups

The assay measuring the adaptive release of volatile methyl groups from halobacterial cells was essentially performed as described by Alam *et al.* (1989) with some modifications. Cells were grown to an OD₆₀₀ of 0.8 to 0.9 as described (Oesterhelt and Krippahl, 1983). 1.8 ODml of cells were centrifuged, washed twice and resuspended in BSH (pH 7.5). After 30 min incubation at 37°C in the presence of 130 µg/ml puromycin, the cells were radiolabeled with 30 µl (30 µCi, 375 pmol) of L-[methyl-³H] methionine (80 Ci/mmol, Amersham Biosciences, Freiburg, Germany) and incubated at 37°C for additional 45 min. After centrifugation the cells were washed twice and resuspended in 1.5 ml of BSH followed by transfer to a 0.22 µm filter-unit (cellulose ester, Roth, Karlsruhe, Germany) using a peristaltic pump (Fig. 4.5).

The chase buffer contained 0.1 mM L-methionine in BSH plus 10 mM KCN. It was pumped over the cells at a constant flow rate of 1.5 ml/min and fractions of 18 s were collected. Light stimuli of 120 W/m² (measured behind the transparent part of the filter-unit) were applied by switching on or off a 450 W xenon lamp equipped with cut-off filters KG3 and OG570 (Schott,

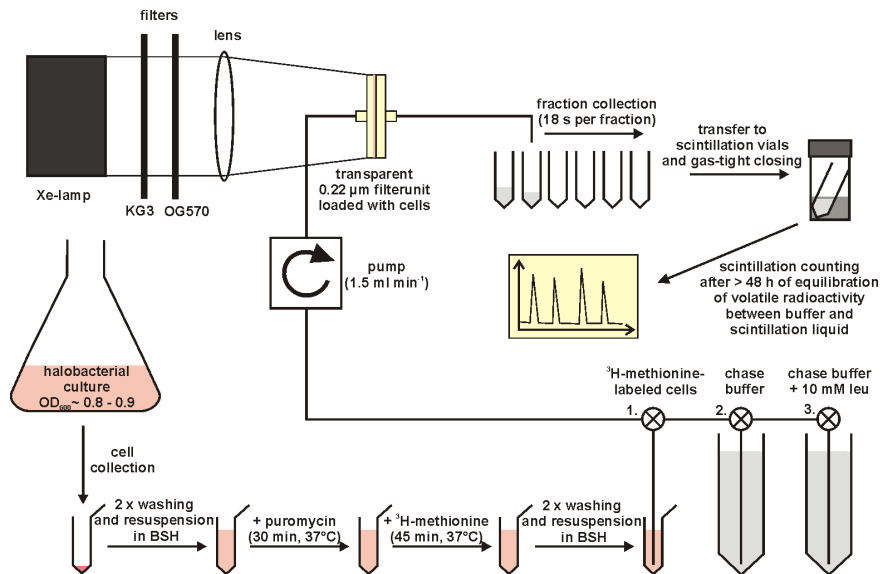


Figure 4.5 Assay to investigate the release of volatile methyl groups from halobacterial cells upon photo- and chemostimuli.

Depicted is an overview of the assay procedure that is described in detail in the text.

Mainz, Germany). Leucine stimuli were applied by switching to chase buffer that additionally contained 10 mM L-leucine and back to chase buffer without leucine, by use of a 3-way valve. Fractions of 450 µl were collected in Eppendorf tubes which were placed upright in vials containing 6 ml of scintillation liquid (EcoSint Plus, Roth, Karlsruhe, Germany). All vials were tightly closed in uninterrupted succession at the end of fraction collection.

Volatile radioactivity was determined after ≥ 48 hours. At that time $\geq 70\%$ of the methanol contained in the chase buffer had entered the scintillation liquid in experiments to determine the kinetics of methanol equilibration between 500 µl of chase buffer and 6 ml of scintillation liquid (Fig. 4.6). In these experiments, known amounts of ^{14}C -labeled methanol (20 mCi/mmol, Sigma-Aldrich, Taufkirchen, Germany) were added to the chase buffer, and after tight closing of the scintillation vials the scintillation activity was measured at different times.

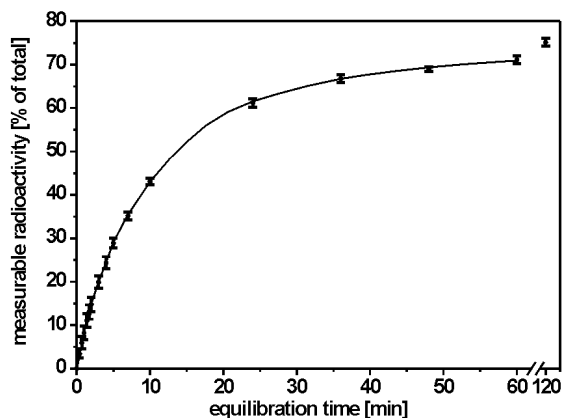


Figure 4.6 Kinetics of methanol equilibration between chase buffer and scintillation liquid.

Amounts of 1, 2, 5 or 10 μl of an aqueous solution of ^{14}C -methanol (10,000 dpm/ μl) were added to 500 μl of chase buffer at pH 5.5 and at pH 7.0 in a microfuge tube, which stood upright in a vial containing 6 ml of scintillation liquid. Immediately after methanol addition the vial was tightly closed. For each of the 8 samples the fraction of the initially added radioactivity that had reached the scintillation liquid via the gas phase was determined after different times via scintillation counting. Each depicted value represents the average of the fractions of radioactivity contained in the scintillation liquids of each of the 8 samples at a given time. The standard deviations are shown as error bars.

4.8 Additional methods

4.8.1 Determination of protein contents and buffering capacities of halobacterial cell fractions

A 350 ml culture of strain S9 or MKK101 was grown at 37°C with swirling at 180 rpm to an OD_{600} of 1.0 and 0.7, respectively. The cells were pelleted by centrifugation, washed three times with 40 ml unbuffered basal salt medium without citrate (BSWC), and finally resuspended in 50% BSWC to an OD_{600} of 10. A lysate corresponding to 200 ODml of cells was generated by sonication (2 x 1.5 min, Branson sonifier 450, 1/2" disruptor horn, 30% duty cycle, level 7) and centrifuged for 20 min at 6,300·g to check for and remove unlysed cells (< 1%). An aliquot of 4 ml (the total lysate fraction) was kept for determination of protein concentration and buffering capacity. The remaining lysate was subjected to ultracentrifugation (60Ti-rotor, Beckman, 200,000·g, 60 min, 4°C). The cytosolic fraction was removed and the membrane pellet was washed with 50% BSWC, centrifuged under the same conditions, and resuspended in 0.9 ml of water. Protein concentrations of all fractions were determined by the BCA assay (Pierce, Rockford).

To determine the buffering capacities of the different fractions first of all 40 ml of 50% BSWC were brought to pH 4.5 by addition of HCl and then titrated under a stream of nitrogen up to pH 9.3 with 0.01 N NaOH and back to pH 4.5 with 0.01 N HCl. In separate experiments, these

titrations were repeated after addition of 2.5 ml total lysate, 5 ml cytosolic fraction, or 600 μ l of membrane fraction, respectively, this time using 0.1 N NaOH and HCl. The buffering capacities at different pH values (in nmol H⁺ per pH unit) were calculated for each fraction as the difference in the slopes of the NaOH titration curves in the presence and absence of the respective fraction. From the volumes of the fractions and their protein concentrations, buffering capacities could be calculated as nmol H⁺ per pH-unit per mg protein.

4.8.2 Measurements of pH changes in cell suspensions upon changes in illumination

Measurements were basically performed as described (Wagner *et al.*, 1978). In brief, MKK101 cells grown to an OD₆₀₀ of 0.94 were washed several times and resuspended in 8 ml of BSWC to a final OD of 0.63, resulting in a total number of $7.0 \cdot 10^9$ cells in the assay. After incubation in a glass vessel at 35°C in the dark under a constant flush of nitrogen for 2 hours, the cells were illuminated with light of 80 W/m² (measured inside the vessel) or fractions thereof, passed through cut-off filters (Schott, Mainz, Germany) KG1, W360 and OG570. Illumination periods of ca. 10 min were interrupted by equally long dark phases. Upon switching off and on the light, the initial rates of external pH-decreases and -increases, respectively, were measured. Finally pH changes were calibrated with a standard solution of HCl.

4.9 Computer programs

In the course of this study the following software was used for analysis or presentation of data: BioEdit (up to version 7.01; <http://www.mbio.ncsu.edu/BioEdit/bioedit.html>) was taken for sequence analysis and alignment editing. Sequence alignments were generated with ClustalW (Thompson *et al.*, 1994), which was started from within BioEdit with the standard settings. Cloning was planned and plasmid maps were generated with Clone Manager 7 (Scientific and Educational Software, Cary, USA).

For the prediction of TM regions the DAS (dense alignment surface method)-prediction server was used (<http://www.sbc.su.se/~miklos/DAS/maindas.html>; Cserzo *et al.*, 1997). Comparative protein modeling was done with the SWISS MODEL server (<http://swissmodel.expasy.org/>; Schwede *et al.*, 2003) using the alignment interface. Inputs were sequence alignments produced with BioEdit. The graphic representations of pdb files or of protein models generated by SWISS MODEL were produced with the molecular visualization software RasTop 2.1 (<http://www.geneinfinity.org/rastop/>).

The HaloLex server (<http://www.halolex.mpg.de>) was used to retrieve sequences and designations of halobacterial genes and predicted proteins, and to investigate the neighborhood of annotated open reading frames. HaloLex is a system which presently (August, 2005) provides public access to the genome of *H. salinarum* and restricted access to that of *N. pharaonis*. It is based on the data obtained from sequencing *H. salinarum* strain R1 (DSM671) and *N. pharaonis* strain DSM2160 in the department Oesterhelt of the Max-Planck-Institute of Biochemistry, and integrates all available information about the genes and predicted gene products, including experimental evidence like mass spectrometrical identifications of proteins.

BLAST searches (Altschul *et al.*, 1990) against public databases were performed with the BLAST server of the national center of biotechnology information (NCBI; <http://www.ncbi.nlm.nih.gov/BLAST/>), whereas searches against sequences from *H. salinarum* and *N. pharaonis* were performed with the publicly not accessible part of the HaloLex system.

Mascot searches were performed with the software from Matrix Science Inc., Boston, USA (<http://www.matrixscience.com>), which was installed on a local server and could therefore use databases which were created either by the bioinformatics group of the department Oesterhelt or in the course of this study. Two types of searches were performed. (i) Peptide mass fingerprint (PMF) analyses were used in case of MALDI-TOF MS to identify the protein(s) of origin for sets of detected peptide masses. (ii) MS/MS ion searches were performed in the case of LC-ESI Q-TOF MS to identify peptides and their corresponding proteins based on raw MS/MS data. These data were obtained via fragmentation of peptides generated by Asp-N-digest of membrane proteins originating from 1-D gel slices.

Additional software was used to generate this dissertation: OpenOffice.org 1.1 for word processing, Origin 6.1 to generate graphs, CorelDraw 11 to compose vector (/bitmap) graphics, CorelPhotoPaint 11 for editing of bitmap-graphics and Endnote 8 to generate the list of references.

5 REFERENCES

- Alam, M., and Oesterhelt, D. (1984) Morphology, function and isolation of halobacterial flagella. *J Mol Biol* **176**: 459-475.
- Alam, M., Lebert, M., Oesterhelt, D., and Hazelbauer, G. (1989) Methyl-accepting taxis proteins in *Halobacterium halobium*. *EMBO J* **8**: 631-639.
- Alam, M., and Hazelbauer, G.L. (1991) Structural features of methyl-accepting taxis proteins conserved between archaeobacteria and eubacteria revealed by antigenic cross-reaction. *J Bacteriol* **173**: 5837-5842.
- Altschul, S.F., Gish, W., Miller, W., Meyers, E.W., and Lipman, D.J. (1990) Basic local alignment search tool. *J Mol Biol* **215**: 403.
- Ames, P., Studdert, C.A., Reiser, R.H., and Parkinson, J.S. (2002) Collaborative signaling by mixed chemoreceptor teams in *Escherichia coli*. *Proc Natl Acad Sci USA* **99**: 7060-7065.
- Appleman, J.A., and Stewart, V. (2003) Mutational analysis of a conserved signal-transducing element: the HAMP linker of the *Escherichia coli* nitrate sensor NarX. *J Bacteriol* **185**: 89-97.
- Aravind, L., and Ponting, C.P. (1999) The cytoplasmic helical linker domain of receptor histidine kinase and methyl-accepting proteins is common to many prokaryotic signalling proteins. *FEMS Microbiol Lett* **176**: 111-116.
- Ashby, M.K. (2004) Survey of the number of two-component response regulator genes in the complete and annotated genome sequences of prokaryotes. *FEMS Microbiol Lett* **231**: 277.
- Baryshev, V.A., Glagolev, A.N., and Skulachev, V.P. (1981) Sensing of $\Delta\mu_{H^+}$ in phototaxis of *Halobacterium halobium*. *Nature* **292**: 338-340.
- Besir, H. (2001) Investigation of lipid-mediated crystallization of the ion pumps bacteriorhodopsin and halorhodopsin from *Halobacterium salinarum*. Munich: Thesis, LMU.
- Bibikov, S.I., Grishanin, R.N., Marwan, W., Oesterhelt, D., and Skulachev, V.P. (1991) The proton pump bacteriorhodopsin is a photoreceptor for signal transduction in *Halobacterium halobium*. *FEBS Lett* **295**: 223-226.
- Bibikov, S.I., Grishanin, R.N., Kaulen, A.D., Marwan, W., Oesterhelt, D., and Skulachev, V.P. (1993) Bacteriorhodopsin is involved in halobacterial photoreception. *Proc Natl Acad Sci U S A* **90**: 9446-9450.
- Bibikov, S.I., Miller, A.C., Gosink, K.K., and Parkinson, J.S. (2004) Methylation-independent aerotaxis mediated by the *Escherichia coli* Aer protein. *J Bacteriol* **186**: 3730-3737.
- Bilwes, A.M., Alex, L.A., Crane, B.R., and Simon, M.I. (1999) Structure of CheA, a signal-transducing histidine kinase. *Cell* **96**: 131.
- Bischoff, D.S., and Ordal, G.W. (1992) *Bacillus subtilis* chemotaxis - a deviation from the *Escherichia coli* paradigm. *Mol Microbiol* **6**: 23-28.
- Blat, Y., and Eisenbach, M. (1996) Oligomerization of the phosphatase CheZ upon interaction with the phosphorylated form of CheY - The signal protein of bacterial chemotaxis. *J Biol Chem* **271**: 1226-1231.
- Boukhvalova, M., VanBruggen, R., and Stewart, R.C. (2002) CheA kinase and chemoreceptor interaction surfaces on CheW. *J Biol Chem* **277**: 23596.
- Boyd, A., and Simon, M.I. (1980) Multiple electrophoretic forms of methyl-accepting chemotaxis proteins generated by stimulus-elicited methylation in *Escherichia coli*. *J Bacteriol* **143**: 809-815.
- Bray, D., Levin, M.D., and Morton-Firth, C.J. (1998) Receptor clustering as a cellular mechanism to control sensitivity. *Nature* **393**: 85.

- Brooun, A., Zhang, W., and Alam, M. (1997) Primary structure and functional analysis of the soluble transducer protein HtrXI in the archaeon *Halobacterium salinarium*. *J Bacteriol* **179**: 2963-2968.
- Brooun, A., Bell, J., Freitas, T., Larsen, R.W., and Alam, M. (1998) An archaeal aerotaxis transducer combines subunit I core structures of eukaryotic cytochrome c oxidase and eubacterial methyl-accepting chemotaxis proteins. *J Bacteriol* **180**: 1642-1646.
- Butler, S.L., and Falke, J.J. (1998) Cysteine and disulfide scanning reveals two amphiphilic helices in the linker region of the aspartate chemoreceptor. *Biochemistry* **37**: 10746-10756.
- Chervitz, S.A., and Falke, J.J. (1996) Molecular mechanism of transmembrane signaling by the aspartate receptor: a model. *Proc Natl Acad Sci U S A* **93**: 2545-2550.
- Chi, Y.I., Yokota, H., and Kim, S.H. (1997) Apo structure of the ligand-binding domain of aspartate receptor from *Escherichia coli* and its comparison with ligand-bound or pseudoligand-bound structures. *FEBS Lett* **414**: 327-332.
- Cline, S.W., Lam, W.L., Charlebois, R.L., Schalkwyk, L.C., and Doolittle, W.F. (1989) Transformation methods for halophilic archaeobacteria. *Can J Microbiol* **35**: 148-152.
- Cserzo, M., Wallin, E., Simon, I., von Heijne, G., and Elofsson, A. (1997) Prediction of transmembrane alpha-helices in prokaryotic membrane proteins: the dense alignment surface method. *Protein Eng* **10**: 673-676.
- DasSarma, S., Rajbhandary, U.L., and Khorana, H.G. (1983) High-frequency spontaneous mutation in the bacterio-opsin gene in *Halobacterium halobium* is mediated by transposable elements. *Proc Natl Acad Sci U S A* **80**: 2201-2205.
- Djordjevic, S., and Stock, A.M. (1998) Chemotaxis receptor recognition by protein methyltransferase CheR. *Nat Struct Mol Biol* **5**: 446.
- Dunten, P., and Koshland, D.E. (1991) Tuning the responsiveness of a sensory receptor via covalent modification. *J Biol Chem* **266**: 1491-1496.
- Eisenbach, M. (1990) Functions of the flagellar modes of rotation in bacterial motility and chemotaxis. *Mol Microbiol* **4**: 161-167.
- Fisher, M., Pick, U., and Zamir, A. (1994) A salt-induced 60-kilodalton plasma-membrane protein plays a potential role in the extreme halotolerance of the alga *Dunaliella*. *Plant Physiol* **106**: 1359-1365.
- Garrity, G.M., Bell, J.A., and Lilburn, T.G. (2004) Taxonomic outline of the prokaryotes. In *Bergey's manual of systematic bacteriology*. New York: Springer-Verlag. DOI:10.1007/bergeysoutline2000405
- Gestwicki, J.E., Lamanna, A.C., Harshey, R.M., McCarter, L.L., Kiessling, L.L., and Adler, J. (2000) Evolutionary conservation of methyl-accepting chemotaxis protein location in Bacteria and Archaea. *J Bacteriol* **182**: 6499-6502.
- Grishanin, R.N., Bibikov, S.I., Altschuler, I.M., Kaulen, A.D., Kazimirchuk, S.B., Armitage, J.P., and Skulachev, V.P. (1996) $\Delta\Psi$ -mediated signalling in the bacteriorhodopsin-dependent photoresponse. *J Bacteriol* **178**: 3008-3014.
- Griswold, I.J., Zhou, H.J., Matison, M., Swanson, R.V., McIntosh, L.P., Simon, M.I., and Dahlquist, F.W. (2002) The solution structure and interactions of CheW from *Thermotoga maritima*. *Nat Struct Biol* **9**: 121.
- Hartmann, R., Sickinger, H.D., and Oesterhelt, D. (1980) Anaerobic growth of halobacteria. *Proc Natl Acad Sci U S A* **77**: 3821-3825.
- Hayashi, S., and Wu, H.C. (1990) Lipoproteins in bacteria. *J Bioenerg Biomembr* **22**: 451-471.
- Hazelbauer, G.L., and Engström, P. (1981) Multiple forms of methyl-accepting chemotaxis proteins distinguished by a factor in addition to multiple methylation. *J Bacteriol* **145**: 35-42.
- Henke, J.M., and Bassler, B.L. (2004) Bacterial social engagements. *Trends Cell Biol* **14**: 648.

- Higuchi, R. (1990) Recombinant PCR. In *PCR Protocols - A Guide to Methods and Applications*. Innis, M.A., Gelfand, D.H., Sninsky, J.J. and White, T.J. (eds). San Diego: Academic Press, Inc.
- Hildebrand, E., and Dencher, N. (1975) Two photosystems controlling behavioral responses of *Halobacterium halobium*. *Nature* **257**: 46-48.
- Holmes, M.L., and Dyall-Smith, M.L. (2000) Sequence and expression of a halobacterial beta-galactosidase gene. *Mol Microbiol* **36**: 114-122.
- Hou, S., Brooun, A., Yu, H.S., Freitas, T., and Alam, M. (1998) Sensory rhodopsin II transducer HtrII is also responsible for serine chemotaxis in the archaeon *Halobacterium salinarum*. *J Bacteriol* **180**: 1600-1602.
- Hou, S., Larsen, R.W., Boudko, D., Riley, C.W., Karatan, E., Zimmer, M., et al. (2000) Myoglobin-like aerotaxis transducers in Archaea and Bacteria. *Nature* **403**: 540-544.
- Jiang, Y.X., Ruta, V., Chen, J.Y., Lee, A., and MacKinnon, R. (2003) The principle of gating charge movement in a voltage-dependent K⁺ channel. *Nature* **423**: 42-48.
- Kehry, M.R., and Dahlquist, F.W. (1982) The methyl-accepting chemotaxis proteins of *Escherichia coli* - Identification of the multiple methylation sites on methyl-accepting chemotaxis protein-I. *J Biol Chem* **257**: 378.
- Kehry, M.R., Bond, M.W., Hunkapiller, M.W., and Dahlquist, F.W. (1983) Enzymatic deamidation of methyl-accepting chemotaxis proteins in *Escherichia coli* catalyzed by the cheB gene product. *Proc Natl Acad Sci U S A* **80**: 3599-3603.
- Kehry, M.R., Doak, T.G., and Dahlquist, F.W. (1984) Stimulus-induced changes in methyltransferase activity during chemotaxis in *Escherichia coli*. *J Biol Chem* **259**: 1828-1835.
- Kim, K.K., Yokota, H., and Kim, S.-H. (1999) Four-helical-bundle structure of the cytoplasmic domain of a serine chemotaxis receptor. *Nature* **400**: 787-792.
- Kim, S.H. (1994) Frozen dynamic dimer model for transmembrane signaling in bacterial chemotaxis receptors. *Protein Sci* **3**: 159-165.
- Kim, S.H., Wang, W.R., and Kim, K.K. (2002) Dynamic and clustering model of bacterial chemotaxis receptors: Structural basis for signaling and high sensitivity. *Proc Natl Acad Sci U S A* **99**: 11611-11615.
- Klein, C. (2005) Proteomeanalyses on *Halobacterium salinarum*. Munich: Thesis, LMU.
- Klein, C., Garcia-Rizo, C., Bisle, B., Scheffer, B., Zischka, H., Pfeiffer, F., et al. (2005) The membrane proteome of *Halobacterium salinarum*. *Proteomics* **5**: 180-197.
- Kokoeva, M.V., and Oesterhelt, D. (2000) BasT, a membrane-bound transducer protein for amino acid detection in *Halobacterium salinarum*. *Mol Microbiol* **35**: 647-656.
- Kokoeva, M.V., Storch, K.-F., Klein, C., and Oesterhelt, D. (2002) A novel mode of sensory transduction in archaea: binding protein-mediated chemotaxis towards osmoprotectants and amino acids. *EMBO J* **21**: 2312-2322.
- Kristich, C.J., and Ordal, G.W. (2002) *Bacillus subtilis* CheD is a chemoreceptor modification enzyme required for chemotaxis. *J Biol Chem* **277**: 25356-25362.
- Laemmli, U.K. (1970) Cleavage of structural proteins during assembly of head of bacteriophage-T4. *Nature* **227**: 680-&.
- Lam, W.L., and Doolittle, W.F. (1992) Mevinolin-resistant mutations identify a promoter and the gene for a eukaryote-like 3-hydroxy-3-methylglutaryl-coenzyme A reductase in the archaeobacterium *Haloferax volcanii*. *J Biol Chem* **267**: 5829-5834.
- Le Moual, H., and Koshland, D.E. (1996) Molecular evolution of the C-terminal cytoplasmic domain of a superfamily of bacterial receptors involved in taxis. *J Mol Biol* **261**: 568-585.

- Lefman, J., Zhang, P., Hirai, T., Weis, R.M., Juliani, J., Bliss, D., *et al.* (2004) Three-dimensional electron microscopic imaging of membrane invaginations in *Escherichia coli* overproducing the chemotaxis receptor Tsr. *J Bacteriol* **186**: 5052-5061.
- Levit, M.N., Liu, Y., and Stock, J.B. (1998) Stimulus response coupling in bacterial chemotaxis: receptor dimers in signalling arrays. *Mol Microbiol* **30**: 459-466.
- Li, M.S., and Hazelbauer, G.L. (2004) Cellular stoichiometry of the components of the chemotaxis signaling complex. *J Bacteriol* **186**: 3687-3694.
- Liu, J.D., and Parkinson, J.S. (1991) Genetic evidence for interaction between the CheW and Tsr proteins during chemoreceptor signaling by *Escherichia coli*. *J Bacteriol* **173**: 4941-4951.
- Lukat, G.S., Lee, B.H., Mottonen, J.M., Stock, A.M., and Stock, J.B. (1991) Roles of the highly conserved aspartate and lysine residues in the response regulator of bacterial chemotaxis. *J Biol Chem* **266**: 8348-8354.
- Lux, R., Munasinghe, V.R.N., Castellano, F., Lengeler, J.W., Corrie, J.E.T., and Khan, S. (1999) Elucidation of a PTS-carbohydrate chemotactic signal pathway in *Escherichia coli* using a time-resolved behavioral assay. *Mol Biol Cell* **10**: 1133-1146.
- Maddock, J.R., and Shapiro, L. (1993) Polar location of the chemoreceptor complex in the *Escherichia coli* cell. *Science* **259**: 1717-1723.
- Marwan, W., and Oesterhelt, D. (1990) Quantitation of photochromism of sensory rhodopsin-I by computerized tracking of *Halobacterium halobium* cells. *J Mol Biol* **215**: 277285.
- Marwan, W., Alam, M., and Oesterhelt, D. (1991) Rotation and switching of the flagellar motor assembly in *Halobacterium halobium*. *J Bacteriol* **173**: 1971-1977.
- Marwan, W., and Oesterhelt, D. (1991) Light-induced release of the switch factor during photophobic responses of *Halobacterium halobium*. *Naturwissenschaften* **78**: 127-129.
- Mattar, S., Scharf, B., Kent, S.B.H., Rodewald, K., Oesterhelt, D., and Engelhard, M. (1994) The primary structure of halocyanin, an archaeal blue copper protein, predicts a lipid anchor for membrane fixation. *J Biol Chem* **269**: 14939-14945.
- Michel, H., and Oesterhelt, D. (1976) Light-induced changes of the pH gradient and the membrane potential in *H. halobium*. *FEBS Lett* **65**: 175-178.
- Michel, H., and Oesterhelt, D. (1980) Electrochemical proton gradient across the cell-membrane of *Halobacterium halobium*: Effect of N,N'- dicyclohexylcarbodiimide, relation to intracellular adenosine-triphosphate, adenosine-diphosphate, and phosphate concentration, and influence of the potassium gradient. *Biochemistry* **19**: 4607-4614.
- Milligan, D.L., and Koshland, D.E., Jr. (1988) Site-directed cross-linking. Establishing the dimeric structure of the aspartate receptor of bacterial chemotaxis. *J Biol Chem* **263**: 6268-6275.
- Monstadt, G.M., and Holldorf, A.W. (1991) Arginine deiminase from *Halobacterium salinarium* - purification and properties. *Biochem J* **273**: 739-745.
- Mukohata, Y., and Kaji, Y. (1981) Light-induced ATP synthesis dependent on halorhodopsin-pH regulation. *Arch Biochem Biophys* **208**: 615-617.
- Ng, W.V., Kennedy, S.P., Mahairas, G.G., Berquist, B., Pan, M., Shukla, H.D., *et al.* (2000) Genomic sequence of *Halobacterium* species NRC-1. *Proc Natl Acad Sci U S A* **97**: 12176-12181.
- Nowlin, D., Bollinger, J., and Hazelbauer, G. (1987) Sites of covalent modification in Trg, a sensory transducer of *Escherichia coli*. *J Biol Chem* **262**: 6039-6045.
- Oesterhelt, D., and Krippahl, G. (1973) Light inhibition of respiration in *Halobacterium halobium*. *FEBS Lett* **36**: 72-76.
- Oesterhelt, D., and Krippahl, G. (1983) Phototropic growth of halobacteria and its use for isolation of photosynthetically-deficient mutants. *Ann Microbiol (Inst Pasteur)* **134 B**: 137-150.

- Oesterhelt, D. (1998) The structure and mechanism of the family of retinal proteins from halophilic archaea. *Curr Opin Struct Biol* **8**: 489-500.
- Oren, A. (1994) The ecology of the extremely halophilic archaea. *FEMS Microbiol Rev* **13**: 415-439.
- Oren, A. (2002) *Halophilic microorganisms and their environments*. Dordrecht: Kluwer Academic Publishers.
- Ottemann, K.M., Xiao, W., Shin, Y.-K., and Jr, D.E.K. (1999) A piston model for transmembrane signaling of the aspartate receptor. *Science* **285**: 1751-1754.
- Patenge, N., Haase, A., Bolhuis, H., and Oesterhelt, D. (2000) The gene for a halophilic beta-galactosidase (*bgaH*) of *Haloferax alicantei* as a reporter gene for promoter analyses in *Halobacterium salinarum*. *Mol Microbiol* **36**: 105-113.
- Perazzona, B., and Spudich, J.L. (1999) Identification of methylation sites and effects of phototaxis stimuli on transducer methylation in *Halobacterium salinarum*. *J Bacteriol* **181**: 5676-5683.
- Pfeiffer, M., Rink, T., Gerwert, K., Oesterhelt, D., and Steinhoff, H.J. (1999) Site-directed spin-labeling reveals the orientation of the amino acid side-chains in the E-F loop of bacteriorhodopsin. *J Mol Biol* **287**: 163-171.
- Rebbapragada, A., Johnson, M.S., Harding, G.P., Zuccarelli, A.J., Fletcher, H.M., Zhulin, I.B., and Taylor, B.L. (1997) The Aer protein and the serine chemoreceptor Tsr independently sense intracellular energy levels and transduce oxygen, redox, and energy signals for *Escherichia coli* behavior. *Proc Natl Acad Sci U S A* **94**: 10541-10546.
- Rose, R.W., Bruser, T., Kissinger, J.C., and Pohlschroder, M. (2002) Adaptation of protein secretion to extremely high-salt conditions by extensive use of the twin-arginine translocation pathway. *Mol Microbiol* **45**: 943-950.
- Rudolph, J., Tolliday, N., Schmitt, C., Schuster, S.C., and Oesterhelt, D. (1995) Phosphorylation in halobacterial signal transduction. *EMBO J* **14**: 4249-4257.
- Rudolph, J., and Oesterhelt, D. (1996) Deletion analysis of the *che* operon in the archaeon *Halobacterium salinarium*. *J Mol Biol* **258**: 548-554.
- Ruepp, A., and Soppa, J. (1996) Fermentative arginine degradation in *Halobacterium salinarium* (formerly *Halobacterium halobium*): Genes, gene products, and transcripts of the *arcRACB* gene cluster. *J Bacteriol* **178**: 4942-4947.
- Sambrook, J., Fritsch, E., and Maniatis, T. (1989) *Molecular cloning: a laboratory manual*. Woodbury: Cold Spring Harbor Laboratory Press.
- Schaegger, H., Cramer, W.A., and von Jagow, G. (1994) Analysis of molecular masses and oligomeric states of protein complexes by blue native electrophoresis and isolation of membrane-protein complexes by 2-dimensional native electrophoresis. *Anal Biochem* **217**: 220-230.
- Schimz, A., and Hildebrand, E. (1979) Chemosensory responses of *Halobacterium halobium*. *J Bacteriol* **140**: 749-753.
- Schmidt, A., Kellermann, J., and Lottspeich, F. (2005) A novel strategy for quantitative proteomics using isotope-coded protein labels. *Proteomics* **5**: 4-15.
- Schnitzer, J.M., Block, S.M., Berg, H.C., and Purcell, E.M. (1990) Strategies for chemotaxis. In *Biology of the chemotactic response*. Armitage, J.P. and Lackie, J.M. (eds). Cambridge, UK: Cambridge University Press, pp. 15 - 34.
- Schwede, T., Kopp, J., Guex, N., and Peitsch, M.C. (2003) SWISS-MODEL: an automated protein homology-modeling server. *Nucleic Acids Res* **31**: 3381-3385.
- Schweiger, U. (1996) Functional characterization of the retinal binding pocket of bacteriorhodopsin via specific mutagenesis. Innsbruck: Dissertation, LFU.

- Seidel, R., Scharf, B., Gautel, M., Kleine, K., Oesterhelt, D., and Engelhard, M. (1995) The primary structure of sensory rhodopsin II: a member of an additional retinal protein subgroup is coexpressed with its transducer, the halobacterial transducer of rhodopsin II. *Proc Natl Acad Sci U S A* **92**: 3036-3040.
- Sourjik, V. (2004) Receptor clustering and signal processing in *E. coli* chemotaxis. *Trends Microbiol* **12**: 569-576.
- Springer, M.S., Goy, M.F., and Adler, J. (1979) Protein methylation in behavioral-control mechanisms and in signal transduction. *Nature* **280**: 279-284.
- Springer, W.R., and Koshland, D.E. (1977) Identification of a protein methyltransferase as the cheR gene product in the bacterial sensing system. *Proc Natl Acad Sci U S A* **74**: 533-537.
- Spudich, E.N., and Spudich, J.L. (1982) Control of transmembrane ion fluxes to select halorhodopsin-deficient and other energy-transduction mutants of *Halobacterium halobium*. *Proc Natl Acad Sci U S A* **79**: 4308-4312.
- Spudich, J.L., and Stoeckenius, W. (1979a) Photosensory behavior of motile *Halobacterium halobium*. *Biophys J* **25**: A78-A78.
- Spudich, J.L., and Stoeckenius, W. (1979b) Photosensory and chemosensory behavior of *Halobacterium halobium*. *Photobiochem Photobiophys* **1**: 43-53.
- Stevens, A., and Greenberg, E. (1997) Quorum sensing in *Vibrio fischeri*: essential elements for activation of the luminescence genes. *J Bacteriol* **179**: 557-562.
- Stock, J.B., and Koshland, D.E. (1978) A protein methyltransferase involved in bacterial sensing. *Proc Natl Acad Sci U S A* **75**: 3659-3663.
- Stock, J.B., and Surette, M.G. (1996) Chemotaxis. In *Escherichia coli and Salmonella typhimurium: cellular and molecular biology*. Vol. 1. Neidhardt, R.C.I., Ingraham, J.L., Lin, E.C.C., Low, K.B., Magasanik, B., Reznikoff, W.S., Schaechter, M. and Umberger, H.E. (eds). Washington, D. C.: American Society of Microbiology, pp. 551-573.
- Storch, K.F., Rudolph, J., and Oesterhelt, D. (1999) Car: a cytoplasmic sensor responsible for arginine chemotaxis in *Halobacterium salinarum*. *EMBO J* **18**: 1146-1158.
- Studdert, C.A., and Parkinson, J.S. (2004) Crosslinking snapshots of bacterial chemoreceptor squads. *Proc Natl Acad Sci U S A* **101**: 2117-2122.
- Sundberg, S.A., Bogomolni, R.A., and Spudich, J.L. (1985) Selection and properties of phototaxis-deficient mutants of *Halobacterium halobium*. *J Bacteriol* **164**: 282-287.
- Szurmant, H., and Ordal, G.W. (2004) Diversity in chemotaxis mechanisms among the bacteria and archaea. *Microbiol Mol Biol Rev* **68**: 301-319.
- Taylor, B.L., Zhulin, I.B., and Johnson, M.S. (1999) Aerotaxis and other energy-sensing behaviour in bacteria. *Annu Rev Microbiol* **53**: 103-128.
- Tebbe, A., Klein, C., Bisle, B., Siedler, F., Scheffer, B., Garcia-Rizo, C., et al. (2005) Analysis of the cytosolic proteome of *Halobacterium salinarum* and its implication for genome annotation. *Proteomics* **5**: 168-179.
- Terwilliger, T.C., and Koshland, D.E. (1984) Sites of methyl esterification and deamination on the aspartate receptor involved in chemotaxis. *J Biol Chem* **259**: 7719-7725.
- Terwilliger, T.C., Wang, J.Y., and Koshland, D.E. (1986) Surface-structure recognized for covalent modification of the aspartate receptor in chemotaxis. *Proc Natl Acad Sci U S A* **83**: 6707-6710.
- Thompson, J.D., Higgins, D.G., and Gibson, T.J. (1994) Clustal-W - Improving the sensitivity of progressive multiple sequence alignment through sequence weighting, position-specific gap penalties and weight matrix choice. *Nucleic Acids Res* **22**: 4673-4680.

- Wadhams, G.H., Warren, A.V., Martin, A.C., and Armitage, J.P. (2003) Targeting of two signal transduction pathways to different regions of the bacterial cell. *Mol Microbiol* **50**: 763-770.
- Wadhams, G.H., and Armitage, J.P. (2004) Making sense of it all: bacterial chemotaxis. *Nat Rev Mol Cell Biol* **5**: 1024.
- Wagner, G., Hartmann, R., and Oesterhelt, D. (1978) Potassium uniport and ATP synthesis in *Halobacterium halobium*. *Eur J Biochem* **89**: 169-179.
- Wagner, G., Oesterhelt, D., Krippahl, G., and Lanyi, J.K. (1981) Bioenergetic role of halorhodopsin in *Halobacterium halobium* cells. *FEBS Lett* **131**: 341-345.
- Wang, L., Fabret, C., Kanamaru, K., Stephenson, K., Dartois, V., Perego, M., and Hoch, J.A. (2001) Dissection of the functional and structural domains of phosphorelay histidine kinase A of *Bacillus subtilis*. *J Bacteriol* **183**: 2795-2802.
- Weis, R.M., Hirai, T., Chalah, A., Kessel, M., Peters, P.J., and Subramaniam, S. (2003) Electron microscopic analysis of membrane assemblies formed by the bacterial chemotaxis receptor Tsr. *J Bacteriol* **185**: 3636-3643.
- West, A.H., and Stock, A.M. (2001) Histidine kinases and response regulator proteins in two-component signaling systems. *Trends Biochem Sci* **26**: 369-376.
- Yao, V.J., and Spudich, J.L. (1992) Primary structure of an archaeobacterial transducer, a methyl-accepting protein associated with sensory rhodopsin I. *Proc Natl Acad Sci U S A* **89**: 11915-11919.
- Zhang, W., Brooun, A., Mueller, M.M., and Alam, M. (1996) The primary structures of the archaeon *Halobacterium salinarium* blue light receptor sensory rhodopsin II and its transducer, a methyl-accepting protein. *Proc Natl Acad Sci U S A* **93**: 8230-8235.
- Zimmer, M.A., Tiu, J., Collins, M.A., and Ordal, G.T. (2000) Selective methylation changes on the *Bacillus subtilis* chemotaxis receptor McpB promote adaptation. *J Biol Chem* **275**: 24264-24272.

6 APPENDIX

6.1 Abbreviations

(d)dNTP	(di)deoxyribonucleoside triphosphate
1(2)-D	one(two)-dimensional
aa	amino acids
ACN	acetonitrile
Amp	ampicillin
APS	ammonium peroxydisulfate
ATP	adenosine triphosphate
BP	binding protein
bp	base pair(s)
BPI	base peak intensity
BR	bacteriorhodopsin
BSA	bovine serum albumin
CCW	counterclockwise
CSPD	disodium 3-(4-methoxy Spiro {1,2-dioxetane-3,2'-(5'-chloro)tricyclo[3.3.1.1 ^{3,7}]decan}-4-yl) phenyl phosphate
CW	clockwise
DIG	digoxigenin
DIG-11-dUTP	digoxigenin-11-2'-deoxyuridine-5'-triphosphate
DMSO	dimethylsulfoxide
DNA	deoxyribonucleic acid
DNaseI	deoxyribonuclease I
dpm	disintegrations per minute
DTT	dithiothreitol
EDTA	ethylenediaminetetraacetate
ESI	electrospray ionization
f.c.	final concentration
Fig.	figure
Glx	glutamate or glutamine
HAP	histidine aspartate phosphorelay
HAMP	histidine kinases, adenylyl cyclases, methyl-binding proteins, phosphatases
HEPES	N-(2-hydroxyethyl)piperazine-N'-(2-ethanesulfonic acid)
HPK(s)	histidine protein kinase(s)
HPLC	high performance liquid chromatography
HPt	histidine phosphotransfer
HR	halorhodopsin
Htr(s)	halobacterial transducer protein
<i>htr(s)</i>	halobacterial transducer gene(s)
indel	insertion/deletion
kb	kilobase(pair)s
kDa	kilodalton
LB	Luria-Bertani
LC	liquid chromatography
λ_{\max}	wavelength of the absorbance maximum
MALDI-TOF	matrix-assisted laser desorption/ionization time-of-flight

Mb	megabase(pair)s
MCS	multiple cloning site
MS	mass spectrometry
MS/MS	tandem mass spectrometry
MW(s)	molecular weight(s)
nt	nucleotide(s)
OD ₆₀₀	optical density at 600 nm
ODml	one ODml corresponds to the amount of cells present in one milliliter of a halobacterial culture at an OD ₆₀₀ of 1.0
orf(s)	open reading frame(s)
PAGE	polyacrylamide gel electrophoresis
PCR	polymerase chain reaction
PEG	polyethylene glycol
pH _e	pH in the extracellular medium
pH _i	intracellular pH
pmf	proton motive force
PVDF	polyvinylidene fluoride
Q-TOF	quadrupole-time-of-flight
RNA	ribonucleic acid
RP	reversed phase
rpm	rotations per minute
RR(s)	response regulator(s)
RT	room temperature
SDS	sodium dodecyl sulfate
SPS	spheroplasting solution
SR	sensory rhodopsin
TB	terrific broth
TEMED	N, N, N', N'-tetramethylethylenediamine
T _m	melting temperature
TM	transmembrane
TM#	transmembrane helix # (# can be 1 to 6)
TPP ⁺	tetraphenylphosphonium ion
Tris	tris(hydroxymethyl)aminomethane
TWEEN20	polyoxyethylene sorbitan monolaurate
UV	ultraviolet light
v/v	volume per volume
w/v	weight per volume
wt	wild-type
X-gal	5-bromo-4-chloro-3-indolyl-beta-D-galactoside

6.2 Lists of Tables and Figures

List of Tables

Table 2.1. Genera and type strains of the family <i>Halobacteriaceae</i>	5
Table 3.1. Rates of net proton transport across MKK101 cell membranes induced by illumination changes.....	44
Table 3.2. Comparison of the number of residues in those Htr-peptides that contain the putative methylation site at heptad position -12 and were generated by digestion with either trypsin or Asp-N	67
Table 3.3. Example of a Mascot MS/MS ions search result: suggested protein-identifications and peptide-list underlying the identification of the first protein.....	75
Table 3.4. Mascot search result for the MS/MS fragmentation of the singly methylated Htr14-peptide DTVSATVEEIAASAN which was specified in the peptide list of Table 3.3.....	77
Table 4.1. Overview of strains.....	96
Table 4.2. Overview of plasmids.....	99
Table 6.1. Oligonucleotide primers.....	140
Table 6.2. Compilation of information on <i>htr</i> genes and their products.....	148
Table 6.3. First entries of the FASTA-formatted lists of peptide sequences, which represent the databases used for the identification of Htr peptides via Mascot MS/MS ions searches.....	150
Table 6.4. Regions, features and methylation sites of Htrs, Tsr, Tar and McpB.....	154

List of Figures

Figure 2.1 Electron micrographs of <i>H. halobium</i> (<i>H. salinarum</i>) cells with (A) bipolar and (B) monopolar flagellation.....	7
Figure 2.2 Random and biased random walk.....	8
Figure 2.3 Structures and interaction pathways of chemosensory components of <i>E. coli</i> and <i>S. typhimurium</i>	10
Figure 2.4 Polar clustering of transducers in <i>E. coli</i> and <i>H. salinarum</i>	11
Figure 2.5 Two-state model of the transducer-kinase complex.....	16
Figure 2.6 Schematic of the three transducer classes, according to Le Moual and Koshland (1996)....	20
Figure 3.1 Overview of the generated strains leading to retinal protein-deficient strain OMI1, and strains MKK101 and MKK102.....	26
Figure 3.2 Schematic of the construction of plasmids pMKK101, pMKK102, pMKK114 and pMKK119 to exemplify the genetic strategies employed.....	27
Figure 3.3 Genotypic analysis of strains OMI1, MKK101 and MKK102.....	28
Figure 3.4 Chromosomal locations of halobacterial genes encoding transducers, opsins and Che-proteins.....	30
Figure 3.5 Comparison of the N-terminal sequences of putative extracellular lipid-anchored ligand-binding proteins, expected to be involved in <i>H. salinarum</i> chemotaxis, with that of halocyanin from <i>N. pharaonis</i>	31

Figure 3.6 Southern-blot analysis of the <i>htr</i> -deletion strains derived from strain MKK101, exemplified by MKK114.....	32
Figure 3.7 Selection of halobacterial transformants via the "double-picking" technique or via red-blue-clone-selection.....	33
Figure 3.8 Cell-tracking experiments with BR-containing strain MKK101 ($\Delta htr1 \Delta htr2 \Delta htr11$) and derived <i>htr</i> -mutants.....	35
Figure 3.9 Stimulus-induced release of ³ H-labeled methanol from whole cells immobilized in a transparent 0.22 μ m filter unit.....	36
Figure 3.10 Immunochemical analysis of the cellular localization and the methylation status of Htr14 in different halobacterial strains with anti-Htr14 _{D585} serum.....	38
Figure 3.11 Mass spectra in the mass-per-charge ranges of the three methylatable peptides of Htr14... 40	40
Figure 3.12 Tracking of MKK101 cells in the presence of 5 mM cyanide after light-off stimuli of varying durations.....	42
Figure 3.13 Determination of the buffering capacities of cell lysates, cytosolic and membrane fractions from halobacterial strains S9 and MKK101 at different pH values.....	43
Figure 3.14 MpcT (Htr14) sequence with relevant features indicated.....	47
Figure 3.15 Alignments of the N- and C-terminal sequences of OE2712R with the N-terminal sequences of MpcT (Htr14) and its putative ortholog from <i>N. pharaonis</i> , and with the C-terminal sequence of KinA, respectively.....	49
Figure 3.16 Proposed structures of halobacterial MpcT (Htr14) and <i>E. coli</i> Tsr.	51
Figure 3.17 Clustering of overexpressed Tsr in the <i>E. coli</i> membrane.....	52
Figure 3.18 Section of the suggested hexagonal array of Tsr molecules, viewed from the plane of the membrane into the cytosol, and proposed arrangement of CheW and CheA in such an array.....	54
Figure 3.19 Overview of the involvement of transducer proteins (Htrs) in halobacterial signal transduction.....	59
Figure 3.20 Hydrophobic heptads in the putative coiled-coil regions of Tsr, Htr14 and McpB.....	63
Figure 3.21 Heptad positions 2 and 3 within the coiled coil of Htr14 (modeled on the cTsrQ-structure).....	64
Figure 3.22 MALDI-TOF mass spectra of some methylatable Htr peptides resulting from tryptic digests of protein spots from 2-D gels.....	66
Figure 3.23 Htr positions on a nitrocellulose blot after SDS PAGE of membrane protein preparations from different <i>htr</i> -deletion mutants derived from strain S9, and calculated gel-band pattern of the Htrs.....	68
Figure 3.24 Positions of the excised gel slices used for LC ESI Q-TOF MS/MS analysis and the Htrs identified in these slices.....	69
Figure 3.25 MS spectra in the mass-per-charge (<i>m/z</i>) ranges of the differently methylated forms of those peptides of Htr4 and Htr5 that contain the first methylatable site, present in heptad -12.....	72
Figure 3.26 Fragments of the b- and y-series comprise the major part of the peptide-fragments generated during ESI-Q-TOF MS/MS analysis.....	76
Figure 3.27 MS/MS spectra of the differently methylated forms of peptide DEMSATIEEVAASA of Htr4.....	79
Figure 3.28 Unambiguous MS/MS identifications of the methylated glutamate residue in different peptides.....	80

Figure 3.29 Examples of an unambiguous identification of the methylation site but not of the methylated glutamate residue (A), and for doubly methylated sites in a peptide derived from strain S9 (B) and in a peptide from the $\Delta cheB$ mutant WFS101 (C).....	81
Figure 3.30 Alignments of the amino acid sequences comprising the first methylatable (A), signaling (B) and second methylatable (C) regions of the 18 Htrs, Tsr and McpB with possible methylation sites indicated.....	84
Figure 3.31 Hypothetical scenario for the generation of class I and class III transducers from a proposed common ancestor.....	87
Figure 3.32 MS/MS spectra of the unmethylated and the methylated form of peptide DLAEETREQAA which originates from the signaling region of Htr14 from strain S9.....	89
Figure 4.1 Schematic description of a halobacterial transformation with a suicide plasmid.....	106
Figure 4.2 Solvent gradient used in the LC ESI Q-TOF experiments.....	119
Figure 4.3 Cell-tracking setup for the analysis of the orange-light response of halobacterial cells.....	121
Figure 4.4 Microscopic slide after parts of the glass surface were coated with pectin.....	122
Figure 4.5 Assay to investigate the release of volatile methyl groups from halobacterial cells upon photo- and chemostimuli.....	123
Figure 4.6 Kinetics of methanol equilibration between chase buffer and scintillation liquid.....	124
Figure 6.1 Maps of the plasmids pMKK100, 101, 102, 114 and 119	139
Figure 6.2 (A) Schematic overview of the gene loci for <i>htrs</i> 3 to 10.....	145
Figure 6.3 Southern blots of <i>Bam</i> HI-, <i>Pst</i> I-, <i>Sac</i> I- or <i>Sca</i> I-digested DNA from strain MKK101 and from the <i>htr</i> -deletion strains derived from it.....	147
Figure 6.4 Zoomed MS/MS spectra of the singly methylated Htr14 peptide DTVSATVEEIAASAN originating from two different membrane protein preparations of strain S9 (wt) and one of WFS101 ($\Delta cheB$).....	151
Figure 6.5 MS/MS spectrum of singly methylated Htr8 peptide DLSAAIEEVAASA points only weakly to a methylation of the first rather than the second glutamate.....	152
Figure 6.6 MS/MS spectra of the unmethylated and singly methylated form of the Htr14 peptide DLAEETREQAA from strain WFS101.....	153
Figure 6.7 Schematic representation of the 18 Htrs, <i>E. coli</i> Tsr and Tar, and <i>B. subtilis</i> McpB with features and methylation sites indicated.....	156

6.3 Plasmid maps

Depicted below are the plasmids from Fig. 3.2 that were produced in the course of this study. pMKK100 is the parent plasmid for the construction of *bgaH*-containing plasmids, which allow for red-blue selection of colonies after transformation. pMKK101 and pMKK102 were used for strain complementation with the *bop* gene and the *hop* gene, respectively. pMKK114 and pMKK119 are prototypes of an *htr*-deletion and an *htr*-complementation plasmid, respectively. To derive maps for the remaining deletion and complementation plasmids, the DNA between the *Spe*I (or *Bam*HI) site and the *Hind*III site has to be replaced by the respective deletion or complementation fragment.

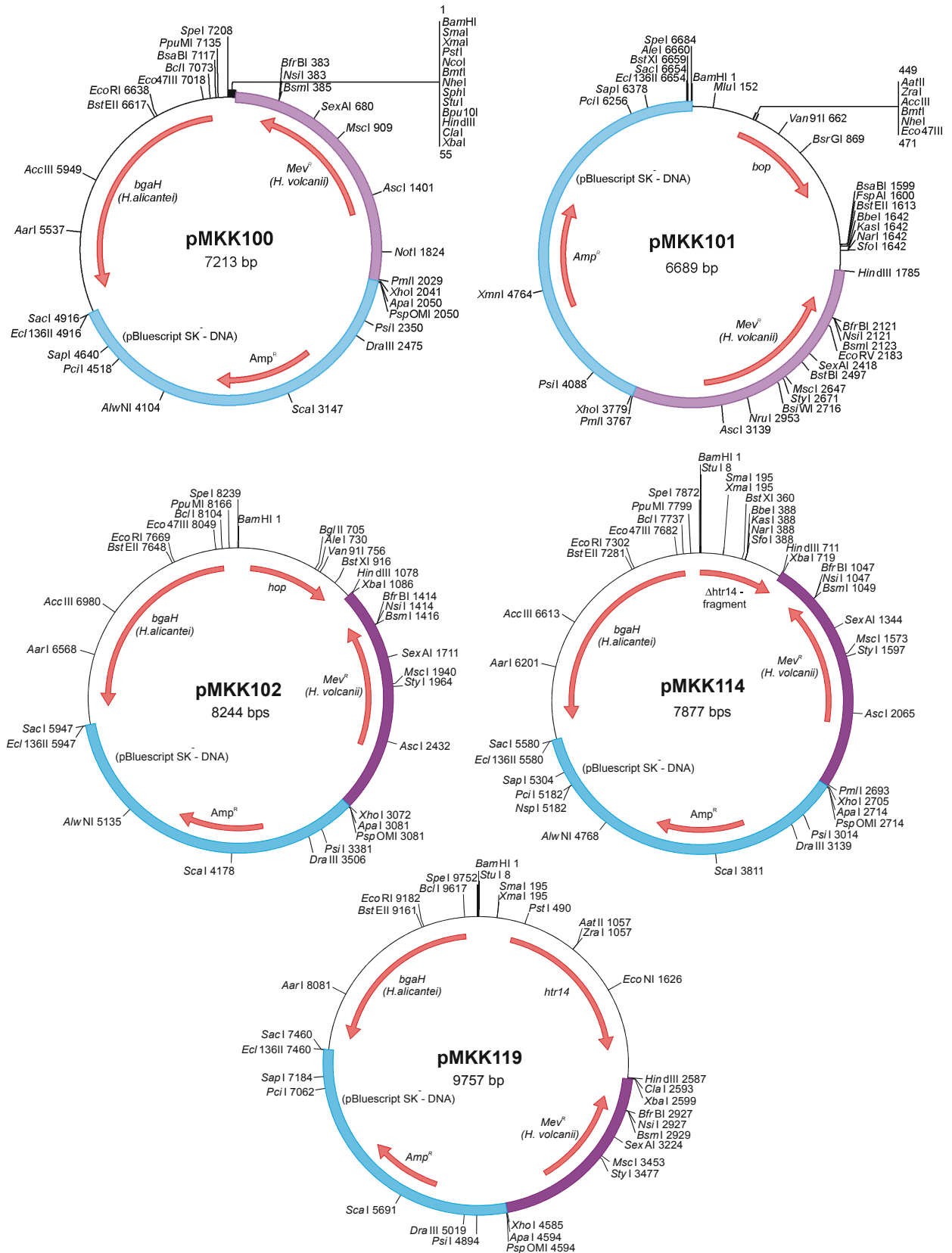


Figure 6.1 Maps of the plasmids pMKK100, 101, 102, 114 and 119

For restriction enzymes which cleave only once within the plasmid, names and cleavage positions are depicted. *Amp^R* and *Mev^R*: markers for ampicillin- and mevinolin-resistance, respectively; *bgaH*: gene encoding the β-galactosidase BgaH; *bop*: bacterioopsin; *hop*: haloopsin; *htr14*: gene encoding Htr14 (MpcT); *Δhtr14*: fused upstream and downstream sequences of *htr14*. Detailed information about all plasmids, including lab designations, is given in Table 4.2.

6.4 Oligonucleotide primers for PCR

The following table provides an overview of the oligonucleotide primers used for the production of DNA fragments in the course of this work. The product names are listed in the first column. If restriction sites are present within the sequence, then they are underlined and the enzyme is given in parentheses. All sequences are given in 5'--> 3' direction and the position of the last nucleotide is given relative to the first base (position +1) of the start codon of the relevant gene. A "PREhtr"-product comprises the upstream sequence of the respective *htr*-gene, whereas the corresponding " Δ htr"-product comprises the fused upstream and downstream sequences of this *htr*.

Table 6.1. Oligonucleotide primers.

<i>Products</i>	<i>Primer name</i>	<i>Primer sequence (restriction site)</i>	<i>Pos. of last nt</i>	<i>T_m^g [°C]</i>
bop-locus	bopall1.seq	TAG <u>CGA ATT CGA</u> CAC GGT CAA CGG GAG G (EcoRI)	-583	60
	bopdown1.rev	GCA <u>TAA GCT TGG</u> TAC ACG TCG CCG AAC C (HindIII)	+1373	60
bop-locus2	bopseq0+	AAA TTC CGT CAC GAG CGT ACC ATA CT	-47	76
	boprev26	GCG AGT ACA AGA CCG AGT GGG GG	+847	76
PREbop	bopseq20	GCT CGT AGC CGC CGT GCG GGA G	-716	78
	boprev37	AAC GAG GAT ATG TGT GTA ACT CTA CGA	-39	76
COREbop	bopseq10	TCG CGT TCA CGA TGT ACC	+211	56
	boprev21	CCA CAA CAC AAC GGT AAC G	+567	58
hop-locus	UShop-1.seq	GCC <u>GGG ATC CCC</u> GGC GAC G (BamHI)	-569	66
	DShop-1.rev	TGG <u>ACA AGC TTC</u> TCC ACG TCC CG (HindIII)	+1687	64
PREhop	HOPU1	CAG ACG TCG AGG TCC TGG TCG G	-1463	74
	HOPU2rev	CGG CGT TCC GCG AGG GCA CC	-1140	72
COREhop	hopseq1	CCT GGC GGT ACC CCA TCG AGA G	-255	74
	HR21	CAG CCC GAG GTA GCT GGA GAT	+220	68
MCS-1	MCS-1.seq	TAG TGG ATC CCC CGG GCT GCA GCC ATG GGC TAG CGC ATG CAG GCC	-	66
	MCS-1.rev	AAG CTC TAG AAT CGA TAA GCT TAG GCC TGC ATG CGC TAG CCC	-	66
PREsopII	PREsopII.seq	TTC TGG TGG TCC ACC ACG	-2952	58
	PREsopII.rev	CTG ATG AAC CGG GTC TCG	-2422	58
COREsopII	COREsopII.seq	ATG GTT TTG GGT CGG CGC	+32	60
	COREsopII.rev	CTC GGT TTG GAG GAT GCC	+547	58
PREsopI	PREsopI.seq	GTC GGG ACC AAC ACG CG	-1868	58
	PREsopI.rev	ATC AGA TCC CTC CAT AAG G	-1640	56
COREsopI	COREsopI.seq	TCA TCG GTG TGA TGG TG	+313	56
	COREsopI.rev	TGC ATG AAC ACG CGA CGC	+645	58
PREhtr8 and Δ htr8	UShtrVIII-1.seq ^a	TTC <u>CTG GAT CCG</u> GAG ACC ACC C (BamHI)	-305	68
	UShtrVIII-1.rev ^b	CTG CGT AAC GCG AAC ACC CTC AGG TGG CGG	-19	64
	DShtrVIII-1.seq ^c	TGA GGG TGT TCG CGT TAC GCA GTG GGT TCG C	+1952	66
	DShtrVIII-1.rev ^d	CCT <u>GAA GCT TGC</u> CGT CGA GTT CG (HindIII)	+2151	70
COREhtr8	COREhtr8.seq	GCA GCG CTG AGA CGA CCG	+43	62
	COREhtr8.rev	CAC CGA CGG GAT CGA CGC	+306	62

Products	Primer name	Primer sequence (restriction site)	Pos. of last nt	T_m^g [°C]
PREhtr10 and Δhtr10	UShemAT-1.seq ^a	AGC GCG <u>GAT CCG</u> TCG AGG ACG (BamHI)	-393	68
	UShemAT-1.rev ^b	CGG CGT CGA GCT TTT CCC CAA GAA TGC CGG ACG	-21	68
	DShemAT-1.seq ^c	TCT TGG GGA AAA GCT CGA CGC CGA GAC CGT CG	+1491	72
	DShemAT-1.rev ^d	GTT GCA <u>AGC TTC</u> GAC GTG ACG GC (HindIII)	+1819	70
COREhtr10	COREhemAT.seq ^e	GCA ACG ATA ATG ACA CTC TCG	+25	62
	COREhemAT.rev ^f	CGG TGT CGT ACT CGC CGC	+314	62
PREhtr15 and Δhtr15	UShtp9-1.seq ^a	GTA <u>CGG ATC CGT</u> TAA CGG CG (BamHI)	-317	64
	UShtp9-1.rev ^b	TGG GTT CAA TGG CAT TCG TCA GTA GGT CGG G	-16	64
	DShtp9-1.seq ^c	CTG ACG AAT GCC ATT GAA CCC ACG CGA GTA CG	+1932	66
	DShtp9-1.rev ^d	CGA TAT ACA CCA <u>AGC TTA</u> GGA CG (HindIII)	+2333	64
COREhtr15	COREhtp9.seq ^e	CAA ACT GCT CGG TCG CGG C	+36	62
	COREhtp9.rev ^f	CCC GCT GAG ACA TCG GCC G	+245	62
PREhtr14 and Δhtr14	UShtp18-1.seq ^a	GCT <u>TGG ATC CGA</u> GGC CTC CC (BamHI)	-375	64
	UShtp18-1.rev ^b	CGC TAC TGG CGC CTA ATC GTC TAT GTC CCC C	-21	66
	DShtp18-1.seq ^c	ACG ATT AGG CGC CAG TAG CGG CCC CGC C	+1894	66
	DShtp18-1.rev ^d	CGA GAA <u>GCT TCT</u> GTT CCG CGG (HindIII)	+2186	64
COREhtr14	COREhtp18.seq ^e	ACA GGC ATA CAA GCG CTC GC	+31	64
	COREhtp18.rev ^f	TGC ATC CCA TCG AAG GAC GC	+352	64
PREhtr9 and Δhtr9	UShtp3-1.seq ^a	ACC ACC <u>CGG ATC CGT</u> TCA GTG (BamHI)	-321	64
	UShtp3-1.rev ^b	CCG CGC CGC ACA TGC AGA TGG GTA CGG GC	-16	64
	DShtp3-1.seq ^c	ATC TGC ATG TGC GGC GCG GAC GAA GTC C	+1467	64
	DShtp3-1.rev ^d	TGC GTG <u>AAG CTT</u> GCG CCG G (HindIII)	+1768	64
COREhtr9	COREhtp3.seq ^e	AAC ATG AAC TGG GGT CGC CG	+33	64
	COREhtp3.rev ^f	TAG TCG CCG GTG AGC AGC G	+287	64
PREhtr18 and Δhtr18	UShtp16-1.seq ^a	GTG <u>AAC TAG TCG</u> TCC TCG ATG C (SpeI)	-448	64
	UShtp16-1.rev ^b	AGT GTG GTC TGG TTG TGT TAT GTG TTC ACA CAC G	-24	66
	DShtp16-1.seq ^c	CAT AAC ACA ACC AGA CCA CAC TGA TCT CTC CC	+2472	66
	DShtp16-1.rev ^d	CGT CTA <u>AGC TTT</u> TGA ACG CGT CC (HindIII)	+2777	66
COREhtr18	COREhtp16.seq ^e	GCA CGT ACG TTC CGA CAG CG	+30	66
	COREhtp16.rev ^f	CGA GGC CCG GAT GGT GTC C	+351	66
PREhtr16 and Δhtr16	UShtp17-1.seq ^a	CCG <u>GAC TAG TGG</u> GGA CGC GC (SpeI)	-315	66
	UShtp17-1.rev ^b	CGC CGC CGC CCC CTC GCT GTT GGT GCC C	-18	66
	DShtp17-1.seq ^c	GCG AGG GGG CGG CGG CGG GCG TGC G	+2396	66
	DShtp17-1.rev ^d	CAA GCG GTA <u>AAG CTT</u> GCG TTC C (HindIII)	+2643	64
COREhtr16	COREhtp17.seq ^e	GAC GCT CGA AGA CAC GCT CC	+31	66
	COREhtp17.rev ^f	CTG CCG TTC TGC CGG CCG	+348	64
PREhtr12 and Δhtr12	UShtp12-1.seq	CCA <u>GGA TCC</u> CGA CCT CGA CG (BamHI)	-282	66
	UShtp12-1.rev	ACC AAC CAG GGT CGT CGG CGT CCA GTG CG	-19	66
	DShtp12-1.seq	GCC GAC GAC CCT GGT TGG TGG ATT TTT TGC G	+1288	66
	DShtp12-1.rev	TCG GAA <u>AGC TTG</u> GCG GCC ACC (HindIII)	+1611	66
COREhtr12	COREhtr12.seq	GGA GGT GTG GCG CGG CGC	+26	66
	COREhtr12.rev	CAC CGT CGT TGT GCA GTG GG	+297	66
PREhtr13 and Δhtr13	UShtp13-1.seq	AAC <u>TGG ATC CGG</u> CTC GTA CCC CAT CCC (BamHI)	-280	68
	UShtp13-1.rev	AAC CCA GTA CGG TCA TTG GAC TGC CTA TGC CC	-16	66
	DShtp13-1.seq	AGT CCA ATG ACC GTA CTG GGT TTC GAG GTG GG	+1294	68
	DShtp13-1.rev	GCA TAA <u>GCT TCA</u> GTA GGG GCG GGG TCC GC (HindIII)	+1558	68
COREhtr13	COREhtr13.seq	GCG TCA CCG TCG ACG CCG G	+55	68
	COREhtr13.rev	CAG CGG GGA TTG GAT GGC CG	+278	68

<i>Products</i>	<i>Primer name</i>	<i>Primer sequence (restriction site)</i>	<i>Pos. of last nt</i>	<i>T_m^g [°C]</i>
PREhtr17 and Δhtr17	UShtr17-1.seq	ATG <u>CGG ATC CGC</u> TGT GCT CCC ACT CAT CGC (BamHI)	-357	66
	UShtr17-1.rev	TGA AGA AAT AGT GGT CGT CAC CCT CGG CGG	-19	66
	DShtr17-1.seq	GGG TGA CGA CCA CTA TTT CTT CAT TCA GAC GAC TCC	+1646	68
	DShtr17-1.rev	CCG <u>TAA GCT TTC</u> ATA CTC TGG GTC GAC CTG G (HindIII)	+1888	66
COREhtr17	COREhtr17.seq	GTT CGA CGT CAT CGC CGT CG	+40	66
	COREhtr17.rev	CGA GAT CGT GCC GGT GGA CG	+251	68
PREhtr7 and Δhtr7	UShtr7-1.seq	GCA <u>TGG ATC CGG</u> AAG TAA GTG TGT GCA ATG G (BamHI)	-281	68
	UShtr7-1.rev	AGA CCG CAG CGC CGT GTC CTC CGT TGC CG	-19	66
	DShtr7-1.seq	AGG ACA CGG CGC TGC GGT CTG GTC AGT CGG	+1661	68
	DShtr7-1.rev	ATA <u>CAA GCT TCG</u> ACG AGA CCG ACA CGG GC (HindIII)	+1921	66
COREhtr7	COREhtr7.seq	CGT CTT CGT TGA CGC GGT CG	+34	66
	COREhtr7.rev	CAC CGC CAC TGT CGT CGC C	+246	66
PREhtr6 and Δhtr6	UShtr6-1.seq	CGA <u>TGG ATC CAC</u> TCC GAC CAG TCG CGC AGC (BamHI)	-282	68
	UShtr6-1.rev	CCC GGC GGC GCC ACC ACC GCC GGC GG	-19	68
	DShtr6-1.seq	GGT GGT GGC GCC GCC GGG TCG CGG CAC G	+2389	68
	DShtr6-1.rev	GTA <u>TAA GCT TTC</u> CCG ACG AGT CCA CTC CCG (HindIII)	+2655	68
COREhtr6	COREhtr6.seq	GCA TCA CTG GCG CAC TCC GG	+30	68
	COREhtr6.rev	ACC GAC CGC GCG TGC GTC C	+245	68
PREhtr4 and Δhtr4	UShtr4-1.seq	AGT <u>AAC TAG TGA</u> CGC CGG CTG CGC GTA CG (SpeI)	-284	68
	UShtr4-1.rev	TCC CGC CGA GTC TCC GGT CAA ACG CGT CTC G	-24	68
	DShtr4-1.seq	TGA CCG GAG ACT CGG CGG GAC GCT CAG GC	+2356	68
	DShtr4-1.rev	CTC <u>GAA GCT TCG</u> GCC GGT CGC GGC TGC C (HindIII)	+2610	68
COREhtr4	COREhtr4.seq	TTT GCG CAT CGA ATA CTG CGG C	+37	68
	COREhtr4.rev	TAC TGA GCG AGC ATC CTG GCG	+246	68
PREhtr5 and Δhtr5	UShtr5-1.seq	TCA <u>TAC TAG TGC</u> ACT GCG GTC GAC GAA GGG (SpeI)	-281	68
	UShtr5-1.rev	GGC TGC GGT GTC AGA TGA AGT CGT TGT TCT GC	-26	68
	DShtr5-1.seq	ACT TCA TCT GAC ACC GCA GCC GGT CAG TCC G	+2456	66
	DShtr5-1.rev	AGA <u>TAA GCT TAG</u> GAG ATC AGT CAG GCG ATG G (HindIII)	+2712	66
COREhtr5	COREhtr5.seq	CGA CGC CGG CGA CAA CTC G	+36	66
	COREhtr5.rev	CCA GCC AGT CGC CGA TCT CG	+246	68
PREhtr3 and Δhtr3	USbasT-1.seq ^a	CAT <u>GGG ATC CCG</u> CGC TCG CGT TGC TCG C (BamHI)	-360	68
	USbasT-1.rev ^b	GTT CGG CGA CAC CAC CGT CCG TGA AGT ATC C	-26	66
	DSbasT-1.seq ^c	GGA CGG TGG TGT CGC CGA ACC CTT TTC TTC G	+2442	66
	DSbasT-1.rev ^d	AGA <u>TAA GCT TTT</u> CCG GAG GCT CAC CGC CG (HindIII)	+2651	66
COREhtr3	COREbasT.seq ^e	ACA TCG ACC GCG GAC TCT TCG	+28	68
	COREbasT.rev ^f	GGT TGA TTC TTT CTG TGT GAG CC	+218	68
PREhtr11 and Δhtr11	UScar-2.seq ^a	TAC <u>TAC TAG TCT</u> CCG CAC CGT ATT AAT AGC CG (SpeI)	-404	68
	UScar-1.rev ^b	TAG CGG CGT TAT TTC TTA TTA TCC TCC TGT TCA CG	-27	66
	DScar-1.seq ^c	GGA TAA TAA GAA ATA ACG CCG CTA AAC ATA CGT CG	+1378	66
	DScar-1.rev ^d	CTT <u>AAA GCT TAG</u> GGC CAT GGG TTC TAT GCC C (HindIII)	+1644	68
COREhtr11	COREcar.seq ^e	GTC AGA CAT GGG TGG CGA AGC	+35	68
	COREcar.rev ^f	GAG GGC GTC CGA TCG AGC C	+252	66
PREoe1534 and Δoe1534	US1534.seq	TGA <u>CGG ATC CTC</u> GCC TAA CCT TTA TCT AGT TCC (BamHI)	-277	66
	US1534.rev	CCC CGC CAG GCA CCA GCG TTG GCG GCG G	-19	68
	DS15341.seq	ACG CTG GTG CCT GGC GGG GCC GCT ACT GG	+790	68
	DS1534.rev	CAG <u>TAA GCT</u> TCA CCG ACG AGG TCG CCG ACC (HindIII)	+1074	70
COREoe1534	CORE1534.seq	CGC CTT CGG ATC GAT CCT AGC	+95	68
	CORE1534.rev	CCG TGA ACG ACG CGA AGA ACC	+305	68

<i>Products</i>	<i>Primer name</i>	<i>Primer sequence (restriction site)</i>	<i>Pos. of last nt</i>	<i>T_m^g [°C]</i>
bgaH-locus	USbgaH-1.seq	TCG <u>CAC TAG TGT</u> CTC TCA CGG (SpeI)	-131	66
	DSbgaH-1.rev	AGT ACA CCG <u>AGC TCG</u> GCG GC (SacI)	+2140	66
<p>a - f: Alternative names for these primers are in the case of a: USht[#].seq, b: USht[#].rev, c: DSht[#].seq, d: DSht[#].rev, e: COREht[#].seq and f: COREht[#].rev, where # stands for the number of the <i>ht^r</i> indicated in the product column. g: The primer melting temperature T_m was calculated by adding up 2° per A-T match and 4° per G-C match of primer and template.</p>				

6.5 Southern blots to verify the *htr*-deletions in strains derived from MKK101

As exemplified with the generation of the *htr14*-deletion strain MKK114 (Fig. 3.6), strain MKK101 was also used as the parent strain for the deletion of other *htr* genes. Depicted below are the gene loci of all *htrs* that were deleted in the course of this study (Fig. 6.2 A and B). The successful deletion of each individual *htr* was verified via Southern blotting using genomic DNA from MKK101 and of the respective *htr*-deletion strain, after digestion with an appropriate restriction enzyme (Fig. 6.3). DIG-11-dUTP-labeled DNA probes which hybridize to either the upstream region (PRE) or a region within the respective *htr* (CORE) were used in this analysis. The sizes of the DNA fragments that were detected by the respective PRE probes, and the absence of signals when using the respective CORE probes on DNA from the deletion strains, confirmed the deletions in all generated strains.

The *htr*-deletion strains generated from parent strain S9 (Table 4.1) were also checked via Southern blots. These blots showed essentially the same band patterns as the ones depicted for the MKK101-derived *htr*-deletion strains (data not shown). This confirmed the deletion-genotype also for these S9-derived strains.

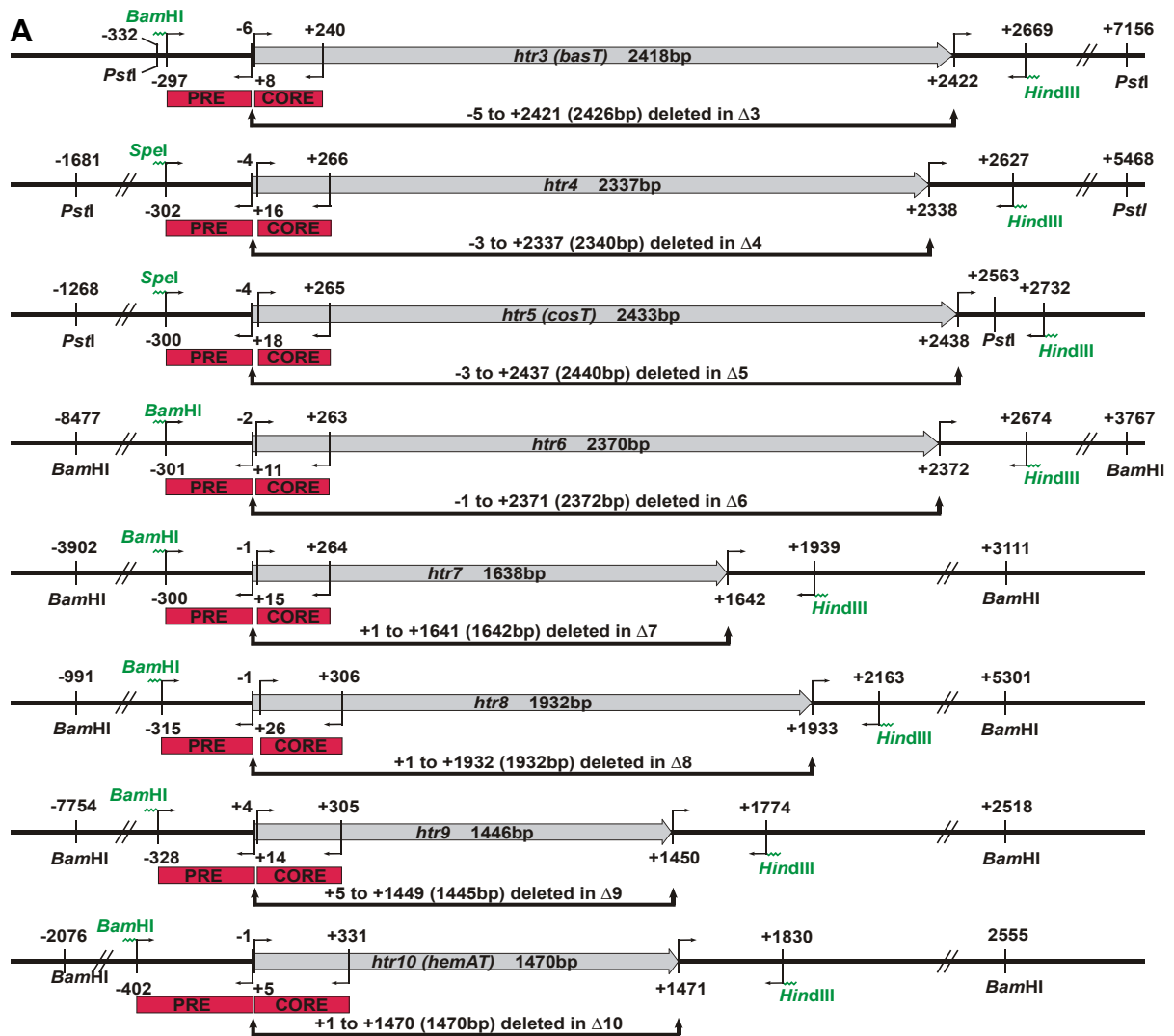


Figure 6.2 (A) Schematic overview of the gene loci for *htrs* 3 to 10.

Wild-type *htr* loci of *H. salinarum* are shown with the indicated nucleotide positions given relative to the start of the orf. PCR primers are depicted as bent arrows, together with the position of the first matching 5'-nucleotide. Restriction sequences attached to the primers are symbolized by a zigzag line. These sequences were used for cloning the PCR-generated Δhtr fragments, which lack the coding region of the respective *htr*, into appropriate plasmids, to produce the respective deletion plasmids (Table 4.2). The positions of recognition sites for restriction enzymes (*Bam*HI, *Pst*I, *Sac*I, *Sca*I) used in Southern blot analysis of the deletion strains are indicated. Furthermore the DIG-11-dUTP-labeled DNA probes used for these Southern blots are shown at their hybridization positions. The DNA regions missing in the generated *htr*-deletion fragments and in the corresponding plasmids and deletion strains are given with respect to the first nucleotide (+1) of the orf. The loci of *htr1*, *htr2* and *htr11* (*car*) are not shown because these genes were already missing in MKK101, the parental strain for the *htr*-deletions.

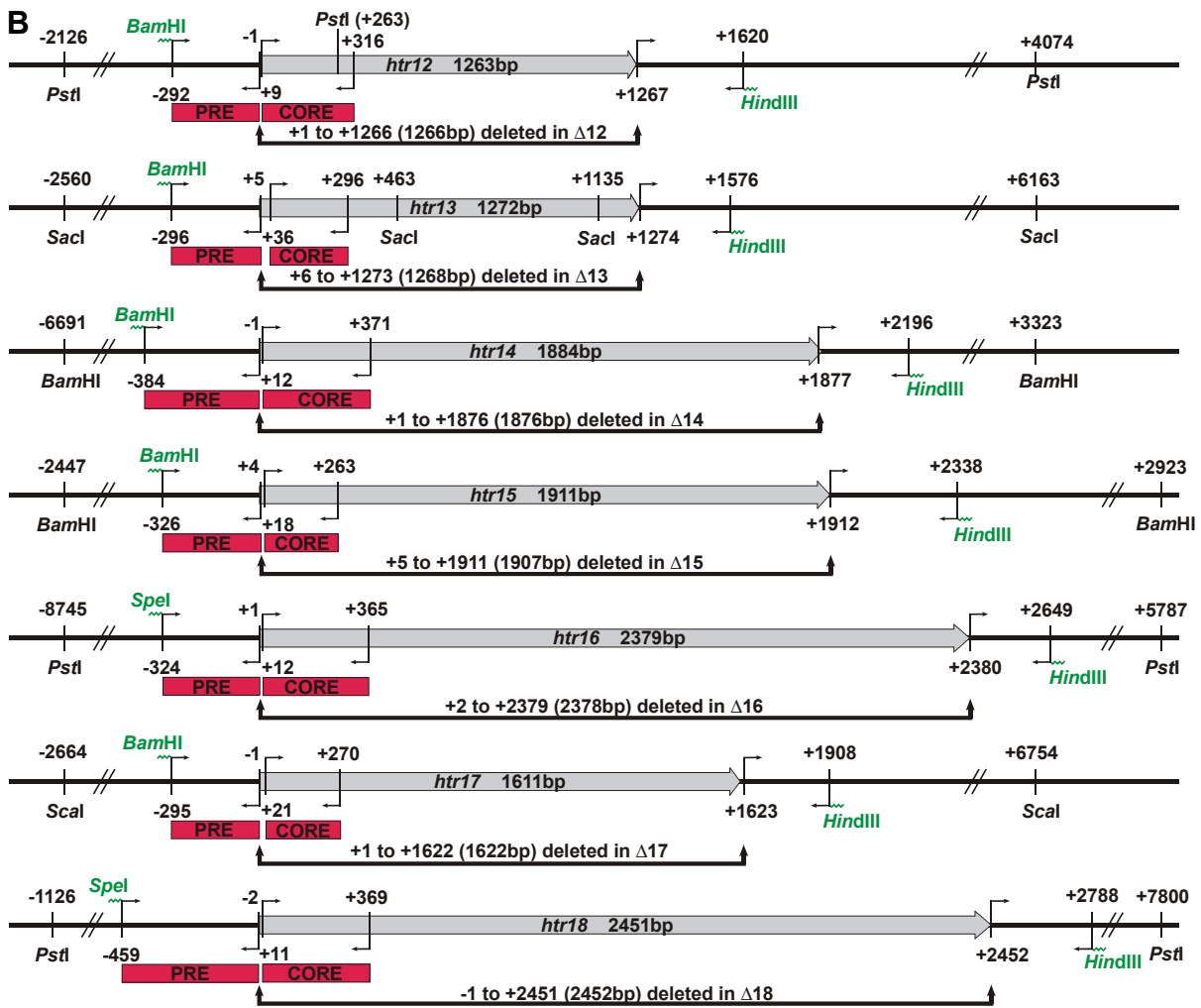


Figure 6.2 (B) Schematic overview of the gene loci for *htrs 12* to *18*.
 For details see Fig. 6.2 A.

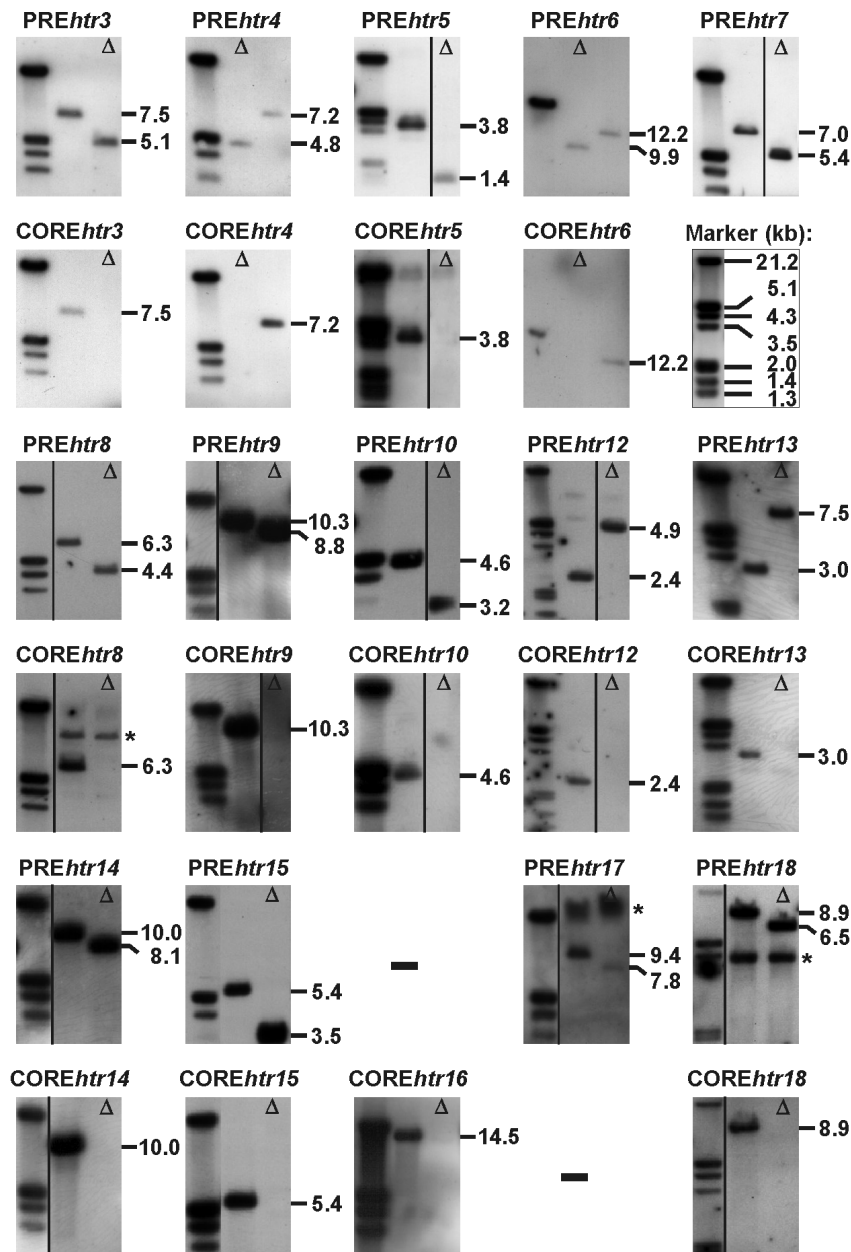


Figure 6.3 Southern blots of *Bam*HI-, *Pst*I-, *Sac*I- or *Sca*I-digested DNA from strain MKK101 and from the *htr*-deletion strains derived from it.

The blots were produced using DIG-11-dUTP-labeled PRE and CORE DNA-probes directed against the upstream region of the respective *htr* gene and a region within this *htr*, respectively (Fig. 6.2). Left lanes show bands of a DNA marker, to which the sizes are attributed at the right of the second row of blots. Genomic DNA from strain MKK101 and from the respective *htr*-deletion strain was digested with *Bam*HI (for *htrs* 6, 7, 8, 9, 10, 14, 15), *Pst*I (for *htrs* 3, 4, 5, 12, 16, 18), *Sac*I (for *htr*13) or *Sca*I (for *htr*17) before use with the respective blot. A lane marked with a Δ contains the DNA of the respective deletion strain, the other lane contains DNA from MKK101. Calculated sizes of the DNA fragments for the respective genotypes are indicated to the right of the blots and are in all cases matching the experimental band position. An asterisk marks the position of bands attributed to unspecific hybridization.

6.6 Details on *htrs* and their gene products

The following table summarizes the currently available information on the 18 halobacterial transducer genes and their products.

Table 6.2. Compilation of information on *htr* genes and their products.

Systematic gene name (Functional gene name) R1-identifier^a / NRC-1-identifier^b	Old gene names	Total length and first 21 nucleotides of the coding region [Chromosomal region / strand]^a	Length of protein / First 7 aa/ Calculated MW [Predicted no. of TM regions /Htr-group]^c (calc. pI)^d	Physiological function of the encoded transducer (Htr) [Transcription unit with neighboring orf at 5' or 3' end of the <i>htr</i>]^a
<i>htr1 (htrI)</i> OE3347F / VNG1659G	<i>htp1</i>	1611 bp: ATGACA ATCGCATGGGCGCGC [1226323-1227933 / F]	536 aa / MTIAWAR / 56.64 kDa [2 TM /group 2] (4.1)	phototaxis-transducer for orange and UV light via photoreceptor SRI [3'-overlap: OE3348F (<i>sopI</i>)]
<i>htr2 (htrII)</i> OE3481R / VNG1765G	<i>htp2</i> <i>htE</i>	2295 bp: ATGGGG TCCGGATTAGTCGCA [1294122-1296416 / R]	764 aa / MGSGLVA / 79.00 kDa [2 TM /group 3] (4.0)	phototaxis-transducer for blue light via photoreceptor SRII [2 bp distant from 3'-end: OE3480R (<i>sopII</i>)]
<i>htr3 (basT)</i> OE3611R / VNG1856G (incorrectly assigned orf for NRC-1 lacks 516 bp at its 5' end)	<i>htp10</i> <i>htC</i>	2418 bp: GTGAGC GACATCGACCGCGGA [1359876-1362293 / R]	805 aa / MSDIDRG / 84.78 kDa [2 TM/group 3] (3.9)	chemotaxis-transducer for Val, Leu, Ile, Met, Cys (only in the presence of putative binding protein BasB) [5'-overlap: OE3612R (<i>basB</i>)]
<i>htr4</i> OE2189R / VNG0806G	<i>htp6</i> <i>htpVI</i> <i>htD</i>	2337 bp: ATGTCG ATACGATCGTTTTGCG [0595645-0597981 / R]	778 aa / MSIRSF A / 82.03 kDa [2 TM/group 3] (4.2)	function not known [no transcription unit]
<i>htr5 (cosT)</i> OE3474R / VNG1760G	<i>htp4</i> <i>htpIV</i> <i>htF</i>	2433 bp: ATGTCC GAACCCACGGCCGAC [1288172-1290604 / R]	810 aa / MSEPTAD / 85.17 kDa [2 TM/group 3] (4.0)	chemotaxis-transducer for compatible osmolytes (putatively via binding protein CosB) [5'-overlap: OE3476R (<i>cosB</i>)]
<i>htr6</i> OE2168R / VNG0793G	<i>htp7</i> <i>htJ</i>	2370 bp: ATGAGC GACGGCATCACTGGC [0585634-0588003 / R]	789 aa / MSDGITG / 83.88 kDa [2 TM/group 3] (4.1)	function not known (putatively mediating chemotaxis via binding protein TmpC) [5'-overlap: OE2170R (<i>tmpC</i>)]
<i>htr7</i> OE3473F / VNG1759G	<i>htp5</i> <i>htpV</i> <i>htI</i>	1638 bp: ATGAGT GGTGCTGCCGTCTTC [1286519-1288156 / F]	545 aa / MSGAAVF / 57.04 kDa [3 TM/group 4] (3.9)	function not known [5'-overlap: OE3472F (encoding a 3 TM protein)]
<i>htr8 (htrVIII)</i> OE3167F / VNG1523G	<i>htp8</i> <i>htK</i>	1932 bp: ATGGGG GAATCCGCACGCGG [1122627-1124558 / F]	643 aa / MGESARG / 67.25 kDa [6 TM/group 5] (4.2)	aerotaxis-transducer for aerophilic response [no transcription unit]
<i>htr9</i> OE2996R / VNG1395G	<i>htp3</i> <i>htpIII</i> <i>htA</i>	1446 bp: ATGTCT AAAAACAACATGAA [1030926-1032371 / R]	481 aa / MSKNKHE / 50.74 kDa [0 TM/group 1] (3.7)	function not known [no transcription unit]

Systematic gene name (Functional gene name) R1-identifier ^a / NRC-1-identifier ^b	Old gene names	Total length and first 21 nucleotides of the coding region [Chromosomal region / strand] ^a	Length of protein / First 7 aa/ Calculated MW [Predicted no. of TM regions /Htr-group] ^c (calc. pI) ^d	Physiological function of the encoded transducer (Htr) [Transcription unit with neighboring orf at 5' or 3' end of the htr] ^a
<i>htr10</i> (<i>hemAT</i>) OE3150R / VNG1505G	<i>htp15</i> <i>htB</i>	1470 bp: ATGAGC AACGATAATGACACT [1110218-1111687 / R]	489 aa / MSNDNDT / 52.82 kDa [0 TM/group 1] (3.9)	aerotaxis-transducer for aerophobic response [no transcription unit]
<i>htr11</i> (<i>car</i>) OE5243F / --- (orf not present in NRC-1)	<i>htp11</i> <i>htrXI</i>	1359 bp: ATGGAT CCAGCATCGTCAGAC Region on plasmid pHS3: [0151230-0152588 / F]	452 aa / MDPASSD / 49.1 kDa [0 TM/group 1] (4.0)	chemotaxis-transducer for Arg [no transcription unit]
<i>htr12</i> OE3070R / VNG1442G	<i>htp12</i> <i>htrXII</i> <i>htG</i>	1263 bp: ATGGGG GAGGAGGTGTGGCGC [1062231-1063493 / R]	420 aa / MGEEVWR / 44.08 kDa [0 TM/group 1] (3.9)	function not known [no transcription unit]
<i>htr13</i> OE2474R / VNG1013G	<i>htp13</i> <i>htrXIII</i> <i>htL</i>	1272 bp: ATGACC GGGCCCGACAACCTCA [0767790-0769061 / R]	423 aa / MTGPDNS / 44.99 kDa [0 TM/group 1] (4.0)	function not known [no transcription unit]
<i>htr14</i> (<i>mpcT</i>) OE1536R / VNG0355G	<i>htp18</i>	1884 bp: ATGAAC ATAACACAGGCATAC [0270633-0272516 / R]	627 aa / MNITQAY / 65.62 kDa [2 TM/group 2] (3.8)	transducer for membrane potential changes and for phototaxis via BR and HR [no transcription unit]
<i>htr15</i> OE2392R / VNG0958G	<i>htp9</i>	1911 bp: ATGCTG CGCATCTTTCGCAAA [0719691-0721601 / R]	636 aa / MLRIFRK / 67.31 kDa [0 TM/group 1] (3.9)	function not known [3'-overlap: <i>OE2390R</i> (<i>flaD</i>)]
<i>htr16</i> OE1929R / VNG0614G (incorrectly assigned orf for NRC-1 lacks 492 bp at its 5' end)	<i>htp17</i>	2379 bp: GTGTCG CGCGTGACGCTCGAA [0458664-0461042 / R]	792 aa / MSRVTLTLE / 84.85 kDa [2 TM/group 3] (4.0)	function not known [no transcription unit]
<i>htr17</i> OE3436R / VNG1733G	<i>htp14</i>	1611 bp: ATGAAC CACCTCATCGTGCTG [1270982-1272592 / R]	536 aa / MNHLIVL / 56.78 kDa [3 TM/group 3] (4.0)	function not known [5'-overlap: <i>OE3438R</i> (<i>encoding a 3 TM protein</i>)]
<i>htr18</i> OE2195F / VNG0812G (incorrectly assigned orf for NRC-1 lacks 78 bp at its 5' end)	<i>htp16</i>	2451 bp: ATGGCG CTGGGCACGTACGTT [0600783-0603233 / F]	816 aa / MALGTYV / 87.01 kDa [2 TM/group 3] (4.1)	function not known (putatively mediating chemotaxis via binding protein PotD) [3'-overlap: <i>OE2196F</i> (<i>potD</i>)]

a: Systematic names and positions of orfs are given according to the database at <http://www.halolex.mpg.de> (Dieter Oesterhelt *et al.*, unpublished); **b:** Systematic orf names according to Ng *et al.* (2000); **c:** transmembrane regions (TM) were predicted via identification of hydrophobic stretches within the transducers' amino acid (aa) sequences by visual inspection. The definitions of groups are as follows: 1: 0 TM, 2: 2 TM but no extracellular domain, 3: 2 TM plus extracellular domain, 4: 3 TM and 5: 6 TM; **d:** isoelectric points, calculated from the amino acid sequence.

6.7 Databases of Htr-peptide sequences

As described in Chapter 3.2.4, in addition to the database containing all predicted *H. salinarum* protein sequences, two additional databases were created for Mascot searches with the peak lists generated in the Q-TOF MS/MS experiments. The second database accounts for potential Q to E exchanges in Htrs only at sites which were assumed to be potential methylation sites. The third database accounts for all thinkable single or multiple N - D or Q - E exchanges.

Table 6.3. First entries of the FASTA-formatted lists of peptide sequences, which represent the databases used for the identification of Htr peptides via Mascot MS/MS ions searches.

Second database ^a :	Third database ^b :
>Htr1_D256 modified: Q258E DVEQVSASAEELIATI	>Htr1_1603 (Htr1_1603) Htr1_M1 MTIAWARRRYGVKLGGLGYIATAGLLVGVGVTTN
>Htr1_D256 modified: Q259E DVQEVASAEELIATI	>Htr1_1604 (Htr1_1604) Htr1_M1_N33D MTIAWARRRYGVKLGGLGYIATAGLLVGVGVTT
>Htr1_D256 modified: Q258E Q259E DVEEVASAEELIATI	>Htr1_1521 (Htr1_1521) Htr1_D34 DVPSTIVAGIAGLLTLGSINAAETVASIKEIAAQTERVANGNLEQEVSTRT
>Htr2_D702 modified: Q709E DEVAGISEETAQAATAVA	>Htr1_1522 (Htr1_1522) Htr1_D34_N53D DVPSTIVAGIAGLLTLGSI
>Htr3_D728 modified: Q730E DEEAASSTEEVVTMI	>Htr1_1523 (Htr1_1523) Htr1_D34_N73D DVPSTIVAGIAGLLTLGSINAAETVASIKEIAAQTERVA
>Htr3_D561 modified: Q568E DVAETVNEAATESERQELGE	>Htr1_1524 (Htr1_1524) Htr1_D34_N75D DVPSTIVAGIAGLLTLGSINAAETVASIKEIAAQTERVANG
>Htr3_D749 modified: Q756E DRTATESEQVSAAAEQAASVSEVAGRA	>Htr1_1525 (Htr1_1525) Htr1_D34_Q67E DVPSTIVAGIAGLLTLGSINAAETVASIKEIAAETERVANGNLEQEVSTRT
>Htr3_D749 modified: Q757E DRTATESQEVSAAAAEQAASVSEVAGRA	>Htr1_1526 (Htr1_1526) Htr1_D34_Q67E_N73D DVPSTIVAGIAGLLTLGSINAAETVASIKEIAAETERVA
>Htr3_D749 modified: Q756E Q757E DRTATESEEVSAAAAEQAASVSEVAGRA	>Htr1_1527 (Htr1_1527) Htr1_D34_Q67E_N75D DVPSTIVAGIAGLLTLGSINAAETVASIKEIAAETERVANG
>Htr3_D518 modified: Q525E DQVSESVEDISA	>Htr1_1528 (Htr1_1528) Htr1_D34_Q67E_Q78E DVPSTIVAGIAGLLTLGSINAAETVASIKEIAAETERVANGNLEEEVSTRT
>Htr4_D735 modified: Q740E DAAAEETTLTSL	>Htr1_1529 (Htr1_1529) Htr1_D34_Q78E DVPSTIVAGIAGLLTLGSINAAETVASIKEIAAQTERVANGNLEEEVSTRT
>Htr4_D535 modified: Q536E DEVAETSQRAAALG	>Htr1_1617 (Htr1_1617) Htr1_N53D DAAETVASIKEIAAQTERVANGNLEQEVSTRT
>Htr4_D692 modified: Q696E DTGVVEISNAM	>Htr1_1618 (Htr1_1618) Htr1_N53D_N73D DAAETVASIKEIAAQTERVA
>Htr5_D732 modified: Q733E (improbable) DEAASSTEEAVSMTEEVA	>Htr1_1619 (Htr1_1619) Htr1_N53D_N75D DAAETVASIKEIAAQTERVANG
>Htr5_D752 modified: Q768E (improbable) DSTAGEAQSVSAAAEAAAASMSSEIS	>Htr1_1620 (Htr1_1620) Htr1_N53D_Q67E DAAETVASIKEIAAETERVANGNLEQEVSTRT
>Htr5_D515 modified: Q528E DAERASQVSESVVEI AGAA	>Htr1_1621 (Htr1_1621) Htr1_N53D_Q67E_N73D DAAETVASIKEIAAETERVA
>Htr5_D720 modified: Q724E DTGVVEIS	>Htr1_1622 (Htr1_1622) Htr1_N53D_Q67E_N75D DAAETVASIKEIAAETERVANG
>Htr6_D518 modified: Q525E DELSASIEEVAASSATVAETAA	>Htr1_1623 (Htr1_1623) Htr1_N53D_Q67E_Q78E DAAETVASIKEIAAETERVANGNLEEEVSTRT
>Htr6_D726 modified: Q729E DAEEVSAAAEEQSASVAEIARSA	>Htr1_1624 (Htr1_1624) Htr1_N53D_Q78E DAAETVASIKEIAAQTERVANGNLEEEVSTRT
>Htr6_D726 modified: Q737E (improbable) DAEQVSAAAEESASVAEIARSA	>Htr1_1625 (Htr1_1625) Htr1_N73D DGNLEQEVSTRT
>Htr6_D726 modified: Q729E Q737E (improbable) DAEEVSAAAAEESASVAEIARSA	>Htr1_1626 (Htr1_1626) Htr1_N73D_Q78E DGNLEEEVSTRT
>Htr6_D473 modified: Q497E DETLQVATGAEIEITTSQTVSERIEEIA	>Htr1_1627 (Htr1_1627) Htr1_N75D DLEQEVSTRT
>Htr6_D687 modified: Q693E DANHGIEEISDATE	>Htr1_1628 (Htr1_1628) Htr1_N75D_Q78E DLEEEVSTRT
>Htr7_D484 modified: Q496E (improbable) DRAENVSAASEEETASITVETSSLQLAAQA	>Htr1_1594 (Htr1_1594) Htr1_D86 DEFGSLA

a: Besides the protein sequences of all 18 Htrs, the database contains peptide sequences created from the original Htr peptides (after Asp-N digest) by Q-E substitutions (*in silico* deamidations) in the putative methylation regions of the Htrs. Fragments are marked "improbable", if the Q-E substitution was not at heptad positions 2 or 3 (65 modified peptide species in total). **b:** The database is produced by *in silico* generation of all possible permutations of deamidated peptides, which can in principle result from Asp-N digestion of Htrs after Q-E or N-D substitutions (2826 modified and unmodified peptide species in total). [sequence permutations were produced with a program written by Volker Hickmann] For each peptide is listed: the Htr of origin, the Htr residue position of the N-terminal Asp and of the modification(s).

6.8 Additional MS/MS spectra

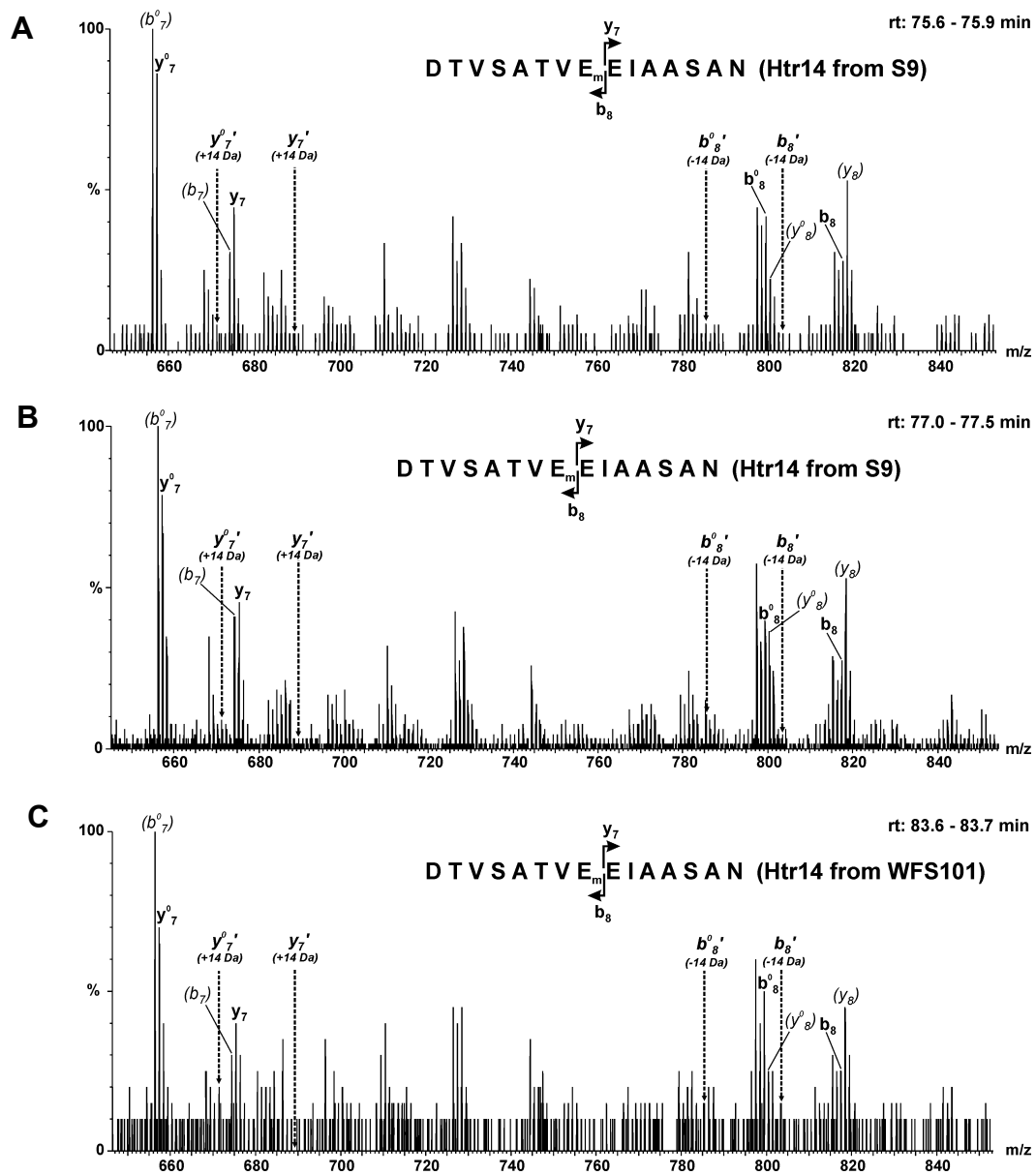


Figure 6.4 Zoomed MS/MS spectra of the singly methylated Htr14 peptide DTVSATVEEIAASAN originating from two different membrane protein preparations of strain S9 (wt) and one of WFS101 ($\Delta cheB$).

Spectra were recorded and annotated as described in Fig. 3.27. (A) Magnified view of the m/z region between 650 and 850 of the spectrum shown in Fig. 3.28. (B) Identical region in a spectrum obtained for the same peptide species in an independent experiment. In the experiment that resulted in the second (first) spectrum the membrane protein preparation was from S9 cells at an OD600 of 1.4 (0.8) and 15 μg (55 μg) of membrane proteins per lane were separated in an 8% gel (10% gel). (C) Spectrum analogous to (A) and (B) but obtained for a peptide derived from a preparation of WFS101 membrane proteins. An MS/MS spectrum of the doubly methylated species was obtained from the same preparation at a retention time (rt) between 86.5 and 86.6 min (shown in Fig. 3.29C). Arrows at the peptide sequence indicate fragments y_7 and b_8 which are crucial for the determination of the methylation position.

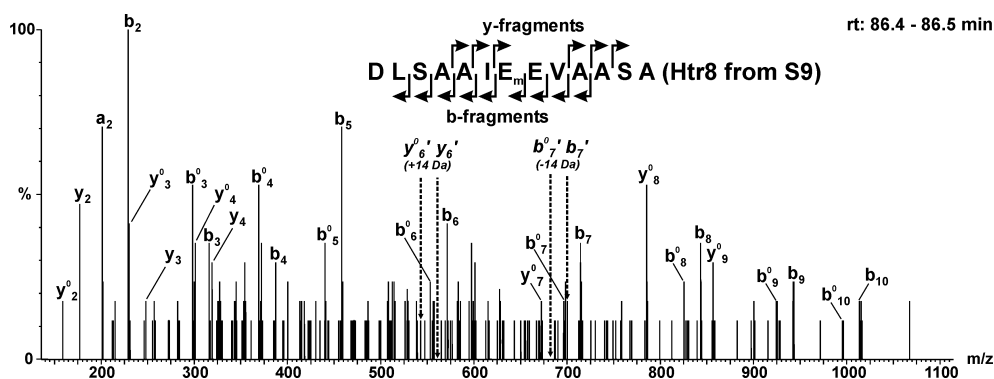


Figure 6.5 MS/MS spectrum of singly methylated Htr8 peptide DLSAAIEEVAASA points only weakly to a methylation of the first rather than the second glutamate.

The spectrum was recorded and annotated as described in Fig. 3.27. In addition to this Htr8 peptide, another peptide of identical sequence and methylation was obtained from a gel position corresponding to lower protein mobility, and was also identified via MS/MS. (Originating from such a gel position this other peptide should not have resulted from Htr8 but rather from CosT (Fig. 3.29). This was concluded from the fact that several other MS/MS spectra identified CosT peptides which originated from that gel position, but no Htr8 peptides were detected.) Neither for the Htr8-derived nor for the Htr5-derived peptide the methylated position could be determined unambiguously, but in both cases the first position seemed to be at least preferred.

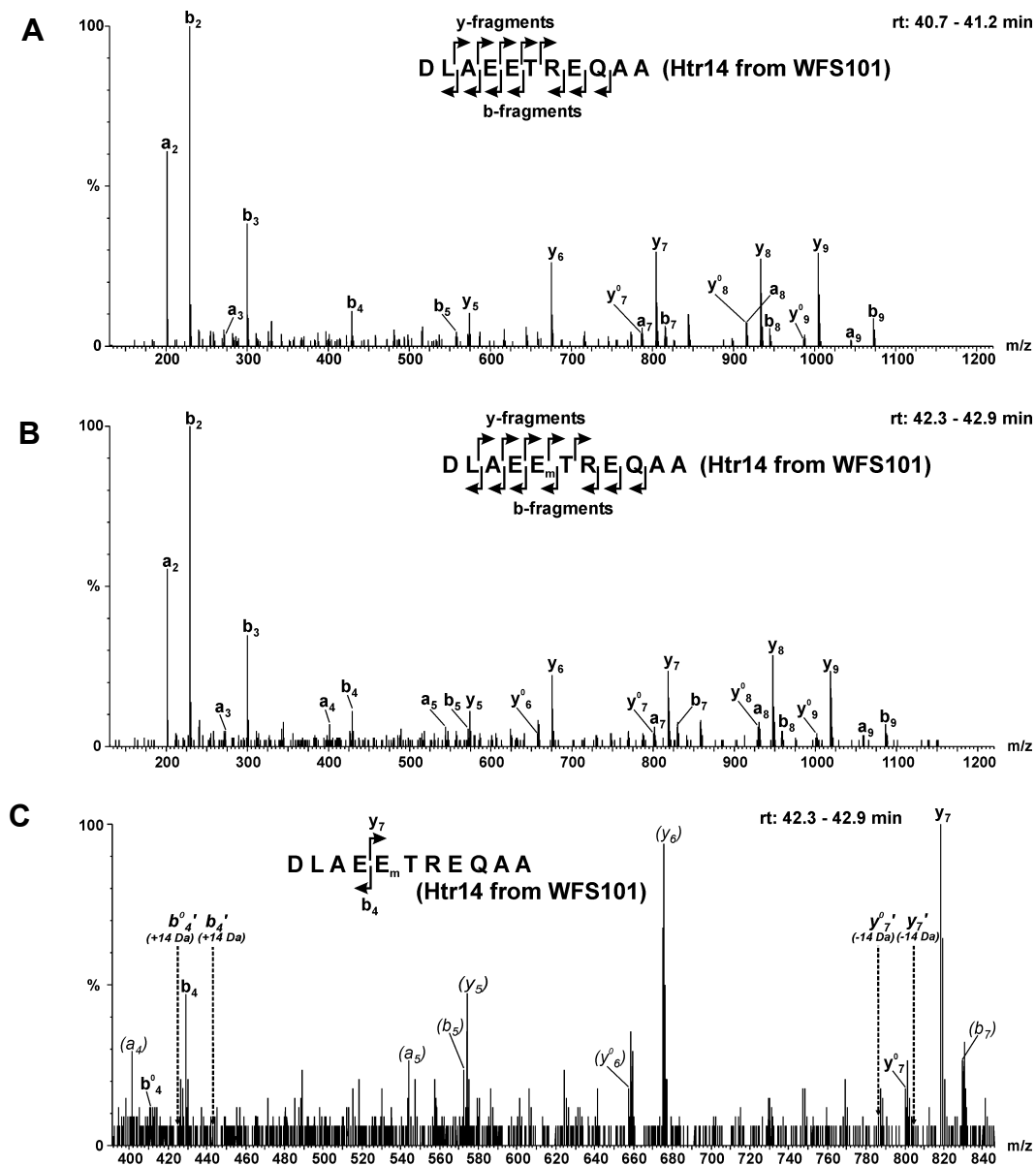


Figure 6.6 MS/MS spectra of the unmethylated and singly methylated form of the Htr14 peptide DLAEETREQAA from strain WFS101.

Spectra were recorded and annotated as described in Fig. 3.27. Spectra of the unmethylated (A) and the singly methylated (B) form of the peptide were obtained from $\Delta cheB$ strain WFS101 and correspond to spectra A and B in Fig. 3.32, which were obtained from wt strain S9. (C) Magnified view of the region of spectrum B, which allows to determine the methylated position within the glutamate pair. Arrows at the peptide sequence indicate fragments y₇ and b₄, which are crucial for the determination of the methylation position. The absence of significant signals for a methylation at the alternative position (indicated by primed fragment designations in combination with dotted arrows) demonstrates that not only in S9 but also in WFS101 the second glutamate of the pair is either the predominantly or the only methylatable residue of this peptide.

6.9 Domain organization of the Htrs, Tsr, Tar and McpB

Table 6.4. Regions, features and methylation sites of Htrs, Tsr, Tar and McpB.

<i>Htr</i> [total aa]	<i>N-terminus</i> location of <i>N-</i> terminus (<i>cy:</i> cytoplasmic; <i>ex:</i> extracellular), aa, number of positively and negatively charged aa	<i>Predicted</i> <i>transmembrane</i> <i>helices (TM)</i> residue numbers, [total residues]	<i>N-terminal-</i> <i>or linker-</i> <i>region</i> (<i>res.</i> <i>between N-</i> <i>terminus or</i> <i>end of last</i> <i>TM and</i> <i>conserved</i> <i>Glx-Glx of</i> <i>heptad -12)</i> [total <i>res.</i>]	<i>Methylation sites</i> <i>identified via Q-</i> <i>TOF MS/MS</i> MS/MS-identified methylatable residues highlighted yellow (main site underlined), assumed additional sites, sites confirmed in the literature	<i>Signaling</i> <i>region</i> (94% identity in all <i>Htrs</i> , <i>inter-</i> <i>rupted by</i> <i>G(D)XXG-</i> <i>motif</i>)	<i>C-</i> <i>terminus</i> residue numbers, [total residues]
Htr1 [536]	cy, 1-13, 4+, 0-	TM1: 14-32 [19] TM2: 35-55 [21]	56-264 [209]	E265/E266 (1 in WT, 2 in ΔB)	332-351 358-374	375-536 [162]
Htr2 [764]	cy, 1-16, 3+, 0-	TM1: 17-37 [21] TM2: 283-302 [20]	303-512 [210]	E513/E514 (1 in WT, ? in ΔB) Q709/E710 (in ΔB)	580-599 604-620	621-764 [144]
Htr3 [805]	cy, 1-24, 5+, 3-	TM1: 25-45 [21] TM2: 297-316 [20]	317-552 [236]	E553/E554 (1 or 2 in ΔB) E735/E736 (1 in ΔB) E763/E764 (2 in ΔB)	620-639 644-660	661-805 [145]
Htr4 [778]	cy, 1-26, 7+, 0-	TM1: 27-47 [21] TM2: 298-317 [20]	318-527 [210]	D521/E522 (0 in ΔB) E528/E529 (1 or 2 in ΔB) <i>D535/Q(E)536</i> A738/E739 (? in ΔB)	595-614 619-635	636-778 [143]
Htr5 [810]	cy, 1-38, 4+, 5-	TM1: 39-59 [21] TM2: 324-344 [21]	345-555 [211]	E556/E557 (1 or 2 in WT and in ΔB) E738/E739 (? in ΔB) E766/E767 (? in ΔB)	623-642 647-663	664-810 [146]
Htr6 [789]	cy, 1-28, 5+, 3-	TM1: 29-49 [21] TM2: 295-314 [20]	315-524 [210]	<i>D518/E519</i> Q(E)525/E526 (? in ΔB) <i>E735/E736</i>	592-611 616-632	633-789 [157]
Htr7 [545]	ex, 1-3, 0+, 0-	TM1: 10-32, 2- [23] TM2: 42-64 [23] TM3: 76-100 [25]	101-279 [180]	E280/E281 (? in ΔB) <i>E494/E495</i>	347-366 375-391	392-545 [154]
Htr8 [643]	cy, 1-47, 7+, 4-	TM1: 48-68, 1- 1+ [21] TM2: 82-102, 1- [21] TM3: 110-128, [19] TM4: 130-148, 1- [19] TM5: 154-173 [20] TM6: 187-208 [22]	210-390 [181]	E391/E392 (1 or 2 in ΔB) <i>E573/E574</i> <i>E601/Q602</i>	458-477 482-498	499-643 [145]
Htr9 [481]	cy, (1-30: 2+, 3-)	---	1-251 [251]	<i>Q252/E253</i> <i>E434/E435</i>	319-338 343-359	360-481 [122]

Htr [total aa]	N-terminus location of N- terminus (cy: cytoplasmic; ex: extracellular), aa, number of positively and negatively charged aa	Predicted transmembrane helices (TM) residue numbers, [total residues]	N-terminal- or linker- region (res. between N- terminus or end of last TM and conserved Glx-Glx of heptad -12) [total res.]	Methylation sites identified via Q- TOF MS/MS MS/MS-identified MS/MS-identified methylatable residues highlighted yellow (main site underlined), assumed additional sites, sites confirmed in the literature	Signaling region (94% identity in all Htrs, inter- rupted by G(D)XXG- motif)	C- terminus residue numbers, [total residues]
Htr10 [489]	cy, (1-30: 2+, 7-)	---	1-264 [264]	E262/E263 E444/E445	329-348 353-369	370-489 [120]
Htr11 [452]	cy, (1-30: 0+, 9-)	---	1-223 [223]	E224/E225 (MALDI) E406/Q407	291-310 315-331	332-452 [121]
Htr12 [420]	cy, (1-30: 2+, 5-)	---	1-184 [184]	Q185/E186 E395/Q396 A367/E368	252-271 276-292	293-420 [128]
Htr13 [423]	cy, (1-30: 1+, 3-)	---	1-195 [195]	E196/Q197 (MALDI) E378/E379 (MALDI)	263-282 287-303	304-423 [120]
Htr14 [627]	cy, 1-27, 4+, 2-	TM1: 28-51 [24] TM2: 55-76 [20]	77-309 [233]	E310/E311 (1 or 2 in WT and in ΔB) E415/E416 (1 in ΔB) E506/E507 (2 in ΔB)	377-396 401-417	418-627 [210]
Htr15 [636]	cy, (1-30: 4+, 2-)	---	1-404 [404] but good homology to Htr9 starting at L170 [404- 169 = 235]!!	Q405/E406 D412/Q(E)413 E419/Q(E)420 Q615/E616	472-491 496-512	513-636 [124]
Htr16 [792]	cy, 1-21, 5+, 3-	TM1: 22-42 [21] TM2: 293-311 [19]	312-548 [237]	E549/E550 E759/E760	616-635 640-656	657-792 [136]
Htr17 [536]	ex, 1-3, 0+, 0-	TM1: 4-24, 1- [21] TM2: 33-56 [24] TM3: 61-83, 1- [23]	84-268 [185]	E269/E270 Q479/Q480	336-355 360-376	377-536 [160]
Htr18 [816]	cy, 1-18, 3+, 0-	TM1: 19-39 [21] TM2: 283-302 [20]	303-538 [236]	E539/E540 (1 in WT, 2 in ΔB) E721/E722 E749/E750	606-625 630-646	647-816 [170]
Tsr (<i>E. coli</i>) [551]	cy, 1-6, 3+	TM1: 7-30 [24] TM2: 192-214 [23]	215-302 [88]	E296/Q(E)297 E303/E304 E310/Q(E)311 E492/E493	370-389 394-410	411-551 [141]
Tar (<i>E. coli</i>) [553]	cy, 1-6, 2+	TM1: 7-30[24] TM2: 189-212 [24]	213-300 [88]	E294/Q(E)295 E301/E302 E308/Q(E)309 Q490/E491	368-387 392-408	409-553 [145]
McpB (<i>B. subtilis</i>) [662]	cy, 1-16, 5+	TM1: 17-37[21] TM2: 279-303 [25]	304-(418) [115]	E370/Q(E)371 E629/E630 E636/E637	486-505 510-526	527-662

6.10 Scheme of the features and methylation sites of Htrs, Tsr, Tar and McpB

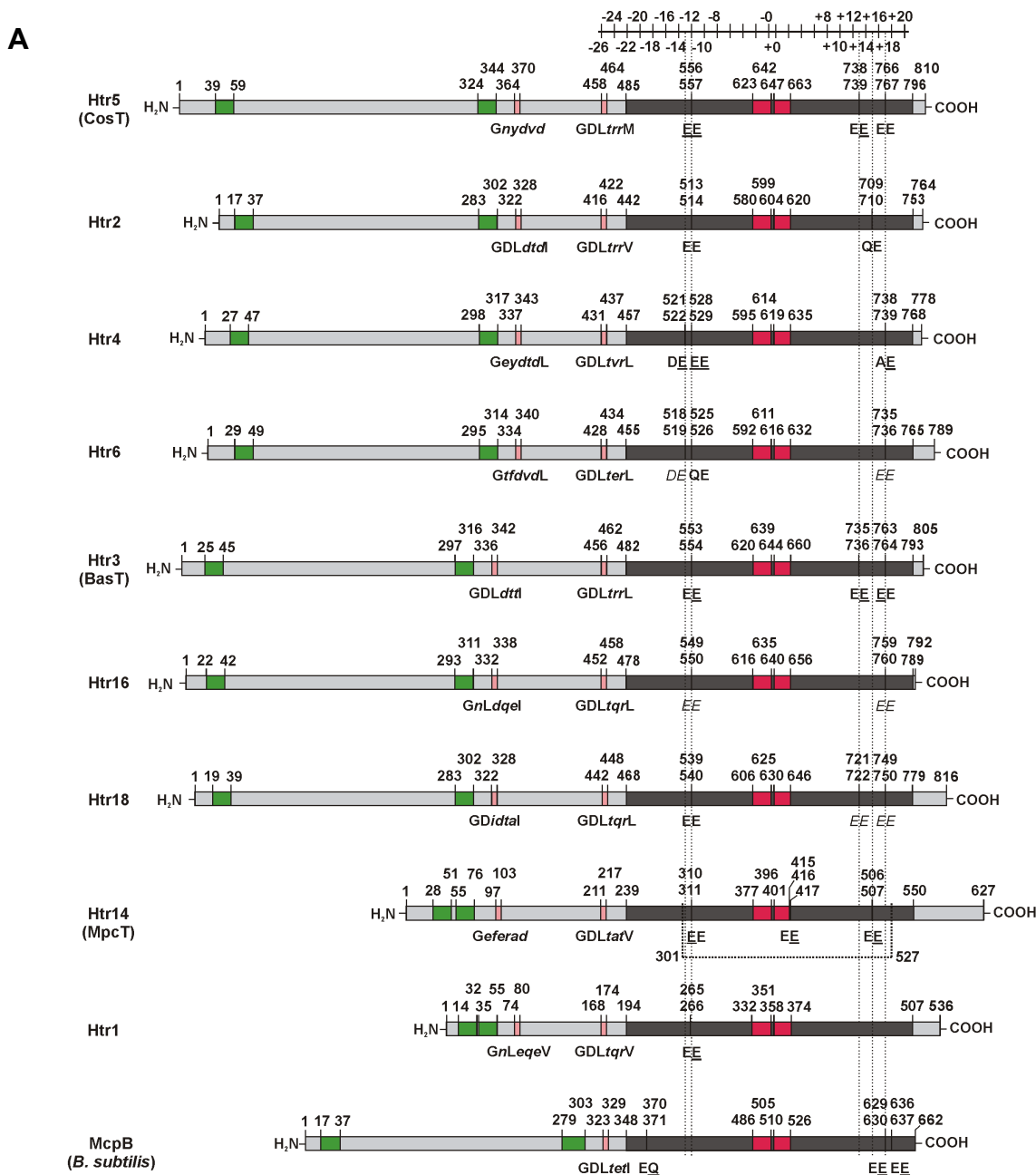
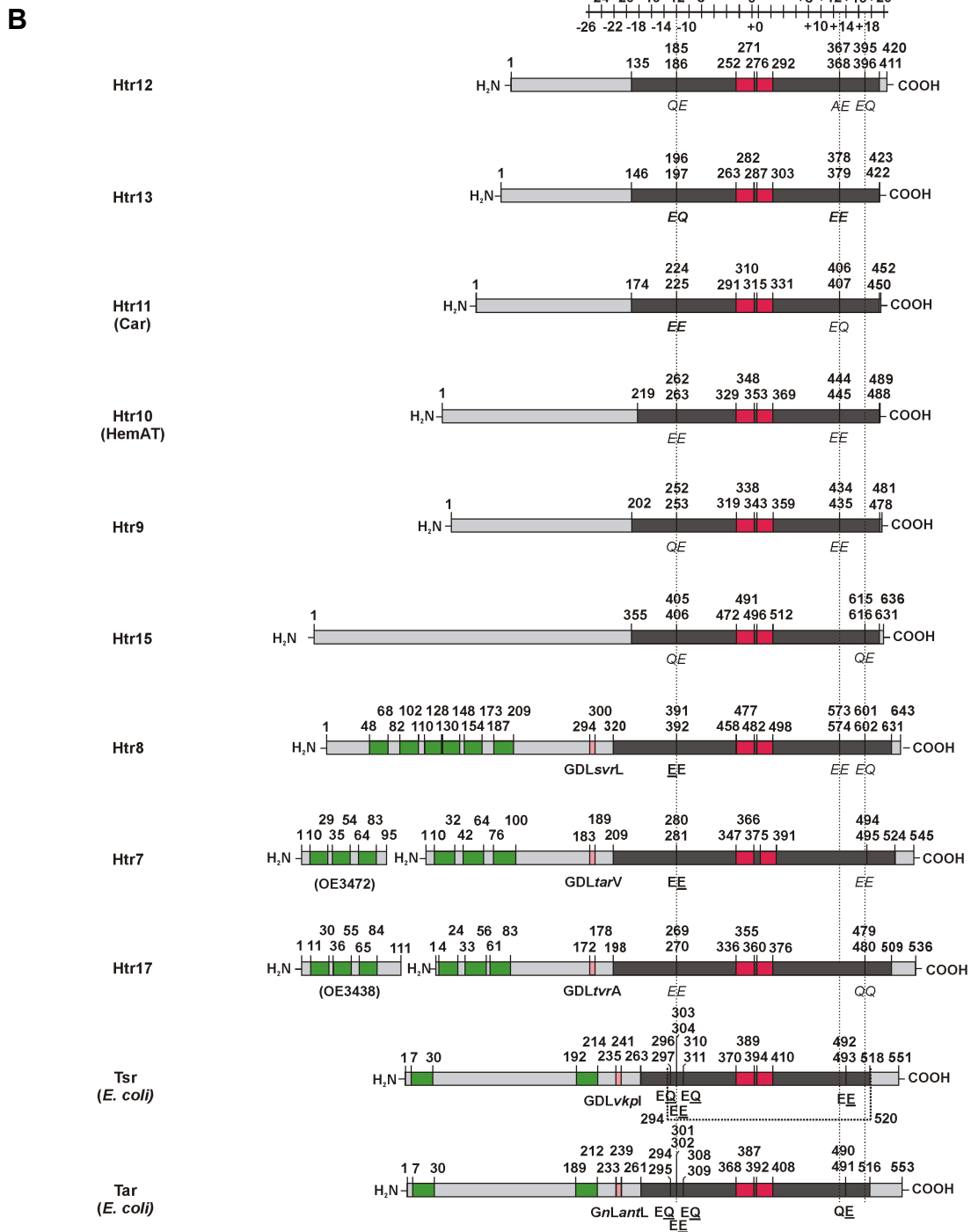


Figure 6.7 Schematic representation of the 18 Htrs, *E. coli* Tsr and Tar, and *B. subtilis* McpB with features and methylation sites indicated.

The graphic transducer representations are aligned at the position of the predicted hairpin turn within the signaling region. Numbers indicate the first and last residue of the depicted features: light grey: complete protein, green: transmembrane (TM) region, pink: GDL-motif within a HAMP domain (capitalized residues indicate matches to the consensus sequence GDLxxxO, with O = hydrophobic residue), dark grey: uninterrupted hydrophobic heptad assumed to comprise a coiled coil region, red: highly conserved signaling region (interrupted by a hairpin turn). A pair of bold letters indicates a methylation site which was either published (McpB, Tsr, Tar) or mass spectrometrically identified (Htrs). For underlined residues a methylation was clearly shown via MS/MS. Italicized letters indicate putative methylation sites as deduced from the surrounding sequences and the residue positions. The positions of the heptads are indicated by a ruler at the top of the figure. (A) Htrs containing 2 TM regions and McpB. Htr methylation was shown within heptads -13, -12, +13, +15 and +17. The dotted line including Htr14 residues 301 to 527 indicates the residues corresponding to those in the cTsrQ structure.

**Figure 6.7**

(B) Htrs containing 0, 6 and 3 TM regions, Tsr and Tar. Htr methylation was shown within heptads -12 and +13, and is assumed within heptad +17. The dotted line including Tsr residues 294 to 520 indicates the residues corresponding to those in the cTsrQ structure. OE3427 and OE3438 are the products of the orfs which form transcription units with Htrs7 and 17, respectively.

Danksagung:

Ich möchte mich an dieser Stelle recht herzlich bei allen bedanken, die zum Gelingen dieser Arbeit beigetragen haben.

An erster Stelle gilt mein Dank Prof. Dr. Dieter Oesterhelt, unter dessen Anleitung diese Arbeit am Max-Planck-Institut für Biochemie in Martinsried entstanden ist. Er hat nicht nur für die Finanzierung dieser Arbeit gesorgt und mir den Besuch diverser Konferenzen im Ausland ermöglicht, sondern mir darüberhinaus maximale Freiheit bei der Planung und Durchführung der einzelnen Projekte gelassen. In den leider seltenen aber dafür oft mehrstündigen Besprechungen, sowie bei den zahlreichen Diskussionen an der Labortür, wenn ich ihn mal wieder mit einem Stück Kreide bewaffnet auf dem Gang abgefangen habe, hat er mir immer wieder mit wissenschaftlichem Rat zur Seite gestanden und mir zahlreiche wertvolle Anregungen geliefert, die wesentlich zum Erfolg dieser Arbeit beigetragen haben.

Weiterhin gilt mein Dank allen Mitgliedern der Abteilung, die, jeder auf seine Weise, dazu beigetragen haben, dass eine Atmosphäre gegenseitiger Hilfsbereitschaft vorherrschte, in der ich immer auf offene Ohren stiess, wenn es mal wieder darum ging, kleinere oder grössere Probleme zu lösen. Insbesondere danke ich den folgenden Personen:

Dr. Kai-Florian Storch, der mich zu Beginn dieser Arbeit in die Thematik der halobakteriellen Signaltransduktion und in diverse molekularbiologische Arbeitsmethoden eingeführt hat.

Dr. Matthias Pfeiffer, für seine permanente Diskussionsbereitschaft bei molekularbiologischen, organisatorischen oder "Halo"-spezifischen Fragestellungen, und für zahllose kurzweilige Abendessen in der "Teeküche", bei denen wir im Lauf der Zeit sicher einige Gefrierschrank-Ladungen der guten alten "Casa Domani" Pizza verspeist haben.

Meinem "Laborbank-Nachbarn" Wilfried Staudinger, für die Konstruktion der *cheB*- und *cheR*-Deletionsstämme, für seine Hilfe bei einigen der "Motion-Messungen", und nicht zuletzt für eine über die Jahre gleichbleibend angenehme Zusammenarbeit in einer Atmosphäre gegenseitiger Hilfsbereitschaft und Verlässlichkeit und für seine Gesellschaft bei den unzähligen gemeinsamen Abendessen im Halocafé.

Allen Mitgliedern der Bioinformatik-Gruppe um Dr. Friedhelm Pfeiffer, die mit HALOLEX ein wunderbares System zur Verwaltung der verschiedensten Informationen über *H. salinarum* geschaffen haben, deren Wert wohl nur diejenigen wirklich einschätzen können, die sich ihre Informationen noch ohne dieses System beschaffen mussten.

Allen in der "Masse" tätigen Kolleginnen und Kollegen; insbesondere Dr. Frank Siedler, der mich in zahlreichen Gesprächen in die Massenspektrometrie eingeführt hat und mir bei der Planung und Durchführung der Experimente immer wieder hilfreich zur Seite stand; weiterhin Bea Scheffer, für die Messungen der zahlreichen Proben an der "Q-TOF", aus deren MS/MS Daten letztlich die Htr-Methylierungsstellen ermittelt werden konnten; und Dr. Sabine Thiessen für ihre Hilfe bei den umfangreichen Vorarbeiten zum Htr-Methylierungsprojekt.

Birgit Bisle und Dr. Christian Klein, die die MALDI Spektren generierten, in denen ich dann später methylierte Htr-Peptide identifizieren konnte.

Dr. Douglas Griffith und Dr. Birgit Wiltschi, für die Durchsicht des MpcT-bezogenen Teils der Arbeit und für viele hilfreiche Kommentare.

Volker Hickmann, für das Schreiben des Computerprogramms, mit dessen Hilfe die Datenbank aus permutierten Htr-Peptiden erstellt werden konnte.

Dr. Masato Otsuka, für die Konstruktion des Stammes OMI1 (NAOMI), der den Ausgangsstamm für das MpcT Projekt darstellte.

Dr. Benjamin Quest, für seine überaus hilfreichen Tips zur Verwendung des Textverarbeitungsprogramms OpenOffice und zur Formatierung der Arbeit.

Und Dank sei natürlich noch dem einen weiteren Menschen, dessen Erwähnung an dieser Stelle nicht fehlen darf, der mir aber leider erst unmittelbar nach dem Binden der Arbeit in den Sinn kommen wird, was ich jetzt schon bedauere!

Schliesslich möchte ich mich an dieser Stelle auch ganz herzlich bei meinen Eltern bedanken, die mir das Studium inclusive des einjährigen Auslandsaufenthaltes in den USA ermöglicht haben und mich über all die Jahre mit einem unerschütterlichen Vertrauen durch alle Höhen und Tiefen begleitet haben. Ihnen ist diese Arbeit gewidmet.

Lebenslauf

Persönliche Daten

Name	Matthias Koch
Geburtsdatum	02.08.1965
Geburtsort	Eschwege

Schulbildung

09/1971 - 07/1975	Struthschule, Eschwege
09/1975 - 07/1981	Friedrich-Wilhelm Gymnasium, Eschwege
09/1981 - 06/1984	Oberstufengymnasium, Eschwege

Wehrdienst

07/1984 - 09/1985	Grundwehrdienst bei der Bundeswehr
-------------------	------------------------------------

Studium

09/1986 - 09/1990	Studium der Chemie an der Albert-Ludwigs-Universität, Freiburg
10/1990 - 09/1991	Auslandsaufenthalt zum Studium der Biochemie am Institute of Molecular Biology an der University of Oregon, Eugene, USA
10/1991 - 03/1998	Studium der Chemie an der Albert-Ludwigs-Universität, Freiburg
05/1998	Diplomhauptprüfung
06/1998 - 03/1999	Diplomarbeit am Institut für Biochemie und Molekularbiologie der Uni Freiburg in der Arbeitsgruppe von Prof. Dr. R. Brandsch zum Thema "Untersuchungen zur Rolle des Proteins MoeA aus <i>Arthrobacter nicotinovorans</i> bei der Biosynthese des Molybdopterin Cofactors"

Promotion

10/1999 - 08/2005	Doktorarbeit am Max-Planck Institut für Biochemie bei Prof. Dr. D. Oesterhelt zum Thema "Investigations on halobacterial transducers with respect to membrane potential sensing and adaptive methylation"
-------------------	---